INVESTIGATION OF FRESHWATER MICROALGAE *PARACHLORELLA*

KESSLERI AS A SOURCE OF ANTI-INFLAMMATORY NATURAL PRODUCTS

by

THOMAS S. VILLANI JR.

A dissertation submitted to the

School of Graduate Studies

Rutgers, The State University of New Jersey

In partial fulfillment of the requirements

For the degree of

Doctor of Philosophy

Graduate Program in Medicinal Chemistry

Written under the direction of

James E. Simon

And approved by

_____

_____

_____

_____

_____

New Brunswick, New Jersey,

January 2018

ABSTRACT OF THE DISSERTATION

Investigation of Freshwater Microalgae *Parachlorella kessleri* as a Source of Anti-inflammatory Natural Products

By THOMAS S. VILLANI JR.

Dissertation Director:

James E. Simon

Considering the tremendous influence that terrestrial plants have had on the identification of bioactive molecules for the modulation of disease, it comes as a surprise that microalgae, which constitute a larger proportion of biomass on earth than terrestrial plants, have not contributed proportionally to the diverse collection of active compounds in pharmacy. As such, microalgae remain an untapped resource for new structures and activities in medicinal chemistry research. The major reason microalgae remain underrepresented in medicinal chemistry exploration is due to the difficulty of obtaining enough biomass to proceed with biochemical and toxicological evaluation of compounds contained within the biomass. Due to recent developments in aquaculture techniques, the biomass-bottleneck has been lifted, and as such, suitable microalgae for a sophisticated exploration of medicinal properties is now obtainable. Using cutting-edge culturing techniques, *Parachlorella kessleri*, a common freshwater microalga, was amassed in quantities sufficient to support a thorough investigation of the natural products contained within, respective to biological activities relevant to the modulation of inflammation. This investigation revealed several compounds exhibiting anti-inflammatory activity, including a known galactolipid previously unidentified in *P. kessleri*, and a novel oxygenated fucoxanthin ester, both compounds exhibiting significant activity in anti-inflammatory assays. This dissertation defense explores the bioactive constituents of *P. kessleri* with respect to anti-inflammatory properties in great detail.

Dedication

To my mother, who taught me how important it was to use my brain, and who always supported me, and always believed in me, even when I doubted myself.

To my father, who taught me to question everything, to get to the root, to never take at face value, to understand, to tinker and to learn.

And to Courtney, my beautiful love, who has been an endless source of support through my struggles, always toward our wonderful life together, and without whom, none of this would have been possible.

Acknowledgements

First and foremost, I would like to thank Dr. Jim Simon and Dr. Qingli Wu, without whose guidance, mentorship, and support, none of this would have been possible. Dr. Simon has tirelessly offered his guidance and direction to my benefit and has been critical to my development by instructing me in the all-important aspects of how to use science to tell an interesting story. Dr. Wu has taught to me his deep and unique perspective on the chemistry of natural products, and his mentorship and extensive knowledge shared with me had a profound influence on my development as a scientist. I would also like to thank Dr. Adolfina Koroch, for spending countless hours mentoring me next to the microscope as we made so many exciting discoveries about Visikol together. Also, I would like to thank Dr. Rodolfo Juliani, for sharing with me his extensive knowledge about GCMS and fatty acid analysis. I would also like to thank Mike DeLuca and Dr. Steve Bushek, who helped more than anyone to keep this project funded and moving forward. I would also like to thank the scientists at AL-G Technologies, without whom there would have been no algae to study.

There are many students who also offered me support during my work at Rutgers. (Soon to be Dr.) Will Reichert has been an important comrade through grad school, my cellmate in Foran. Harna Patel, my right hand in the lab, offered so much of her time to help my burden in the lab, and I will forever be grateful for your help and friendship. Thanks also to Michael Johnson and Nick Crider, who spent countless hours hearing me talking about algae, and offered their ears and helpful criticism whenever I needed.

Table of Contents

List of Tables

List of Figures

Chapter 1 Introduction

The identification and use of biologically active chemical components derived from natural sources has been the primary source of compounds with therapeutic activity throughout human history. Over half of pharmaceutical drugs that have been developed and approved on the market are natural products, or derived from natural products[1]. Natural products continue to be a source of rich structural diversity, giving rise to a diverse array of components with a seemingly infinite variety of chemical permutations. Natural products are typically better suited for interactions with biological systems due to their evolution across time to interact in the biological realm. Even with the advent of high-throughput combinatorial synthesis, giving pharmaceutical researchers access to unprecedented numbers of novel chemical structures, there has not been a proportionate increase in the number of new chemical entities identified for use in therapy. As such, natural products continue to be of great interest in the field of medicinal chemistry as a source of novel, structurally diverse molecules for screening within biological systems. In the last 50 years, as sources of natural products from terrestrial plants were extensively investigated, focus shifted toward new origins for natural products.

Aquatic organisms have long been known to be a rich source of novel and interesting chemistries. By 1974, two natural products, cytarabine and vidaribine, arabinosides of cytosine and adenine respectively, were approved for the treatment of types of leukemia[2]. Inspired by the staggering diversity of marine and freshwater algae, a number

of researchers have taken to exploring species of macro and microalgae for natural products in the continuing effort to identify new sources of interesting molecules.

In this dissertation research, several strains of algae were evaluated for nutritional content, screened for bioactivity and bioactive compounds identified and characterized to assess the viability of the natural products of these microalgae as potential nutraceutical agents for addressing inflammation related to metabolic syndrome. Based on preliminary screening results, one of the algal strains, *Parachlorella kessleri*, was rigorously examined for biological activity, utilizing bio-guided fractionation to assess and identify the chemical constituents that are responsible for medicinal activity with a focus on inflammation.

1.1   Natural Products Derived from Microalgae

Microalgae are eukaryotic single-celled photosynthetic organisms which are taxonomically distinct from cyanobacteria (blue-green algae), which are prokaryotic. Microalgae obtain energy from photosynthesis and live in aquatic environments. Microalgae, like terrestrial plants, require adequate sunlight, water, carbon dioxide, phosphorus and fixed nitrogen. Also like land plants, microalgae store food in the form of hydrocarbons, and are therefore a target of predators and parasitic microorganisms[3]. Microalgae are critically important to the biosphere because they produce approximately 70-80% of the total photosynthetic oxygen released into the atmosphere, supporting all respiring organisms[4]. The biodiversity of microalgae species is remarkable; it is estimated that between 200,000-800,000 species of microalgae exist, of which less than 50,000 species have been documented[5]. Cardozo et al. detail that over 15,000 novel compounds have been characterized from algal biomass. Clearly, due to the huge diversity of species and plethora of rich chemistries, microalgae have been of great interest in natural products research over the last 50 years.

1.1.1   Omega-3 Unsaturated Fatty Acids

Omega-3 unsaturated fatty acids, known to most consumers as "fish oil," has in the last 30 years become a fountain of basic, molecular and clinical research with a wide range of reported health benefits in the treatment of cardiovascular disease, inflammation, rheumatoid arthritis, depression, and cancer, as well as many other therapeutic areas, which are reviewed in detail in this section. Omega-3 fatty acids are single-chained carboxylic acid groups, typically with >16 carbons, unsaturated at the omega (e.g. 3rd)

position from the end of the carbon chain (Figure 1-1). The three most important omega-3 fatty acids to human physiology are α-linolenic acid (ALA, 18:3n3), eicosapentaenoic acid (EPA, 20:5n3), and docosahexaenoic acid (DHA, 22:6n3), shown in Figure 1-1.
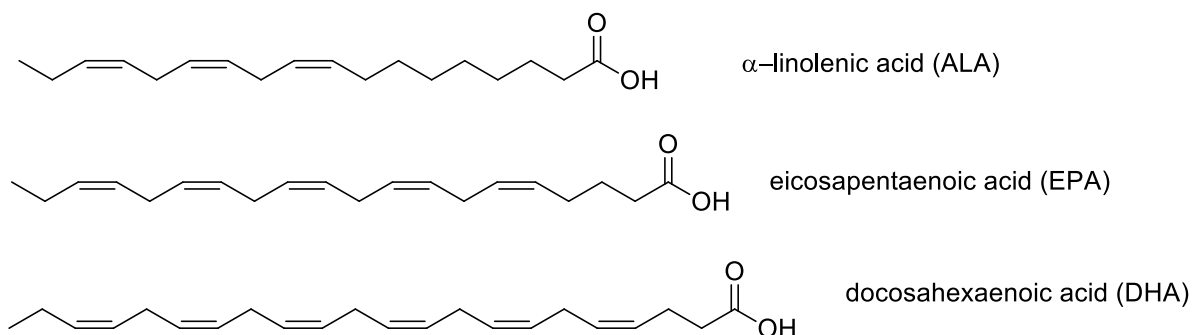
Figure 1-1. Structures of omega-3 fatty acids relevant to human physiology

α-linolenic acid (ALA) is one of the two essential fatty acids; required in human diet because they cannot be innately synthesized by human metabolism. Due to the fact that human cells do not express the required 12- and 15-desaturase enzymes (cite),, synthesis of linolenic acid from stearic acid is not possible, and therefore ALA must be obtained from the diet. In human cells (as well as other animal cells), ALA is a vital component of the phospholipid bilayer, required for proper functionality[6]. A diet deficient in ALA was demonstrated to cause skin scaling, hair loss, and poor wound healing[7], as well as dermatitis[8]. Studies have also correlated diets deficient in ALA to coronary heart disease[6]. Typically, ALA is obtained from dietary sources of seeds (chia, flaxseed), nuts, and oils (flaxseed, canola, soy)[9].

Eicosapentaenoic acid and docosahexaenoic acid, while not technically *essential* fatty acids, are critically important for human health and nutrition. Eicosapentaenoic acid (EPA) and docosahexaenoic acid (DHA) is a major constituent of central nervous system

tissue, particularly in the brain, and is required by all animals for proper metabolic function. Obligate herbivores typically synthesize DHA from ALA, whereas animals with access to seafood and/or algae obtain the majority of their DHA from the environment[10]. In humans, DHA is considered "provisionally essential for infant nutrition;" developmental abnormalities such as in the development of the retina and occipital cortex have been tied to deficiency[11,12].

A wide variety of biological activities have been attributed to omega-3 fatty acids through in vitro and in vivo studies, epidemiological research, as well as clinical trials. Of all the indications for omega-3s, there is perhaps the strongest evidence to support the usage of omega-3s for the mitigation of cardiovascular and heart disease. Meta-analysis of 70 randomized controlled clinical trials established that EPA+DHA supplementation reduced systolic blood pressure by 1.52 mmHg and diastolic blood pressure by 0.99 mmHg with a 95% confidence interval, with the strongest impact on previously untreated hypertensive patients[13]. Omega-3 fatty acids and esters have also been demonstrated to significantly reduce levels of triglycerides in patients—there are currently 6 prescription formulations of omega-3 fatty acids available for the treatment of elevated triglycerides [14]. The mechanism of this interaction remains somewhat elusive, although it has been proposed that inhibition of acyl-CoA:1,2-diacylglycerol acyltransferase[15], decreased lipogenesis in the liver[16,17], and increased plasma lipoprotein lipase activity and β-oxidation[14]. Based upon a systematic review of randomized clinical trials, ALA does not confer the cardiovascular health benefits attributed to EPA and DHA[18]. Wu and Parhofer reported

that they did not find sufficient evidence in the literature to show that omega-3 fatty acids play a role in allaying levels of LDL-cholesterol in diabetic dyslipidemia[19].

There is mounting epidemiological evidence to support that increased dietary omega-3 fatty acids can play a role in the diminution of the risk of stroke caused by plaque buildup in the arteries of the brain, as reviewed by Ehrlich (2011)[20]. Large-population studies have demonstrated a significant decrease in incidence of stroke amongst women who consume at least two servings of fish per week[21]. A systematic meta-analysis of 452 clinical trials and randomized controlled trials was conducted to evaluate the evidence of omega-3 intake on the rate of cardiovascular events[22]. This study revealed an overall decrease of suffering a cardiovascular event of any kind by 10% (p=0.001), a 9% decrease in cardiac death (p=0.03), and a substantial decrease of coronary events, fatal and non-fatal, of 18% over placebo ($p < 1\times10^{-4}$)—there was an overall trend toward lower total mortality, accounting for a 5% reduction of risk (p=0.15).

Omega-3, as well as omega-6 (possessing the first double bond 6 bonds from the terminus), fatty acids are the direct precursors for a number of eicosanoids. Eicosanoids are biologically important molecules which influence a wide array of cellular signaling pathways in the human body. EPA, for example, is a direct precursor for prostaglandin-3, an inhibitor of platelet aggregation, thromboxane-3 (also involved in platelet aggregation) and leukotriene-5 groups [23]. Different structures of eicosanoids can influence inflammation in different ways; omega-3 eicosanoids are anti-inflammatory, whereas omega-6 eicosanoids are pro-inflammatory[24]. Due to their influence on the eicosanoid

cellular signaling pathway, omega-3 fatty acids have been thoroughly investigated for their impact on inflammation and inflammatory diseases. The evidence supporting the roles of omega-3 fatty acids in the regulation of inflammation—the role of omega-3s and eicosanoids on inflammation is discussed in great detail in section 1.2.3 in this dissertation.

The ratio as well as presence of omega-6 to omega-3 fatty acids in human diet is important and has been determined to play a role in a variety of diseases. A very high ratio of omega-6 to omega-3 (as typically found in Western diets) has been shown to "promote the pathogenesis of many diseases, including cardiovascular disease, cancer, and inflammatory and autoimmune diseases" (Simopoulus, 2003, other (cite). Increased levels of Omega-3s help to attenuate a number of disease pathologies. For example, in the prevention of cardiovascular disease, a ratio of 4:1 Omega-6/Omega-3 was associated with a 70% decrease in mortality whereas a ratio of 2-3:1 suppressed inflammation in patients with rheumatoid arthritis[25].

The major source of omega-3 fatty acids in human diets derives from plant or seafood sources[20]. ALA is a major component in a number of seed oils, including chia, flax, and hemp; ALA is also a major component in phospholipids derived from freshwater and marine algal sources[25]. DHA and EPA are more difficult to find in the human diet, the principle source deriving from fish oil or krill oil. Fish oil and krill oil are rich in DHA and EPA, obtained through their diets of other fish and/or algae[20]. Marine algae are the principle source of DHA and EPA in the food chain, generating up to 10-20% EPA/DHA by

mass[26]. Based on this evidence, algae as a source of these and other fatty acids have grown in interest due to their high content of omega-3 fatty acids, and have been extensively evaluated for fatty acid content.

There are many strains of algae that are significant sources of fatty acids, and have gained serious interest in lipid research, especially in the emerging and rapidly developing field of biofuels. Freshwater algae typically contain fatty acids with a chain length of fewer than 20 carbons. *Chlorella vulgaris*, for example, may contain up to 10% (as percentage of freeze-dried biomass) lipids, primarily alpha linolenic, linoleic, and palmitic acid[27]. Marine algae have attracted significant interest due to the high content of long chain polyunsaturated fatty acids found in a wide range of species.

1.1.2   Carotenoids and Xanthophylls

Carotenoids are an important part of human diet and nutrition: β-carotene is a precursor to Vitamin A in humans. Insufficient intake of carotenoids and pro-vitamin A derivatives has been shown to contribute to improper development of the retina[28,29]. Pro-vitamin A derivatives include only α-, β-, and γ-carotene, as well as β-cryptoxanthin, which can be converted directly into retinol (the major form of vitamin A) by β-carotene 15-15'-dioxygenase in the intestinal lumen[30]. Vitamin A is essential to vision; it is required by the retina in the aldehyde form retinal which combines with opsin to form rhodopsin, a light sensitive molecule which is necessary to stimulate retinal cells upon absorption of light[31]. Deficiency in Vitamin A leads to the inhibition of rhodopsin synthesis, which leads to symptoms affecting sight, especially night-vision[32]. Vitamin A also plays a key role in

regulation of skin health, apparently by activating genes in keratinocytes in order to induce differentiation, and retinol esters have been prescribed for skin conditions such as acne[33].

Carotenoids, apart from their nutritious properties, also have demonstrated activity in treating a number of disease pathologies[34]. β-carotene supplementation has been shown to reduce lung cancer incidence in non-smokers [35] . It should be noted that supplementation to smokers actually has been correlated to increased cancer incidence, thought to be related to a suppression of enzymes required in vitamin A synthesis and reuptake and the synthesis of oxidized byproducts in the lung[36].

Due to a continually expanding body of research, xanthophylls have also become a significant topic in the context of human health and nutrition. Xanthophylls are oxygenated carotenoid derivatives produced by plants, algae, and cyanobacteria. Functioning as accessory pigments in the photosynthetic pathway, xanthophylls function to dissipate excess energy which cells are exposed to during high-light photoperiods, and are up-produced during these periods [37] . The distinguishing molecular feature that xanthophylls share is an extended conjugated system flanked by cyclized moieties. This system constitutes the chromophore, which imparts to xanthophylls a dark red, yellow, or orange color. Unlike carotenoids, which are hydrocarbons, xanthophylls possess oxygen-containing functional groups such as hydroxy, keto, or epoxide functionality.

Xanthophylls have been demonstrated to exhibit a number of effects important to human health. Xanthophylls are well-known and widely described for their ability to scavenge

free-radicals, therefore possessing anti-oxidant activity[38] which has been demonstrated by many researchers[39]. Astaxanthin, lutein, β-cryptoxanthin, and other xanthophylls have been sold commercially as antioxidants purported to have numerous health effects. Anti-oxidants have been shown to influence inflammatory and immune responses due to their ability to quench free radical oxygen species (ROS). ROS are known to cause damage to DNA and proteins in cells, thus antioxidants convey a protective effect to tissues. Anti-oxidants can also influence the inflammatory response. ROS are generated during inflammation, which serves as a cellular signal which induces the perpetuation of inflammation since ROS stimulate pro-inflammatory cellular signaling pathways (See section 1.3.4 for a more detailed discussion). Anti-oxidants can quench ROS, which inhibits this immune signaling pathway.

A growing body of clinical evidence supports the hypothesis that xanthophylls, especially lutein and zeaxanthin, play an important role in the attenuation of age-related macular degeneration[40]. The mechanisms through which xanthophylls act relevant to age-related macular degeneration have been reviewed extensively in the literature[41,42,43] and will be described briefly here. Age related macular degeneration (AMD) is the leading cause of legal blindness in patients in the US, and there is currently no treatment available for most patients. The *macula lutea* is the name given to a yellow pigmented immediately surrounding the middle of the retina, called the fovea. The yellow pigments stored in this region offer photoprotection to the cells, protecting through their anti-oxidant effect the retinal tissue. Though the pathogenesis of AMD is still poorly understood, it is thought that a confluence of factors lead to oxidative damage in the cells in the retina which

accumulate with age. This eventually leads to a loss of retinal function in certain regions, causing blind spots, severely impacting the quality of life in afflicted patients.

Lutein has also been demonstrated to inhibit tumor development in BALB/c mice[44]. The algal-derived xanthophyll astaxanthin has been evaluated for its role in the mitigation of cardiovascular inflammation (such as artherosclerosis) due to its ability to quench reactive oxygen species; evidence from multiple species supports the use of astaxanthin for this purpose[45] (see section 1.3.4 for a more detailed discussion). Additionally, at least 8 clinical trials conducted to date have demonstrated safety, bioavailability, and reduced markers of oxidative stress and inflammation upon supplementation with xanthophylls— reviewed by Fasset and Coombes (2009)[46]. Xanthophylls isolated from *Halocynthia roretzi* have been demonstrated to suppress expression of pro-inflammatory IL-1β and IL-6 in RAW264.7 murine macrophage cells. Gao et al. (2012) showed that supplementation of xanthophylls in the diets of chickens decreased pro-inflammatory and increased anti-inflammatory cytokine[47]. Researchers have demonstrated that fucoxanthin possesses a number of bioactivities: fucoxanthin has been shown to induce apoptosis on human colon cancer cells[48], prostate cells[49], and inhibit the growth of human neuroblastoma cells[50].

1.1.3   Sterols

Sterols deriving from non-animal sources, known as phytosterols, have been studied extensively in the past few decades due to the fact that many phytosterols are capable of mitigating high-cholesterol levels in people. Coronary heart disease arising from atherosclerosis and related pathology is a major contributor to overall mortality in

modern industrialized nations, and there is overwhelming evidence tying heart disease to inflammation arising from poor diet, the excess of LDL cholesterol particles, and obesity. The pathophysiology of atherosclerosis is discussed in detail in section *1.3.1* later in this chapter.

Sterols are collectively the class of naturally occurring alcohols typified by the ring structure shown in Figure 1-2, consisting of a fused tetracyclic ring system composed of a cyclopentyl ring fused to a tetradecahydro-phenanthrene, with a hydroxy functional group. The most common sterol in animals is cholesterol, also shown in Figure 1-2. Cholesterol plays a critical role in stabilizing animal cell membrane structure and ensuring proper functioning—absence of cholesterol in diet leads to severe disruption in the integrity and proper functioning of cell membranes[51]. The biosynthesis of cholesterol is described in Voet, Voet, and Pratt[52]; the pathway is shown in Figure 1-2 and briefly described. All animal cells synthesize cholesterol, starting from one molecule of acetyl CoA, one molecule of acetoacetyl-CoA, which through a hydration reaction, form 3-hydroxy-3-methylglutaryl CoA (HMG-CoA). HMG-CoA is subsequently reduced by HMG-CoA reductase to mevalonic acid. Inhibition of HMG-CoA is the mechanism of action of the statins, a therapeutic class of drugs including atorvastatin (Lipitor®) marketed for their efficacy in lowering blood cholesterol levels[53]. Mevalonic acid is converted to isopentenyl diphosphate by decarboxylation. Three molecules of isopentenyl diphosphate condense to form farnesyl pyrophosphate. Two molecules of farnesyl pyrophosphate are subsequently condensed to form squalene by action of squalene synthase. Oxidosqualene cyclase oxidizes squalene to the epoxide, which then spontaneously cyclizes to form

lanosterol, which through many more steps, is subsequently converted to cholesterol. Approximately 75% of the cholesterol in the body is synthesized in this route, while the remainder is absorbed through diet—diets high in saturated fats lead to a higher production of cholesterol by the liver[54].

Fatty acids

Acetyl-CoA + Acetoacetyl-CoA

Lyase   Synthase

HMG-CoA

HMG-CoA reductase

statins

CH$_2$OPP

Sterol - general structure

squalene synthase

CH$_2$OPP

squalene epoxide

H$^+$

carbocation rearrangements

cholesterol

lanosterol
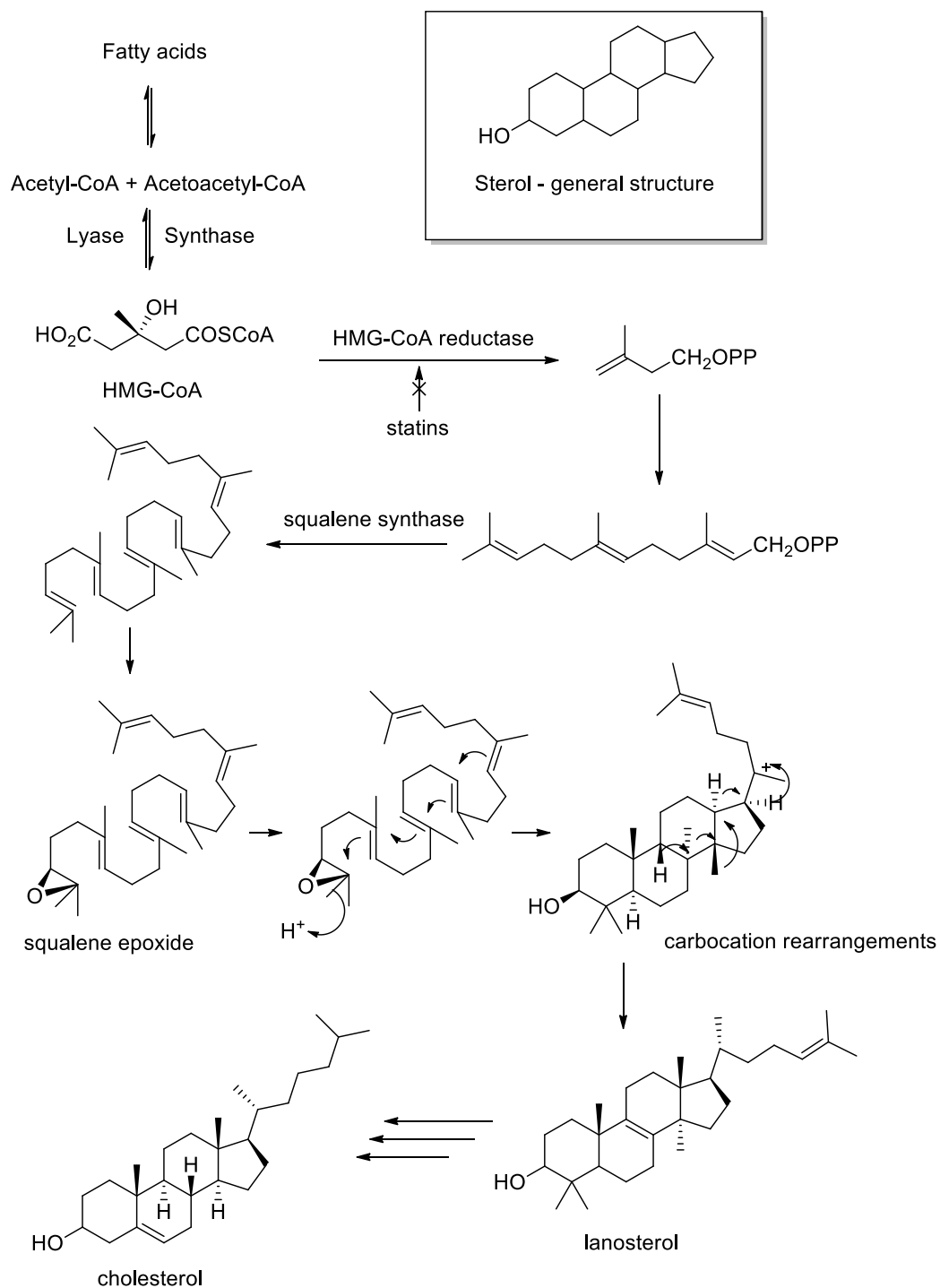
Figure 1-2. Structure and biosynthesis of Sterols (adapted from Nes (2011)[55] and Voet, Voet, & Pratt (2004)[52]

The absorption of cholesterol constitutes a major source of cholesterol in the body, nearly 25% of cholesterol is obtained in this fashion[56]. Due to the high lipophilicity of cholesterol, it can only be absorbed by incorporation into bile acid micelles. As such, only non-esterified cholesterol may be incorporated readily into bile acid micelles, and since nearly 15% of dietary sterols occur as fatty acid esters, the enzyme cholesterol esterase is critical to free cholesterol from its ester form[56]. Bile acid micelles are mixed micelles containing bile acids, free cholesterol, phospholipids and lysophospholipids, as well as triglycerides, monoacylglycerides, and free fatty acids. These micellar complexes facilitate the transport of cholesterol and other lipid soluble vitamins across the cell membranes. Due to the involvement of bile acids, the liver is the primary regulator of cholesterol levels in the body.

β-sitosterol   campesterol   stigmasterol   brassicasterol
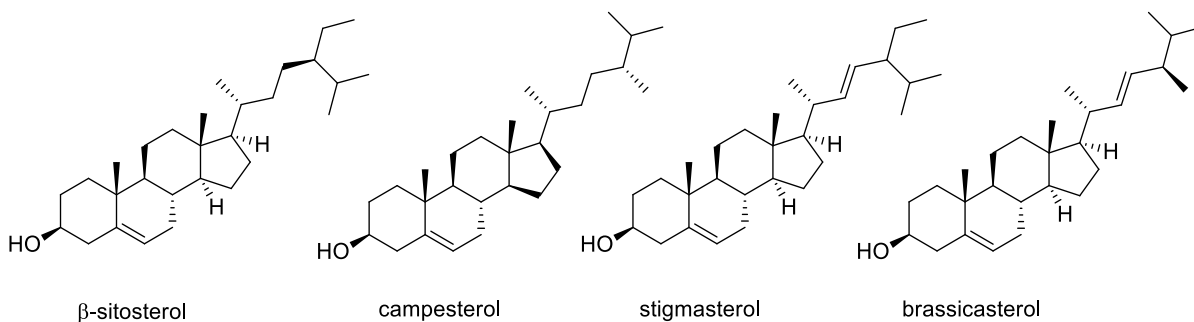
Figure 1-3. Chemical structures of common dietary phytosterols

Phytosterols, hereto defined as referring collectively to all non-animal sterols, have gained a marked interest in pharmaceutical and nutraceutical applications due to their ability to interact with cholesterol-acting enzymes[57]—the market for phytosterols has

grown to over $500M (as of 2015) annually in the US, and is expected to grow at 9% CAGR through 2024[58]. The structures of the 4 most common phytosterols found in algae species[59] are shown in Figure 1-3: β-sitosterol, stigmasterol, and campesterol, typical of terrestrial plants, and brassicasterol, typically found in a wide array of terrestrial plants, and in several marine species. The absorption rate of phytosterols is much lower than for cholesterol; only 5% of dietary phytosterols are absorbed, (campesterol is absorbed better than β-sitosterol, stigmasterol is minimally absorbed) compared to 40% absorption for cholesterol[60]. Phytosterols can be incorporated into the cellular membranes of animal tissues analogously to cholesterol—researchers have shown that a 3 week supplementation of rat diets with 5% dietary phytosterols (β-sitosterol and campesterol) led to the incorporation of phytosterols into liver microsomes, and a corresponding decrease in membrane fluidity[61]. Interestingly, the saturated phytosterols, known as phytostanols, show the same activities with higher potency in comparison to the phytosterols.

The impact of dietary phytosterols on human health has been extensively studied in the past decades. The usage of phytosterols as agents for the treatment of hypercholesterolemia in adults has been described since the 1950s (cite),. A number of clinical studies have been performed to investigate the impact of phytosterols preparations on cholesterol, as well as low density lipoprotein (LDL) levels, colloquially known as "bad cholesterol." (cite), Sitosterol supplementation at 0.7-2 g/day in hypercholesterolemic patients resulted in a 11-20% reduction in serum cholesterol levels after 3 weeks[62,63]. There has been variation between results observed which has been

attributed to differences in the phytosterols formulations utilized in the studies[64]. Purified

phytosterols form highly stable and insoluble crystals, which can take days or even weeks

to solubilize in bile acids[65], and as such it appears that the vehicle utilized for phytosterols

supplementation is critical. Consistent lowering with LDL has been reported in many

studies which utilized food matrices to solubilize the phytosterols and increase their

bioavailability: oil[66], egg fat[67], aqueous emulsion with triglycerol mono-oleate[68], and also

by micronization with fatty foods[69] such as margarine. As is summarized in Figure 1-4,

dietary phytosterols reduce LDL cholesterol levels in a dose dependent manner.

Researchers have shown that the maximum level of inhibition for cholesterol absorpton

is 20-30% even with saturating doses of phytosterols[70]. These results have been

confirmed in dozens of clinical studies, and supplementation with phytosterols is

currently a course of therapy prescribed to patients at risk for coronary heart disease and

atherosclerosis.
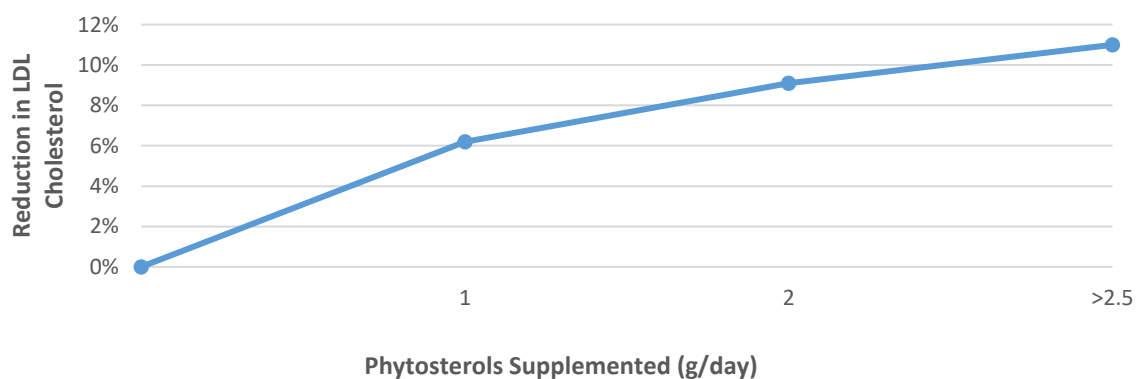
Figure 1-4. Reduction of LDL levels in patients supplemented with phytosterols over six-week treatment. Results compiled from 26 clinical studies[71].

Due to the incontrovertible evidence supporting the role of phytosterols in lowering

blood serum LDL and cholesterol levels, many studies have been conducted to elucidate

the mechanism of action through which phytosterols influence their effects. The mechanism first posited, which has withstood a battery of researchers examining it in great detail, was that phytosterol consumption inhibits cholesterol absorption[60]. The mechanism is thought to be supramolecular effects in the micelles—researchers have demonstrated that sitosterol has an increased affinity for bile acid micelles over cholesterol, and as such the competition between sitosterol and cholesterol favors sitosterol energetically[72] Additionally, competition between sitosterol and cholesterol for uptake in the intestinal epithelium has been demonstrated. Inhibition of cholesterol absorption competitively by phytosterols causes a relative state of cholesterol deficiency. To compensate, animal cells upregulate cholesterol biosynthesis, as well as up regulate LDL receptors expression and activity[71]. Cholesterol precursor biosynthesis increases by 10-46%, and correspondingly, cholesterol biosynthesis increases by 38-53%[71]. LDL receptors are membrane surface receptors which facilitate the endocytosis of LDL particles, particularly in the liver, leading to an overall increase in hepatic LDL clearance, and a corresponding decrease in serum LDL levels[73]. Researchers have demonstrated 25-43% increase in LDL receptor levels, as well as a corresponding reduction in LDL production in the liver by 20% and plasma concentration reduced by 20%[71].

There is overwhelming clinical, biochemical, and mechanistic evidence that supports the role of phytosterols in the attenuation of hypercholesterolemia and therefore atherosclerosis. Terrestrial plants have long been that major source of phytosterols, and their bioactivities have been extensively reviewed in section 1.2. Algae are a great source

of a plethora of sterols with a wide range of unique structures. An overview of sterols contained in algae relevant to this project is described in section 1.2.

1.1.4   Unique natural products derived from algal sources

A thorough review of some interesting and unique classes of natural products derived from algal sources, specifically from green and brown algae, is presented in this section, and will provide a context for the rich complexity innate to algal natural products. For a more complete review of the topic, Blunt et al. (2003 - 2010) publish yearly reviews updating the progress made in the marine natural products research field which are quite extensive[74-83]. In 2001, the structure of kahalalide F, a complex cyclic peptide, was first reported. Kahalalide F (compound **1.1**), is a cyclic depsipeptide originally isolated from the mollusk *Elysia rufescens*, and subsequently found in the primary food source, the green alga *Bryopsis sp*[84]. Kahalalide F was introduced into Phase I clinical trials, effective against prostate cancer, in 2005 (Blunt et al., 2005). As of 2009, kahalalide F had progressed to Phase II clinical trials, and showed efficacy against several types of cancer[85]. The compounds are shown in Figure 1-5.

A unique set of brominated, prenylated hydroquinones (compounds **1.2**, **1.3**, and **1.4**) was isolated from the Cuban green algae *Cymopolia barbata* whose structures were assigned by NMR[86]. Capisterone B (compound **1.5**) and acetyl derivative Capisterone A were isolated from *Panicillus capitatus*, originating from Cat Cay, Bahamas—these compounds exhibited potent antifungal activity[87]. A number of novel diterpenoids (compounds **1.6-1.8**) were discovered in *Caulerpa brownii,* originating from Tasmania[88].
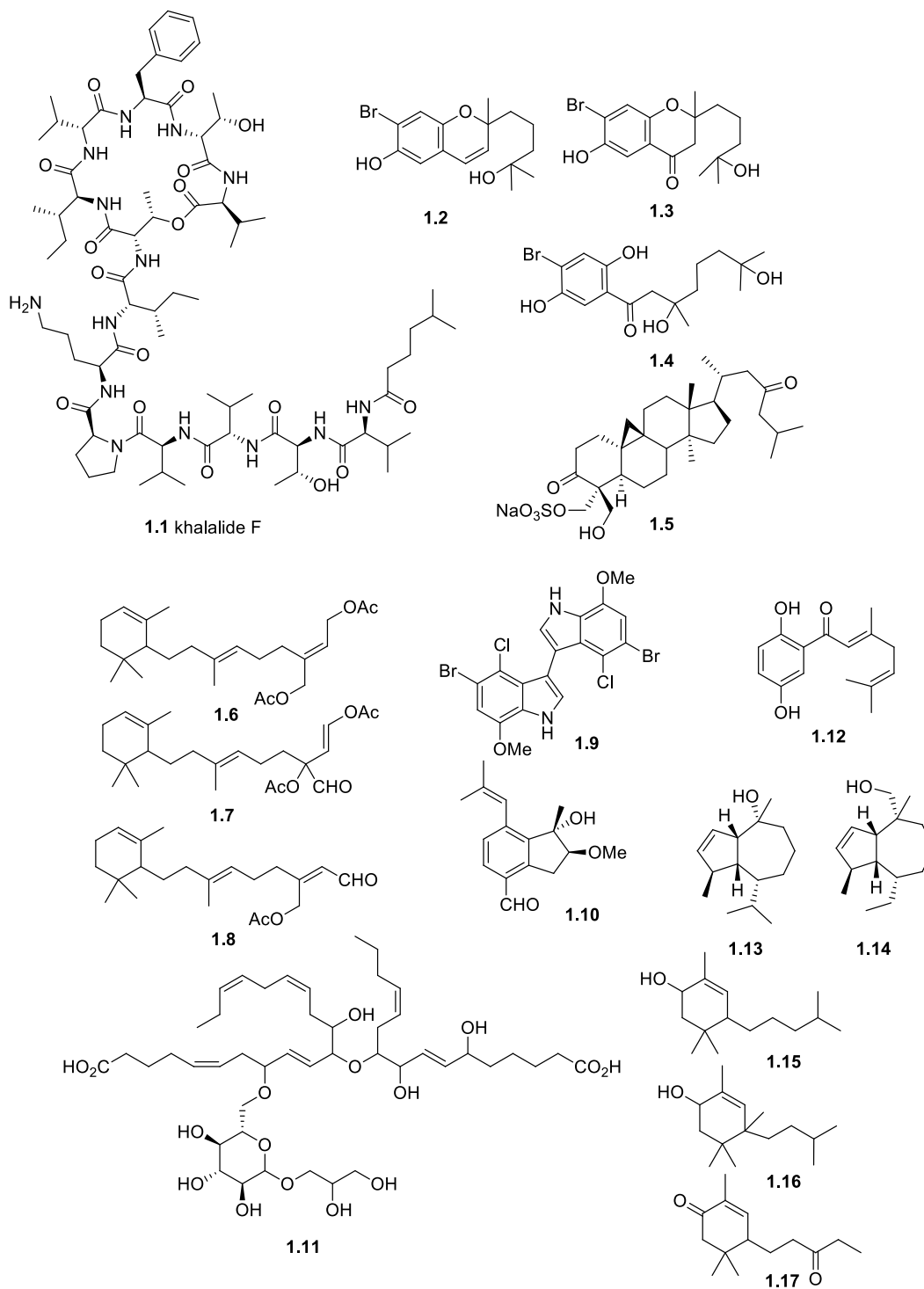
Figure 1-5. Structures of natural products isolated from various green algae, discussed in text

A highly unusual halogenated bis-indole was isolated from *Chaetomorpha basiretorsa* (compound **1.9**), a particularly unusual structure for natural products[89]. A group working with algae from Chinese origins isolated to sesquiterpene aldehyde Caulerpal A (compound **1.10**) from *Caulerpa taxifolia*[90]. A novel ether-linked glycoglycerolipid (compound **1.11**) was isolated as its methyl ester from the green algae *Avrainvillea nigrans* which was found to be a potent anti-mitotic agent—stimulating the polymerization of tubulin and inhibiting the proliferation of MCF-7 breast cancer and HCT-116 colorectal cancer[91]. From the Jamaican strain of *Cymopolia barbata* algae, the first non-halogenated cymopol (compound **1.12**) was isolated and characterized[92]. Two guaiane sesquiterpenoids were identified in extracts of *Ulva fasciata* by bio-guided fractionation in order to identify components responsible for anti-oxidant activity[93]. Additionally, several unusal non-terpenoid compounds were also detected in extracts of *Ulva fasciata*, with free radical scavenging activity superior to tocopherol[94].

1.2   Review of algal species used in this dissertation

1.2.1   *Isochrysis galbana*

Isochrysis galbana Parke, a haptophyte, is a unicellular brown marine alga which is an excellent food source for bivalves, and is commonplace in the aquaculture industry. This algae, *I. galbana* is one of the major species grown at the New Jersey Aquaculture Innovation Center to support their bivalve breeding effort, where two strains, the Tahitian and Caribbean strain, were grown in quantities sufficient for chemical investigation. Possessing two equal length flagella, *I. galbana* is able to swim smoothly in calm water[95].

The chromatophores of *I. galbana* are colored yellowish brown due to a high content of the xanthophyll fucoxanthin[96]. In cultures that grow to 3-6 months-old, cyst formation may occur, wherein a hardened shell is formed encasing the algae cell, a process described in detail by the monograph by Mary Parke (1949)[95]. Individuals shed their flagella, and develop a membrane around the external cell wall. The cellulose membrane of the cyst then begins to thicken and becomes impregnated with silica. The chromataphores pass into the cyst and finally the cytoplasm shrinks considerably in size.

Isochrysis galbana is prevalent in the literature, however mostly a topic of focus in aquaculture due to its usage as an ideal feed for shellfish and other marine species. There is a minimum of information on medicinally active compounds, but the nutritional components have been well characterized by a number of studies: *I. galbana* is rich in protein, carbohydrates and lipids, especially omega-3 fatty acids such as eicosapentaenoic acid and docosahexaenoic acid [97-101].

Few studies have been conducted which seek to investigate the medicinal properties of *I. galbana*. In a very thorough study, the effects of lyophilized extracts of *I. galbana* on aspects of the nervous system of mice were quantified[102]. The authors found that *I. galbana* exerted a time-dependent effect on spontaneous motor activity, as well as an increase in exploratory activity after 30 minutes of inoculation, and the authors posit that these effects suggest a benzodiazepine-like activity and suggest an anxiolytic agent exists within the *I. galbana* extract. An algal/bacterial growth inhibitor was isolated from the ethyl-acetate extract of *I. galbana* and shown to be 1-(hydroxyl-diethyl malonate)-

isopropyl dodecenoic acid through ^{1}H, ^{13}C and 2D NMR techniques[103]. Interestingly, this compound was shown to greatly inhibit the growth of *Isochrysis galbana*, as well *C. muelleri* and several other algae. In a publication by B. Scholz and G. Liebezeit, proximate analysis was carried out to test for the presence of alkaloids, phenols, flavonoids, tannins, and saponins[104], which were discovered, although no study could be found which characterizes the specific components.

1.2.2   *Pavlova lutheri*

Pavlova lutheri has been studied primarily for its fatty acid content, and as such only few references exist in the literature outside this topic. Similar to *Isochrysis galbana* discussed above, *P. lutheri* contains a variety of polyunsaturated fatty acids and shows promise as a dietary supplement. *P. lutheri* has been demonstrated to contain the very long chain polyunsaturated fatty acids eicosapentaenoic acid (20:5n-3) and docosahexaenoic acid (22:6n-3) in a study by *Tonon et al*[105]. Phospholipids and glycolipids have been characterized in *P. lutheri* in a publication by Dijkman and Kromkamp by GCMS[106]. The same study characterized pigments in this species by HPLC/PDA/FD, although specific compounds were not listed in the study. In another study, betaine-lipids (glycerides linked by an ether linkage to another group, structurally similar to phosphatidyl-choline) were characterized by Kato et al.[107] Betaine-lipids have been marketed as nutritional supplements, however there is evidence to suggest that elevated levels of betaine-lipids in man is related to an elevation in plasma lipids associated with coronary artery disease[108]. A low-molecular weight peptide has been isolated and characterized from the fermentation of *P. lutheri* which has been shown to effect important factors for bone

formation, remodeling and mineralization, and the researchers pose that it may be used as a supplement to aid bone-growth[109].

1.2.3   *Parachlorella kessleri*

There is relatively little known about the freshwater green algae *Parachlorella kessleri,* although it is closely related to species of *Chlorella*. *Parachlorella kessleri* was originally classified as *Chlorella kessleri*; taxonomical revision was made subsequent to pioneering chemotaxonomic and phylogenetic work of Kessler and collaborators[110-112], rectifying many discrepancies within the *Chlorella* genus[113]. *P. kessleri* belongs to the phylum Chlorophyta. P. kessleri was found to be exceptionally stable to acidic conditions; *P. kessleri* is the dominant algae found in *Laguna Verde*, an acidic, mesothermal pond that is part of a series of water bodies influenced by the Copahue Volcano, where the pH ~2.5, and temperature about 30-35˚C. The severe conditions in which this algae is found would typically be expected to come at a detriment to growth density, yet the evidence runs quite contrary, wherein *P. kessleri* obtains exceptional growth densities at these conditions at about 2 x 10^7 cells per mL. *P. kessleri* grows about 2-10 µm, is spherical and possesses no flagella.

Very few publications exist within indexed literature in which *P. kessleri* is a topic of study. A search on SciFinder [114] (provided by CAS) revealed only 78 entries for publications/patents as of June 20, 2015. The majority of publications examine the use of *P. kessleri* for fermentation of wastewater, or aquaculture applications of *P. kessleri* and are outside the scope of this dissertation. In terms of studies which focus on chemistry,

only 13 journal articles have been published to date, the bulk of literature available evaluates the usage of *P. kessleri* for the production of lipid and starch-rich biomass for energy applications, as numerous authors have reported high lipid yields from *P. kessleri*[115-120]. Only two papers have been published evaluating the nutritional or chemical composition of *P. kessleri*. Ivánová et al. (2012) evaluated the functional group composition in *P. kessleri* by a potentiometric titration technique, and detected 3.99 mmol/g organic acid, 2.13 mmol/g strongly acidic 1.28 mmol/g weakly acidic organic functionality[121]. Researchers have also evaluated the antioxidant potential of *P. kessleri* and its relationship to carotenoid and phenol content, demonstrating high anti-oxidant capacity[122].

There are 15 patents and patent applications which name *Parachlorella kessleri* as a component of an invention or process. The majority of patents have been filed by Solazyme, a commercial algae producer, which protect lipid-rich microalga compositions for use in foods[123-129] and beverages[130]. One interesting application filed in Japan protects the usage of polysaccharides derived from *P. kessleri* as an immunostimulant which promotes the production of antiviral antibodies[131,132]. In a similar vein, an American group filed protection for usage of polysaccharides derived from *P. kessleri* in personal care products and cosmetics[133,134].

1.3 Inflammation and Human Health

The importance of the role that inflammatory responses play in the survival of animal species is evidenced clearly by the ubiquity and highly conserved nature of the cells,

genes, and biochemistries involved. Deficits in inflammatory response result in compromise of the health and survival of an organism. Inflammation is a localized protective response to damage caused to tissues through mechanical injury, chemical corrosion, temperature damage, or microbial invasion (cite),. The inflammatory pathways serve to isolate, dilute, destroy and regenerate tissues which have been compromised. The inflammatory response is an aspect of nearly every disease state and is a key regulator of pain, thus the modulation of the inflammatory response is a key aspect of the therapeutic strategy for most diseases, from the common cold to serious injury [138]. Excessive inflammation can be life threatening—trauma to the brain causes inflammation, leading to swelling which can be lethal due to excessive pressure on the brain. Inflammation can also be the source of disease state as well (cite),; there is ample evidence which demonstrates how dysregulation of the inflammatory response contributes to the pathophysiological basis for diseases[138,152] such as atherosclerosis, rheumatoid arthritis and other autoimmune diseases, and Alzheimer's disease.

1.3.1 Inflammation and Disease

The homeostasis that exists within the intricate pathways which control the inflammatory and immune responses are critical to the survival of advanced lifeforms. Organisms deficient in natural inflammatory response are left prone to infections which quickly become lethal when they are not attenuated. Similarly, dysregulation or excessive inflammatory response is itself the cause of many diseases, and can likewise lead to lethality in the affected organism[152]. As Lewis Thomas, a leading physician who pioneered work in understanding the immune response to infection, eloquently stated, "Our

arsenals for fighting off bacteria are so powerful and involved so many defense mechanisms, that we are more in danger of them than the invaders. We live in the midst of explosive devices; we are mined."[135] Inflammatory response is characteristic of nearly all infections, injuries, and many types of disease[138]. The pathology of a number of diseases is characterized by excessive or dysregulated inflammatory response[152] including pneumonia, rheumatoid arthritis, gastrointestinal ulceration, and atherosclerosis.

Pneumonia is an inflammatory condition in the lung caused by one or more of many possible factors, the most common of which is bacterial or viral infection[136]. Characterized by coughing, chest pain, fever, and dyspnea, pneumonia results in inflammatory edema which affects the ability of the alveoli to allow air transfer to the blood stream[137]. Bacterial pneumonia is treated with antibiotics, and usually resolved within 2-3 weeks. Prior to the advent of antibiotics, pneumonia was a leading cause of death, and to this day carries the highest morbidity and mortality rate of any infection[138]. Pneumonia affects over 450 million people each year (7% of human population), resulting in approximately 4 million deaths annually[139]. Typically, the respiratory tract is sterile beyond the vocal cords; the mucosal membranes and cilia in the nasal passage and upper respiratory tract capture and clear the majority of pathogens and materials before reaching the lung[138]. Small numbers of bacteria which gain access to the lower respiratory tract, the innate immune response is activated and can typically effectively contain the spread of pathogens. However, with large numbers or particularly virulent pathogens, the innate immune response can be overwhelmed, and lead to the triggering of a far more substantial

inflammatory response[138]. This leads to excessive fluid and edema, resulting in the obstruction of airways that in severe cases can lead to death[138].

Rheumatoid arthritis (RA) is an autoimmune disorder characterized by chronic inflammation and pain, stiffening of joints, eventually leading to the destruction of the cartilaginous tissue. While the causes of RA are not completely understood, the disease has been extensively studied. RA appears to have roots in genetic factors, since several genes have been associated with an increased incidence of RA[140]. Additionally, support for the role in genetic factors, however demonstrating other factors are at play as well, is evidenced by the fact that the coincidence rate of RA in monozygotic twins is 15-20%[141]. RA is approximately 3 times more common in smokers than in non-smokers[140]. RA progression occurs through three phases: 1) initiation phase, due to innate inflammatory response; 2) amplification, due to T cell activation; 3) chronic inflammatory phase, where cytokines such as interleukins IL-1 and IL-6, and TNF-α perpetuate the inflammatory response[142]. TNF-α plays a major role in RA, and several anti-TNF-α therapeutics currently exist for the treatment of RA, such as infliximab, etanercept, and adalimumab, which are associated with significant improvement in therapeutic outcome[143]. TNF-α plays a major role in inflammation and cellular signaling, and is discussed in detail in section 1.3.5. The cytokines go on to activate macrophages, which go on to produce cellular signals that go on to activate fibroblasts and osteoclasts, which begin to turn cartilaginous material in the joints to ossified bone, eventually restricting and locking joints[143].

Atherosclerosis is a form of arterial sclerosis in which the arterial wall thickens as a result of chronic inflammatory response of leukocytes which have invaded the walls of arteries[144]. A chronic disease, atherosclerosis often presents no signs until a heart attack or sudden cardiac death. Though not fully understood, the mechanism of atherosclerosis is initiated by inflammatory processes in the endothelial cells of the blood vessels as they respond to particles of low-density lipoprotein (LDL) retained in the vessel walls[146]. LDL particles become oxidized which causes the endothelial cells to attract leukocytes (macrophages and T-cells) to ingest and remove oxidized LDL particles[144]. The LDL particles are usually absorbed and removed after the phages recruit high-density lipoprotein particles (HDL) to remove the lipoprotein, however if there is insufficient HDL to keep up with LDL production, the phages continue to absorb LDL until the point of rupture. The ruptured phages spill cellular materials, oxidized lipids and cholesterols which lead eventually to the deposition of plaques throughout the arterial wall[146]. Lysed cells and re-exposed oxidized LDL particles contributes to the recruitment of more phages, continuing the cycle that leads to chronic inflammation of the vessel or artery. Eventually arteries become narrowed and hardened, restricting blood flow and causing angina. If a piece of plaque should break off suddenly from the arterial wall, it may become lodged in the narrowed blood vessels, which causes heart attack or stroke[144].

1.3.2 Biology

The inflammatory response incorporates two major pathways: the innate response and the adaptive response. The innate inflammatory response is the first response to injurious stimuli, and occurs within minutes of injury. The innate response is intended to mitigate

the damage or infection until it can be stopped, or until the adaptive immune response has time to mount a highly selective attack. The adaptive immune response is what is typically characterized as the "immune system" colloquially, and consists of a variety of cells that generate antibodies. Antibodies are proteins (immunoglobulins) which adsorb strongly to pathogens, allowing for their recognition by circulating leukocytes. These two pathways constituting the immune response will be discussed in turn in the following sections.

1.3.2.1 Innate Immune Response

The innate immune response constitutes acute inflammatory response, recruitment of neutrophils to eliminate infectious agent, and resolution to homeostasis. Acute, or short-term, inflammation of tissue appears within a few minutes to a few hours of damage or infection, and can be recognized by five cardinal signs: redness (*rubor*) and heat (*calor*) is seen in inflamed tissue, caused due to increased blood flow at the site of inflammation[146]. Swelling (*tumor*) and pain (*dolor*) are caused due to the accumulation of fluid in inflamed tissues[146]. Pain is also caused due to the release of chemical signals such as histamine or bradykinin[146]. Finally, loss of function is seen in inflamed tissue, with roots in multiple causes[146]. The hallmark of chronic, or long-term, inflammation is the presence of fibrous connective tissue, resulting in scarring and impairment of tissue function.

There are a number of structural and biochemical changes that occur to allow the innate inflammatory response to proceed on a cellular level, described in detail by Serhan, Ward, & Gilroy (2010) in their text *The Fundamentals of Inflammation*[145], is briefly described

below. The first change occurs within endothelial cells, which coat the inner lining of blood and lymphatic vessels. Endothelial cells become activated, and begin to express adhesion factors (e.g. ICAM-1, VCAM-1) on their surfaces, which allow neutrophils to attach themselves at the site of injury. Activated endothelial cells begin a biochemical cascade (described in detail in the following section) leading to the generation of pro-inflammatory cytokines and chemokines, which stimulate the acute immune response in other cells, and begin the attraction of neutrophils. The expression of Tissue Factor by endothelial cells promotes a cascade leading to coagulation and thrombus formation on the surface of the vascular tissue. Following activation, endothelial cells undergo systemic changes to allow the flow of acute inflammatory exudate, a mixture of proteins, fluid, and cells, to flood the area to initiate localized defenses, causing swelling of the tissue (edema). The exudate is rich in leukocytes (white blood cells), mostly neutrophils, which follow biochemical signals emitted by infected or damaged cells and attach themselves at the point of injury using adhesive molecules.

The major function of innate inflammatory response is to destroy or eliminate the causative agent, mitigating the immediate damage while the adaptive immune system mounts a selective attack against the invading organism, if needed. The leukocytes quickly isolate and destroy the infected or damaged cells and/or microorganisms through phagocytosis[145]. During phagocytosis, the microorganism, infected cell, or causative agent is engulfed by the leukocyte after recognition from pathogen-associated molecular patterns (PAMPs) from Toll-like receptors (TLRs)[145]. The adaptive immune system, in order to mount a highly selective attack, generates pathogen specific antibodies, which

then selectively coat pathogens in a process called opsonization, which greatly facilitates

recognition by leukocytes and phagocytosis. After absorption, the leukocyte uses an

NADPH dependent oxidase system which generates a *respiratory burst* wherein large

quantities of reactive oxygen species (ROS) such as nitric oxide, O_2^-, and H_2O_2 are

generated in the cell, causing severe oxidative damage to the engulfed body[146]. The

absorbed body is lysed and liquefied, allowing the debris to be removed and recirculated.

This allows for the regeneration process to begin following the resolution of inflammatory

cycle. The inflammatory response is resolved following the removal of the irritant,

wherein leukocytes are cleared through apoptosis, vascular tissue resumes normal

functioning, and homeostasis is attained[147]. In some tissues, following the resolution of

inflammatory response, cellular regeneration begins. The acute inflammatory response

allows the body to rid itself of irritants, infectious agents, and caustic materials, as well as

initiate a first response to cellular damage. The cascade leading to platelet activation and

subsequent blood clotting is also activated in order to stop hemorrhage and restrict blood

loss[146].

While the acute inflammatory response seeks to restore the body to its pre-injury state,

complications due to the consequences of response can lead to further injury, and in

many cases even cause fatality. Extensive edema within enclosed compartments, such as

the skull or joints, which resist the flow of fluids, can lead to drastically increased

hydrostatic pressure within the compartment[148]. The increased pressure can seriously

impair organ function, as in the spraining of articular joints, which can eventually lead to

death, as is the case with bacterial meningitis[145]. In the lung, excessive edema in the

alveolar air compartments precedes alveolar flooding in which air exchange is significantly impaired, such as in bacterial pneumonia[145]. As such, while the inflammatory response serves as a first response to protect an organism from infection, injury and damage, regulation and resolution of the inflammatory response is just as crucial to the survival of the organism.

While the acute inflammatory response occurs within hours of infection or injury, and resolves typically within several days, chronic inflammation is marked by persistent inflammatory symptoms that may last for months or even years (cite),. Chronic inflammation is not simply persistent acute inflammation, but characterized by morphologically distinct features such as the presence of lymphocytes and macrophages and an absence of neutrophils, whereas the acute response is characterized by the presence of neutrophils, and few lymphocytes/macrophages[148]. Chronic inflammation is due to consistent innate and adaptive inflammatory response caused from persisting inflammatory trigger (chronic infection, splinter, auto-immune diseases, etc.), a persistence in the presence of activated inflammatory cells, or a dysregulation in inflammatory resolution [149] . Macrophages release a number of pro-inflammatory mediators which go on to activate fibroblasts, which secrete collagen and activate further macrophage response[146]. This cross-linked collagen is rigid and leads to a lack of function, i.e. scarification. Scarified tissue is a major component of chronic inflammatory diseases. In patients with rheumatoid arthritis, collagen-filled joint tissue is ossified, leading eventually to a loss of joint function[150]. Fibrous collagen formation in the liver, caused

from chronic exposure to hepatotoxins such as acetaminophen, can to an irreversible loss of liver function in affected areas[151].

Chronic inflammation and inflammatory diseases demonstrate that the inflammatory response is a dual-edged sword. While inflammatory and immune response is a vital mechanism required for the survival of all animals, careful regulation and control of this response is equally important. As is discussed in detail in the following section, dysregulation of inflammatory response has been linked to a huge number of diseases.

1.3.2.2 Adaptive Immune Response

The adaptive immune response, also known as the humoral immune response, is the second phase of the inflammatory response which allows the body to mount a specific and selective attack against invading pathogens. That nature allowed for the evolution of such complex and elegant mechanisms for dealing with microscopic invaders is certainly inspiring. As infection begins, macrophages present at the point of infection ingest invading microorganisms (called phagocytosis), lyse them, and present particles of the infectious agent (called antigens) on the cell surface[146]. The macrophages release interleukin-1 (IL-1) to attract T-helper cells[152]. Special cells called antigen presenting cells (APCs) absorb pathogens through phagocytosis, lyses the pathogen, and presents the fragments, known as antigens, on the surface of the cell[146]. Endothelial cells as well as macrophages utilize the same process to display antigens to leukocytes. Cells under attack from viruses and microorganisms present antigens on their surfaces in order to signal the infection to T and B cells[152].

T-helper cells bind to the antigens to stimulate the release a number of cytokines, the most important of which are interleukin-2 (IL-2) and interferon gamma (IFN-γ)[145]. These cytokines attract, activate, and stimulate proliferation of T and B cells. Cytokines involved with inflammation are discussed in detail in section 1.3.5. The phages follow the cytokine gradient to the point of infection. There are millions of types of cytotoxic T cells (activated by IL-2) and each one able to recognize a different antigen[152]. When the cytotoxic T cell encounters the antigen it matches on an infected cell, it binds to the infected cell, release perforin, a protein complex which causes membrane perforation and subsequent cell lysis[146]. After the infection is brought under control, regulatory T cells deactivate cytotoxic T cells, and stimulate the release of memory T cells, which remain in circulation should the virus/microorganism attack again. B cells operate in a parallel pathway to affect an immune defense against infected cells and invading microorganisms.

Millions of types of B cells are also produced, each of which match a specific antigen. When B cells become activated by T helper cells, they differentiate into plasma cells and B memory cells[145]. Plasma cells begin to generate and secrete antibodies which match the antigens displayed by the invading organism or infected cells. Antibodies are immunoglobulin based proteins which bind to antigens on the pathogen, allowing for a "tagging" of foreign materials for destruction by phages[142]. Antibodies flood the bloodstream, actively binding and tagging infected cells and pathogens for destruction, called "opsonization." Opsonized microorganisms are actively targeted for lysis by phages, allowing for facile and selective recognition of the invasive species or infected cells[142]. Opsonized microorganisms are actively lysed by Blood Complement, which

immediately destroys the invading species pathogen[146]. Some B cells survive and differentiate into memory B cells, allowing for a swifter and stronger reaction to subsequent diseases by the immediate production of antibodies which recognize antigens on the pathogen[148]. This biochemical memory allows the organism to quickly recognize and respond to future infections from the same or very similar pathogens, and is the basis for vaccination and adaptive immunity from disease.

1.3.3 Lipid signaling

In normal cellular functioning, the inflammation pathway maintains homeostasis through a balance of molecular, protein, and genetic controls. Lipid signaling is a crucial part of the regulatory process and signal cascade which controls inflammatory response (Figure 1-6). When cellular lysis occurs, membrane phospholipids are exposed in the extracellular environment[153]. At this stage, 2-arachidonyl-phostphatidylethanolamines will undergo cleavage catalyzed by cytosolic Phospholipase A2 (PLA2), which hydrolyzes the *sn*-2 position ester, releasing free arachidonic acid as well as lysophospholipid[153]. Free arachidonic acid is subsequently cyclized; this reaction is catalyzed by the inducible form of cyclooxygenase, cyclooxygenase-2 (COX-2), to form Prostaglandin H_2 (PGH_2)[154]. PGH_2 is the precursor for all prostanoids, which are synthesized through a number of different prostaglandin synthases. PGD_2, PGE_2 and PGF_2 are the major prostaglandins involved with inflammatory response, as well as thromboxane (TXA_2, not shown). These prostaglandins bind to G-protein coupled receptors specific to each prostaglandin, and through conformational change, and subsequent phosphorylation, stimulate the Gα protein subunit to dissociate[155]. The freed Gα protein can now bind to Adenylate Cyclase (as well

as a variety of other proteins) to continue the signal transduction cascade. Binding to adenylate cyclase activates conversion of adenosine triphosphate (ATP) to cyclic adenine monophosphate (cAMP), a cellular signaling molecule used by a number of pathways to promote stimulatory responses[156].
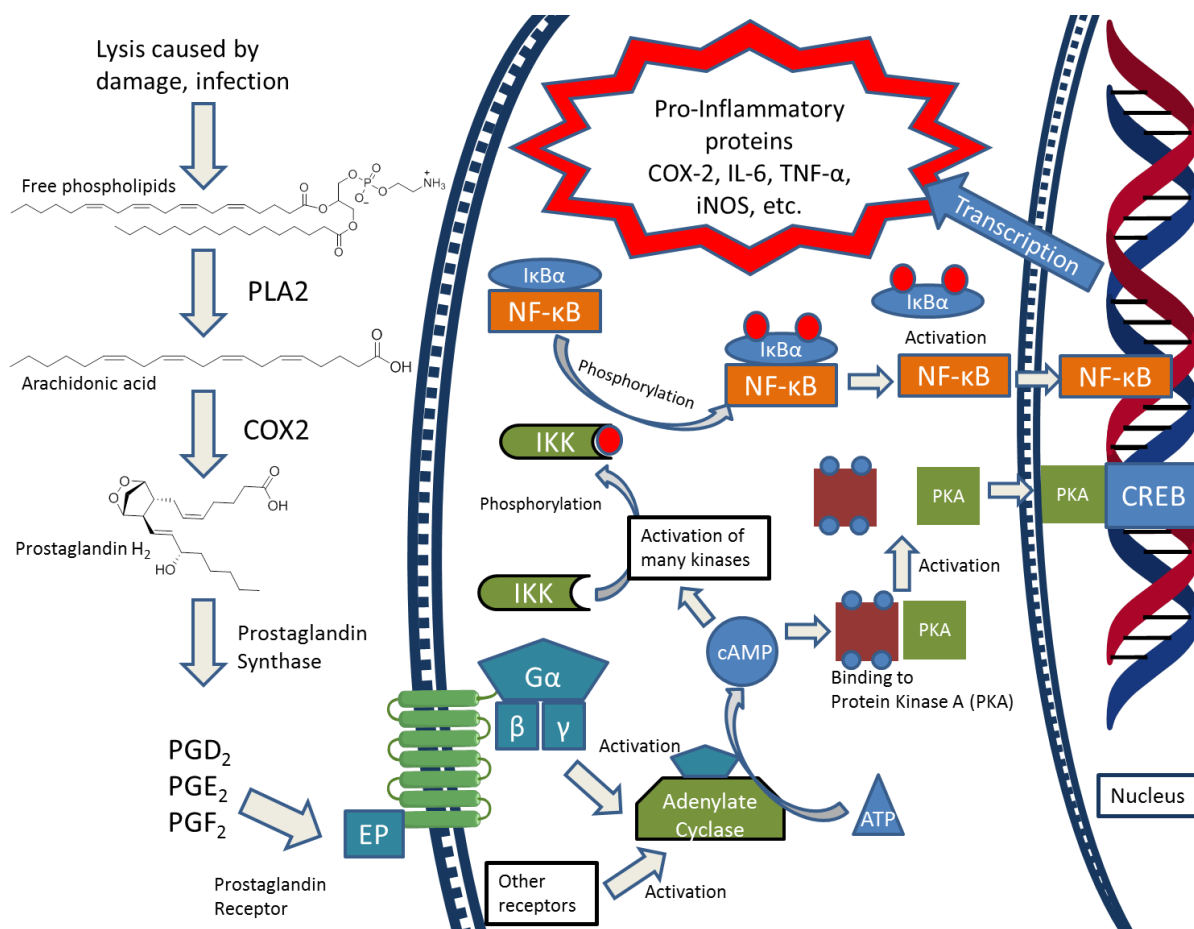
Figure 1-6. Cellular Inflammatory Signaling pathway, compiled from references cited within the text of this chapter

cAMP formation in the cells goes on to activate a number of signaling kinases. Four molecules of cAMP bind to Protein Kinase A (PKA), which is an important kinase involved in cellular signaling[52]. After binding 4 molecules cAMP, PKA dissociates from its catalytic domains, activating them. The catalytically activated PKA translocates to the cell nucleus,

where it activates cAMP response element-binding protein (CREB). CREB then binds to cre-binding protein (CBP); the complex is a cellular transcription factor and when bound to other transcription elements induces transcription of a number of genes, including many important pro-inflammatory cytokines, such as IL-6, IL-8, and TNF-α[157], as well as pro-inflammatory iNOS as well as further expression of COX-2[158]. The pro-inflammatory proteins induce a feedback effect, stimulating more cells to produce a further inflammatory response, and to recruit a response from immune cells. See section 1.3.5 for a detailed discussion of cytokine pathways. A schematic of this process is shown in

Figure 1-6.

1.3.4 NF-κB: Rapid Acting Transcription Factor

Nuclear factor kappa light-chain-enhancer of activated B cells (NF-κB) is a ubiquitous protein complex in animal cells which activates an orchestra of gene transcription, leading to cellular response from a wide array of eliciting phenomena. NF-κB is considered a rapidly-acting transcription factor because it does not require protein synthesis to initiate the cellular response. This is because NF-κB is in constant circulation in an inactivated form, and can be activated by a wide variety of stimuli[159]. Activation of NF-κB can occur through a variety of membrane bound receptors, allowing many stimuli to directly activate gene transcription through NF-κB[160]. NF-κB plays a key role in the regulation and signaling of inflammation response; dysregulation of NF-κB has been tied to inflammatory and autoimmune diseases. Due to its role as a signaler of inflammation and cellular stress, NF-κB has been extensively studied.

1.3.4.1 Activation of NF-κB.

When in homeostasis, NF-κB in the cytosol is bound to IκBα, which inhibits the ability of NF-κB to enter the nucleus. One of many possible stimuli interacts with receptors on the cell surface, causing a signaling cascade leading to the activation of IκB kinase (IKK). After activation, IKK phosphorylates IκBα. Phosphorylation of IκBα causes dissociation of IκBα, releasing NF-κB, which is now free to enter the nucleus. NF-κB then binds to CBP to induce transcription of a great number of proteins[159], and plays a key role in regulating immune response[160].

There is a wide range of stimuli that can illicit NF-κB activation and subsequent response. Physiological stresses such as hypoxia [161] and acidic cellular pH [162] have been demonstrated to activate NF-κB in vivo. Physical stresses have been tied to activation of NF-κB by a number of different researchers. NF-κB activation has been found associated with traumatic brain injury in rats[163]. Double-strand DNA breaks[164], as well as gamma radiation[165], have been shown to induce NF-κB. Obesity[166] and high-fat diet[167] have been correlated with increased NF-κB activation. NF-κB is also activated by fungi and viral pathogens, such as Ebola[168], HIV-1[169], Herpes simplex[170], Influenza[171] and many others.

A huge number of bacteria are endogenously recognized and activate NF-κB. Bacterial infection promotes the activation of NF-κB through recognition of specific bacterial products, such as lipopolysaccharide, and thus prompts an immune response for infection[172]. Lipopolysaccharide is bound by lipopolysaccharide-binding protein (LBP); this complex in turn binds to CD14 or TLR4 receptors located on the cell surface. Receptor

interactions stimulate TRAF6, which goes on to activate MEKK1, which in turn activates

IKK, which phosphorylates IκBα, causing dissociation from NF-κB, and finally activating

NF-κB[173].

There exists a vast collection of signaling proteins, called cytokines, which induce

activation of NF-κB, in a process critical to intracellular signaling and cell-cycle regulation.

A number of interleukins, so named because they were first found in leukocytes, induce

activation of NF-κB[174]. Interleukins are a group of cytokines critical to the functioning and

regulation of the immune system and inflammatory response; a number of interleukins

are associated with the recruitment of inflammatory and immune response. [175].

Interleukin 1 (IL-1) is produced by macrophages, B lymphocytes and natural killer cells,

and signals an increase in the expression of factors that allow phagocytes and

lymphocytes to transmigrate to sites of infection. IL-1 also affects the activity of the

hypothalamus, resulting in increased body temperature, leading to fever response[176]. IL-

1 binds to IL-1R receptors located on the cell-surface, beginning the kinase signal cascade,

releasing IRAK, and then by way of TRAF2, activating MEKK1[174]. MEKK1 goes on to activate

IKK, which in turn activates NF-κB.

Tumor necrosis factor-α (TNF-α) is another important cellular signaling molecule involved

in inflammation and apoptosis. First, TNF-α binds to the TNF-α receptor (TNFR) on the cell

surface, which causes an adapter protein inside the cell to become activated. TNF-α

Receptor-associated factors (TRAFs) go on to transduce the signal via NF-κB inducing

kinase (NIK), which leads to the activation of IKK, which finally activates NF-κB by causing the dissociation of IκBα[177]. TNF-α is discussed in detail in the following section.

Radical oxygen species (ROS) have also been demonstrated to play a key role in the activation of NF-κB during periods of stress. As macrophages and neutrophils actively produce micromolar levels of free radicals in order to target and attack bacterial cells[178], when cells come into contact with ROS, they prepare themselves for possible attack by activating inflammatory response. It has been shown that hydrogen peroxide stimulated activation of IKK via SHIP-1, a tyrosine kinase, or via activation of PKD through Src and Abl, although the exact mechanism of activation has yet to be elucidated[179].

1.3.4.2 Genes activated by NF-κB

After induced activation of NF-κB by one of the stimuli described above, NF-κB passes into the nucleus where it binds with CBP to promote gene transcription. There are hundreds of proteins whose genes are regulated by NF-κB. An extremely extensive (although not necessarily exhaustive) list of genes activated by NF-κB is maintained by the Gilmore Research group at Boston University[180]. In the context of inflammation, there are a number of important genes activated by NF-κB. Many of the interleukins are promoted by NF-κB, as part of an important feedback loop that induces NF-κB in other cells. Interleukins-1a and 1b (IL-1) are activated for transcription by NF-κB, both are pro-inflammatory cytokines, and activate an inflammatory response in other cells[181,182]. Transcription of IL-2 is also induced by NF-κB[183], leading to T-Cell and NK-cell activation[184]. IL-6 is also up-regulated by activation of NF-κB, which in turn stimulates production and

differentiation of B cells, T cells, as well as promoting a host of gene transcription activity in other cells through feedback stimulation of NF-κB[185].

Interferon-gamma (IFN-γ) is also up-regulated by induction of NF-κB[186]. IFN-γ has a wide range of stimulatory functions within immune and inflammatory response. IFN-γ is involved with cellular responses to viral infections. Briefly, IFN-γ activates macrophages and stimulates the release of ROS through iNOS, as well as matrix zinc-finger proteases. IFN-γ goes on to stimulate a further inflammatory response through IFN-γ receptors which stimulate feedback response through CREB, STAT3, and also NF-κB.

Tumor necrosis factor α (TNF-α) is another critically important cellular signaling protein involved in inflammation response. TNF-α is produced principally by macrophages, although it is also produced by neutrophils, eosinophils, and natural killer cells, and is a primary signaling molecule in acute inflammatory response[187]. Expression of TNF-α is induced by NF-κB activation[188], which evokes feedback reinforcement since TNF-α also stimulates activation of NF-κB[189]. Additionally, the expression of TNF-α receptor p75/80 (CD120B) is stimulated by NF-κB, leading to an increased sensitivity to TNF-α level[190]. NF-κB also stimulates the transcription of TNF-α receptor associated factors (TRAF), required by TNF-α receptors to transduce the cellular signal to activate NF-κB in turn[191].

Inducible nitric oxide synthase (iNOS) is an important enzyme involved in the regulation of inflammatory responses. Nitric oxide (NO) is an important cellular signaling molecule which is generated *in situ* by oxidation of L-arginine by iNOS involved in immune response to cellular damage[192]. iNOS is expressed by macrophages and T-cells where the high

content of NO produced by iNOS goes on to generate ROS, causing cytotoxicity to infected cells and bacteria. Expression of iNOS has been shown to be upregulated by NF-κB[193].

Additionally, NF-κB stimulates a number of other pro-inflammatory enzymes. Lipopolysaccharide binding protein is expressed upon stimulation of NF-κB[194], leading to an increase in inflammatory response due to bacterial infection. COX-2 is also upregulated by NF-κB[195], leading to an increase in prostaglandin synthesis as shown in the above section. 5- and 12-lipoxygenase are also regulated by NF-κB; the lipoxygenases metabolize eicosanoids into leukotrienes and other inflammatory mediators[196,197].

1.3.5 Cytokines

Cytokines are an important class proteins involved in cellular signal transduction. Cytokines are utilized by cells during the inflammatory process in order to initiate, propagate, and eventually resolve the inflammatory response[175]. Different cytokines are responsible for activating different cells, and activate different functions. Cytokines produced by cells act to produce a response in one of three fashions: from cell to cell, known as paracrine, transported from glands through vesicles to cells throughout the body, known as endocrine, and cytokines produced within a cell can affect the activity of itself, known as autocrine[201]. Cytokines act by all three mechanisms to illicit complex and intricate control over cellular responses to inflammation. Immune cells follow cytokine gradients to the point of injury or infection, while endocrine cytokines act to stimulate fever, modulate metabolism, and alter gene expression patterns[201].

There are three major categories of cytokines discussed within this introduction chapter: interleukins (ILs), tumor necrosis factor (TNF-α), and interferon gamma (IFN-γ). A summary of the cytokines discussed within this dissertation is shown below in Table 1-1, itemized by source, target cells, and function. The following sub-sections discuss the biology and biochemistry of these cytokines in detail.

Table 1-1. Cytokines involved in inflammation: sources, targets, and functions*

Cytokine	Source	Target Cells	Function
IL-1	• Macrophages • B cells • Monocytes • epithelial cells • endothelial cells	• T cells; B cells	• Activation and stimulation
		• Endothelial cells	• Acute phase response
		• Hypothalmus	• Fever
		• Liver	• Acute phase reactants
IL-2	• T cells • NK cells	• T cells; B cells	• Growth
		• Monocytes	• Activation
IL-4	• T cells	• T cell; B cells	• Growth and activation
IL-6	• T cells • Macrophages • Fibroblasts	• T cells; B cells	• Stimulation
		• Mature B cells	• Growth
		• Liver	• Acute phase reactants
IL-8	• Macrophages • Epithelial cells • Platelets	• Neutrophils	• Activation and chemotaxis
IL-10	• T cells	• Macrophages	• Inhibits Antigen presenting cells
		• T cells	• Inhibits cytokine production
IFN-γ	• T cells • NK cells	• Monocytes	• Activation
		• Endothelial cells	• Activation
		• Antigen presenting cells	• Increase MHC I and II (proteins that present antigens)
TNF-α	• Macrophages • T cells • Epithelial cells	• T cells; B cells	• Activation and stimulation
		• Endothelial cells	• Acute phase response
		• Hypothalmus	• Fever
		• Liver	• Acute phase reactants

*Data compiled from Dinarello (1996)[198], Liles & Van Voorhis (1995)[201], and Brocker et al. (2010)[175].

1.3.5.1 TNF-α

Tumor necrosis factor alpha (TNF-α) was first discovered in 1975, when Dr. Old, working at Memorial Sloan-Kettering Cancer Center in New York, reported a cytotoxic factor produced by macrophages which was able to induce cell-death in murine fibrosarcoma cells[199]. The primary role of TNF-α is in the regulation of immune cells and is one of the

cytokines involved in the acute inflammatory response: TNF-α can induce fever, apoptosis, and elicits the primary symptoms of inflammation (pain, redness, swelling)[200]. This protein is critical to cellular signaling in order to bring about the inflammatory response upon stimulation by lipopolysaccharide (LPS), as well as other bacterial products, and interleukin 1 (IL-1). TNF-α activates T cells, B cells, and elicits the acute response through a biochemical cascade ending with the activation of NF-κB[200].

There are two cellular receptors which can bind TNF-α, TNFR1 which is expressed in most tissue types, and TNFR2, which is expressed only in immune cells[200]. First, TNF-α binds to TNFR which causes a conformational change to occur in the receptor protein; this leads to the dissociation of SODD, an inhibitory protein, freeing TRADD to bind[200]. TRADD recruits TRAF2 and RIP. TRAF2 recruits IKK which is then activated by RIP. Activated IKK goes on to phosphorylate IκBα, which then dissociates from NF-κB. NF-κB goes on to activate the transcription of a wide array of pro-inflammatory factors and perpetuates the inflammatory response, as described later in section 1.3.4.

1.3.5.2 Interleukins

Interleukins (ILs) are a group of over 15 distinct families of low weight cytosolic cytokines which serve as intercellular messengers and are responsible for the regulation of inflammatory and immune response, cell growth and differentiation. ILs are secreted by cells and elicit their activity through a paracrine pathway, wherein ILs directly modulate the activity of other cells by binding with receptors found on the cell surface (cite). Originally discovered in leukocytes (cite), ILs trigger a biochemical cascade once bound

which leads to a diverse array of responses from other leukocytes (as well as other cell types), hence the name "interleukin."

There is a wide array of interleukins, each interacting with different receptor sub-types, and eliciting a variety of physiological and biochemical responses. There exist many overlapping signal redundancies, wherein a single IL can activate multiple differing receptors, and many ILs can activate the coincidental receptors, providing access to a great degree of control over IL promoted responses by biochemical mechanisms[201]. The interleukins exist to carry the complex signals that mediate the adaptive immune response. Some interleukins are pro-inflammatory, such as Interleukin-1 (IL-1), which is primarily responsible for T-cell and B-cell activation, as well as stimulating fever and hyperalgesia[202]. Interleukin-1 attracts helper T cells, which bind to antigen presenting cells (APCs) and subsequently release interleukin-2 (IL-2). IL-2 goes on to stimulate T and B cell proliferation, proliferating the immune response cascade (the adaptive immune response is discussed in section 1.3.1). On the contrary, some interleukins show anti-inflammatory effects, such as IL-10, which suppresses immune response and inflammation, inhibits the formation of antigen presenting cells, and arrests proliferation of leukocytes. A table of interleukins and their various targets and activities is shown in Table 1-1.

1.3.5.3 Interferon gamma

Interferon gamma (IFN-γ) is a cytokine which is critical to the cell signaling process involved with innate and adaptive immune response to viral, as well as some bacterial,

infections[203]. Interferons are a class of chemicals composed of two major classes, type I and type II interferons; IFN-γ is a type II interferon and is the only member of this class[207]. Originally discovered in 1957, interferons were first described because of their ability to cause infected and non-infected cells to recruit proteins that inhibit viral replication[204], however it was later shown that IFN-γ plays a key role in regulating immune response. IFN-γ displays weak anti-viral and anti-proliferative activity, but more importantly, IFN-γ is involved in nearly all phases of inflammatory and immune responses, including the activation, proliferation, and differentiation of leukocytes such as B cells, T cells, macrophages, as well as signaling to endothelial cells (see Table 1-1). IFN-γ also enhances the cytotoxicity of T cells, macrophages, and NK cells. Additionally, IFN-γ stimulates immune response by enhancing major histocompatibility complex (MHC) proteins, which are used to present antigens from pathogens on the surface of cells to trigger and signal immune response.

IFN-γ interacts with cells by binding IFN-γ receptors (IFNGR) found on the cell surface in an autocrine, paracrine, and endocrine fashion[205]. Binding to IFNGR stimulates the activation of JAK1, which induces phosphorylation of STAT1[206]. STAT1 subsequently dimerizes, crosses into the nucleus, and stimulates transcription of IFN-γ activated sequences (GAS) elements which induce transcription of a number of genes involved in inflammation and immune response. The collection of genes activated by IFN-γ is known as the *interferome*, the targets of which are compiled in the Interferome Database maintained by Monash University[207]. IFN-γ can also bind IFN-α receptors (IFNAR) which also induces activation of JAK1. JAK1 induces activation of MAPKK kinase, leading to

activation of MAPKK3 and MAPKK6, causing activation of MSK1 and MSK2, which diffuse into the nucleus and activate CREB transcription[207] (CREB is discussed in detail in section 1.3.3).

1.4   Dissertation hypotheses and objectives

Since chronic inflammatory diseases pervade modern society manifesting in large part due to dietary metabolic syndrome, we hypothesized that the development of a highly nutritious, biologically active extract would serve a great need within public health and medicine. As discussed in previous sections, chronic inflammatory symptoms require treatment for years, often indefinitely, and so there is great interest in identifying methods of modulating inflammatory response. Due to the mountain of evidence which supports the conjecture that microalgae is a rich source of chemically and biologically interesting compounds, it was hypothesized that a thorough investigation of the natural products contained in algal biomass by way of bio-activity guided fractionation would yield extracts and compounds that would modulate biological activity, particularly inflammation.

As such, this study was designed to accomplish the evaluation a number of microalgae from marine and freshwater sources for interesting bioactivity. This study focuses on biological activities relevant to inflammation and metabolic syndrome, such as pancreatic lipase inhibition activity, cyclooxygenase-2 inhibition and endo-cannabinoid reuptake inhibitor activity. A detailed natural products investigation was conducted on *Parachlorella kessleri*, a freshwater green microalga related closely to the widely known

and commercially available *Chlorella vulgaris,* in order to isolate and characterize molecular compounds found in the biomass. A number of assays were utilized to screen the extracts and fractions for bio-active constituents to select separation strategy. Active constituents were evaluated for potency, and chemically characterized.

1.5 References

[1] Newman, D. J., Cragg, G. M., & Snader, K. M. (2003). Natural products as sources of new drugs over the period 1981– 2002. *Journal of natural products*, *66*(7), 1022-1037.

[2] Mayer, A. M., Glaser, K. B., Cuevas, C., Jacobs, R. S., Kem, W., Little, R. D., McIntosh, J.M., Newman, D.J., Potts, C.B., & Shuster, D. E. (2010). The odyssey of marine pharmaceuticals: a current pipeline perspective. *Trends in pharmacological sciences*, *31*(6), 255-265.

[3] Graham, L. E., & Wilcox, L. W. (2000). Algae. Upper Saddle River, NJ: Prentice Hall

[4]Kasting, J. F., & Siefert, J. L. (2002). Life and the evolution of Earth's atmosphere. *Science*, *296*(5570), 1066-1068.

[5] Cardozo, Karina H.-M.; Thais, Guaratini; Marcelo P., Barros; Vanessa R., Falcão; Angela P., Tonon; Norberto P., Lopes; Sara, Campos; Moacir A., Torres; Anderson O., Souza; Pio, Colepicolo; Ernani, Pinto (2006). "Metabolites from algae with economical impact". In *Comparative Biochemistry and Physiology Part C: Toxicology & Pharmacology* (Elsevier) **146** (1-2): 60–78.

[6] deGomezdumm N. T., Giammona A. M., Touceda, L. A., and Raimondi C. 2001. Lipid Abnormalities in Chronic Renal Failure Patients Undergoing Homeodialysis. *Medicina*. 61:142-146.

[7] Ruthig, D. J., & Meckling-Gill, K. A. (1999). Both (n-3) and (n-6) fatty acids stimulate wound healing in the rat intestinal epithelial cell line, IEC-6. *The Journal of nutrition*, 129(10), 1791-1798.

[8] Horrobin, F.D. 1993. Fatty Acid Metabolism in Health and Disease: the role of Δ-6 desaturase. *American Journal of Clinical Nutrition*, 57 (S), 732S-736S.

[9] Chin, S. F., Liu, W., Storkson, J. M., Ha, Y. L., & Pariza, M. W. (1992). Dietary sources of conjugated dienoic isomers of linoleic acid, a newly recognized class of anticarcinogens. *Journal of food composition and analysis*, *5*(3), 185-197.

[10] Narayan, B., Miyashita, K., & Hosakawa, M. (2006). Physiological effects of eicosapentaenoic acid (EPA) and docosahexaenoic acid (DHA)—A review. *Food Reviews International*, *22*(3), 291-307.

[11] Salem Jr, N., Litman, B., Kim, H. Y., & Gawrisch, K. (2001). Mechanisms of action of docosahexaenoic acid in the nervous system. *Lipids*, *36*(9), 945-959.

[12] Guesnet, P., & Alessandri, J. M. (2011). Docosahexaenoic acid (DHA) and the developing central nervous system (CNS)–Implications for dietary recommendations. *Biochimie*, *93*(1), 7-12.

[13] Miller PE, Van Elswyk M, Alexander DD (July 2014). "Long-chain omega-3 fatty acids eicosapentaenoic acid and docosahexaenoic acid and blood pressure: a meta-analysis of randomized controlled trials". *American Journal of Hypertension,* 27 (7): 885–96.

[14] Weintraub HS (November 2014). "Overview of prescription omega-3 fatty acid products for hypertriglyceridemia". *Postgraduate medicine,* 126 (7): 7–18.

[15] Harris WS, Bulchandani D. Why do omega-3 fatty acids lower serum triglycerides? *Current Opinions Lipidology,* 2006;17(4):387-393.

[16] Omtryg [package insert]. Arlington, VA: Trygg Pharma, Inc.; 2014.

[17] Vascepa [package insert]. Bedminster, NJ: Amarin Pharma Inc.; 2013.

[18] Wang, C., Harris, W. S., Chung, M., Lichtenstein, A. H., Balk, E. M., Kupelnick, B., Jordan, H.S. & Lau, J. (2006). n− 3 Fatty acids from fish or fish-oil supplements, but not α-linolenic acid, benefit cardiovascular disease outcomes in primary-and secondary-prevention studies: a systematic review. *The American journal of clinical nutrition,* 84(1), 5-17.

[19] Wu L, Parhofer KG (December 2014). "Diabetic dyslipidemia". *Metabolism: clinical and experimental*, 63 (12): 1469–79.

[20] Ehrlich, S. D. (2011, May 11). Omega-3 fatty acids. Retrieved March 25, 2015, from http://umm.edu/health/medical/altmed/supplement/omega3-fatty-acids

[21] Iso H, Rexrode KM, Stampfer MJ, Manson JE, Colditz GA, Speizer FE et al. Intake of fish and omega-3 fatty acids and risk of stroke in women. JAMA. 2001;285(3):304-312.

22 Delgado-Lista, J., Perez-Martinez, P., Lopez-Miranda, J., & Perez-Jimenez, F. (2012). Long chain omega-3 fatty acids and cardiovascular disease: a systematic review. British Journal of Nutrition, 107(S2), S201-S213.

[23] Salmon, J. A., & Higgs, G. A. (1987). Prostaglandins and leukotrienes as inflammatory mediators. *British medical bulletin*, *43*(2), 285-296.

[24] Wall, R., Ross, R. P., Fitzgerald, G. F., & Stanton, C. (2010). Fatty acids from fish: the anti-inflammatory potential of long-chain omega-3 fatty acids. *Nutrition reviews*, *68*(5), 280-289.

[25] Simopoulos, A. P. (2002). The importance of the ratio of omega-6/omega-3 essential fatty acids. *Biomedicine & pharmacotherapy*, *56*(8), 365-379.

[26] Medina, A. R., Grima, E. M., Giménez, A. G., & González, M. I. (1998). Downstream processing of algal polyunsaturated fatty acids. *Biotechnology Advances*, 16(3), 517-580.

[27] Converti, A., Casazza, A. A., Ortiz, E. Y., Perego, P., & Del Borghi, M. (2009). Effect of temperature and nitrogen concentration on the growth and lipid content of Nannochloropsis oculata and Chlorella vulgaris for biodiesel production. *Chemical Engineering and Processing: Process Intensification*, 48(6), 1146-1151.

[28] Handelman, G. J., Dratz, E. A., Reay, C. C., & Van Kuijk, J. G. (1988). Carotenoids in the human macula and whole retina. *Investigative ophthalmology & visual science*, 29(6), 850-855.

[29] Li, B., & Bernstein, P. S. (2012). Macular Pigment Carotenoids and Their Roles in Human Eye Health and Diseases. In Studies on Retinal and Choroidal Disorders (pp. 613-627). Humana Press.

[30] DeMan, John (1999). *Principles of Food chemistry* (3rd ed.). Maryland: Aspen Publication Inc. p. 358.

[31] Wolf G (2001). "The discovery of the visual function of vitamin A". The Journal of Nutrition 131 (6): 1647–1650.

[32] McGuire, Michelle; Beerman, Kathy A. (2007). *Nutritional sciences: from fundamentals to food*. Belmont, CA: Thomson/Wadsworth.

[33] Fuchs E, Green H (1981). "Regulation of terminal differentiation of cultured human keratinocytes by vitamin A". *Cell* **25** (3): 617–25.

[34] Snodderly, D. M. (1995). Evidence for protection against age-related macular degeneration by carotenoids and antioxidant vitamins. *The American journal of clinical nutrition*, *62*(6), 1448S-1461S.

[35] Omenn, G. S., Goodman, G. E., Thornquist, M. D., Balmes, J., Cullen, M. R., Glass, A., & Hammar, S. (1996). Effects of a combination of beta carotene and vitamin A on lung cancer and cardiovascular disease. *New England journal of medicine*, *334*(18), 1150-1155.

[36] Heinonen, O. P., & Albanes, D. (1994). The effect of vitamin E and beta carotene on the incidence of lung cancer and other cancers in male smokers.*The New England journal of medicine*, *330*.

[37] Demmig-Adams, B., & Adams, W. W. (1996). The role of xanthophyll cycle carotenoids in the protection of photosynthesis. *Trends in Plant science*, *1*(1), 21-26.

[38] Edge, R., McGarvey, D. J., & Truscott, T. G. (1997). The carotenoids as anti-oxidants—a review. *Journal of Photochemistry and Photobiology B: Biology*,*41*(3), 189-200.

[39] Paiva, S. A., & Russell, R. M. (1999). β-carotene and other carotenoids as antioxidants. *Journal of the American College of Nutrition*, *18*(5), 426-433.

[40] Koo, E., Neuringer, M., & SanGiovanni, J. P. (2014). Macular xanthophylls, lipoprotein-related genes, and age-related macular degeneration. *The American Journal of Clinical Nutrition*, *100*(Supplement 1), 336S-346S.

[41] Snodderly DM. (1995) Evidence for protection against age-related macular degeneration by carotenoids and antioxidant vitamins. *The American Journal of Clinical Nutrition*, **62**(suppl):1448S–61S.

[42] Krinsky NI, Landrum JT, Bone RA. (2003) Biologic mechanisms of the protective role of lutein and zeaxanthin in the eye. *Annual Review of Nutrition,* 23:171–201.

[43] Whitehead, A. J., Mares, J. A., & Danis, R. P. (2006). Macular pigment: a review of current knowledge. *Archives of ophthalmology*, *124*(7), 1038-1045.

[44] Park, J. S., Chew, B. P., & Wong, T. S. (1998). Dietary lutein from marigold extract inhibits mammary tumor development in BALB/c mice. *The Journal of nutrition*, *128*(10), 1650-1656.

[45] Pashkow, F. J., Watumull, D. G., & Campbell, C. L. (2008). Astaxanthin: a novel potential treatment for oxidative stress and inflammation in cardiovascular disease. *The American journal of cardiology*, *101*(10), S58-S68.

[46] Fassett, R. G., & Coombes, J. S. (2009). Astaxanthin, oxidative stress, inflammation and cardiovascular disease. *Future Cardiology*, *5*(4), 333-342.

[47] Gao, Y. Y., Xie, Q. M., Jin, L., Sun, B. L., Ji, J., Chen, F. Ma J. Y. & Bi, Y. Z. (2012). Supplementation of xanthophylls decreased proinflammatory and increased anti-inflammatory cytokines in hens and chicks. *British Journal of Nutrition*, *108*(10), 1746-1755.

[48] Hosokawa, M., Kudo, M., Maeda, H., Kohno, H., Tanaka, T., & Miyashita, K. (2004). Fucoxanthin induces apoptosis and enhances the antiproliferative effect of the PPARγ ligand, troglitazone, on colon cancer cells. *Biochimica et Biophysica Acta (BBA)-General Subjects*, *1675*(1), 113-119.

[49] Kotake-Nara, E., Asai, A., & Nagao, A. (2005). Neoxanthin and fucoxanthin induce apoptosis in PC-3 human prostate cancer cells. *Cancer letters*, *220*(1), 75-84.

[50] Okuzumi, J., Nishino, H., Murakoshi, M., Iwashima, A., Tanaka, Y., Yamane, T & Takahashi, T. (1990). Inhibitory effects of fucoxanthin, a natural carotenoid, on N-*myc* expression and cell cycle progression in human malignant tumor cells. *Cancer letters*, *55*(1), 75-81.

[51] Nes, W. R. (1974). Role of sterols in membranes. *Lipids*, *9*(8), 596-612.

[52] Voet, Voet & Pratt (2006). Fundamentals of Biochemistry. Wiley. Pg 493

[53] Sever, P. S., Dahlöf, B., Poulter, N. R., Wedel, H., Beevers, G., Caulfield, M., Collins, R., Kjeldsen, S.E., Kristinsson, A., McInnes, G., Mehlsen, J., Nieminen, M., O'Brien & E., Östergren, J. (2003). Prevention of coronary and stroke events with atorvastatin in hypertensive patients who have average or lower-than-average cholesterol concentrations, in the Anglo-Scandinavian Cardiac Outcomes Trial—Lipid Lowering Arm (ASCOT-LLA): a multicentre randomised controlled trial. *The Lancet*, *361*(9364), 1149-1158.

[54] About Cholesterol. (2014, April 21). American Heart Association Website. *Heart.org* Retrieved April 20, 2015.

[55] Nes, W. D. (2011). Biosynthesis of cholesterol and other sterols. *Chemical reviews*, *111*(10), 6423-6451.

[56] Cohn, J. S., Kamili, A., Wat, E., Chung, R. W. S., & Tandy, S. (2010). Dietary Phospholipids and Intestinal Cholesterol Absorption. *Nutrients*, *2*(2), 116–127. doi:10.3390/nu2020116

[57] Ostlund, R. E. (2007). Phytosterols, cholesterol absorption and healthy diets. *Lipids*, *42*(1), 41-45.

[58] Global Market Insights Inc., (Sept. 2016). *Phytosterols Market Size By Product (Beta-Sitosterol, Campesterol, Stigmasterol), By Application (Pharmaceuticals, Food ingredients, Cosmetics), Regional Outlook (U.S., Canada, Mexico, Germany, UK, France, Italy, Russia, Poland, China, India, Japan, Indonesia, Malaysia, Thailand, Australia, Brazil, South Africa, Saudi Arabia, UAE), Growth Potential, Price Trend, Competitive Market Share & Forecast, 2016 – 2024;* Global Market Insights Market Reports. Retrieved from: https://www.gminsights.com/industry-analysis/phytosterols-market.

[59] Patterson, G. W. (1971). The distribution of sterols in algae. *Lipids*, *6*(2), 120-127.

[60] Ling, W. H., & Jones, P. J. H. (1995). Dietary phytosterols: a review of metabolism, benefits and side effects. *Life sciences*, *57*(3), 195-206.

[61] Leikin, A. I., & Brenner, R. R. (1992). In vivo phospholipid modification induces changes in microsomal Δ5-desaturase activity. *Biochimica et Biophysica Acta (BBA)-Lipids and Lipid Metabolism*, *1165*(2), 189-193.

[62] Heinemann, T., Axtmann, G., & Bergmann, K. V. (1993). Comparison of intestinal absorption of cholesterol with different plant sterols in man*.*European journal of clinical investigation*, *23*(12), 827-831.

[63] Denke, M. A. (1995). Lack of efficacy of low-dose sitostanol therapy as an adjunct to a cholesterol-lowering diet in men with moderate hypercholesterolemia. *The American journal of clinical nutrition*, *61*(2), 392-396.

[64] Moghadasian, M. H., & Frohlich, J. J. (1999). Effects of dietary phytosterols on cholesterol metabolism and atherosclerosis: clinical and experimental evidence. *The American journal of medicine*, *107*(6), 588-594.

[65] Ostlund RE Jr, Spilburg CA, Stenson WF. 1999. Sitostanol administered in lecithin micelles potently reduces cholesterol absorption in humans. Am. J. Clin. Nutr. 70: 826–31

[66] Miettinen TA, Puska P, Gylling H, Vanhanen H, Vartiainen E. 1995. Reduction of serum cholesterol with sitostanolester margarine in a mildly hypercholesterolemic population. N. Eng. J. Med. 333: 1308–12

[67] Mattson FH, Grundy SM, Crouse JR. 1982. Optimizing the effect of plant sterols on cholesterol absorption in man. Am. J. Clin. Nutr. 35:697–700

[68] Grundy SM, Mok HYI. 1977. Determination of cholesterol absorption in man by intestinal perfusion. J. Lipid Res. 18:263– 71

[69] Jones PJH, Howell T, MacDougall DE, Feng JY, Parsons W. 1998. Short-term administration of tall oil phytosterols improves plasma lipid profiles in subjects with different cholesterol levels. Metabolism 47:751–56

[70] Lees AM, Mok HYI, Lees RS, McCluskey MA, Grundy SM. 1977. Plant sterols as cholesterol-lowering agents: clinical trials in patients with hypercholesterolemia and studies of sterol balance. Atherosclerosis 28:325–38

[71] Ostlund Jr, R. E. (2002). Phytosterols in human nutrition. *Annual review of nutrition*, *22*(1), 533-549.

[72] Armstrong MJ, Carey MC. 1987. Thermodynamic and molecular determinants of sterol solubilities in bile salt micelles. J. Lipid Res. 28:1144–55

[73] Brown MS, Goldstein JL (1984). "How LDL Receptors Influence Cholesterol and Atherosclerosis". *Scientific American* **251** (3): 52–60.

[74] Faulkner, D. J. (2001). Marine natural products. *Natural product reports*, *18*(1), 1R-49R.

[75] Blunt, J. W., Copp, B. R., Munro, M. H., Northcote, P. T., & Prinsep, M. R. (2003). Review: Marine natural products. *Natural Product Reports*. 20,1-48

[76] Blunt, J. W., Copp, B. R., Munro, M. H., Northcote, P. T., & Prinsep, M. R. (2003). Review: Marine natural products. *Natural Product Reports*. 21,1-49.

[77] Blunt, J. W., Copp, B. R., Munro, M. H., Northcote, P. T., & Prinsep, M. R. (2005). Review: Marine natural products. *Natural Product Reports*. 22(1), 15-61

[78] Blunt, J. W., Copp, B. R., Munro, M. H., Northcote, P. T., & Prinsep, M. R. (2006). Marine natural products. *Natural Product Reports*. 23(1), 26-78

[79] Blunt, J. W., Copp, B. R., Hu, W. P., Munro, M. H., Northcote, P. T., & Prinsep, M. R. (2007). Marine natural products. *Natural Product Reports*, *24*(1), 31-86.

[80] Blunt, J. W., Copp, B. R., Hu, W. P., Munro, M. H., Northcote, P. T., & Prinsep, M. R. (2008). Marine natural products. *Natural product reports*, *25*(1), 35-94.

[81] Blunt, J. W., Copp, B. R., Hu, W. P., Munro, M. H., Northcote, P. T., & Prinsep, M. R. (2009). Marine natural products. *Natural product reports*, *26*(2), 170.

[82] Blunt, J. W., Copp, B. R., Munro, M. H., Northcote, P. T., & Prinsep, M. R. (2010). Marine natural products. *Natural product reports*, *27*(2), 165-237.

[83] Blunt, J. W., Copp, B. R., Munro, M. H., Northcote, P. T., & Prinsep, M. R. (2011). Review: marine natural products.

[84] Hamann, M. T., & Scheuer, P. J. (1993). Kahalalide F: a bioactive depsipeptide from the sacoglossan mollusk Elysia rufescens and the green alga Bryopsis sp. *Journal of the American Chemical Society*, *115*(13), 5825-5826.

[85] Cruz, L. J., Luque-Ortega, J. R., Rivas, L., & Albericio, F. (2009). Kahalalide F, an antitumor depsipeptide in clinical trials, and its analogues as effective antileishmanial agents. *Molecular pharmaceutics*, *6*(3), 813-824.

[86] Dorta, E., Darias, J., San Martín, A., & Cueto, M. (2002). New Prenylated bromoquinols from the green alga Cymopolia barbata. *Journal of natural products*, *65*(3), 329-333.

[87] Puglisi, M. P., Tan, L. T., Jensen, P. R., & Fenical, W. (2004). Capisterones A and B from the tropical green alga Penicillus capitatus: unexpected anti-fungal defenses targeting the marine pathogen Lindra thallasiae. *Tetrahedron*, *60*(33), 7035-7039.

[88] Handley, J. T., & Blackman, A. J. (2005). Secondary metabolites from the marine alga Caulerpa brownii (Chlorophyta). *Australian journal of chemistry*, *58*(1), 39-46.

[89] Ramesh, C., Kavala, V., Kuo, C. W., Raju, B. R., & Yao, C. F. (2010). An Unprecedented Route for the Synthesis of 3, 3′-Biindoles by Reductive Cyclization of 3-[2-Nitro-1-(2-nitrophenyl) ethyl]-1H-indoles Mediated by Iron/Acetic Acid. *European Journal of Organic Chemistry*, *2010*(20), 3796-3801.

[90] Mao, S. C., Guo, Y. W., & Shen, X. (2006). Two novel aromatic valerenane-type sesquiterpenes from the Chinese green alga Caulerpa taxifolia. *Bioorganic & medicinal chemistry letters*, *16*(11), 2947-2950.

[91] Williams, D. E., Sturgeon, C. M., Roberge, M., & Andersen, R. J. (2007). Nigricanosides A and B, antimitotic glycolipids isolated from the green alga Avrainvillea nigricans collected in Dominica. *Journal of the American Chemical Society*, *129*(18), 5822-5823.

[92] Gallimore, W. A., Sambo, T., & Campbell, T. (2009). Debromocymopolone from the green alga, Cymopolia barbata. *Journal of Chemical Research*, *2009*(3), 160-161.

[93] Chakraborty, K., Lipton, A. P., Paulraj, R., & Chakraborty, R. D. (2010). Guaiane sesquiterpenes from seaweed Ulva fasciata Delile and their antibacterial properties. *European journal of medicinal chemistry*, *45*(6), 2237-2244.

[94] Chakraborty, K., & Paulraj, R. (2010). Sesquiterpenoids with free-radical-scavenging properties from marine macroalga Ulva fasciata Delile. *Food Chemistry*, *122*(1), 31-41.

[95] Parke, M. (1949). Studies on marine flagellates. Journal of the Marine Biological Association of the United Kingdom 28: 255-288.

[96] Kim, S. M., Kang, S. W., Kwon, O. N., Chung, D., & Pan, C. H. (2012). Fucoxanthin as a major carotenoid in Isochrysis aff. galbana: Characterization of extraction for commercial application. *Journal of the Korean Society for Applied Biological Chemistry*, *55*(4), 477-483.

[97] Brown, M. R., Jeffrey, S. W., Volkman, J. K., & Dunstan, G. A. (1997). Nutritional properties of microalgae for mariculture. *Aquaculture*, *151*(1), 315-331.

[98] Araujo, G. S., Matos, L. J., Gonçalves, L. R., Fernandes, F. A., & Farias, W. R. (2011). Bioprospecting for oil producing microalgal strains: evaluation of oil and biomass production for ten microalgal strains. *Bioresource technology*, *102*(8), 5248-5250.

[99] Seychelles, L. H., Audet, C., Tremblay, R., Fournier, R., & Pernet, F. (2009). Essential fatty acid enrichment of cultured rotifers (Brachionus plicatilis, Müller) using frozen-concentrated microalgae. *Aquaculture Nutrition*, *15*(4), 431-439.

[100] Farhadian, O., Yusoff, F. M., & Mohamed, S. (2008). Nutritional values of Apocyclops dengizicus (Copepoda: Cyclopoida) fed Chaetocerous calcitrans and Tetraselmis tetrathele. *Aquaculture Research*, *40*(1), 74-82.

[101] Milke, L. M., Bricelj, V. M., & Parrish, C. C. (2008). Biochemical characterization and nutritional value of three Pavlova spp. in unialgal and mixed diets with Chaetoceros muelleri for postlarval sea scallops, Placopecten magellanicus. *Aquaculture*, *276*(1), 130-142.

[102] Laguna, M. R., Villar, R., Cadavid, I., & Calleja, J. M. (1993). Effects of extracts of Tetraselmis suecica and Isochrysis galbana on the central nervous system. *Planta medica*, *59*(3), 207-214.

[103] Yingying, S., Changhai, W., & Jing, C. (2008). Growth inhibition of the eight species of microalgae by growth inhibitor from the culture of Isochrysis galbana and its isolation and identification. *Journal of Applied Phycology*, *20*(3), 315-321.

[104] Scholz, B., & Liebezeit, G. (2006). Chemical screening for bioactive substances in culture media of microalgae and cyanobacteria from marine and brackish water habitats: first results. *Pharmaceutical biology*, *44*(7), 544-549.

[105] Tonon, T., Harvey, D., Larson, T. R., & Graham, I. A. (2003). Identification of a very long chain polyunsaturated fatty acid Δ4-desaturase from the microalga Pavlova lutheri. *FEBS letters*, *553*(3), 440-444.

[106] Dijkman, N. A., & Kromkamp, J. C. (2006). Phospholipid-derived fatty acids as chemotaxonomic markers for phytoplankton: application for inferring phytoplankton composition. *Marine Ecology Progress Series*, *324*.

[107] Advanced Research on Plant Lipids, *Proceedings of the International Symposium on Plant Lipids*, 15th, Okazaki, Japan, May 12-17, 2002 Pages19-22 (2003)

[108] Lever M, George PM, Atkinson W, Molyneux SL, Elmslie JL, et al. (2011) Plasma Lipids and Betaine Are Related in an Acute Coronary Syndrome Cohort. *PLoS ONE* 6(7): e21666.

[109] Abstracts of Papers, 243rd ACS National Meeting & Exposition, San Diego, CA, United States, March 25-March 29, 2012 Pages AGFD-149 (2012)

[110] Kessler E. (1982) Chemotaxonomy in the Chlorococcales. In F.E. Round & D.J. Chapman (Eds.) *Progress in phycological research.* (pp. 111–135). Elsevier, Amsterdam

[111] Kessler E. 1984. A general review on the contribution of chemotaxonomy to the systematics of green algae. In D.E.G. Irvine & D.M. John (Eds.), *Systematics of the green algae* (Ed. by), pp. 391–407. Academic Press, London

[112] Kessler E. & Soeder C.J. (1962). Biochemical contributions to the taxonomy of the genus Chlorella. *Nature* 194: 1096–1097.

[113] Juárez, Á. B., Vélez, C. G., Iñiguez, A. R., Martínez, D. E., Rodríguez, M. C., Vigna, M. S., & de Molina, M. D. C. R. (2011). A Parachlorella kessleri (Trebouxiophyceae, Chlorophyta) strain from an extremely acidic geothermal pond in Argentina. *Phycologia*, *50*(4), 413-421.

[114] *SciFinder*; Chemical Abstracts Service: Columbus, OH; https://scifinder.cas.org (accessed June 20, 2015); Results for search query: *Parachlorella kessleri*.

[115] Klassen, V., Blifernez-Klassen, O., Hoekzema, Y., Mussgnug, J. H., & Kruse, O. (2015). A novel one-stage cultivation/fermentation strategy for improved biogas production with microalgal biomass. *Journal of Biotechnology*.

[116] Pádrová, K., Lukavský, J., Nedbalová, L., Čejková, A., Cajthaml, T., Sigler, K., Vítová, M., & Řezanka, T. (2014). Trace concentrations of iron nanoparticles cause overproduction of biomass and lipids during cultivation of cyanobacteria and microalgae. *Journal of Applied Phycology*, 1-9.

[117] Takeshita, T., Ota, S., Yamazaki, T., Hirata, A., Zachleder, V., & Kawano, S. (2014). Starch and lipid accumulation in eight strains of six Chlorella species under comparatively high light intensity and aeration culture conditions. *Bioresource technology*, *158*, 127-134.

[118] LiLi, J., XiaoBin, W., YaHong, G., Hong, M., & YeGuang, L. (2013). A newly selected lipid-rich microalgae strain and its molecular identification. *Acta Hydrobiologica Sinica*, *37*(4), 606-612.

[119] Fernandes, B., Teixeira, J., Dragone, G., Vicente, A. A., Kawano, S., Bišová, K., Přibyl, P, Zachleder, V., & Vítová, M. (2013). Relationship between starch and lipid accumulation induced by nutrient depletion and replenishment in the microalga Parachlorella kessleri. *Bioresource technology*, *144*, 268-274.

[120] Dyo, Y. M., Vonlanthen, S. E., Purton, S., & Zayadan, B. K. (2013). Evaluating new isolates of microalgae from Kazakhstan for biodiesel production. *Russian journal of plant physiology*, *60*(4), 549-554.

[121] Ivánová, D., Kaduková, J., Kavuličová, J., & Horváthová, H. (2012). Determination of the Functional Groups in Algae Parachlorella Kessleri by Potentiometric Titrations. *Nova Biotechnologica et Chimica*, *11*(2), 93-99.

[122] Goiris, K., Muylaert, K., Fraeye, I., Foubert, I., De Brabanter, J., & De Cooman, L. (2012). Antioxidant potential of microalgae in relation to their phenolic and carotenoid content. *Journal of applied phycology*, *24*(6), 1477-1486.

[123] Druon, A., Le Ruyet, M., Segueilha, L. (2015). PCT Int. Appl., WO 2015022469 A2 20150219.

[124] Brooks, G., Franklin, S., Avila, J., Devker, S., Baliu, E., Rakitky, W., Piechocki, J., Zdanis, D., Norris, L. (2013). U.S. Pat. Appl. Publ., US 20130122180 A1 20130516.

[125] Brooks, G., Franklin, S., Avila, J., Devker, S., Baliu, E., Rakitky, W., Piechocki, J., Zdanis, D., Norris, L. (2012). U.S. Pat. Appl. Publ., US 20120128851 A1 20120524.

[126] Brooks, G., Franklin, S., Avila, J., Devker, S., Baliu, E., Rakitky, W., Piechocki, J., Zdanis, D., Norris, L. (2010). U.S. Pat. Appl. Publ., US 20100303957 A1 20101202.

[127] Brooks, G., Franklin, S., Avila, J., Devker, S., Baliu, E., Rakitky, W., Piechocki, J., Zdanis, D., Norris, L. (2010). U.S. Pat. Appl. Publ., US 20100297323 A1 20101125.

[128] Brooks, G., Franklin, S., Avila, J., Devker, S., Baliu, E., Rakitky, W., Piechocki, J., Zdanis, D., Norris, L. (2010). U.S. Pat. Appl. Publ., US 20100297325 A1 20101125.

[129] Brooks, G., Franklin, S., Avila, J., Devker, S., Baliu, E., Rakitky, W., Piechocki, J., Zdanis, D., Norris, L. (2010). U.S. Pat. Appl. Publ., US 20100297296 A1 20101125.

[130] Brooks, G., Franklin, S., Avila, J., Devker, S., Baliu, E., Rakitky, W., Piechocki, J., Zdanis, D., Norris, L. (2010). U.S. Pat. Appl. Publ., US 20100297295 A1 20101125.

[131] Sato, T. (2014). Jpn. Kokai Tokkyo Koho, JP 2014105202 A 20140609.

[132] Sato, T., Lee, JB. (2014). Jpn. Kokai Tokkyo Koho, JP 2014025035 A 20140206.

[133] Coragliotti, A., Franklin, S., Day, A., Decker, S. (2012) From U.S. Pat. Appl. Publ., US 20120202768 A1 20120809.

[134] Coragliotti, A., Franklin, S., Day, A., Decker, S. (2010). PCT Int. Appl., WO 2010111710 A1 20100930.

[135] Thomas, L. (1972). Germs. *New England Journal of Medicine*, 287:553-5

[136] McLuckie, A., ed. (2009). *Respiratory disease and its management.* New York: Springer. p. 51.

[137] Ashby, Bonnie; Turkington, Carol (2007). *The encyclopedia of infectious diseases (3rd ed.)*. New York: Facts on File. p. 242. ISBN 0-8160-6397-4.

[138] Levy, B. D. (2010). Lung In Gilroy, D.W. (Ed.), *Fundamentals of Inflammation* (pp. 253-5). New York, NY: Cambridge University Press.

[139] Mitzgerd, J.P. 2008. Acute lower respiratory tract infection. *New England Journal of Medicine* 358, 716-27

[140] Scott DL, Wolfe F, Huizinga TW (Sep 25, 2010). "Rheumatoid arthritis". *Lancet* **376** (9746): 1094–108.

[141] Silman AJ, MacGregor AJ, Thomson W, Holligan S, Carthy D, Farhan A, Ollier WE (1993). "Twin concordance rates or rheumatoid arthritis: Results from a nationwide study". *British journal of rheumatology* **32**(10): 903–907.

[142] Shah, Ankur. *Harrison's Principle of Internal Medicine* (18th ed.). United States: McGraw Hill. p. 2738.

[143] Raza, K. & Gordon, C. (2010). Rheumatoid Arthritis/SLE In Gilroy, D.W. (Ed.), *Fundamentals of Inflammation* (pp. 267-275). New York, NY: Cambridge University Press.

[144] Suri, J., Kathuria, C., & Molinari, F. (Eds.). (2010). *Atherosclerosis disease management*. Springer Science & Business Media.

[145] Serhan, C. N., Ward, P. A., & Gilroy, D. W. (2010). *Fundamentals of inflammation*. Cambridge University Press.

[146] Ward, P. A. (2010). Acute and chronic inflammation. *Fundamentals of Inflammation*, 1-16.

[147] Willoughby, D. A., Moore, A. R., Colville-Nash, P. R., & Gilroy, D. (2000). Resolution of inflammation. *International journal of immunopharmacology*,*22*(12), 1131-1135.

[148] Roy, S., Bagchi, D., & Raychaudhuri, S. P. (Eds.). (2012). *Chronic Inflammation: Molecular Pathophysiology, Nutritional and Therapeutic Interventions*. CRC Press.

[149] Radbruch, A., & Lipsky, P. E. (Eds.). (2006). *Current concepts in autoimmunity and chronic inflammation* (Vol. 305). Springer Science & Business Media.

[150] Anderson, K. O., Bradley, L. A., Young, L. D., McDaniel, L. K., & Wise, C. M. (1985). Rheumatoid arthritis: review of psychological factors related to etiology, effects, and treatment. *Psychological bulletin*, *98*(2), 358.

[151] Blazka, M. E., Wilmer, J. L., Holladay, S. D., Wilson, R. E., & Luster, M. I. (1995). Role of proinflammatory cytokines in acetaminophen hepatotoxicity.*Toxicology and applied pharmacology*, *133*(1), 43-52.

[152] Aliberti, J. (Ed.). (2011). *Control of innate and adaptive immune responses during infectious diseases*. Springer Science & Business Media.

[153] Piomelli, D. (1993). Arachidonic acid in cell signaling. *Current opinion in cell biology*, 5(2), 274-280.

[154] Ulrich, C. M., Bigler, J., & Potter, J. D. (2006). Non-steroidal anti-inflammatory drugs for cancer prevention: promise, perils and pharmacogenetics. *Nature Reviews Cancer*, 6(2), 130-140.

[155] Digby GJ, Lober RM, Sethi PR, Lambert NA (2006). "Some G protein heterotrimers physically dissociate in living cells". *Proc. Natl. Acad. Sci.* 103 (47): 17789–94.

[156] Sodeman W, Sodeman T (2005). "Physiologic- and Adenylate Cyclase-Coupled Beta-Adrenergic Receptors". *Sodeman's Pathologic Physiology: Mechanisms of Disease*. W B Saunders Co. pp. 143–145

[157] Hsiao, H. Y., Mak, O. T., Yang, C. S., Liu, Y. P., Fang, K. M., & Tzeng, S. F. (2007). TNF-α/IFN-γ-induced iNOS expression increased by prostaglandin E2 in rat primary astrocytes via EP2-evoked cAMP/PKA and intracellular calcium signaling. *Glia*, *55*(2), 214-223.

[158] Spooren, A., Kooijman, R., Lintermans, B., Van Craenenbroeck, K., Vermeulen, L., Haegeman, G., & Gerlo, S. (2010). Cooperation of NFκB and CREB to induce synergistic IL-6 expression in astrocytes. *Cellular signalling*,*22*(5), 871-881.

[159]Gilmore TD (2006). "Introduction to NF-κB: players, pathways, perspectives".*Oncogene* **25** (51): 6680–4.

[160]Gilmore TD (1999). "The Rel/NF-κB signal transduction pathway: introduction". *Oncogene* **18**(49): 6842–4.

[161] Greenberg, H., Ye, X., Wilson, D., Htoo, AK, Hendersen, T., & Liu, S.F. (2006). Chronic intermittent hypoxia activates nuclear factor kappaB in cardiovascular tissues in vivo. *Biochemical and Biophysical Research Communications*, 343(2), 591-6

[162] Bischoff, D. S., Zhu, J. H., Makhijani, N. S., & Yamaguchi, D. T. (2008). Acidic pH stimulates the production of the angiogenic CXC chemokine, CXCL8 (interleukin-8), in human adult mesenchymal stem cells via the extracellular signal-regulated kinase, p38 mitogen-activated protein kinase, and NF-κB pathways. *Journal of cellular biochemistry*, *104*(4), 1378-1392.

[163] Hang, C. H., Shi, J. X., Li, J. S., Li, W. Q., & Yin, H. X. (2005). Up-regulation of intestinal nuclear factor kappa B and intercellular adhesion molecule-1 following traumatic brain injury in rats. *World journal of gastroenterology: WJG*,*11*(8), 1149-1154.

[164] Habraken, Y., & Piette, J. (2006). NF-κB activation by double-strand breaks.*Biochemical pharmacology*, *72*(9), 1132-1141.

[165] Brach, M. A., Hass, R., Sherman, M. L., Gunji, H., Weichselbaum, R., & Kufe, D. (1991). Ionizing radiation induces expression and binding activity of the nuclear factor kappa B. *Journal of Clinical Investigation*, *88*(2), 691.

[166] Ghanim, H., Aljada, A., Hofmeyer, D., Syed, T., Mohanty, P., & Dandona, P. (2004). Circulating mononuclear cells in the obese are in a proinflammatory state. *Circulation*, *110*(12), 1564-1571.

[167] Zhang, X., Dong, F., Ren, J., Driscoll, M. J., & Culver, B. (2005). High dietary fat induces NADPH oxidase-associated oxidative stress and inflammation in rat cerebral cortex. *Experimental neurology*, *191*(2), 318-325.

[168] Martinez, O., Valmas, C., & Basler, C. F. (2007). Ebola virus-like particle-induced activation of NF-κB and Erk signaling in human dendritic cells requires the glycoprotein mucin domain. *Virology*, *364*(2), 342-354.

[169] Bachelerie, F., Alcami, J., Arenzana-Seisdedos, F., & Virelizier, J. L. (1991). HIV enhancer activity perpetuated by NF-κB induction on infection of monocytes. *Nature*, *350*(6320), 709-712.

[170] Yedowitz, J. C., & Blaho, J. A. (2005). Herpes simplex virus 2 modulates apoptosis and stimulates NF-κB nuclear translocation during infection in human epithelial HEp-2 cells. *Virology*, *342*(2), 297-310.

[171] Ronni, T., Matikainen, S., Sareneva, T., Melen, K., Pirhonen, J., Keskinen, P., & Julkunen, I. (1997). Regulation of IFN-alpha/beta, MxA, 2', 5'-oligoadenylate synthetase, and HLA gene expression in influenza A-infected human lung epithelial cells. *The Journal of Immunology*, *158*(5), 2363-2374.

[172] Sen, R. & Baltimore, D. (1986). Inducibility of kappa immunoglobulin enhancer binding protein Nf-kappa B by a post-translational mechanism. *Cell*, 47(6), 921-8.

[173] Kitchens RL (2000). "Role of CD14 in cellular recognition of bacterial lipopolysaccharides". *Chemical Immunology and Allergy* 74: 61–82.

[174] Malinin, N. L., Boldin, M. P., Kovalenko, A. V., & Wallach, D. (1997). MAP3K-related kinase involved in NF-kB induction by TNF, CD95 and IL-1. *Nature*, 385, 540-4

[175] Brocker C, Thompson D, Matsumoto A, Nebert DW, Vasiliou V (2010). Evolutionary divergence and functions of the human interleukin (IL) gene family. *Human Genomics*, 5 (1): 30–55.

[176] Contassot E, Beer HD, French LE (2012). "Interleukin-1, inflammasomes, autoinflammation and the skin". *Swiss Med Wkly* 142: w13590

[177] Osborn, L., Kunkel, S., & Nabel, G. J. (1989). Tumor necrosis factor alpha and interleukin 1 stimulate the human immunodeficiency virus enhancer by activation of the nuclear factor kappa B. *Proceedings of the National Academy of Sciences*, *86*(7), 2336-2340.

[178] Lander H.M. (1997). An essential role for free radicals and derived species in signal transduction. FASEB J, 11 (2), 118–124

[179] Gloire, G., Legrand-Poels, S., & Piette, J. (2006). NF-κB activation by reactive oxygen species: fifteen years later. *Biochemical pharmacology*, *72*(11), 1493-1505.

[180] NF-kB Target Genes » NF-kB Transcription Factors | Boston University. (n.d.). Retrieved March 30, 2015, from http://www.bu.edu/nf-kb/gene-resources/target-genes/

[181] Mori, N., & Prager, D. (1996). Transactivation of the interleukin-1alpha promoter by human T-cell leukemia virus type I and type II Tax proteins. *Blood*, *87*(8), 3410-3417.

[182] Hiscott, J., Marois, J., Garoufalis, J., D'addario, M., Roulston, A., Kwan, I., & Bensi, G. (1993). Characterization of a functional NF-kappa B site in the human interleukin 1 beta promoter: evidence for a positive autoregulatory loop. *Molecular and cellular biology*, *13*(10), 6231-6240.

[183] Hoyos, B., Ballard, D. W., Bohnlein, E., Siekevitz, M., & Greene, W. C. (1989). Kappa B-specific DNA binding proteins: role in the regulation of human interleukin-2 gene expression. Science, 244(4903), 457-460.

[184] Serfling, E., Barthelmäs, R., Pfeuffer, I., Schenk, B., Zarius, S., Swoboda, R., Mercurio, F., & Karin, M. (1989). Ubiquitous and lymphocyte-specific factors are involved in the induction of the mouse interleukin 2 gene in T lymphocytes. *The EMBO journal*, *8*(2), 465.

[185] Libermann, T. A., & Baltimore, D. (1990). Activation of interleukin-6 gene expression through the NF-kappa B transcription factor. *Molecular and cellular biology*, *10*(5), 2327.

[186] Sica, A., L. Dorman, V. Viggiano, M. Cippitelli, P. Ghosh, N. Rice, H., A. Young. 1997. Interaction of NF-kappaB and NFAT with the interferon-gamma promoter. *Journal of Biological Chemistry*, 373: 30412.

[187] Locksley RM, Killeen N, Lenardo MJ (2001). The TNF and TNF receptor superfamilies: integrating mammalian biology. *Cell* **104** (4), 487–501.

[188] Beg, A. A., & Baltimore, D. (1996). An essential role for NF-κB in preventing TNF-α-induced cell death. *Science*, *274*(5288), 782-784.

[189] Shakhov AN, Collart MA, Vassalli P, Nedospasov SA, Jongeneel CV. (1990) Kappa B-type enhancers are involved in lipopolysaccharide-mediated transcriptional activation of the tumor necrosis factor alpha gene in primary macrophages. *Journal of Experimental Medicine* 171(1), 35-47

[190] Santee, S. M., & Owen-Schaub, L. B. (1996). Human tumor necrosis factor receptor p75/80 (CD120b) gene structure and promoter characterization. *Journal of Biological Chemistry*, *271*(35), 21151-21159.

[191] Schwenzer R, Siemienski K, Liptay S, Schubert G, Peters N, Scheurich P, Schmid RM, Wajant H. (1999). The human tumor necrosis factor (TNF) receptor-associated factor 1 gene (TRAF1) is up-regulated by cytokines of the TNF ligand family and modulates TNF-induced activation of NF-kappaB and c-Jun N-terminal kinase. *Journal of Biological Chemistry*, 274(27), 19368-74.

[192] Hong, C. H., Hur, S. K., Oh, O. J., Kim, S. S., Nam, K. A., & Lee, S. K. (2002). Evaluation of natural products on inhibition of inducible cyclooxygenase (COX-2) and nitric oxide synthase (iNOS) in cultured mouse macrophage cells.*Journal of Ethnopharmacology*, 83(1), 153-159.

[193] Xie, Q. W., Kashiwabara, Y., & Nathan, C. (1994). Role of transcription factor NF-kappa B/Rel in induction of nitric oxide synthase. *Journal of Biological Chemistry*, 269(7), 4705-4708.

[194] Schumann, R. R. (1994). Mechanisms of transcriptional activation of lipopolysaccharide binding protein (LBP). *Progress in clinical and biological research*, 392, 297-304.

[195] Yamamoto K, Arakawa T, Ueda N, Yamamoto S. (1995). Transcriptional roles of nuclear factor kappa B and nuclear factor-interleukin-6 in the tumor necrosis factor alpha-dependent induction of cyclooxygenase-2 in MC3T3-E1 cells. *Journal of Biological Chemistry*, 270(52), 31315-20

[196] Chopra, A., Ferreira-Alves, D. L., Sirois, P., & Thirion, J. P. (1992). Cloning of the guinea pig 5-lipoxygenase gene and nucleotide sequence of its promoter. *Biochemical and biophysical research communications*, 185(2), 489-495.

[197] Arakawa T, Nakamura M, Yoshimoto T, Yamamoto S (1995) The transcriptional regulation of human arachidonate 12-lipoxygenase gene by NF kappa B/rel. *FEBS Letters,* 363, 105-10

[198] Dinarello, C. A. (1996). Role of pro-and anti-inflammatory cytokines during inflammation: experimental and clinical findings. *Journal of biological regulators and homeostatic agents*, 11(3), 91-103.

[199] Carswell EA, Old LJ, Kassel RL, Green S, Fiore N, Williamson B. (1975). An endotoxin-induced serum factor that causes necrosis of tumors. *Proceedings of the National Academy of Science,USA*. 72(9), 3666-70.

[200] Wajant H, Pfizenmaier K, Scheurich P (2003). "Tumor necrosis factor signaling". *Cell Death Differ.* **10**(1): 45–65.

[201] Liles, W. C., & Van Voorhis, W. C. (1995). Review: nomenclature and biologic significance of cytokines involved in inflammation and the host immune response. *Journal of Infectious Diseases*, 172(6), 1573-1580.

[202] Dinarello CA (2011). "Interleukin-1 in the pathogenesis and treatment of inflammatory diseases". *Blood* 117 (14): 3720–32.

[203] Schoenborn, J. R., & Wilson, C. B. (2007). Regulation of interferon-γ during innate and adaptive immune responses. *Advances in immunology*, 96, 41-101.

[204] Plotnikoff NP, Ed.(1999) Cytokines: stress and immunity. Boca Raton: CRC Press.

[205] Gray, P. W., & Goeddel, D. V. (1982). Structure of the human immune interferon gene. *Nature*, 298(5877):859-63.

[206] Lee, Y. J., & Benveniste, E. N. (1996). Stat1 alpha expression is involved in IFN-gamma induction of the class II transactivator and class II MHC genes. *The Journal of Immunology*, 157(4), 1559-1568.

[207] Rusinova, I., Forster, S., Yu, S., Kannan, A., Masse, M., Cumming, H., & Hertzog, P. J. (2013). Interferome v2. 0: an updated database of annotated interferon-regulated genes. *Nucleic acids research*, 41(D1), D1040-D1046.

Chapter 2 Nutritional Content of Algae

The overall goal of this research was to investigate the potential for algal biomass to be utilized as a nutraceutical product or ingredient with anti-inflammatory, and potentially other valuable health modifying properties. A nutraceutical is a "nutritious pharmaceutical" i.e. a food ingredient that bestows medical or health benefits "including the prevention and/or treatment of disease"[1]. Nutraceuticals are nutritious functional foods, however go further than functional foods to include foods and ingredients with specific health modifying properties or concentrated extracts that are used because of their unique chemical profile. The content of vitamins, protein, minerals and carbohydrates contained within nutraceuticals constitutes the difference between a nutraceutical and pharmaceutical. The Dietary Supplement Health and Education Act (DSHEA) of 1994 was passed to establish definitions, criteria, and guidelines for labeling and for the regulation of natural products, nutritional supplements and nutraceuticals. DSHEA defines a nutritional supplement as any product "intended to supplement the diet that bears or contains one or more of the following dietary ingredients: a vitamin, a mineral, an herb or other botanical, an amino acid, a dietary substance for use by man to supplement the diet by increasing the total dietary intake, or a concentrate, metabolite, constituent, extract, or combination of any of the aforementioned ingredients"[2]. While the burden of proof required to market nutritional supplements and nutraceuticals is considerably lower than required for FDA approval of pharmaceuticals, the label-claims

permitted for use on nutritional supplements limit their use in treating disorders and disease prior to FDA approval.

The major aspect of identifying nutraceuticals and the development thereof is to evaluate the nutritional content and bioactivity in order to fully elucidate its potential benefits to health. Chronic illnesses such as atherosclerosis, coronary heart disease, diabetes and cancer have been closely tied to diet, and there is ample evidence to support the attenuation of many disease states by modulation of the diet. Additionally, a key goal of the collaboration undertaken on this project with the New Jersey Aquaculture Innovation Center and private biofuel company AL-G Technologies (defunct since 2016, now a Canadian subsidiary jointly owned by Exxon) was to identify the potential for algae grown by NJAIC and/or AL-G could be used and eventually marketed as a nutraceutical. Thus, a key goal of this dissertation project was to thoroughly investigate the nutritional content of the algal biomass and ascertain functional applications. The roles played by the nutrients found in algal biomass will be described in this chapter.

2.1 Material

Due to the innumerable species of algae available and nearly infinite permutations of variables to consider when selecting a strain of algae for study, it was crucial to address the specific considerations outlined for the selection of the algal strains utilized throughout the course of this dissertation. First, it is necessary to explain some of the difficulties involved in the chemical and biological investigation of algal biomass.

The biggest single factor affecting the choice of microalgal species to utilize in this project was the availability of >100 g quantities (freeze dried). For the study of natural products, generally more than 1 kg starting material is utilized in order to ensure that a sufficient quantity of any compounds isolated will be obtained for complete characterization. When evaluating terrestrial plant material, this concern is easy to address due to the easy availability of large quantities of raw material. However, due to the cellular nature of algae, large quantities of relatively pure algal biomass cannot be obtained by harvesting from natural sources. Therefore, cultured algal biomass must be used in order to obtain the quantities required for this project. There are very few strains of algae that can be obtained commercially, and of those available, most are processed or mixtures of algae, or consist primarily of cyanobacteria. This research was done in collaboration with the New Jersey Aquaculture Innovation Center (NJAIC) which maintains a shellfish breeding program in Cape May, NJ to support offshore shellfishery populations. As part of their effort, they maintain large cultures of several marine microalgae which became the first targets of our investigation. Researchers at NJAIC graciously helped this effort by collecting, concentrating, centrifuging, freezing, and transporting algae biomass.

After several months of effort in collecting marine algae biomass, the second major factor involved in the selection of biomass became apparent. The quantity we required was too great for the processing capabilities of the NJAIC. After months of effort, only 10-15 g biomass had been collected. In order to address this issue, different methods of growing algae were systematically evaluated. Through our work we began collaborating with researchers working for AL-G Technologies, a company devoted to the exploration of a

new aeroponic algae growing technique. The AL-G aeroponic technique greatly reduced the amount of water utilized in algae biomass production, and thus eliminated much of the effort required to process and dry the algae for investigation[3]. AL-G technologies had experimented with several strains, but found that acidophilic green freshwater algae *Parachlorella kessleri* worked best on their system. In a matter of weeks, 100 g of algal biomass was collected for use in this project. It is for these reasons that this dissertation focuses on marine algae as well as freshwater species of algae that were available for this project.

2.1.1   Growth and Harvesting

2.1.1.1 Marine algal species

Marine species were obtained courtesy of Prof. Dave Bushek of the New Jersey Aquaculture Innovation Center, and Rutgers University where faculty maintain broodstock of shellfish such as oysters to support the offshore fishery population of New Jersey. As part of their operation, many species of algae are cultured using large bioreactors—essentially large transparent tubes filled with continuously aerated media and exposed to sunlight. The strains of algae grown for use at this facility are *Isochrysis galbana* (both Caribbean and Tahitian strain, C-Iso and T-Iso respectively), *Pavlova lutheri*, *Chaetoceros calcitrans*, *Chaetoceros negracile,* and *Tetraselmis chuii*. Since the shellfish consume the algae at the concentration grown in the bioreactors, the algae biomass is not concentrated in their normal efforts, and for this project, algae-containing media was

centrifuged to collect a concentrated algal paste which was immediately frozen and stored at -20°C prior to lyophilization.

2.1.1.2 *Parachlorella kessleri*

Parachlorella kessleri biomass was cultured and harvested as described by Johnson et al. (2015)[3] utilizing a novel aeroponic membrane substrate technique. *P. kessleri* was initially transferred to a 2 liter Erlenmeyer flask containing respective media and placed 20 cm below an LED lighting array with a light intensity of 200 $\mu mol*m^{-2}s^{-1}$ (16 hours light, 8 hours dark). The media used for the *P. kessleri* experimentation was as follows: KNO_3 (200 mg/L), NH_4Cl (106 mg/L), $CaCl_2*2H_2O$ (25 mg/L), $MgSO_4*7H_2O$ (25 mg/L), K_2HPO_4 (25 mg/L), $Na_2EDTA*2H_2O$ (1.1 mg/L), $FeSO_4*7H_2O$ (10 mg/L). The media used for *P. kessleri* was made using New Brunswick, NJ tap water and acidified by dropwise addition of HCl to a pH of 5.5. The inoculation flasks were aerated at a rate of 2 liters per minute (2:1 v/v) with ambient air and following 10 days of growth the biomass concentration was sufficient to begin experimentation.

Then 1000 mL of the *P. kessleri* inoculum was used to inoculate ten proprietary aeroponic membranes (15x25x1 cm) for cultivation. To inoculate aeroponic membranes with algae they were soaked in 200 ml of the inoculum for 20 seconds and then rolled through a mechanical roller press (ATLAS, sku #AT01) to allow for infiltration of the inoculum throughout the membrane structure. These membranes were then hung from a stainless steel scaffolding system by plastic loops such that the membranes are 1 cm below a 1/16" irrigation dripper and are spaced 5 cm apart from one another. In addition to the ten

membranes that are inoculated, an additional membrane is placed at either side of the ten membranes such that the ten membranes experience equal lighting. The membranes are illuminated with an LED array consisting of seven 60 cm LED strips (Mouser Electronics, 901-SB-6500-TR) spread 3 cm apart which is placed 8 cm above the membranes and provides a light intensity of 200 $\mu mol*m^{-2}s^{-1}$ measured at the top of the membranes on a 16 hours-on/8-hours-off light cycle. The set of 10 *P. kessleri* membranes were placed on a shelf within a 75x75x40 cm growth chamber with an aeration rate of 1 vol/hr and a temperature of 24-27˚C with a relative humidity of 96-99%. The sets of ten membranes in total were irrigated with 5.7 liters of media per day using a peristaltic pump (Masterflex, HV-07522-20). The volume from the pump to the ten membranes is 4 mL/min and is administered 8 mL every 2 minutes at a flow rate of 60 mL/min. Following inoculation, the membranes are harvested using the mechanical roller press every 3-4 days and the effluent is collected for subsequent evaluation. The algal biomass was stored at -80˚C prior to freeze drying to remove all water. Freeze-dried algae was stored in a sealed opaque plastic container at -20˚C prior to analysis.

2.1.2   Processing

The centrifuged algae concentrates obtained from Dr. Dave Bushek, Rutgers were freeze dried (Labconco, 4.5 L lyophilizer system, Kansas City, MO). The yields of algae biomass collected in this manner are shown in Table 2-1.

Table 2-1. Yield of algal biomass from freeze-drying process

Strain	Centrifuged Volume	Dry weight	Yield (m/v)
Isochrysis galbana **(Caribbean strain) aka C-iso**	284mL	12.0619g	4.2%
Isochrysis galbana **(Tahitian strain) aka T-iso**	10mL	0.468g	4.6%
Pavlova lutheri	52mL	7.0885	13.6%
Chaetoceros neogracile	5mL	0.284g	14.2%
Chaetoceros calcitrans	10mL	0.500g	5.0%
Tetraselmis chuii	5mL	0.161g	3.2%

2.2 Fatty Acid Content

Due to the high content of fatty acids in marine algae, many species of algae have been investigated; however the bulk of the available literature focuses on the utilization of algal biomass for biodiesel applications. As is discussed in detail earlier (See sections 1.1.1 and 1.3.3) there is strong evidence linking omega-3 fatty acid derivatives to cardiovascular, inflammatory, and other health benefits. As such, a thorough investigation of the algal biomass relative to fatty acids including these unique ones were examined for this project.

2.2.1 Method Development

Typically for plant and animal samples, to measure total fatty acid content one extracts the lipid materials with a nonpolar solvent such as chloroform or hexane using Soxhlet extraction, followed by concentration of the lipid extract. Due to the nonpolar nature of the lipid material, gas chromatography (GC) is employed for analysis. However, due to the instability of many fatty acids, a derivatization procedure is employed to convert the fatty acids to esters, allowing for facile separation, identification, and quantitation by GC using

flame ionization detection. However, due to different nature of lipids found in microalgae, non-polar extraction is inefficient.

Unlike animals and plants which store fats as triglycerides, fatty acids contained within microalgae are typically found in polar lipid forms, such as phospholipids and galactolipids. Phospholipids are the major component of cellular membranes and consist of two fatty acids connected via ester bond to glycerol, possessing a phosphate group on the remaining hydroxyl group. A variety of functional moieties can be found attached to the phosphate group. Galactolipids consist of two fatty acid esters to glycerol, with one or more galactoside groups attached to the remaining glycerol hydroxyl. Phospholipids and galactolipids are significantly more polar than their corresponding triglyceride relatives, and as such require specific considerations for extraction and analysis.

Due to the specific chemical nature of the fatty acids derived from algae species, the majority of methods cited in the literature have been developed for use on fish oils[4-10] and are thus inadequate for a matrix which is as compositionally different as algae, without subsequent validation and in our hands were insufficiently reproducible for our use. As such, using NIH guidelines for the study of natural products which we developed for botanicals, we first needed to optimize and then validate a method specifically for authenticate algae matrices, where water content is a major concern, and a variety of fatty acid conjugates exist bound in cell membranes and organelles.

Fatty acids cannot be accurately quantified directly due to the instability of free carboxylic acids, as well as thermal instability of conjugated forms, so typically they are derivatized

as esters prior to analysis[5,7,8]. This transformation step introduces a new opportunity for error, and must be carefully optimized and validated to ensure results are accurate. There are several aspects that must be considered for the successful quantitation of fatty acids in algae, and progress toward the optimization of each step is discussed below.

2.2.1.1 Extraction

Quantitative extraction of the analytes into a medium suitable for transformation into derivatives for GC analysis is a crucial step that must be carefully optimized to ensure that the analytes are completely extracted for subsequent measurement. Incomplete extraction will lead to a result that reports a lower than accurate quantity of fatty acids.

Two major methods that are widely cited in the literature are the Folch method (Folch et al., 1957)[4], which employs 2:1 Chloroform-Methanol, and the Bligh and Dyer method (Bligh and Dyer, 1959)[5], which employs 1:2:0.2 Chlorofom-methanol-water. Nearly all lipid analyses employ a modification of one of these techniques, and the Folch and Bligh/Dyer method have accrued >50,000 and >35,000 citations, respectively. These methods are rapid and simple, designed for evaluation of triglycerides and phospholipids in a range of tissue. Through countless citations, this method has been employed in a wide range of tissues. Issues appeared to arise in the algal material due to the cellular wall restricting the ability of phospholipids to dissolve. To address this issue, a detailed quantitative comparison between the two techniques was undertaken by Iverson, Lang, & Cooper (2001)[6] in a broad range of marine tissues. They showed that the Bligh & Dyer method significantly underreports the lipid content in a number of marine tissues. Based

on these results, it was determined that optimization of lipid extraction would have to be performed specific to the algal biomass utilized in this project. Di-heptadecanoyl-phosphocholine (Chromadex, Irvine, CA) was chosen to utilize as an internal standard for validation of recovery. Each of these techniques was attempted as described by the authors multiple times, and also with a number of modifications.

Table 2-2. Results of Lipid Extraction Trials exploring Folch and Bligh-Dyer methods with varying conditions

	Heat	Stirring	Sonication	Comments	Recovery (%)
Folch	✔	✔	X	No modifications, heat and mechanical stirring – lack of reproducibility, time-consuming	65 ± 12.6%
Folch	X	X	✔	Folch method – sonication, no heat, no mechanical stirring – much better reproducibility	67 ± 4.4%
Folch	X	X	✔	Folch method – sonication, no heat, no mechanical stirring, first methanol added, sonicated, then chloroform added – no difference from above	63 ± 9.7%
Folch	X	X	✔	Folch method – sonication, 3x extracts combined – time consuming, higher recovery	85 ± 11.1%
Bligh-Dyer	✔	✔	X	Bligh-Dyer – no modifications, heat and mechanical stirring – emulsion formation severely limited scale, difficult to dry extracts	58 ± 15.5%
Bligh-Dyer	X	X	✔	Bligh-Dyer – sonication, no heat – still emulsions formed when trying to separate layers – lack of reproducibility	81 ± 9.9%
Bligh-Dyer	X	X	✔	Bligh-Dyer – sonication, repeated extraction with chloroform – still emulsions formed, improved results	88 ± 6.7%

	Heat	Stirring	Sonication	Comments	Recovery (%)
Bligh-Dyer	X	X	✓	Bligh-Dyer – sonication, centrifugation to break emulsion – finally seemed to work properly, reproducible results – however extracts contain some water and requiring drying before subsequent steps.	91 ± 5.9%

From the results generated and illustrated in Table 2-2, a wide number of issues arose due to formation of emulsions and remaining water in the extractions. The most efficient extraction of lipids was obtained utilizing the Bligh/Dyer approach by centrifugation to break the emulsions. While this technique was effective for single sample trials, due to the practical complexity, it was not amenable to large numbers of samples utilized during growth optimization experiments. Due to these issues with the extractions, it was theorized that the extraction/esterification step could be combined in order to achieve simpler and more robust analytical procedure.

2.2.1.2 Transesterification

In order to prepare the fatty acids from the algae for analysis, they must first be chemically esterified, converting them into what is essential biodiesel for their analysis by GC. This step is also crucial, as any lipids which are not rendered entirely as their esters will be underestimated by the analysis. Water is a major concern in this reaction, since any water drives the reaction towards incompletion. Choice of reaction conditions and catalyst is also critical to ensure complete solubility of lipid conjugates in reaction medium. Due to the complexities involved with lipid extraction, it was decided to develop

a one-step technique to derivatize the fatty acids for subsequent GC analysis. A number

of conditions were tested on the course to optimize this reaction. Di-heptadecanoyl-

phosphocholine (Chromadex, Irvine, CA) was chosen to utilize as an internal standard for

validation of recovery. A summary of the experiments is shown in Table 2-3.

Table 2-3. Methodology and results for various transesterification methods used to derivatize algal biomass.

BF$_3$/Methanol

- BF$_3$/Methanol, 70˚C, sealed in a vial with rubber septum and phenolic cap: Resulted in decomposition of the septum and cap, resulting in a loss of pressure and evaporation of solvent
- BF$_3$/Methanol, 70˚C, sealed in a vial with a PTFE septum and a screw-on cap (ReactiVial): No problems with cap or septum, however reaction did not go to completion after 2 hours. Clear evidence of decomposition of the glass by HF, indication of water reacting with BF$_3$ during reaction.
- BF$_3$/Methanol, 85˚C, sealed under N$_2$, 1 hour: No problem with decomposition of reagent anymore, however reaction did not proceed past 20% completion (by internal standard via GC-FID)
- BF$_3$/Methanol, 85˚C, sealed under N$_2$, 3 hours: No problem with decomposition of reagent anymore, however reaction did not proceed past 20% completion (by quantity of internal standard)
- BF$_3$/Methanol, 85˚C, sealed under Ar, 3 hour: No problem with decomposition of reagent anymore, however reaction did not proceed past 20% completion (by quantity of internal standard)

Methanol/HCl

- 5% HCl/methanol (purchased from Sigma-Aldrich, several months old) – sealed under N$_2$ in a capped culture tube heated to 60˚C – no problems with degradation of reaction vial, although reaction only went to 70% completion.
- This reaction was repeated with temperatures ranging from 60-95C, varied reaction times from 30mins to 5 hours, but the highest recovery was 75%.

Methanol/AcCl

- This reaction gave much higher recoveries (~75%) however still too low for validation.
- Solubility appears to be an issue with this reaction, as particulates of algae extract can be observed around the edges of the reaction vial. It was theorized that poor solubility of algal biomass was causing incomplete reaction.
- The reaction was repeated with the incorporation of toluene as a co-solvent. Finally, the reaction yielded completion (98-102%) by GC analysis.

The most commonly cited techniques for derivatization of fatty acids to esters for analysis by GC employ the utilization of solutions of BF_3 in Methanol, based on the original method described by Metcalfe & Schmitz (1961)[7]. This technique has been thoroughly employed for the analysis of omega-3 fatty acids in fish oil, which owes in large part to the >1500 citing articles employing this technique. While this technique is highly effective for usage on purified triglycerides, it proved problematic in usage with the complex matrix of freeze-dried algal biomass. It was apparent from etching of the glass vial during the reaction that excess hydroxyl content contained in the biomass in the form of proteins, starches, and nucleic acids was reacting with BF_3 to release fluoride ion *in situ*. As such, it was decided to abandon usage of BF_3 for esterification of algal biomass.

The next most popularly utilized technique for the conversion of fatty acids to esters involves the usage of dry HCl dissolved in methanol to effect transesterification[8]. In algae, this method is commonly employed for evaluation and comparison of fatty acid lipid profiles[9]. This technique proved more reliable than the BF3 technique, however due to the hygroscopicity of the methanolic HCl, the reaction did not go to completion. As such, it was decided to prepare methanolic HCl fresh prior to analysis by decomposition of AcCl

in methanol. While results were improved slightly, it appeared that incomplete solvation of algal biomass was preventing access to phospholipid retained in vesicles. We hypothesized that the use of a nonpolar co-solvent such as benzene or toluene could substantially increase the recovery for this analytical derivatization by better solubilizing lipid and membrane structures for the reaction. A review of techniques in the literature showed this technique is effective at evaluating fatty acids from foodstuffs and feces[10]. This hypothesis was then confirmed by the addition of 40% toluene (v/v) into the reaction mixture, which gave complete recovery of the analytical standard. This method was selected for the evaluation of fatty acid content in the algal biomass utilized in this project.

2.2.2 Methodology

2.2.2.1 One Step Extraction and Derivatization of Fatty Acids

Six 2x20cm culture tubes and a 25mL volumetric flask, and a 50mL Erlenmeyer flask were rinsed with methanol and dried in an oven at 105˚C overnight. The glassware was removed from the oven and placed in a $CaCl_2$ desiccator to cool to room temperature before use. 97.1mg diheptanoyl-phosphocholine acid (di-17:0-PhoCho) was diluted to 25.00mL with toluene (3.884mg/mL) and used as an internal standard to validate recovery.

Approximately 50mg freeze-dried algal sample was added quickly to each culture tube, followed by 1.00mL internal standard solution (3.884mg/mL in toluene), and 1.00mL toluene. 3.00mL freshly prepared methanolic HCl was added, followed by a magnetic

stirbar. The samples were very gently vortexed to avoid splashing sample on the side of

the vials. The culture tubes were flushed with N_2 (atmospheric pressure) and sealed

tightly. The sealed culture tubes were placed in a water bath at 80˚C for 3 hours with

magnetic stirring. Periodically the reaction vials were checked for leaks. Tubes which

leaked were not included in subsequent analyses.

The reaction tubes were removed from heat and allowed to come to room temperature.

5.00mL Na_2CO_3 solution (6% m/v) was added, followed by 2.00mL toluene. The resultant

biphasic mixture was thoroughly vortexed (~30 seconds). The tubes were centrifuged to

settle the emulsion. Approximately 2mL of the clear brown/yellow upper layer (toluene

layer) was aliquoted and dried over Na_2SO_4. The dried solutions were placed in amber

autosampler vials and analyzed immediately by GC-FID. All samples were repeated in

triplicate.

2.2.2.2   Two-step extraction and esterification

Approximately 50mg freeze-dried algal biomass was added to 10mL glass centrifuge

tubes. 1.00mL 2:1 chloroform/methanol (v/v). The tube was capped with a red-rubber

septum, and placed in the sonicator bath for 5 minutes. The sonicated extracts were

centrifuged (add speed and make of unit), and the liquid was decanted. The algal cake

was broken up and re-sonicated in an additional 1.00mL 2:1 chloroform/methanol. The

extract was centrifuged, and the liquid was combined with the previous extract. The

combined extracts were dried under N_2 at 35˚C. The extracts were dried in a vacuum

desiccator overnight. 1.00mL internal standard solution (3.884mg/mL di-heptanoyl-

phosphocholine in toluene) was added to the lipid extracts with an additional 1.00mL toluene and 0.5mL anhydrous methanol. This solution was transferred to a dried culture tube.

3.00mL freshly prepared methanolic HCl was added, followed by a magnetic stirbar. The samples were very gently vortexed to avoid splashing sample too high on the side of the vials. The culture tubes were flushed with N_2 (atmospheric pressure) and sealed tightly. The sealed culture tubes were placed in a water bath at 80˚C for 3 hours with magnetic stirring. Periodically the reaction vials were checked for leaks. Tubes which leaked were not included in subsequent analyses.

The reaction tubes were removed from heat and allowed to come to room temperature. 5.00mL Na_2CO_3 solution (6% m/v) was added, followed by 2.00mL toluene. The resultant biphasic mixture was thoroughly vortexed (~30 seconds). The tubes were centrifuged to settle the emulsion. Approximately 2mL of the clear brown/yellow upper layer (toluene layer) was aliquoted and dried over Na_2SO_4. The dried solutions were placed in amber autosampler vials and analyzed immediately by GC-FID. All samples were repeated in triplicate.

2.2.2.3 GC-FID analysis for fatty acid methyl esters

All analyses for the quantitation of fatty acid methyl esters (FAMEs) utilized the same gas chromatograph program, described herein. All samples were repeated in triplicate. 0.5 μL toluene FAME solution was injected on an HP1125 Gas Chromatograph with Flame Ionization Detector (FID), using a 1:25 split injection. The column used was an Alltech EC-

WAX, 30m, 0.25 mm I.D., 0.25 μm film. The inlet was set at 220 ˚C, Helium carrier gas flow set at 71.8 kPa, 23.7 mL/min. The following temperature gradient was employed which provided adequate separation of all fatty acids: Initial temperature, 60˚C, hold 1 min; 10 ˚C/min to 220˚C, hold 23 min, 5˚C/min to 240 ˚C, hold for 16 minutes.

2.2.3 Results and Discussion

2.2.3.1 *Comparison of One-Step and Two-Step Extraction/Derivatization*

Pavlova lutheri was selected for the comparison of the one and two-step extraction/derivatization methods. The results of the fatty acid analysis for the one-step extraction/derivatization is shown in Table 2-4. The one-step method exhibited excellent recovery (98 ± 1.4%) compared to the two-step (~80%), and as such, the one-step method reported higher quantities of fatty acids than the two-step by 1.13% of freeze-dried biomass (Table 2-5).

Table 2-4. Results of one step extraction/derivatization of fatty acids in *Pavlova lutheri*

ID	Common name	% of total FAs	% dry weight	Absolute Deviation	RSD
14:0	Myristic	14.95%	1.202%	0.045%	1.77%
16:0	Palmitic	17.45%	1.402%	0.001%	0.10%
16:1n7	Palmitoleic	13.86%	1.114%	0.001%	0.07%
18:1n7	Oleic	1.25%	0.100%	0.037%	0.37%
18:2n6	Linolenic	2.08%	0.167%	0.001%	0.62%
18:3n3	Alpha linolenic	2.39%	0.192%	0.001%	0.48%
18:4n3	Stearidonic	5.68%	0.456%	0.002%	0.45%
20:5n3	Eicosapentaenoic (EPA)	32.86%	2.640%	0.010%	0.37%
22:6n3	Docosahexaenoic (DHA)	9.49%	0.762%	0.008%	1.08%
	Total	100.00%	8.035%	0.066%	
	Total omega-3	50.421%	4.051%		Recovery

ID	Common name	% of total FAs	% dry weight	Absolute Deviation	RSD
	Total omega-6	2.08%	0.167%		98 ± 1.4 %
	Total unsat'd	67.602%	5.432%		
	Total Saturated	32.398%	2.603%		

Table 2-5. Comparison of one-step and two-step methods for quantitation of fatty acids in Pavlova lutheri

ID	Percentage total FA	Average % composition	RSD	Difference from one step method
14:0	14.20%	0.991%	2.25%	-0.210% *
16:0	16.76%	1.170%	1.95%	-0.232% *
16:1n7	13.27%	0.926%	2.38%	-0.188% *
18:1n7	1.25%	0.087%	3.68%	-0.013%
18:2n6	2.04%	0.142%	10.27%	-0.025% *
18:3n3	2.37%	0.165%	1.16%	-0.027% *
18:4n3	5.78%	0.403%	1.39%	-0.053% *
20:5n3	35.26%	2.461%	1.96%	-0.179% *
22:6n3	9.07%	0.634%	7.73%	-0.129% *
Total	100.00%	6.906%	2.31%	-1.129% *
Total omega-3	52.480%	3.663%		
Total omega-6	2.04%	0.14%		**Recovery of IS**
Total unsat'd	69.039%	4.819%		**79% ± 6.5%**
Total Sat'd	30.961%	2.161%		

* statistically significant difference ($p < 0.05$), determined by two-tailed, unpaired t-test

The fatty acids were underrepresented in all classes using the two-step method; a 20% relative decrease in each fatty acid was found with respect to the one-step method. This is consistent with the recovery found for the two-step technique, which was found to be 79 ± 6.5%. There was clear evidence that the one-step technique was superior to the two-step technique for the quantitation of fatty acid content in freeze-dried algae biomass.

2.2.3.2 Validation of Method

The GC/MS method and instrument used in this study exhibited excellent separation of the fatty acids contained within the algal biomass. A representative flame ionization detector (FID) chromatogram is shown in Figure 2-1. This method demonstrated excellent peak shape, and good separation for all major fatty acids contained within algae biomass. Retention time reproducibility was excellent, as well as peak area precision.
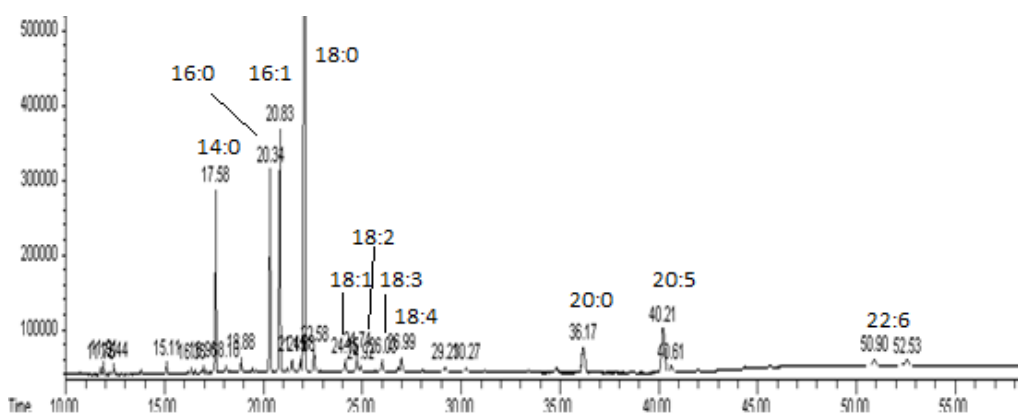
Figure 2-1. Representative GC-FID chromatogram of *Chaetoceros negracile* fatty acids

In order to validate recovery and precision of this method, Di-heptadecanoyl-phosphocholine was selected for use in spiked recovery experiments. A calibration curve was constructed for the peak response of heptadecanoic acid methyl ester spanning 200 µg/mL to 48.8 ng/mL which showed excellent linearity (0.9998) across this range. The sensitivity and linearity characteristics for the calibration curve are shown in Table 2-6. The limit of detection (LOD) was determined to be 6.1 ng/mL; the limit of quantitation (LOQ) was determined to be 20.3 ng/mL (n = 6).

Table 2-6. Sensitivity, linearity, accuracy, precision, and ruggedness for one-step extraction, derivatization and GC analysis.

Linear range	LOD	LOQ	Slope (ng*mL^{-1}/Area)	Intercept	R^2
48.8 ng/mL - 200 µg/mL	6.1 ng/mL	20.3 ng/mL	0.0131	8.19	0.9998

Single-operator Intraday precision (n=6)*				Inter-day, Inter-operator precision (n=6)*			
Added (ng)	Found (ng)	Recovery (%)	RSD (%)	Added (ng)	Found (ng)	Recovery (%)	RSD (%)
202.1	201.4 ± 4.3	99.6	2.13	211.0	206.7 ± 10.3	97.9	4.97
99.8	100.4 ± 2.4	100.6	2.39	104.2	105.3 ± 5.5	101.0	5.22
54.3	53.4 ± 1.2	98.3	2.27	51.2	49.8 ± 3.6	97.2	7.22

* Validated by spiking with diheptadecanoyl-phosphocholine.

Varying concentrations of the synthetic phospholipid were spiked into algae biomass prior to analysis in order to evaluate precision and accuracy. The precision and accuracy were excellent with the one-step technique. Intraday precision for single-operator analysis was 2.13-2.39%; recoveries ranged from 99.6-100.6%, demonstrating the high degree of accuracy achieved across a range of concentrations when using this method. Ruggedness of this method was also evaluated between two operators on different days of analysis. The ruggedness of this method was not quite as good as with single operator analysis, although still showed good inter-operator precision: RSD of recovery ranged from 4.97-7.22%. The inter-operator accuracy was excellent, ranging from 97.2-101.0% recovery.

2.2.3.3 Fatty acid content

Using the technique developed and validated in the prior sections, the fatty acid content of all algae strains was evaluated. The results are itemized in Table 2-7 and graphically depicted in Figure 2-2. *P. lutheri* contained the highest content of saturated fatty acids, with 2.60% by mass, consisting of 1.40% hexadecanoic acid (16:0) and 1.20% tetradecanoic acid (14:0). Long chain saturated fatty acids 24:0 and 22:0 were detected only in *Chaetoceros sp.* The saturated stearic acid (18:0) was only detected in significant quantities in *P. kessleri* (0.24%).

Palmitoleic (16:1n7) and oleic (18:1n9) acid were present in all algal samples tested, the highest content found in *P. kessleri*. Only *I. galbana* (C-iso), *C. calcitrans*, and *P. kessleri* were found to contain myristoleic acid (14:1n5), although in trace amounts excepting *P. kessleri*. Linoleic acid (18:2n6) was found in all samples; *P. kessleri* had the highest content of linoleic acid by a large margin, with 3.99 ± 0.069% by weight. Alpha linolenic acid (18:3n3) was also present in the highest quantity in *P. kessleri* (2.27 ± 0.037%).

As expected, long chain (>18 carbons) polyunsaturated fatty acids were only detected in the marine species. The well-known and commercially available Docosahexaenoic acid (DHA, 22:6) was detected in every species of marine algae tested. *P. lutheri* contained the highest content of DHA, with 0.76%. Eicosapentaenoic acid (EPA, 20:5) was detected in every species although only trace amounts were detected in the two strains of *I. galbana*. The marine species with the highest content of Omega-3's was *P. lutheri*, which contained a total of 4.22% by mass Omega-3's. Eicosatrienoic acid was detected only in *Chaetoceros*

neogracile and *Chaetoceros calcitrans* at approximately the same quantities (0.41% and

0.48% respectively). Stearidonic acid (18:4n3) was detected in every marine species, but

was not detected in *P. kessleri. Isochrysis galbana* (C-iso) contained the highest content

of stearidonic acid at 1.19 ± 0.014%. All marine species had >10x omega-3s compared to

omega-6s. *P. kessleri* had an omega-6 to omega-3 ratio of approximately 1.76.

Table 2-7. Absolute fatty acid content of all six algal species used in this project

Fatty Acid	*Isochrysis galbana* (C-iso)[A]	*Isochrysis galbana* (T-iso)[A]	*Pavlova lutheri*[A]	*Chaetoceros neogracile*[A]	*Chaetoceros calcitrans*[A]	*Parachlorella kessleri* (PK-T)[A]
14:0	0.61 ± 0.060	0.41 ± 0.017	1.20 ± 0.045	0.75 ± 0.036	1.16 ± 0.104	0.29 ± 0.013
16:0	0.36 ± 0.015	0.48 ± 0.019	1.40 ± 0.001	1.03 ± 0.023	0.36 ± 0.004	1.69 ± 0.021
18:0	-	-	-	0.04 ± 0.001	0.03 ± 0.001	0.26 ± 0.003
22:0	-	0.04 ± 0.000	-	0.04 ± 0.001	0.03 ± 0.000	-
24:0	-	-	-	0.06 ± 0.002	0.04 ± 0.001	-
Saturated	*0.97*	*0.93*	*2.60*	*1.92*	*1.62*	*2.24*
14:1n5	0.02 ± 0.001	-	-	-	0.05 ± 0.01	0.22 ± 0.013
16:1n7	0.24 ± 0.011	0.13 ± 0.011	1.11 ± 0.001	1.37 ± 0.04	0.98 ± 0.05	0.86 ± 0.003
18:1n9	0.21 ± 0.002	0.48 ± 0.016	0.10 ± 0.000	0.04 ± 0.003	0.09 ± 0.002	0.81 ± 0.031
20:1n9	0.17 ± 0.001	0.06 ± 0.002	-	-	0.06 ± 0.003	-
Monounsat'd	*0.65*	*0.67*	*1.21*	*1.41*	*1.17*	*1.89*
18:2n6	0.2 ± 0.000	0.10 ± 0.003	0.17 ± 0.001	0.06 ± 0.002	0.12 ± 0.004	3.99 ± 0.069
18:3n3	0.42 ± 0.003	0.22 ± 0.008	0.19 ± 0.001	-	0.11 ± 0.009	2.27 ± 0.037
18:4n3	1.19 ± 0.014	0.71 ± 0.013	0.46 ± 0.002	0.06 ± 0.005	0.41 ± 0.021	-
20:3n3	-	-	-	0.41 ± 0.014	0.48 ± 0.047	-
20:5n3	0.05 ± 0.003	0.04 ± 0.003	2.64 ± 0.010	1.00 ± 0.032	0.89 ± 0.124	-
22:6n3	0.5 ± 0.045	0.63 ± 0.010	0.76 ± 0.008	0.09 ± 0.003	0.19 ± 0.003	-
Polyunsat'd	*2.35*	*1.69*	*4.22*	*1.62*	*2.19*	*6.25*
Omega-3	2.15	1.59	4.05	1.56	2.08	2.27
Omega-6	0.20	0.10	0.17	0.06	0.12	3.99
6/3 ratio	0.09	0.06	0.04	0.04	0.06	1.76
Total	**3.97**	**3.28**	**8.03**	**4.95**	**4.98**	**10.33**

[A] content of fatty acids as % of freeze dried weight
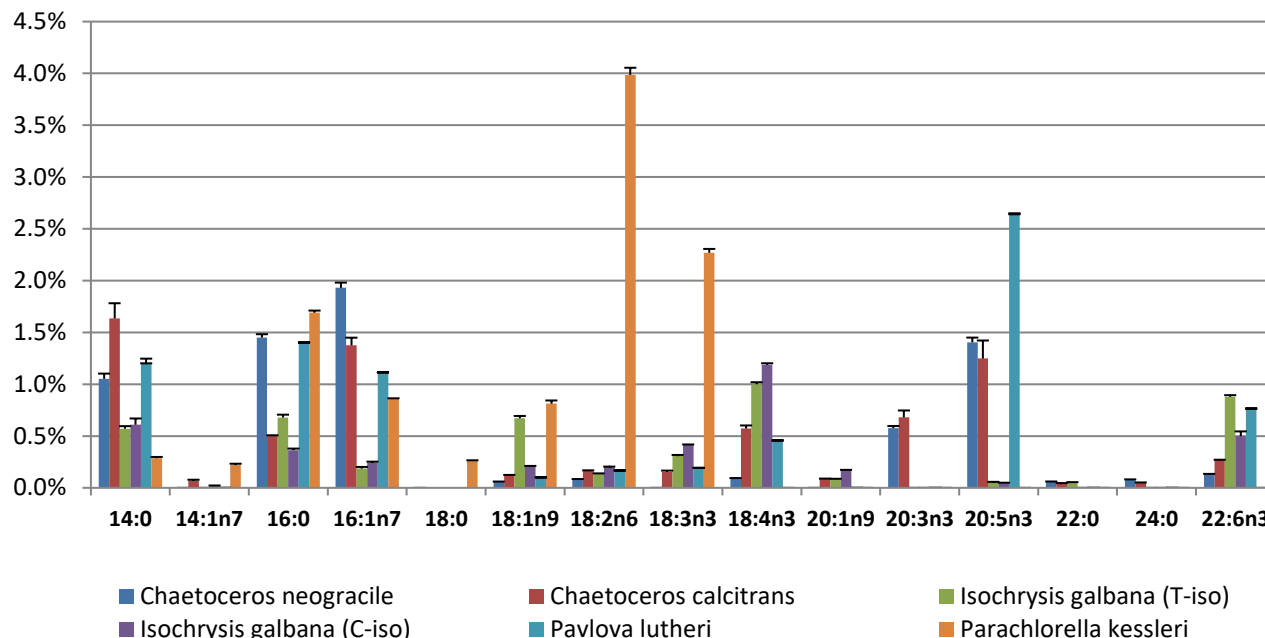
Figure 2-2. Absolute fatty acid content of six algal species used in this project

Parachlorella kessleri exhibited a unique fatty acid profile due to the fact that it is the sole freshwater algae evaluated. Very few freshwater algae have been reported to contain long-chain (≥ 20 carbons) fatty acids. *P. kessleri* contained the highest content of fatty acids per dry weight, at 10.33%. The highest content of omega-3 fatty acids was detected in *P. kessleri*—the two omega-3 fatty acids contained in *P. kessleri* were linoleic acid, at 3.99 ± 0.069% of dry weight, and α-linolenic acid at a content of 2.27 ± 0.037% of dry weight. Together these fatty acids represent 3/5 of the total content of fatty acids. Linoleic acid and linolenic acid are essential to human (and animal) nutrition because they cannot be synthesized and must be consumed in all diets. See section 1.1.1 for a complete review of the importance of linoleic acid and α-linolenic acid to diet and nutrition. Additionally, linoleic acid and α-linoleic acid were identified as active constituents in *P. kessleri* responsible for anti-inflammatory activity via COX-2 inhibition (See section 5.3.2

for a thorough discussion).   Furthermore, *P. kessleri* contained the highest content of saturated fats by mass, at 2.24% consisting of myristic acid (14:0) at 0.29 ± 0.013%, palmitic acid (16:0) at 1.69 ± 0.021, and stearic acid (18:0) 0.26 ± 0.003% by mass of dry weight. Finally, *P. kessleri* possessed the highest content of mono-unsaturated fatty acids at 1.89%, comprising of myristoleic acid (14:1n5) at 0.22 ± 0.013%, palmitoleic acid (16:1n7) at 0.86 ± 0.003%, and oleic acid (18:1n9) at 0.81 ± 0.031% of dry weight. Based on these results, there is support for the role of marine and freshwater algae utilized in this study as nutritious sources of bioactive fatty acids.

2.3   Carotenoids

β-carotene and other carotenoids are a critical aspect of nutrition and health due to their facile conversion to vitamin A in the body. Carotenoids are the major source of vitamin A in non-animal foods. The role of carotenoids in nutrition and health has been described earlier (See section 1.1.2). Typically, the analysis of carotenoids is accomplished using spectrophotometric techniques, due to the unique UV-Vis absorption spectra that is characteristic of carotenoids. The technique for measuring total carotenoid content involves hydrolysis and subsequent extraction into non-polar solvent[11]. Quantitation is accomplished by the construction of a calibration curve correlating the absorption in the UV-Vis spectrum to the concentration of commercially available β-carotene. However, this method has major drawbacks, since interfering pigments can cause over-representative results, and so many researchers have developed techniques utilizing High Performance Liquid Chromatography (HPLC); and at the same time, when only using one

carotenoid to estimate total carotenoids it could under represent the actual values. Original methods typically utilize normal phase conditions due to the high lipophilicity of carotenoids[12,13,14]. There are major drawbacks to utilizing normal-phase conditions for modern HPLC equipment without major modifications to the seals and gaskets such that the harsh organic solvents utilized in normal phase do not destroy the mechanical apparatus. Since our lab uses HPLCs optimized to reverse-phase conditions, and our ESI-MS is especially unsuited to normal phase conditions, it was decided to extend our search of the literature to find a method optimized for reverse-phase conditions suitable for our HPLC/MS. Additionally, it was decided to utilize a method amenable to MS analysis so that subsequent characterization of xanthophylls and other pigments could be accomplished.

While an exhaustive review of current methodology in chromatographic techniques used in carotenoid analysis is outside the scope of this dissertation, an excellent review was published by de Quirós and Costa (2006)[15]. By comparing methodology which utilized acceptable solvents (acetonitrile, methanol, water, and small volumes of organic solvent such as methyl-tert-butyl ether) and acceptable stationary phases (C8, C18, C30), it was determined that the usage of methanol and aqueous ammonium acetate was a common feature of successful methodology[16,17], in some cases accompanied by more non-polar solvents[18], isopropanol[19], or methyl $tert$-butyl ether (MtBE)[20,21]. After a careful review, we was opted to utilize the C30 phase column for optimum separation of pigments, with tertiary mobile phase gradient of 0.1% NH_4OAc in H_2O, methanol, and MtBE.

2.3.1 Methodology

Approximately 25 mg freeze-dried algal samples were added to a 10 mL glass centrifuge tube. Samples were extracted 3x with 5 mL 1:1 Acetone/MtBE. Combined extracts were freed of solvent under reduced pressure. Dried extracts were re-dissolved into 1.00 mL 1:1 Acetone/MtBE, centrifuged to remove particulates, and stored immediately in amber autosampler vials. Samples were analyzed the same day of preparation, and extra care was taken to minimize the exposure to light and oxygen. A calibration curve for β-carotene was constructed using a reference standard solutions spanning a concentration range of 42.5 μg/mL to 41.5 ng/mL (R^2 = 0.9997). The limit of detection for this method is 5.18 ng/mL, with a limit of quantitation is 41.5 ng/mL.

HPLC samples were prepared by filtering each extract through a 0.4 μm nylon syringe filter into an amber HPLC autosampler vial. HPLC separation was performed on an YMC-C_{30} Carotenoid column, 250 x 4.6 mm, 5 μm (Phenomonex Inc., Torrence, CA). For LC-MS analysis, a Hewlett Packard Agilent 1100 Series LC/MS (Agilent Technologies, Waldbronn, Germany) equipped with autosampler, quaternary pump system, DAD detector, degasser, MSD trap with an electrospray ion source (ESI) was applied, and software HP ChemStation was used for data processing. The HPLC mobile phase contains solvent A (0.2% acetic acid with 0.1% NH_4OH in water) and B (Methanol with 0.1% formic acid) and C (MtBE with 0.1% formic acid) in gradient shown in Table 2-8. The flow rate was set at 0.8 mL/min with a 1:10 splitter after the output of the UV detector leading ~100 μL/min to the ESI-MS. The UV detector was set at 210, 254, 280, 370, 450 nm. The eluent was monitored by electrospray ion mass spectrometer (ESI-MS) scanned from *m/z* 100 to

1200. ESI was conducted by using a needle voltage of -3.5 KV (negative mode). High purity

nitrogen (99.999%) was used as dry gas at a flow rate of 8 L/min and capillary temperature

was at 350°C. Nitrogen was used as nebulizer at 45 psi, and Helium as collision gas.

Table 2-8. HPLC gradient program used for the analysis of carotenoids in algal biomass

Time (min)	%A[1]	%B[2]	%C[3]
0	5	90	5
5	5	75	20
10	4	70	26
16	3	57	40
34	3	57	40
35	5	75	20

1. 0.2% acetic acid with 0.1% NH_4OH in water
2. Methanol with 0.1% formic acid
3. *tert*-butyl methyl ether (MtBE) with 0.1% formic acid

2.3.2   Results

The HPLC method selected for use demonstrated excellent separation and peak shape

(Figure 2-3). β-carotene eluted at 34.5 minutes, and was well separated from interfering

xanthophylls and chlorophyll pigments. β-carotene was identified by its characteristic

absorption spectrum, shown in Figure 2-4, and by comparison with retention time of

known standards. No other carotene isomers (α, γ, etc.) were detected. A representative

chromatogram is shown in Figure 2-5. The calibration curve constructed using

commercially available β-carotene demonstrated excellent linearity (0.9997) over a range

spanning 42.5 µg/mL to 41.5 ng/mL. The method provided excellent precision and results were obtained with very low relative standard deviations (<5%).
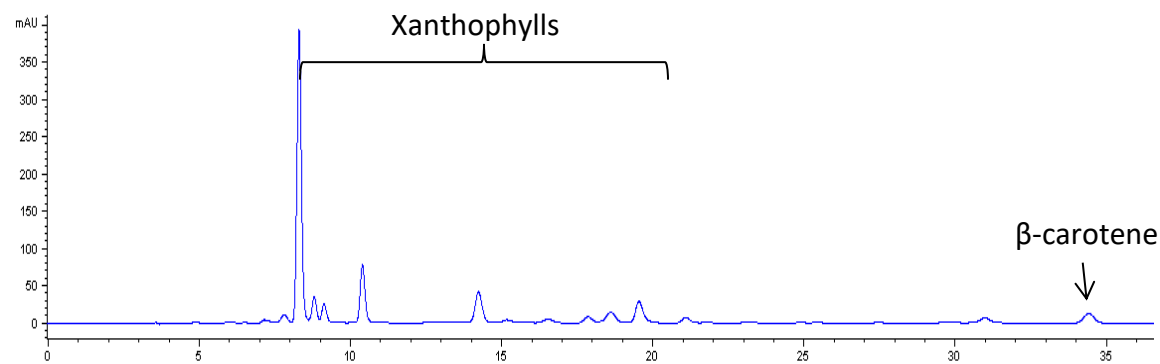
Figure 2-3. Representative UV-Vis chromatogram at 450 nm of pigment extract of *Parachlorella kessleri*
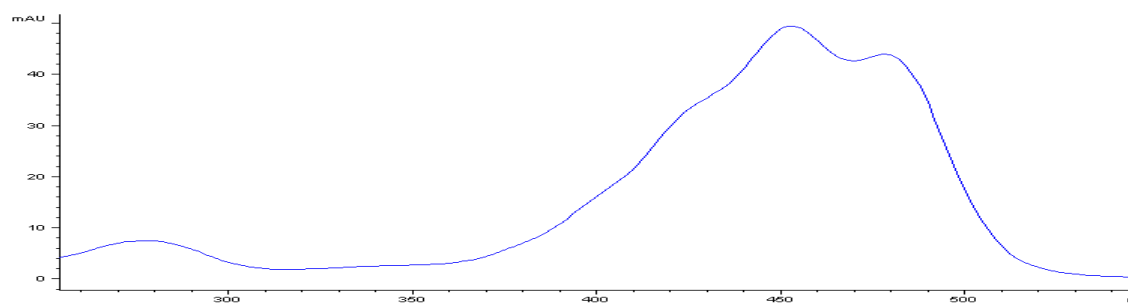
Figure 2-4. Characteristic UV-Vis spectrum of β-carotene

All species of algae tested contained high levels of β-carotene. The difference in the levels of β-carotene between samples was statistically significant ($p<0.05$). The marine species contained higher levels of β-carotene than the freshwater species (*Parachlorella kessleri).* *Pavlova lutheri* contained the highest content of β-carotene, at 315.1 ± 10.20 mg/kg. The strain with the second highest β-carotene content was C-iso, the Caribbean strain of *Isochrysis galbana,* which contained 292.6 ± 6.48 mg/kg. Interestingly, there was a

significant difference between the Caribbean and Tahitian strain of *I. galbana*; the Tahitian strain (T-iso), with 196.8 ± 5.51 mg/kg, contained 33% less β-carotene than C-iso. The reason for this difference remains unclear; however, it is likely related to harvesting factors. *Chaetoceros calcitrans* contained 139.4 ± 7.54 mg/kg, nearly 4x the quantity found in *Chaetoceros neogracile*, which contained 49.0 ± 1.12 mg/kg.

By comparison to common vegetables know to be rich in β-carotene such as spinach, carrots, lettuce, and sweet potato (Figure 2-5, data from USDA nutrient database[23]), the algal species had a substantial content of β-carotene. *Pavlova lutheri*, for example, contained nearly 6x more β-carotene per kg than raw spinach which is an excellent source of β-carotene[22]. Based on these results, in can be concluded that the algal biomass analyzed in this project is a rich source of β-carotene, and thus extracts derived from these species are nutritious sources of pro-vitamin A derivatives.
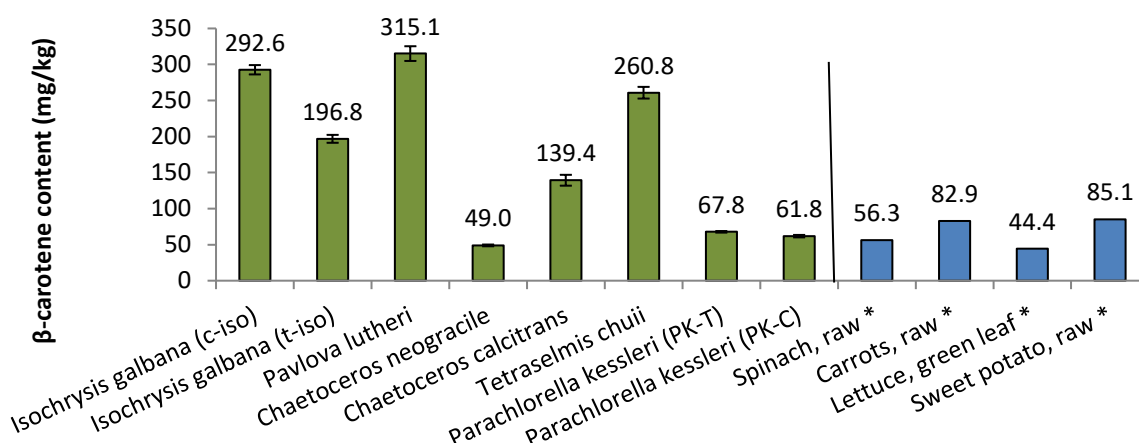
Figure 2-5. β-carotene content of algal species determined by HPLC analysis.
[*]Data obtained from USDA nutrient database[23].
All results showed statistical significance by two-tailed, unpaired student's t-test (p<0.05)

2.4 Tocopherols

The class of compounds that includes Vitamin E and derivatives are collectively known as the "tocopherols." Tocopherols are lipophilic vitamins which contain α-tocopherol, the specific form that is preferred for absorption in humans[24]. The structure of α-tocopherol is shown below in Figure 2-6. Tocopherols are an important vitamin and therefore an important aspect of diet—deficiency causes neurological problems such as spinocerebellar ataxia and myopathy, as well as anemia[25].
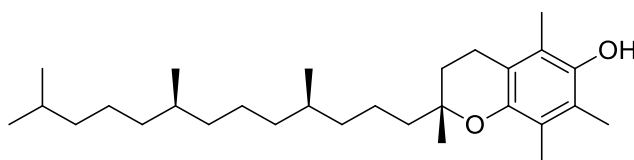
Figure 2-6. Chemical structure of α-tocopherol

Tocopherols have been implicated in a wide range of effects on human health, however there is an overall lack of agreement between clinical results for many of these reported effects. While vitamin E supplementation alone was not able to slow the progression or the development of age-related macular degeneration[26], however a protective effect was observed when vitamin E was combined with other antioxidants such as β-carotene and vitamin C[27]. The impact of Vitamin E supplementation on the onset of Alzheimer's disease has shown mixed effects. As reviewed and concluded by Frank and Gupta (2005)[28] some research has suggested vitamin E may reduce risk of developing AD, while other trials have found no clinical benefit. The impact of tocopherols on cancer also has shown a mixture of promising and negative results. One study correlated a higher intake of

tocopherols to a decreased incidence of prostate and breast cancer[29], however a recent study followed 18,000 women in NY and found no positive benefit from Vitamin E supplementation[30].

2.4.1 Methodology

It was found through development of methodology for the extraction and analysis of β-carotene (See section 2.3) that the tocopherol content contained within the algal biomass was readily extracted alongside the carotenoids. As such, the same methodology was applied for the quantitation of tocopherols in the algal biomass.

Approximately 25 mg freeze-dried algal samples were added to a 10 mL glass centrifuge tube. Samples were extracted 3x with 5 mL 1:1 Acetone/MtBE. Combined extracts were freed of solvent under reduced pressure. Dried extracts were re-dissolved into 1.00 mL 1:1 Acetone/MtBE, centrifuged to remove particulates, and stored immediately in amber autosampler vials. Samples were analyzed the same day of preparation, and extra care was taken to minimize the exposure to light and oxygen. A calibration curve was constructed for α-tocopherol using a reference standard solutions spanning a concentration range of 1020 μg/mL to 1.99 μg/mL (R^2 = 0.9992).

HPLC samples were prepared by filtering each extract through a 0.4 μm nylon syringe filter into an amber HPLC autosampler vial. HPLC separation was performed on an YMC-C_{30} Carotenoid column, 250 x 4.6 mm, 5 μm (Phenomonex Inc., Torrence, CA). For LC-MS analysis, a Hewlett Packard Agilent 1100 Series LC/MS (Agilent Technologies, Waldbronn, Germany) equipped with autosampler, quaternary pump system, DAD detector,

degasser, MSD trap with an electrospray ion source (ESI) was applied, and software HP

ChemStation was used for data processing. The HPLC mobile phase contains solvent A

(0.2% acetic acid with 0.1% NH_4OH in water) and B (Methanol with 0.1% formic acid) and

C (MtBE with 0.1% formic acid) in gradient shown in Table 2-8. The flow rate was set at

0.8 mL/min with a 1:10 splitter after the output of the UV detector leading ~100 μL/min

to the ESI-MS. The UV detector was set at 210, 254, 280, 370, 450 nm. The eluent was

monitored by electrospray ion mass spectrometer (ESI-MS) scanned from *m/z* 100 to

1200. ESI was conducted by using a needle voltage of -3.5 KV (negative mode). High purity

nitrogen (99.999%) was used as dry gas at a flow rate of 8 L/min and capillary temperature

was at 350°C. Nitrogen was used as nebulizer at 45 psi, and Helium as collision gas.

Table 2-9. HPLC gradient program used for the analysis of tocopherols in algal biomass

Time (min)	%A[1]	%B[2]	%C[3]
0	5	90	5
5	5	75	20
10	4	70	26
16	3	57	40
34	3	57	40
35	5	75	20

1. 0.2% acetic acid with 0.1% NH_4OH in water
2. Methanol with 0.1% formic acid
3. *tert*-butyl methyl ether (MtBE) with 0.1% formic acid

2.4.2 Results

The extraction and HPLC method utilized gave excellent peak shape and separation of the tocopherol derivatives detected in the algae biomass. The tocopherols in the extracts were identified by the characteristic UV-Vis spectrum of α-tocopherol, shown in Figure 2-7, obtained from a commercially available standard (Sigma-Aldrich, St. Louis, MO), and by the characteristic quasimolecular ion $(M+H)^+$ at 431.2 m/z.
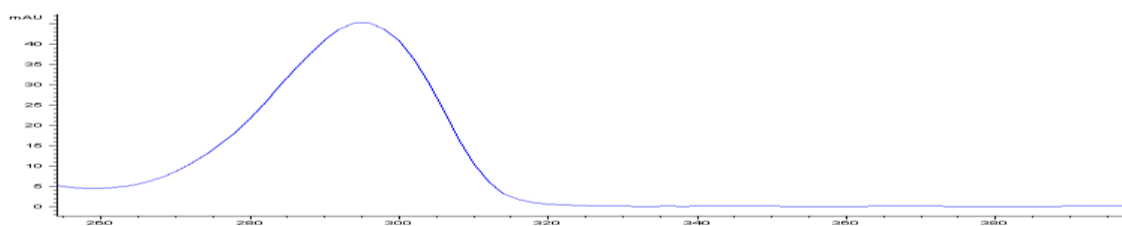
Figure 2-7. Characteristic UV-Vis spectrum of α-tocopherol exhibiting broad absorbance (λ_{max} = 295nm)
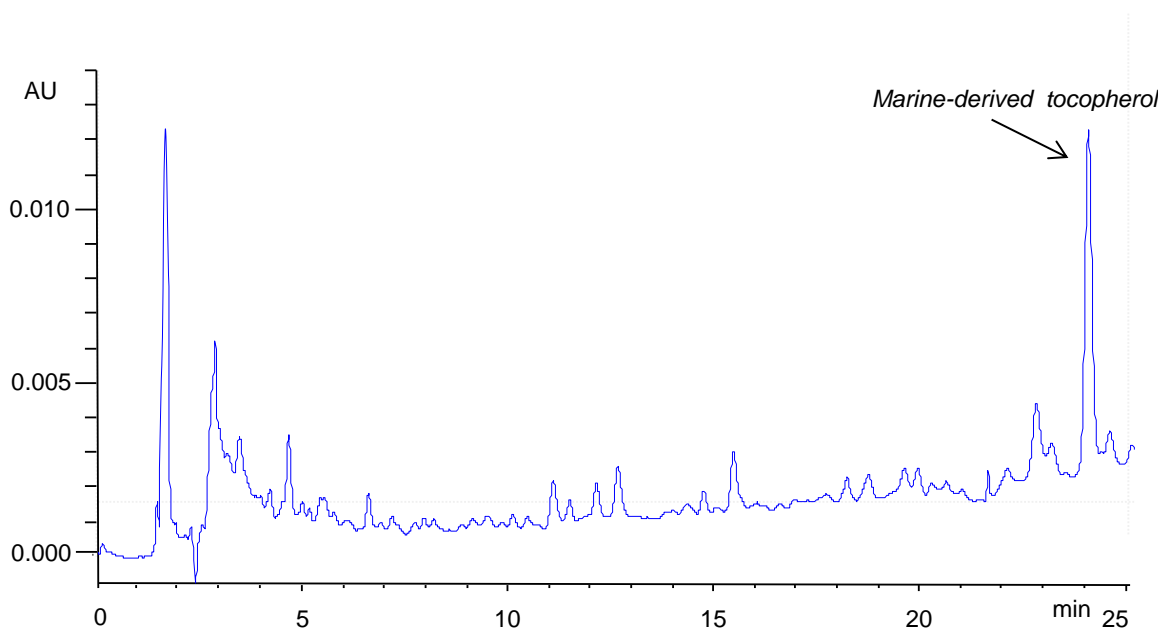
Figure 2-8. Representative UV-Vis HPLC chromatogram at 280 nm of α-tocopherol extract of *Isochrysis galbana* (C-iso)

Interestingly, α-tocopherol was not detected in any of the algal samples except for *Parachlorella kessleri*. A single compound with a similar retention time and identical UV-Vis spectrum was detected in each of the marine algal species which was characterized as a tocopherol derivative; the quasimolecular ion (M+H)+ suggested a single additional unsaturation was present in the tocopherol skeleton (*m/z* = 429.5). A representative chromatogram of the tocopherol-containing extract is shown in Figure 2-8.

In order to identify the structure of the tocopherol derivative detected in the marine algal extracts, the extracts were subjected to in-line electrospray mass spectrometry (ESI-MS) in positive ion mode. Characterized by a quasimolecular ion of 429.5 (M+H)$^+$, the tocopherol derivative in marine algae was apparently the singly unsaturated derivative of α-tocopherol, designated "marine-derived tocopherol" by Yamamoto et al. (2001)[31]. In order to further confirm the identity, MS/MS was performed on the 429.5 quasimolecular ion, yielding 4 major fragments. The proposed fragmentation mechanism is depicted in Figure 2-9. Decomposition of the quasimolecular ion by loss of the terminal allyl radical gives the fragment corresponding to 388.3 *m/z*. Cleavage between the ε and ζ carbon of the chain leads to the fragment corresponding to 289.3 *m/z*. Cleavage between the α and β position yields the 219.2 *m/z* fragment. Finally, the retro Diels-Alder pathway leads to the o-quinone methide.
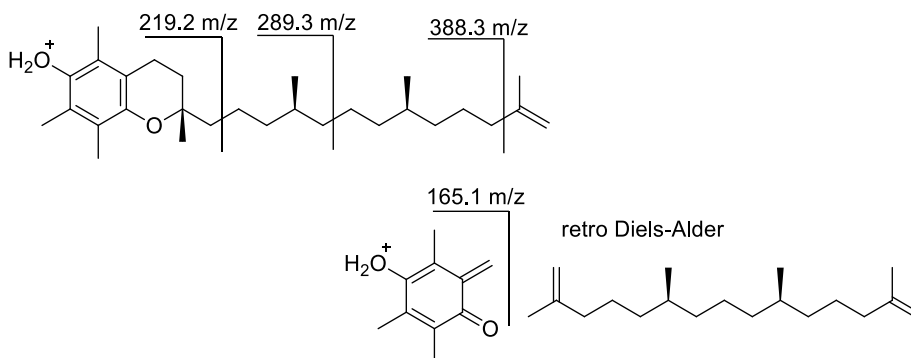
Figure 2-9. Proposed mass spectrum fragmentation pathway for marine derived tocopherol detected in marine algal species.

The results of the α-tocopherol quantitation for all algal species used in this project as well as common foodstuffs are shown in Figure 2-10. The strains of *Isochrysis galbana* showed the highest tocopherol content: the Caribbean strain (C-iso) contained the highest content of tocopherol at 438 ± 8.3 μg/g freeze-dried biomass, significantly higher (p = 0.004) than the content detected in the Tahitian strain (T-iso) at 364 ± 20.4 μg/g. These results were consistent with those reported by Bandarra et al. (2003) for the tocopherol content of *I. galbana*[32].
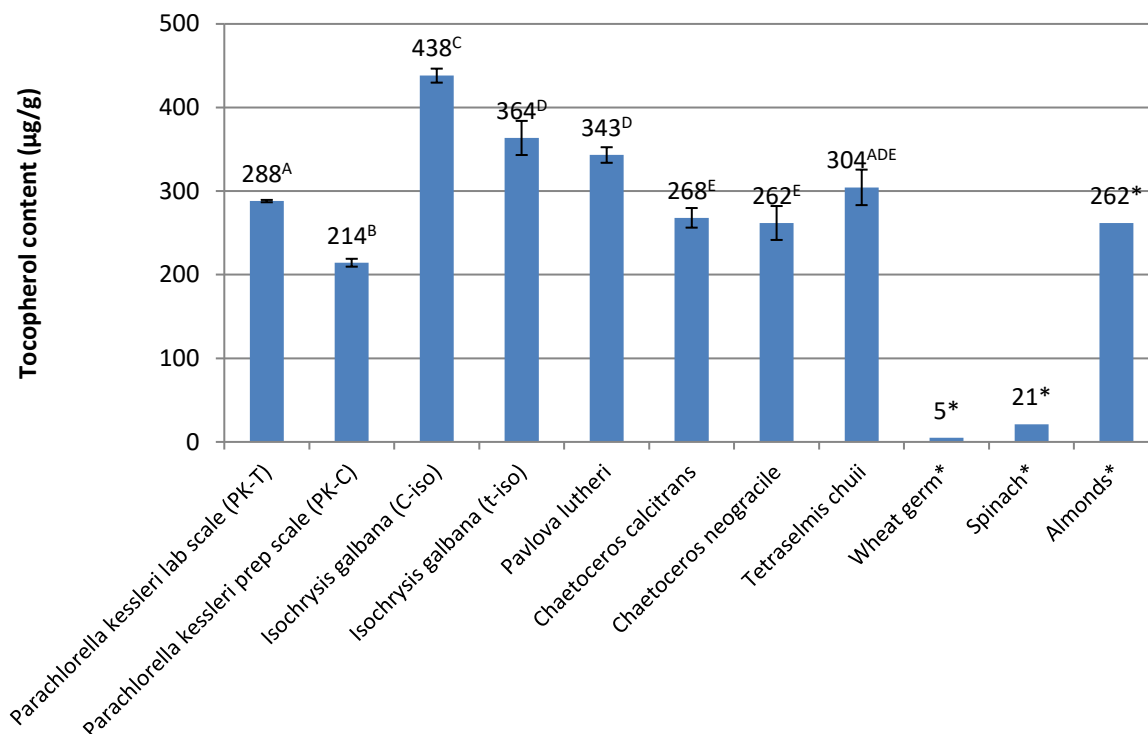
Figure 2-10. α-tocopherol content of algal biomass measured by HPLC
[A-E]Bars that do not share any letter in superscript differed significantly by two-tailed unpaired student's t-test (p < 0.05)
*Data obtained from USDA nutrient database[23]

Pavlova lutheri proved to be a rich source of tocopherol, found to contain 343 ± 9.3 µg/g, which is comparable to the content in the Tahitian *I. galbana* strain (p = 0.19). *Tetraselmis chuii* contained 304 ± 21.2 µg/g tocopherol, slightly more than detected for both *P. kessleri* laboratory scale (PK-T, p = 0.521) and prep-scale (PK-C, p = 0.052), and *Chaetoceros sp.* (p = 0.219-0.244), but significantly less than C-iso. The *Chaetoceros sp.* exhibited statistically indistinguishable results (p = 0.673), with tocopherol content of 268 ± 11.7 µg/g (*C. calcitrans*) and 261 ± 20.3 µg/g (*C. neogracile*).

Interestingly, the laboratory scale strain of *P. kessleri* (PK-T) demonstrated statistically significant (p = 10^{-5}) increase in tocopherol production compared to the preparative scale

P. kessleri (PK-C), showing an increase from 214 ± 4.7 µg/g to 288 ± 1.4 µg/g tocopherol by HPLC. The accumulation of tocopherol could be impacted by light and night. Thus, the regular light cycles and controlled nutrients, as well as protection from bacterial and fungal contamination, although other variables such as time of harvest, light cycle, or seasonal cycles may have contributed due to natural lighting.

Compared to common foods such as wheat germ and spinach, containing 5 µg/g and 21 µg/g tocopherol by mass[23], the algal biomass evaluated in this study contains a far higher concentration of tocopherols, ranging from 214 − 438 µg/g. Algal biomass contains a comparable quantity of tocopherols to Vitamin E-rich foods such as almonds, which contain 262 µg/g α-tocopherol by mass[23]. Based on these results, it is clear that algal biomass has a potential as a source of tocopherols, fulfilling the dietary requirement for Vitamin E with minimal biomass due to the high concentration. Due to the high concentration of tocopherols, we can conclude that algal biomass may serve as a nutritionally supplementary material to enhance to Vitamin E content of common flours and foodstuffs.

2.5 Proximate Analysis

2.5.1 Methodology
2.5.1.1 Protein Content

One of the most well-known and widely cited methods for the determination of protein content is the Bradford method[33] Bradford method is a colorimetric technique based on the absorbance shift of the dye Coomassie blue G-250. Protein binds to the dye, shifting

the absorption maximum, causing the dye to turn blue. The intensity of this response is proportionate to the quantity of protein present, and can therefore be used to measure the protein present in extracts. Bovine serum albumin is utilized as a standard to construct a calibration curve to allow for quantitation.

The method was executed as described in the product pamphlet provided by Sigma Aldrich with the Bradford reagent. Approximately 10 mg freeze-dried algal biomass was placed into a 10.00 mL volumetric flask; ~8 ml 0.1M phosphate buffered saline (PBS) was added. The flask was placed in a sonicator bath for 30 minutes, let cool to room temperature, and 0.1M PBS was added to the mark. A calibration series was prepared by serial dilution of Bovine Serum Albumin (Sigma-Aldrich) spanning 2.04 mg/mL to 3.984 μg/mL. Bradford reagent was obtained (Sigma-Aldrich) and stored at 3-5°C until use.

100 μL each sample and calibration standard was added to a 1.5 mL semi-micro polystyrene cuvette. A blank containing 100 μL of 0.1M PBS was also prepared. 750 μL Bradford reagent was added. The samples were incubated for 25 minutes at room temperature. After 25 minutes, absorbance at 595 nm was measured. Calibration standards were fitted to a second-order polynomial (R^2 = 0.998).

2.5.1.2 Total Lipid Content

The total content of lipids in the algal biomass was determined using the Folch method as described in the original paper[34]. Briefly, approximately 100 mg freeze-dried algal biomass was ground at room temperature in a mortar and pestle. The ground material was transferred into a glass centrifuge tube. 3.00 mL 2:1 chloroform/methanol was

added. An additional 0.75 mL 0.88% KCl was added. The centrifuge tube was sonicated

for approximately 30 seconds followed by vigorous vortexing. Finally, the centrifuge tubes

were placed into a centrifuge and spun at 10,000 rpm for 5 minutes (6 inch, 45 degree

angled rotor). The lower phase was transferred and an additional 3.00 mL 2:1

chloroform/methanol was added, followed by a repeat vortexing. The lower phase was

transferred and combined with the previous extract in a dried massed vial, and the solvent

was removed by drying under a stream of N_2 and warmed gently to 40˚C. The yield of

lipids was measured gravimetrically.

2.5.1.3   Carbohydrate Content

Total carbohydrate content was determined utilizing the commonly employed phenol-

sulfuric acid assay, optimized by Masuko et al. (2005) for microplate format with a

detection limit of 10 nmol[35], with minor modifications. Briefly, 10 mg freeze-dried algal

biomass was placed in an Eppendorf tube with 150 µL concentrated sulfuric acid. 30 µL of

5% phenol in ddH_2O. The Eppendorf tube was heated in a water bath to 90˚C for 5

minutes. The solution was transferred the microplate and absorbance at 490 nm was

measured. A calibration curve was prepared utilizing serially diluted solutions of glucose

in ddH2O spanning 20 mg/mL to 20 ng/mL.

2.5.1.4   Ash content

Approximately 200 mg freeze-dried algal biomass was added to a pre-dried, pre-weighed

ceramic crucible and quickly covered with aluminum foil. The crucibles were placed in an

electric kiln furnace heated to 400˚C for 24 hours. The crucibles were removed when the

kiln had come to a temperature of 120°C and placed in a CaCl$_2$ desiccator. When cooled to room temperature, the crucibles were weighed to determine residual ash content. Values were measured in triplicate for algae with enough biomass available.

2.5.2 Results and Discussion

The summarized results are shown in Table 2-10 for the proximate analyses of the freeze dried algal biomass materials. The algae biomass evaluated for this study demonstrated high protein content, ranging between 15.91 – 27.99% mass of freeze-dried weight. This level of protein is comparable to dietary meats such as chicken, which contains 20.85% protein (05057, Chicken, broilers or fryers, breast, meat and skin, raw)[23]. Strains of *Parachlorella kessleri* grown in lab (PK-T) or large-scale conditions (PK-C) exhibited exceptional protein content at 27.52 ± 1.414% and 25.77 ± 1.130% respectively; these results did not differ significantly (p = 0.169). The only marine species with comparable protein content was *Chaetoceros neogracile* which contained 27.99 ± 0.135% protein, the highest value detected, although not significantly different from the *P. kessleri* samples. Both strains of *Isochrysis galbana* demonstrated the lowest protein content at 15.91 ± 3.391% (Caribbean strain, C-Iso), and 15.08 ± 2.298% (Tahitian strain, T-iso); these values did not differ significantly (p = 0.743). *Pavlova lutheri* contained 18.99 ± 1.014% protein by mass.

One of the primary reasons that the freshwater and marine algae utilized in this study are used in aquaculture is due to their high lipid content. Hence, it was not surprising to find a relatively high content of lipids in the algal biomass, ranging from 13.6 – 21.2% by mass

of freeze-dried algae. The marine species had a slightly but markedly higher lipid content

(17.2 − 21.2%) than the freshwater *P. kessleri* samples (13.6 - 15.8%). The *I. galbana*

strains contained 20.1 ± 0.88% (C-iso) and 19.8 ± 1.34% (T-iso), respectively. These results

are consistent with results reported in the literature for *I. galbana* at a range of growth

conditions[36]. The results for *P. kessleri* are consistent with those reported for *C. vulgaris*

at normal growth conditions[37]. Finally, the results for lipid composition of *P. lutheri* and

Chaetoceros sp. are also consistent with reported results[38,39].

Table 2-10. Results from proximate analyses determined for algal biomass

Sample	Protein (%)	Lipid (%)	Carbohydrates (%)	Ash (%)
Parachlorella kessleri **(PK-T)**	27.52 ± 1.414 [ABD]	15.8 ± 1.26 [AB]	42.4 ± 5.10 [AB]	1.5 ± 0.41 [A]
Parachlorella kessleri **(PK-C)**	25.77 ± 1.130 [B]	13.6 ± 1.61 [A]	45.7 ± 3.96 [B]	1.8 ± 0.45 [A]
Pavlova lutheri	18.99 ± 1.014 [C]	21.2 ± 1.55 [C]	45.2 ± 2.81 [B]	4.9 ± 0.66 [B]
Isochrysis galbana **(C-iso)**	15.91 ± 3.391 [C]	20.1 ± 0.88 [CD]	48.1 ± 3.27 [B]	9.2 ± 0.46 [B]
Isochrysis galbana **(T-iso)**	15.08 ± 2.298 [C]	19.8 ± 1.34 [CE]	47.6 ± 2.99 [B]	8.8 ± 0.51 [B]
Chaetoceros neogracile	27.99 ± 0.135 [AD]	17.2 ± 1.86 [ADE]	31.2 ± 6.58 [A]	5.2 ± 0.41 [B]
Chaetoceros calcitrans	21.83 ± 4.935 [ABCD]	18.1 ± 0.75 [BE]	34.0 ± 3.91 [A]	4.5 ± 0.38 [B]

Superscripts A-E. = entries in a column that share a letter in the superscript did not differ statistically significantly (P<0.05) by two-tailed, unpaired students t-test

2.6   Elemental Analysis

2.6.1   Methodology

Freeze-dried samples of *Parachlorella kessleri*, *Isochrysis galbana* and *Pavlova lutheri*

were prepared. Unfortunately, due to the high quantity of sample required for analysis,

the other species of marine algae could not be evaluated. The samples (x grams freeze-dried) were ground using xxx to what particulate size, and sent for analysis by Inductively Coupled Plasma Mass Spectrometry (ICP-MS) at the Penn State Agricultural Analysis Laboratory.

2.6.2 Results and Discussion

The results of the elemental analysis by ICP-MS are shown in **Table 2-11**. The nitrogen content was consistent with the protein content found in section 2.5.2, confirming our lab results. The lab scale *P. kessleri* (PK-T) contained substantially more potassium and phosphorus than the prep-scale (PK-C) grown in the greenhouse. The prep scale *P. kessleri* (PK-C) had a 10X-fold increase in calcium content (0.62% vs 0.06% for PK-T), likely due to the usage of tap water to dilute media rather than $_{dd}H_2O$ as in the lab scale. Other mineral increases (Na, Mn, Fe) found in PK-C vs. PK-T are likely due to this same variable.

The marine algae *I. galbana* and *P. lutheri* had several distinct differences compared to the freshwater *P. kessleri*. Firstly, since the marine algae were grown in saltwater media, there was substantially more sodium detected in the marine species, and in addition, there was an increased content of Mg, S, B, and Fe. Interestingly, *P. lutheri* contained almost 4X the quantity of iron as *I. galbana*. Additionally, *P. lutheri* contained significantly more Mn than *I. galbana*—452 ppm vs 67 ppm respectively. Finally, the nitrogen content of *I. galbana* is inexplicably lower than the protein content would suggest.

Table 2-11. Results of elemental analysis of freeze dried algae biomass by ICP-MS

	Parachlorella kessleri prep scale (PK-C)	*Parachlorella kessleri* lab scale (PK-T)	*Isochrysis galbana* (Caribbean strain)	*Pavlova lutheri*
N (%)	7.60	6.94	2.58	5.20
P (%)	2.12	3.18	0.31	0.81
K (%)	2.61	4.13	1.54	1.09
Ca (%)	0.62	0.06	0.76	0.44
Mg (%)	0.41	0.26	2.40	1.96
S (%)	0.49	0.39	2.15	1.24
Na (%)	0.115	0.0054	8.098	4.316
Mn (ppm)	80	56	67	452
Fe (ppm)	280	122	1000	3958
Cu (ppm)	38	11	13	29
B (ppm)	22	10	134	190
Al (ppm)	85	11	21	76
Zn (ppm)	68	39	26	68

2.7   References

[1] Kalra, E. K. (2003). Nutraceutical-definition and introduction. *Aaps Pharmsci*,5(3), 27-28.

[2] Janet Rehnquist (March 2003), Department of Health and Human Services - Office of the Inspector General - Dietary Supplement Labels: Key Elements, United States Department of Health and Human Services, OEI-01-01-00120, retrieved 20 May 2015

[3] Johnson, M., Villani, T. S., Azmat, A., Simon, J. E., & Both, A. J. (2015). Evaluation of algal biomass production on vertical aeroponic substrates. *Algal Research*, 10, 240-248.

[4] Folch, J., Lees, M., & Sloane-Stanley, G. H. (1957). A simple method for the isolation and purification of total lipids from animal tissues. *Journal of Biological Chemistry*, 226(1), 497-509.

[5] Bligh, E. G., & Dyer, W. J. (1959). A rapid method of total lipid extraction and purification. *Canadian journal of biochemistry and physiology*, 37(8), 911-917.

[6] Iverson, S. J., Lang, S. L., & Cooper, M. H. (2001). Comparison of the Bligh and Dyer and Folch methods for total lipid determination in a broad range of marine tissue. *Lipids*, 36(11), 1283-1287.

[7] Metcalfe, L. D., & Schmitz, A. A. (1961). The rapid preparation of fatty acid esters for gas chromatographic analysis. *Analytical Chemistry*, 33(3), 363-364.

[8] Christie, W. W. (1993). Preparation of ester derivatives of fatty acids for chromatographic analysis. *Advances in lipid methodology*, 2(69), e111.

[9] Patil, V., Källqvist, T., Olsen, E., Vogt, G., & Gislerød, H. R. (2007). Fatty acid composition of 12 microalgae for possible use in aquaculture feed. *Aquaculture International*, 15(1), 1-9.

[10] Sukhija, P. S., & Palmquist, D. L. (1988). Rapid method for determination of total fatty acid content and composition of feedstuffs and feces. *Journal of Agricultural and Food Chemistry*, 36(6), 1202-1206.

[11] Biswas, A. K., Sahoo, J., & Chatli, M. K. (2011). A simple UV-Vis spectrophotometric method for determination of β-carotene content in raw carrot, sweet potato and supplemented chicken meat nuggets. *LWT-Food Science and Technology*, *44*(8), 1809-1813.

[12] Ramadan, M., & Mörsel, J. T. (2002). Direct isocratic normal-phase HPLC assay of fat-soluble vitamins and β-carotene in oilseeds. *European Food Research and Technology*, 214(6), 521-527.

[13] Manzi, P., Panfili, G., & Pizzoferrato, L. (1996). Normal and reversed-phase HPLC for more complete evaluation of tocopherols, retinols, carotenes and sterols in dairy products. *Chromatographia*, 43(1-2), 89-93.

[14] Aaran, R. K., & Nikkari, T. (1988). HPLC method for the simultaneous determination of beta-carotene, retinol and alpha-tocopherol in serum. *Journal of pharmaceutical and biomedical analysis*, 6(6), 853-857.

[15] de Quirós, A. R. B., & Costa, H. S. (2006). Analysis of carotenoids in vegetable and plasma samples: A review. *Journal of Food Composition and Analysis*, *19*(2), 97-111.

[16] Barlow, R. G., Cummings, D. G., & Gibb, S. W. (1998). Improved resolution of mono-and divinyl chlorophylls a and b and zeaxanthin and lutein in phytoplankton extracts using reverse phase C-8 HPLC. *Oceanographic Literature Review*, 8(45), 1362.

[17] Slavin, M., & Yu, L. L. (2012). A single extraction and HPLC procedure for simultaneous analysis of phytosterols, tocopherols and lutein in soybeans. *Food chemistry*, 135(4), 2789-2795.

[18] Khachik, F., Beecher, G. R., & Whittaker, N. F. (1986). Separation, identification, and quantification of the major carotenoid and chlorophyll constituents in extracts of several green vegetables by liquid chromatography. *Journal of Agricultural and Food Chemistry*, 34(4), 603-616.

[19] Akhtar, M. H., & Bryan, M. (2008). Extraction and quantification of major carotenoids in processed foods and supplements by liquid chromatography. *Food chemistry*, 111(1), 255-261.

[20] Schierle, J., Pietsch, B., Ceresa, A., Fizet, C., & Waysek, E. H. (2004). Method for the determination of β-carotene in supplements and raw materials by reversed-phase liquid chromatography: Single laboratory validation. *Journal of AOAC International*, 87(5), 1070.

[21] Li, H., Tyndale, S. T., Heath, D. D., & Letcher, R. J. (2005). Determination of carotenoids and all-trans-retinol in fish eggs by liquid chromatography–electrospray ionization–tandem mass spectrometry. *Journal of chromatography B*, 816(1), 49-56.

[22] Yadav, S. K., & Sehgal, S. (1995). Effect of home processing on ascorbic acid and β-carotene content of spinach (*Spinacia oleracia*) and amaranth (*Amaranthus tricolor*) leaves. *Plant foods for human nutrition*, *47*(2), 125-131.

[23] U.S. Department of Agriculture, Agricultural Research Service. 2014. USDA National Nutrient Database for Standard Reference, Release 27. Nutrient Data Laboratory Home Page, http://www.ars.usda.gov/ba/bhnrc/ndl

[24] Rigotti, A (2007). "Absorption, transport, and tissue delivery of vitamin E". *Molecular Aspects of Medicine* **28** (5–6): 423–36.

[25] Brigelius-Flohé R, Traber MG (1999). "Vitamin E: function and metabolism".*FASEB J.* **13** (10): 1145–55.

[26] Taylor, H. R; Tikellis, G; Robman, LD; McCarty, CA; McNeil, JJ (2002). "Vitamin E supplementation and macular degeneration: randomised controlled trial". *BMJ,* **325** (7354): 11.

[27] Age-Related Eye Disease Study Research Group (2001). "A randomized, placebo-controlled, clinical trial of high-dose supplementation with vitamins C and E, beta carotene, and zinc for age-related macular degeneration and vision loss: AREDS report no. 8".*Archives of ophthalmology,* **119** (10): 1417–36.

[28] Frank, B; Gupta, S (2005). "A Review of Antioxidants and Alzheimer's Disease". *Annals of Clinical Psychiatry,* **17** (4): 269–86.

[29] Helzlsouer, K. J.; Huang, HY; Alberg, AJ; Hoffman, S; Burke, A; Norkus, EP; Morris, JS; Comstock, GW (2000). "Association Between alpha-Tocopherol, gamma-Tocopherol, Selenium, and Subsequent Prostate Cancer". *Journal of the National Cancer Institute,* **92** (24): 2018–23.

[30] Heinonen, O. P., & Albanes, D. (1994). The effect of vitamin E and beta carotene on the incidence of lung cancer and other cancers in male smokers.*The New England journal of medicine* 330(15):1029-35..

[31] Yamamoto, Y., Fujisawa, A., Hara, A., & Dunlap, W. C. (2001). An unusual vitamin E constituent (α-tocomonoenol) provides enhanced antioxidant protection in marine organisms adapted to cold-water environments.*Proceedings of the National Academy of Sciences*, *98*(23), 13144-13148.

[32] Bandarra, N. M., Pereira, P. A., Batista, I., & Vilela, M. H. (2003). Fatty acids, sterols and α-tocopherol in *Isochrysis galbana*. *Journal of Food Lipids*, 10(1), 25-34.

[33] Bradford, M.M. (1976), "Rapid and sensitive method for the quantitation of microgram quantities of protein utilizing the principle of protein-dye binding", *Analytical Biochemistry*. 72: 248–254

[34] Folch, J., Leesm M., and Sloane-Stanley, G.H. (1957). A Simple Method for the Isolation and Purification of Total Lipides from Animal Tissues. *Journal of Biological Chemistry*, 226, 497-509

[35] Masuko, T., Minami, A., Iwasaki, N., Majima, T., Nishimura, S. I., & Lee, Y. C. (2005). Carbohydrate analysis by a phenol–sulfuric acid method in microplate format. *Analytical biochemistry*, *339*(1), 69-72.

[36] Zhu, C. J., Lee, Y. K., & Chao, T. M. (1997). Effects of temperature and growth phase on lipid and biochemical composition of Isochrysis galbana TK1. *Journal of Applied Phycology*, 9(5), 451-457.

[37] Converti, A., Casazza, A. A., Ortiz, E. Y., Perego, P., & Del Borghi, M. (2009). Effect of temperature and nitrogen concentration on the growth and lipid content of Nannochloropsis oculata and Chlorella vulgaris for biodiesel production. *Chemical Engineering and Processing: Process Intensification*, 48(6), 1146-1151.

[38] Guihéneuf, F., Mimouni, V., Ulmann, L., & Tremblin, G. (2009). Combined effects of irradiance level and carbon source on fatty acid and lipid class composition in the microalga Pavlova lutheri commonly used in mariculture. *Journal of experimental marine biology and ecology*, 369(2), 136-143.

[39] McGinnis, K. M., Dempster, T. A., & Sommerfeld, M. R. (1997). Characterization of the growth and lipid content of the diatom Chaetoceros muelleri. *Journal of Applied Phycology*, 9(1), 19-24.

Chapter 3   Natural Products Investigation of *Parachlorella kessleri*

Due to the absence of prior chemical investigations into *Parachlorella kessleri* and our goal of identifying bioactive natural products in these algal species it was decided to explore and pursue all major components which are isolable for characterization. As such, the general approach employed was to extract the widest range of constituents utilizing repeated ethanol extraction on the *P. kessleri* biomass, followed by concentration. The concentrated extract was then dried onto an appropriate quantity of silica gel (about 3x the weight of extract) and loaded onto a wide diameter column (20 cm) containing a 10 cm bed of silica gel. The column was eluted sequentially (and exhaustively) with hexanes, chloroform, ethyl acetate, n-butanol, and methanol to achieve five well-separated fractions. These fractions were subjected to alternating and repeated column chromatography across Sephadex LH-20 and silica gel (G and/or H) as well as preparative TLC in order to isolate major constituents.   Sub-fractions were later screened for bioactivity using bioassays described later in Chapter 4 and Chapter 5. Active sub-fractions were subsequently sub-fractionated and re-screened repeatedly to narrow down active constituents. Isolated components were characterized chromatographically by LC and GC coupled to UV-Vis and/or mass spectroscopy. Structures were solved by comparison and co-injection with known standards, or by using HRMS, ^{1}H-NMR, ^{13}C-NMR, and COSY-NMR techniques where applicable. Using this traditional bio-guided fractionation approach, several biologically active compounds were identified, along with several common biochemical compounds.

3.1 General Experimental Procedures

Nuclear magnetic resonance (NMR) spectra were recorded on a Bruker 500 MHz spectrometer (Palo Alto, CA) and a Bruker Avance 400 MHz spectrometer (Billerica, MA). Unless otherwise specified, chemical shifts (δ) are expressed in ppm with reference to the trimethylsilyl (TMS) signal. All solvents and HPLC-grade water used for chromatographic separation and isolation were HPLC-grade (Fisher Scientific, Springfield, NJ); Column chromatography was performed using silica gel (230 – 400 mesh; Selecto Scientific, Suwanee, GA), Sephadex LH-20 (25 – 100 μ, Sigma-Aldich, St. Louis, MO), and Polyamide CC 6 (50 – 160 μm, Sorbent Technologies, Atlanta, GA). Preparative HPLC was performed on a Waters 600/2487 instrument with UV detector (Varian Microsorb C18 column, 10 μm, 41.4 x 300 mm). HPLC-DAD-electrospray ionization/mass spectrometry (ESI/MS) was performed on an Agilent 1100 series instrument (Santa Clara, CA). GC/MS analysis was conducted using a Shimadzu TQ8040 Triple-Q GC/MS (Somerset, NJ).

3.2 Extraction

After a sufficient quantity (> 100 g) of freeze-dried biomass from *Parachlorella kessleri* cultured by AL-G had been obtained, a large-scale extraction procedure was developed. It was determined by small-scale experimentation that the most effective extraction method to extract the widest range of compounds contained within the *P. kessleri* biomass was the usage of mechanical agitation by way of stirring with a large content of glass beads through repeated extractions in dry ethanol and aqueous methanol.

To pilot this technique in large scale, 25.8 g *P. kessleri* biomass was added to a 1000 mL Erlenmeyer flask. 31 g of fine glass beads (1 mm diameter) was added. 600 mL dry 95% ethanol (Acros Organics, Belgium) was added. Vigorous mechanical stirring was accomplished by way of Janke Kunkel Werk mechanical stirrer adapted with a stainless steel propeller-style stirrer at maximum speed (1000 rpm). The flask was wrapped tightly with Al foil and left stirring overnight (24 hours) in the dark. The following morning, the mixture was vacuum filtered (Whatman #2). The filtrate was collected and concentrated, and the filter cake was returned to the mixing flask and re-extracted using 600 mL ethanol. The flask was left stirring overnight. The mixture was filtered as described above; the filtrate was combined with the previous filtrate and concentrated by rotary evaporation. The filter-cake was re-extracted using 500 mL 25% H_2O in methanol; the flask was left stirring overnight. The mixture was filtered as described above and the filtrate was combined with the previous extracts. The solvent was removed by rotary evaporation and repeated azeotropic removal of water by addition of absolute ethanol. Once the extract had achieved a constant mass, the removal of water was complete. 6.52 g (25% yield) of a dark green residue that smelled like low-tide was obtained. This yield was deemed acceptable and the extraction was scaled up.

The scale-up procedure was very similar to the pilot procedure except that smaller volumes of solvent are used for each extraction, and more total extractions are performed due to limitations in the size of flasks and solvent available. 104.1 g freeze-dried *P. kessleri* was added to a 2L round-bottom flask. 100 g fine glass beads (1 mm diameter) were added. 1500 mL dry 95% ethanol was added to the flask. Vigorous

mechanical stirring was applied as described above. Five successive extractions and filtrations were completed using dry 95% ethanol. Two further extractions were conducted using 25% H_2O in methanol. The combined extracts were thoroughly dried with azeotropic removal of water by dry ethanol, followed by letting the extract sit overnight under vacuum. Finally, to ensure complete dryness, the extract was gently heated (40˚C) under a stream of dry N_2. 33.8 g (32.4% yield) of a black-green malodorous adhesive emulsion-like substance was obtained. This yield was deemed sufficient to begin work on the bio-guided fractionation, isolation, and characterization of this material.

3.3   Preliminary fractionation of crude extract

The primary sub-fractions were obtained by adsorbing the crude extract of *P. kessleri* to Silica gel (Selecto, particle size: 32-63). This was accomplished by dissolving the extract in minimum 80:20 95% ethanol/water and allowing dry by passing dry N_2 over the mixture in a small ceramic dish in the fume hood, protected from light. The sticky silica mixture was stirred repeatedly while drying to ensure smooth adsorption of the extract to the silica. For the pilot extract, 9.8g extract was dissolved and adsorbed to 10g silica gel. 20 g silica was added to a 5 cm diameter column packed in hexane. Some buffering sand and silica was added to the top of the column to bring the solid-phase level above the solvent. The algae-adsorbed silica was loaded on to the column and elution was begun with hexane and gentle pressure. 500 mL portions of solvent were added to the column until clear elution, then the following solvent would begin. The solvents used were, in order, hexane (1200 mL), chloroform (2000 mL), ethyl acetate (3650 mL), n-butanol (2000 mL)

and methanol (2000 mL). The fractions were stripped of solvent by rotary evaporation. A total recovery of 74.8% of the mass of the extract loaded onto the column was obtained. Recoveries by fraction are given in Table 3-1. This method was determined to give acceptable yield of the interesting fractions by polarity (ethyl acetate and butanol) and thus it was decided to apply this same methodology to the large-scale extract.

Table 3-1. Recovery by fraction of primary sub-fractions of pilot scale and large scale extract

Fraction	Hexane (H)	Chloroform (C)	Ethyl acetate (E)	n-butanol (B)	Methanol (m)
Pilot scale (9.8g)	147 mg (1.5%)	1.38 g (14.1%)	3.40 g (34.7%)	0.50 g (5.1%)	1.90 g (19.4%)
Large scale (33.2g)	7.10 g (21.3%)	9.60 g (28.9%)	2.50 g (7.53%)	8.30 g (25.0%)	3.10 (9.1%)

The large-scale extract (33.2 g) was adsorbed to 50 g silica gel as described in the above text. Briefly, a wide-bore column (15 cm) was packed to a bed height of 5 cm using Silica gel (Sigma Aldrich, 230-400 mesh, 40-63 μm) in hexanes (Fisher Scientific, city). The algae was loaded atop the column bed dry of solvent, and repeatedly extracted subsequently with hexanes (1500 mL), chloroform (5000 mL), ethyl acetate (5800 mL), n-butanol (4200 mL), and methanol (2200 mL). The extracts were concentrated by rotary evaporation to give an overall recovery of 91.8%. The distribution of recovery by fraction is shown in Table 3-1. Interestingly, the recoveries of fractions in the large-scale fractionation was markedly different than the recoveries obtained in the pilot extraction. Substantially more mass was recovered in the hexane fraction of the large-scale extract (21.3%) than the pilot scale hexane extract (1.5%). The relative recovery of the chloroform fraction nearly doubled, from 14.1% in the pilot scale to 28.9% in the large scale. The ethyl acetate fraction was significantly smaller, with only 7.53% recovery in the large scale vs. 34.7% in the pilot scale. The butanol fraction was substantially bigger in the large scale (25%)

compared to the pilot scale (5.1%). The variability is likely due to batch-to-batch differences in algal biomass in the production technique. The TLC profiles were comparable between the fractions, and so it was decided to combine the corresponding fractions for subsequent separations. Sub-fractions deriving from the hexane fraction are prefixed with "H", chloroform by "C", ethyl acetate by "E", butanol by "B" and methanol by "M" in the following sections.

3.4   Investigation of Ethyl acetate fraction (E)

3.4.1   Isolation of components in ethyl acetate fraction (E)

The ethyl acetate fraction (E) was selected first for fractionation due to the complexity by TLC, the polarity is mid-range and is most likely to harbor components with the lipophilicity required to demonstrate bioactivity. Additionally, principal bioactivity screening on the ethyl acetate fraction compared to the other obtained fractions demonstrated higher activity in the PLA-2 assay (See section 5.2) and pancreatic lipase assay (See section 4.4). It was decided based on the high content of high-polar chlorophyll derivatives to utilize polyamide gel fractionation to separate the bulk of the constituents in Fraction E from the chlorophyll derivatives. This separation is based on the premise that polyamide gel interacts with substrates based on hydrogen bonding, hence chlorophyll derivatives, with the heteratom-rich and high-surface area tetrapyrrole structure, would be separable from the bulk on the basis of the high degree of hydrogen bonding expected between this structure and the polyamide resin.

3.1 g of fraction E (ethyl acetate fraction) was dissolved in 100 mL ethyl acetate (Fisher Scientific, city) and thoroughly mixed by glass stirrer into 3.1g polyamide (MP Polyamide, EcoChrom™, MP Biomedicals) in a beaker. The beaker was covered to protect from dust and left to dry in a fume hood overnight. The mixture was periodically mixed by glass stirrer. The following morning, the residue was scraped together and thoroughly mixed, divided, and recombined to ensure thorough adsorption to the polyamide. A 45 mm column was packed with a bed of polyamide approximately 22 cm in height. The column was conditioned through a gradient from methanol to 10% methanol in water. The ethyl acetate fraction adsorbed to the polyamide was loaded atop the column bed. Successive elutions by stepwise gradient with solutions of methanol and water (500-2000 mL) increasing toward 100% methanol were utilized to separate the ethyl acetate fraction. As hypothesized, the chlorophylls were well-retained on the polyamide resin, and allowed for effective separation through the gradient. A total of 76 fractions of 250 mL volume were taken, and fractions were combined by TLC analysis (1:9 methanol/CHCl$_3$ on Silica H plates with UV$_{254}$ indicator and subsequent visualization by heating after spraying with 1:9 H$_2$SO$_4$/ethanol) to obtain 9 fractions, E-a through E-h. A flowchart of this separation is shown in Figure 3-1. These fractions showed good separation of components by LC/MS

as   well   (
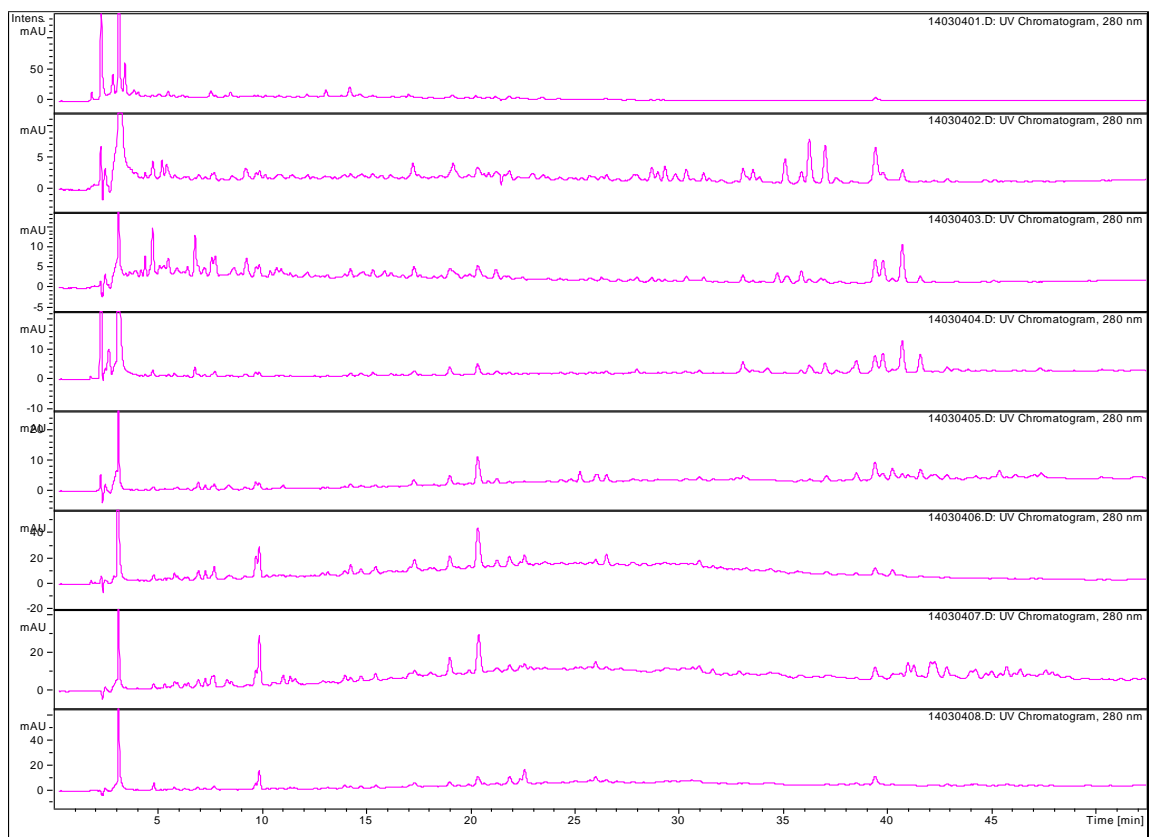
Figure **3-2**).
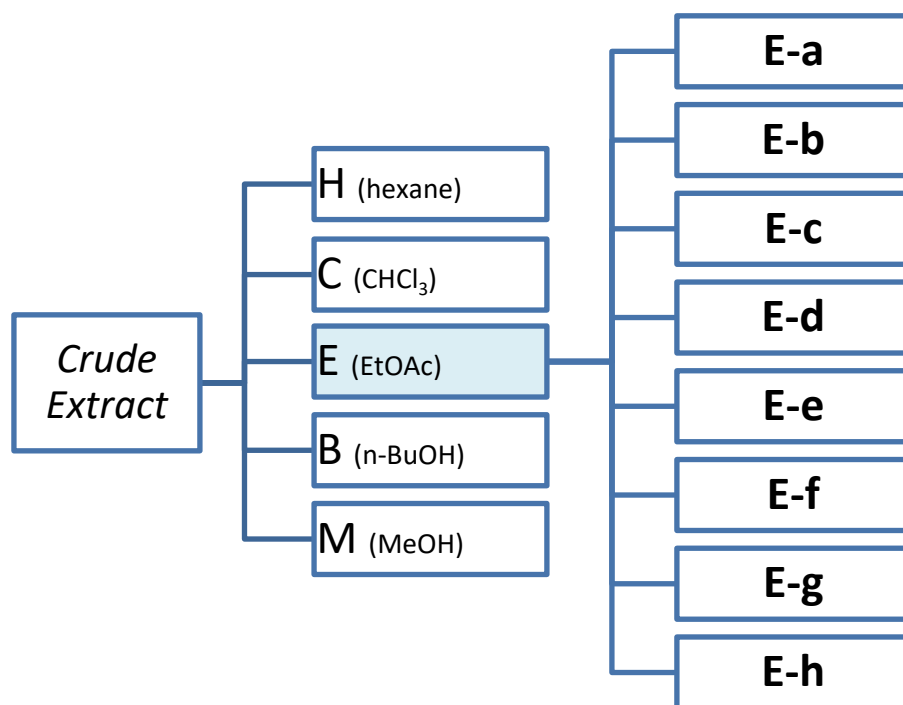
Figure 3-1. Flowchart for the sub-fractionation of fraction E (ethyl acetate fraction)
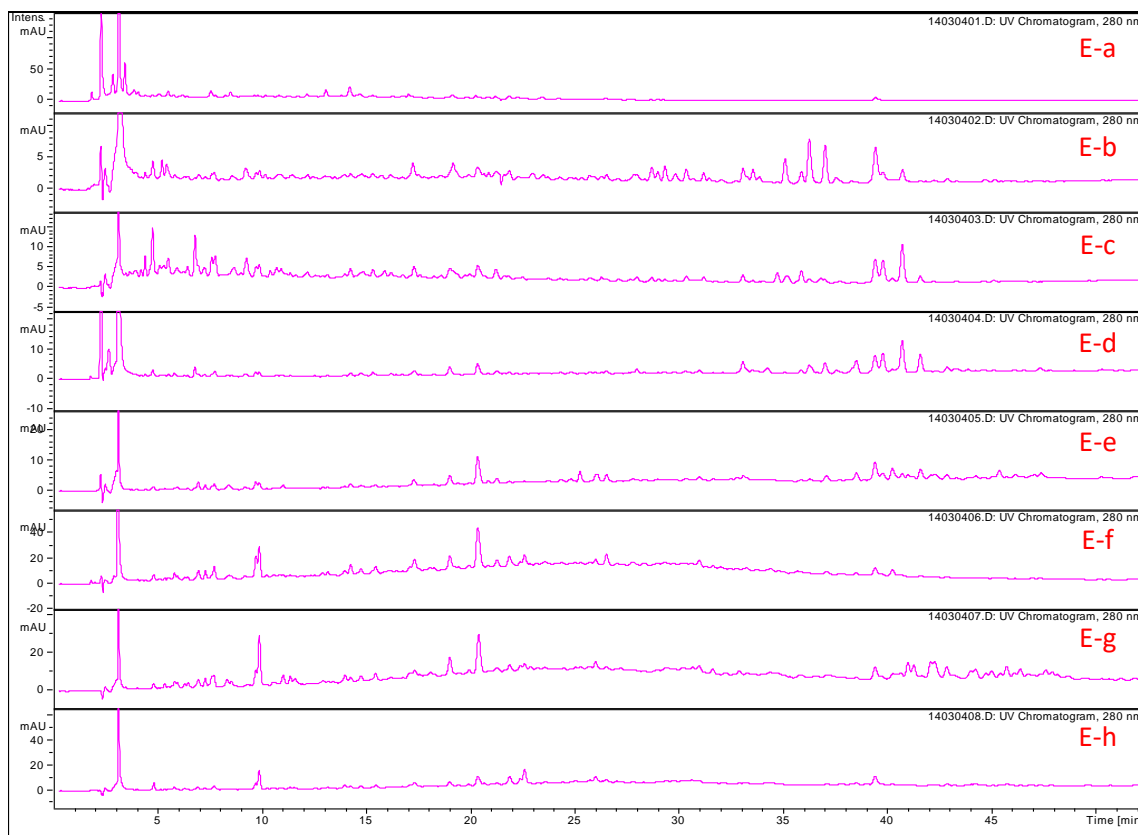
Figure 3-2. Comparison of HPLC/UV chromatograms at 280 nm of sub-fractions of fraction E; E-a through E-h

These fractions were utilized in a subsequent screen in the PLA2, lipase, and, anti-fungal inhibition assay which demonstrated the active sub-fractions. In the case of sPLA2 inhibition, fraction E-h was the sole fraction exhibiting statistically significant activity

versus   vehicle   control   (
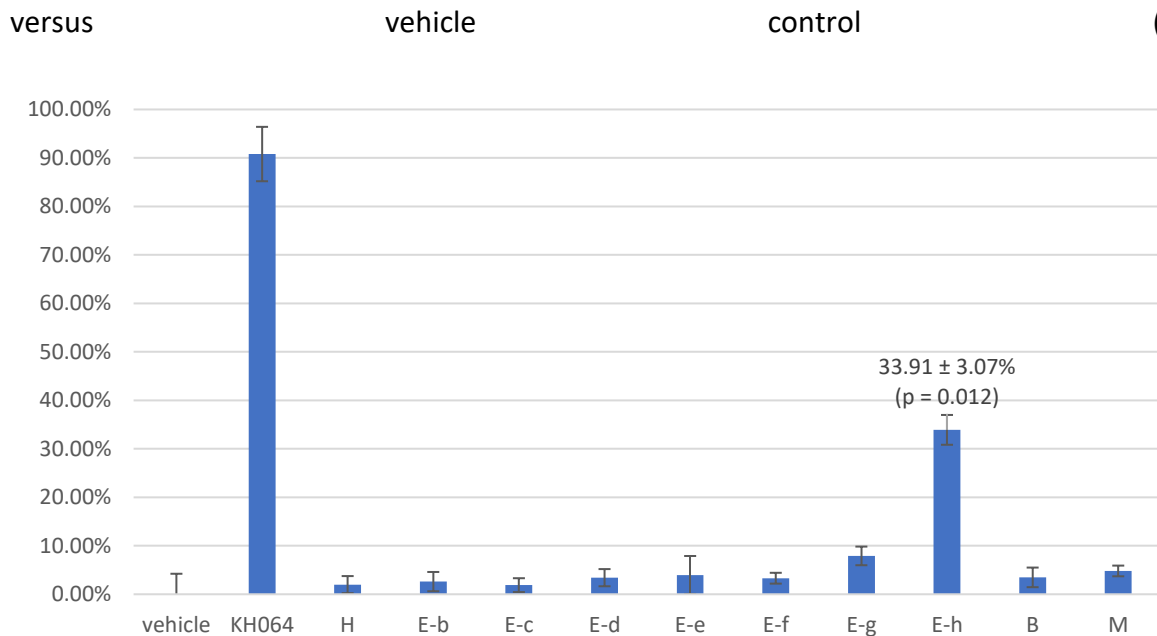
Figure 5-4, pg. 248). Fraction E-g and E-h demonstrated the highest lipase inhibition activity (Figure 4-7, pg. 222). The anti-fungal assay demonstrated only slight activity in fraction E-e. As such, fractions E-g, E-h, and E-e were selected for sub-fractionation via Sephadex column chromatography.

Fractions E-g and E-h appeared to contain some similarities by TLC profile, exhibiting a medium-polarity compound which turned bright red-purple after visualization with 1:9 H_2SO_4/Ethanol. Fraction E-h, however, contained substantially pigmented compounds, identified as xanthophylls by the characteristic UV spectrum. Fraction E-g was selected for separation via column chromatography on a 25 mm diameter, 15 cm height packed column of Sephadex LH-20 in methanol, thoroughly equilibrated. 260 mg of Fraction E-g was dissolved in approximately 2 mL methanol and loaded onto the column. The column was eluted with methanol. Seven initial fractions were collected and combined after TLC

analysis to yield three fractions: E-g-1 (25.5 mg), E-g-2 (163.6 mg), and E-g-3 (67.9 mg).

The major red-purple spot was contained in E-g-2 with minor impurities, and so this

fraction was dissolved in methanol and loaded on the same Sephadex LH-20 column.

There was poor separation achieved, although a small portion of impurity was separable

(E-g-2B) in this method, giving E-g-2A (132.4 mg).
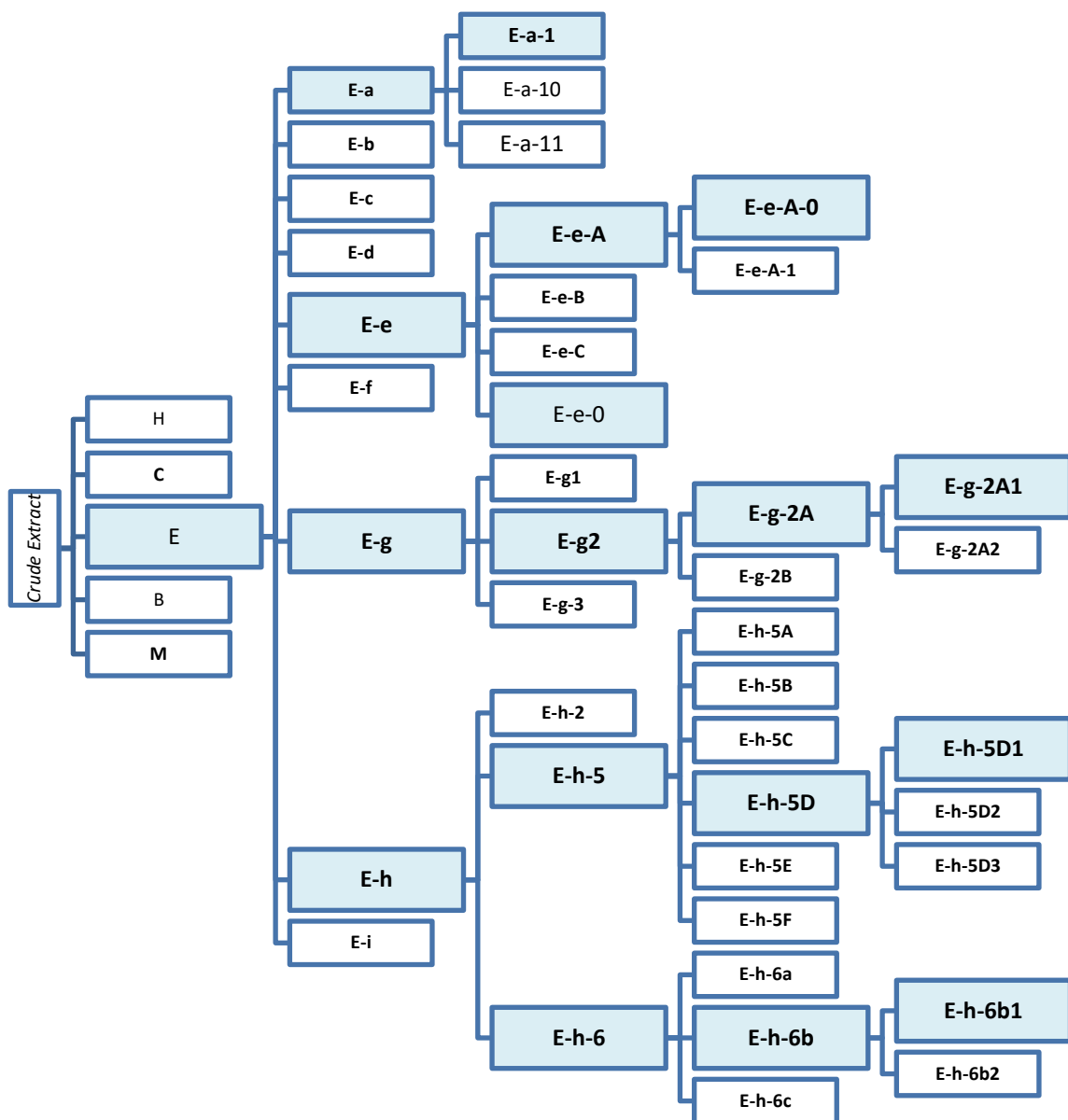
Figure 3-3. Flowchart of isolation of active components in fraction E

HPLC/MS analysis of E-g-2A showed a series of 6 compounds which had very similar retention characteristics, similar quasimolecular ions, but exhibited a common fragmentation pattern and core structure (Figure 3-4).
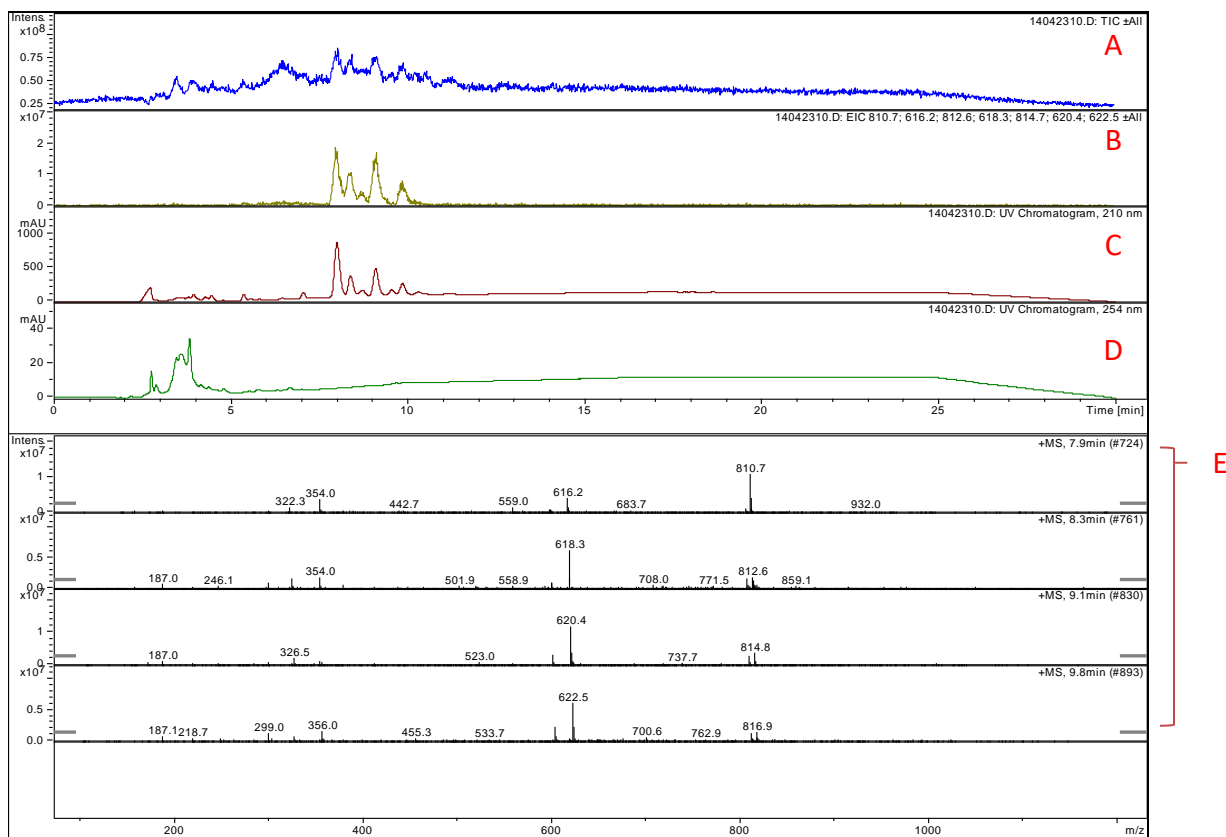
Figure 3-4. UV-Vis, MS Chromatograms and mass spectra of E-g-2A.
A) Total ion chromatogram; B) Extracted ion chromatogram for characterizing ions detected in E-g-2A; C) UV Chromatogram at 210 nm; D) UV Chromatogram at 254 nm; E) Mass spectra of compounds in E-g-2A

In order to isolate one of the compounds to confirm the skeleton of the analogues contained in E-g-2A, preparative scale TLC on silica was employed. Onto a prep-TLC plate (20x20cm Silica gel at 250 μm thickness on glass, Silica F60, Alfa Aesar) was loaded 5.4 mg E-g-2A dissolved in minimum 3:7 methanol/chloroform by careful spotting with a glass capillary tube. The TLC plate was thoroughly dried before elution. The TLC plate was eluted with 8:92 methanol/chloroform. The bands were visualized by covering all but 3-4 mm of the plate perpendicular to the elution flow to spray with 10% H_2SO_4 in ethanol, followed by heating with heat gun. Two bands were collected; E-g-2A1 (2.4 mg) which contained >85% of a single analogue by TLC and in-line ESI-MS injection, and E-g-2A2 (2.8

mg), which contained the remaining analogues. Fraction E-g-2A1 was submitted for a cascade of NMR experiments, as well as HR-MS in order to characterize these structures.

The same technique used for E-g was utilized to separate E-h—separation via Sephadex LH-20 and subsequent prep-TLC separation to isolate analytically pure components. Using the same Sephadex column described above, E-h was separated into 3 fractions, E-h-2 (21.0 mg), E-h-5 (34.0mg), and E-h-6 (95 mg). E-h-5 contained the pigmented xanthophylls and a small quantity of the major red/purple spot by TLC. E-h-6 was nearly pure, but contained a trace amount of xanthophylls. E-h-6 showed significant activity compared to E-h-2, E-h-5, and vehicle control in the sPLA2 inhibition assay (Figure 5-5, pg. 249). E-h-5 demonstrated substantial lipase inhibition activity, with E-h-6 demonstrating slight activity. As such, these fractions were selected for sub-fractionation on Sephadex.

E-h-5 (34.0 mg) was dissolved in 1 mL methanol and loaded onto the Sephadex LH-20 column described in the above text. E-h-5 was separated into 6 fractions, E-h-5A through E-h-5F. The major fraction was E-h-5D (10.6 mg) which contained the yellow compound(s) (presumably xanthophylls). To further separate the constituents, prep-TLC was utilized as described above to obtain E-h-5D1 (1.2 mg) and E-h-5D2 (0.6 mg). These compounds were selected for characterization (see following section). E-h-5D1 exhibited the highest pancreatic lipase inhibition activity.

Due to the high sPLA2 activity exhibited by E-h-6, this fraction was separated in the same manner as E-h-5. E-h-6 (85 mg) was dissolved in minimal methanol and loaded onto the same Sephadex LH-20 column described in the text above. Methanol was used to elute

the column to obtain 3 fractions: E-h-6a (0.7 mg), E-h-6b (71 mg) which contained the

major red spot, and E-h-6c (12 mg). E-h-6a and E-h-6c were inactive, while E-h-6b was

highly active. As such, this fraction was selected for fractionation by prep-TLC with

identical conditions described for E-g-2A. Two major fractions were obtained, E-h-6b1

(57.7 mg), which contained the compound of interest, and E-h-6b2 (12 mg). By HPLC/MS,

E-h-6b1 contained similar compounds as E-g-2A1, with one compound in common,

although all compounds sharing a similar backbone (Figure 3-5). Since fraction E-h6b1 was

the most active fraction in the sPLA2 assay, it was selected for characterization (section

3.4.2).
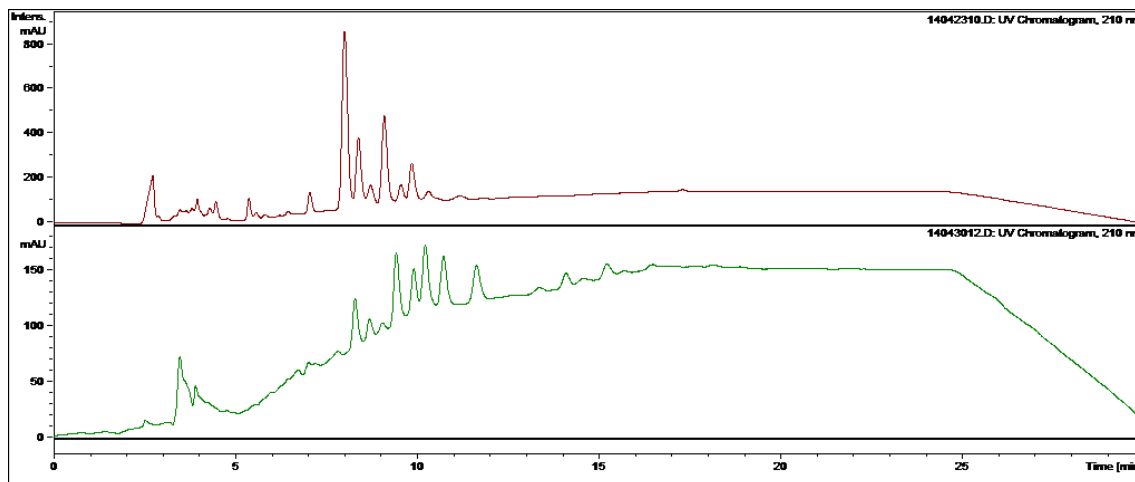
Figure 3-5. HPLC/UV/MS chromatograms comparing E-g-2A1 (top) to E-h-6b1 (bottom)

Due to the anti-fungal activity exhibited by Fraction E-e (Table 4-3, pg. 216) was selected

for separation by column chromatography across Sephadex LH-20. Fraction E-e was

dissolved in a minimum quantity of methanol and loaded onto a 25 mm diameter column

packed to a height of 15 cm. The column was eluted with methanol providing 4 major

fractions: E-e-A, E-e-B, E-e-C, and the final washing fraction, E-e-0. As Fraction E-e-A was

evaporating under ambient conditions in the fume hood, a precipitate was formed which was encouraged by placing the fraction in the refrigerator for several hours. The crystals were mechanically isolated, giving the major compound in Fraction E-e-A-0 (33 mg) as a white solid, and the mother liquor, E-e-A-1. Each of these sub-fractions of E-e was examined under the anti-fungal assay. Fraction E-e-A-0 demonstrated the most potent anti-fungal activity, and was highly pure by HPLC (data shown in following section selected for subsequent characterization (section 3.4.2).

Fraction E-e-0, the final washing fraction, begin to precipitate a waxy solid on evaporation of methanol from the fraction overnight. The solid was filtered and appeared quite pure by HPLC (Figure 3-6). This compound was characterized by LC/MS and NMR, however did not exhibit bioactivity in any of the assays used in this project.

Finally, Fraction E-a was selected for fractionation due to its relatively simple profile by TLC and HPLC/UV (Figure 3-7). After passing through a Sephadex column, 3 significant fractions were obtained, E-a-1, E-a-10, and E-a-11. E-a-1, upon standing, crystallized to give E-a-1-ppt, quite pure by TLC. This compound was selected for characterization.
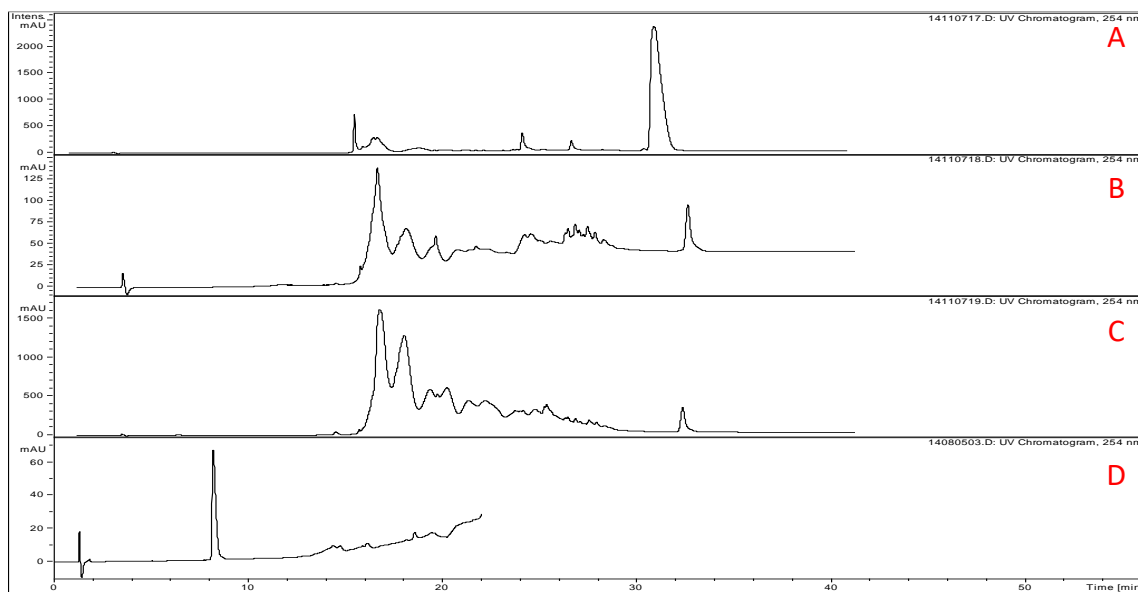
Figure 3-6. HPLC Chromatograms of E-e-0, E-e-b, E-e-c, and E-e-a1
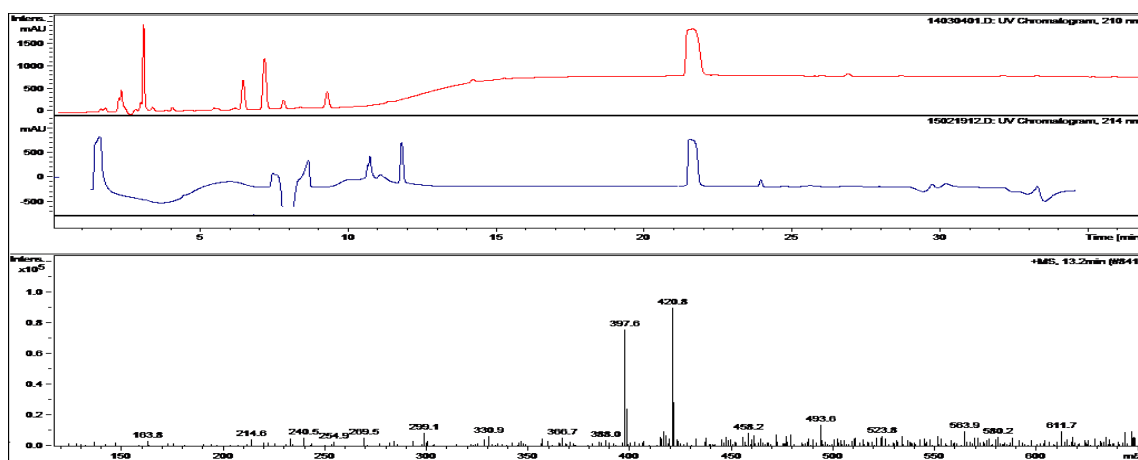
Figure 3-7. HPLC chromatogram of E-a and E-a-1-ppt

3.4.2 Characterization of components in ethyl acetate fraction (E)

3.4.2.1 Compounds E-g-2A1 and E-h-6b1

Preliminary characterization of compounds E-g-2A1 and E-h-6b1 was carried out using

HPLC/MS. LC/MS chromatograms showed that E-g-2A1 contained a mixture of four

closely-eluting compounds with very similar mass spectra, differing by only 2 *m/z* in most circumstances. E-h-6b1 had one compound in common with E-g-2A1, and several other similar isomers. These compounds were largely inseparable; however, one isomer was isolated via repeated preparative-scale TLC. It was hypothesized that if a single compound's skeleton could be determined, the MS fragmentation patterns could be used to identify the adjacent compounds.

In negative ion mode, the compounds in E-h-6b1 all exhibited at fragment peak at 283.2 *m/z*. Because the molecular weight of stearic acid is 284, and it was known that fatty acid derivatives were common within this biomass, it was presumed that the compounds contained a stearic acid moiety which fragmented upon ionization in the MS. The compound which was most isolable had a characteristic ion at 768.5 *m/z* in positive ion mode. As mentioned above, through repeated preparative TLC fractionations, a sufficiently pure sample of this compound was obtained in milligram quantities (1.1 mg). H^1-NMR, C^{13}-NMR and COSY analysis on this compound was conducted—the compound was dissolved in D_6-acetone for analysis. ^{1}H-NMR and COSY spectra are shown in Appendix.

H^1-NMR and COSY analysis proved decisive in the characterization this compound. At first analysis, in ^{1}H-NMR, there were no signals downshifted past 5.4 ppm, and so there were no aromatic constituents in this compound. There were many signals in the aliphatic region, and several signals between 3.5-4.5 ppm, indicating a number of de-shielded protons in the structure, indicating presence of electronegative elements within the

structure. The signals will be annotated and described from least shifted to most shifted across the H^1-NMR spectrum. In signal A, there were 6 protons within two separate, overlapping multiplets, indicative of two independent terminal CH_3- group on a structure separated by at least 2 bonds from electron-withdrawing groups (EWGs), as indicated by integral and shift of 0.8983 ppm. Signal B was the largest signal detected at 1.31 ppm, and integrating to 68 with respect to other signals. Signal B was a complex multiplet, and was taken to represent 68 aliphatic protons as chains of methylene groups with at least 2 bond separation from EWGs. COSY analysis showed that signal B interacted with signal A, indicating that the terminal methyl groups were attached to the methylene groups at one end. Signal C consisted of a complex multiplet of 4 protons detected at 1.62 ppm, consistent with two slightly de-shielded methylene groups. COSY analysis showed these protons coupled with protons in signal B, indicating that these compounds were likely to form the bridge between the long methylene chains and an EWG. Signal D consisted of 4 protons in a complex multiplet at 2.37 ppm which coupled to signal C in COSY analysis. A shift of 2.37 is consistent with alpha-keto methylene protons, and this signal suggests two independent but chemically identical alpha-keto methylene groups. Since signal C couples with signal D in COSY analysis, this suggests C is the signal corresponding to the beta protons adjacent to the alpha-keto protons. Combined with the evidence of signal B and A, it was postulated that signals A-D represent a two long, independent chains of aliphatic groups terminated at one end to keto groups. Given that two independent stearic acid moieties, as suggested to be contained by this molecule through LC/MS analysis, would contain 68 methylenes non-adjacent to EWGs, 6 terminal methyl protons, 4 alpha-keto

protons and 4 beta-keto protons, it was postulated that signals A-D represent two independent stearic acid chains attached to another moiety by acyl-bonds.

Moving to the second cluster of interacting groups, as shown by COSY analysis, we shall skip signal E until further structural analysis, since it was not determined until after the rest of the structure. Signal F contained 2 protons in an overlapping complex multiplet at 3.53 ppm. These protons appeared to be independent of one another, showing a differential coupling pattern in COSY analysis, and were consistent of protons adjacent to EWGs such as oxygen, suggesting alcohol moieties in this quadrant of the molecule. Further signals between 3.5 and 4.5 were in agreement with this. Signal G consisted of 3 protons arranged in a complex overlap of multiplets at 3.73 ppm whose analysis proved difficult independently. COSY analysis demonstrated that these signals coupled to signal F, signal H, and signals I and J. It was hypothesized that signal G consisted of 3 independent protons adjacent to EWGs such as alcohol moieties at different locations, since the coupling pattern in COSY suggested unique coupling partners. Signal H consisted of two protons in a complex multiplet at 3.93 ppm. At this stage, it was hypothesized that a monosaccharide moiety may be present in this compound, as prior experience with the NMR of monosaccharide-containing compounds have shown similar patterns in NMR. Signals F, G and H were hypothesized to derive from a sugar moiety, representing the protons adjacent to the alcohol groups in the sugar ring. Signal L at 5.37 ppm, representing one proton in a complex-splitting multiplet represents the proton adjacent to the bridging oxygen in the sugar ring and the oxygen extending to bond with other groups.

However, given these assumptions, there were still 2 unaccounted protons not within these groups (signals I, J), and one unaccounted proton within signal G (named signal G2), also not contained within these groups. Based on COSY analysis, signal J couples to signal G2, which couples to signal I. This pattern suggests a linear arrangement: J -> G2 -> I; since these signals are located at 4.39 ppm, 4.24 ppm, and 3.76 ppm respectively, it was hypothesized that this arrangement represented a linear arrangement of carbons, each with independent, highly EWGs adjacent to them on the molecule. Since two acyl moieties had yet to be placed, it was presumed that ester-bonds connected the long chains discussed above and protons G2 and I—signal I well-corresponded to protons adjacent to -O-Ac moiety. Since signal G2 was downshifted with respect to signal I, it was hypothesized that signal G2 was also adjacent to an EWG moiety. Based on signal J, consisting of two protons at 4.39 ppm, it was postulated that signal J was adjacent to an oxygen on the end of the chain, corresponding to the connection to the sugar moiety postulated above. As such, the molecule showed NMR data consistent with di-stearoyl glyceryl-hexoside. Since the most common form of sugar-bound lipid is the galactolipid, it was hypothesized that the structure of this compound was di-stearoyl-glyceryl-galactoside. The coupling patterns of the protons contained within the sugar moiety were consistent with known galactolipids reported in the literature[1]. ^{13}C-NMR data was obtained but of little use due to the low concentration of this compound obtained.

Based on the evidence obtained from ^{1}H-NMR and COSY analysis, and data from LC/MS analysis, it was concluded that the structure of the isolated compound contained within fraction E-h-6b1 was di-stearoyl-glyceryl-galactoside.
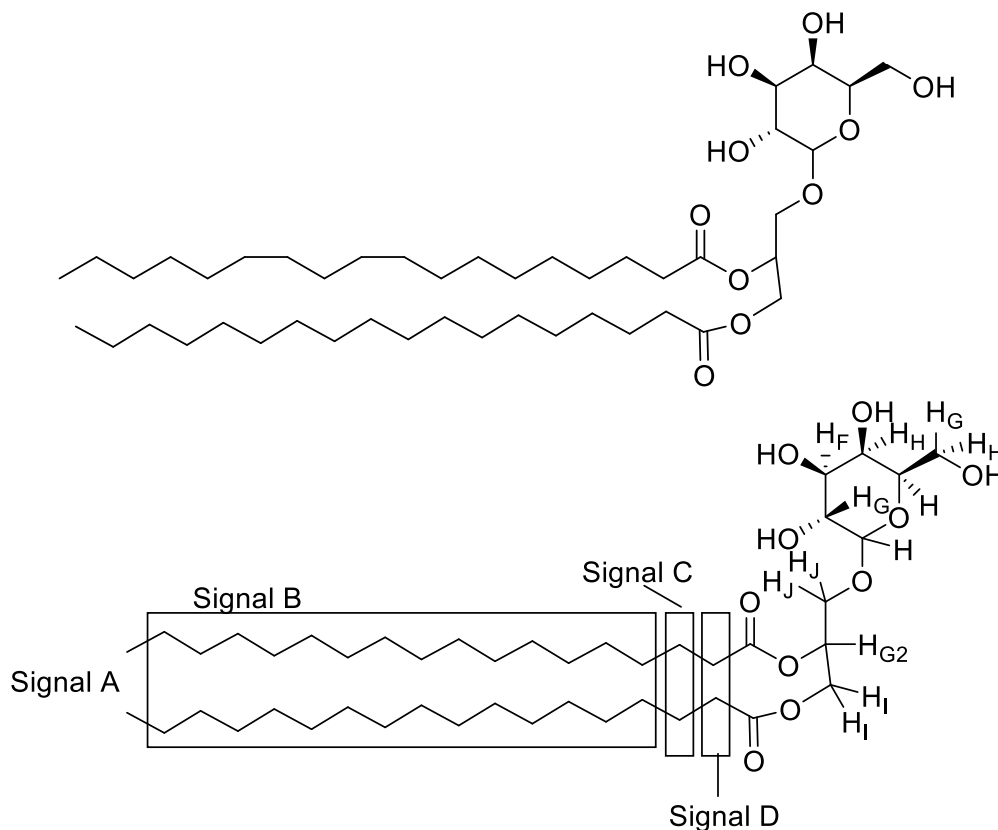
Figure 3-8. Structure of major galactolipid isolated from E-h-6B1 and E-g-2A1 (top) and corresponding signal identities, where subscript represent signal discussed in text.

The proposed structure of this compound is shown in Figure 3-8 with corresponding ^{1}H-NMR signal identities. Based on this structure, the MS fragmentation pattern was re-examined to look for consistencies with expected fragments; the mass spectrum of this compound is shown in Figure 3-10. The postulated fragmentation pattern is shown in Figure 3-9. The mass spectrum in positive ESI-mode showed quasimolecular ion at 767.6 *m/z* [M+H]$^+$ with several major fragmentations, the first at 759.6 *m/z*, corresponding to loss of water by rearrangement of the primary alcohol in the galactose moiety. The second major fragmentation observed was the transition to 283.2 *m/z*, representing fragmentation of stearoyl moiety ($C_{18}H_{41}COO$) from the molecule. The next major fragmentation was a split of a 14 carbon chain from a stearoyl moiety, leading to the peak

observed at 589 *m/z*. This piece further fragmented, losing a water from the sugar moiety, resulting in the peak at 571 *m/z*. This peak lost yet another water molecule, yielding the peak at 553 *m/z*.

Determination of the H^1-NMR coupling patterns and LC/MS fragmentation patterns allowed for the structural assignment of one of the major compounds contained within fractions E-h-2B1 and E-g-2A1. Since the other compounds within these fractions were not separable, but contained analogous components, similarities found in the fragmentation patterns in the LC/MS data were applied to determine the structure of these analogous compounds.

In fraction E-h-6B1, four compounds were detected: the di-stearoyl-glyceryl-galactoside discussed above, and three analogous compounds with similar molecular weights (Figure 3-12). The characteristic quasi-molecular ion detected for the compounds in E-h-6B1 were E-h-6b1.a: 786.6 *m/z* [M+H]$^+$; E-h-6b1.b: 784.3 *m/z* [M+H]$^+$; E-h-6b1.c: 776.8 *m/z* [M+H]$^+$; and E-h-6b1.d: 779.2 [M+H]$^+$. The compound corresponding to 786.6 *m/z* (E-h-6b1.a) was identified as di-stearoyl-glyceryl-galactoside, and as such, it was hypothesized that the compound corresponding to 784.3 *m/z* (E-h-6b1.b) was likely the analogue containing a single double-bond: stearoyl-oleoyl-glyceryl-galactoside. Unfortunately, not enough data was obtained to determine whether the oleoyl moiety is contained within the primary (SN1) or secondary chain (SN2) of the glycerol on the galactolipid compound.
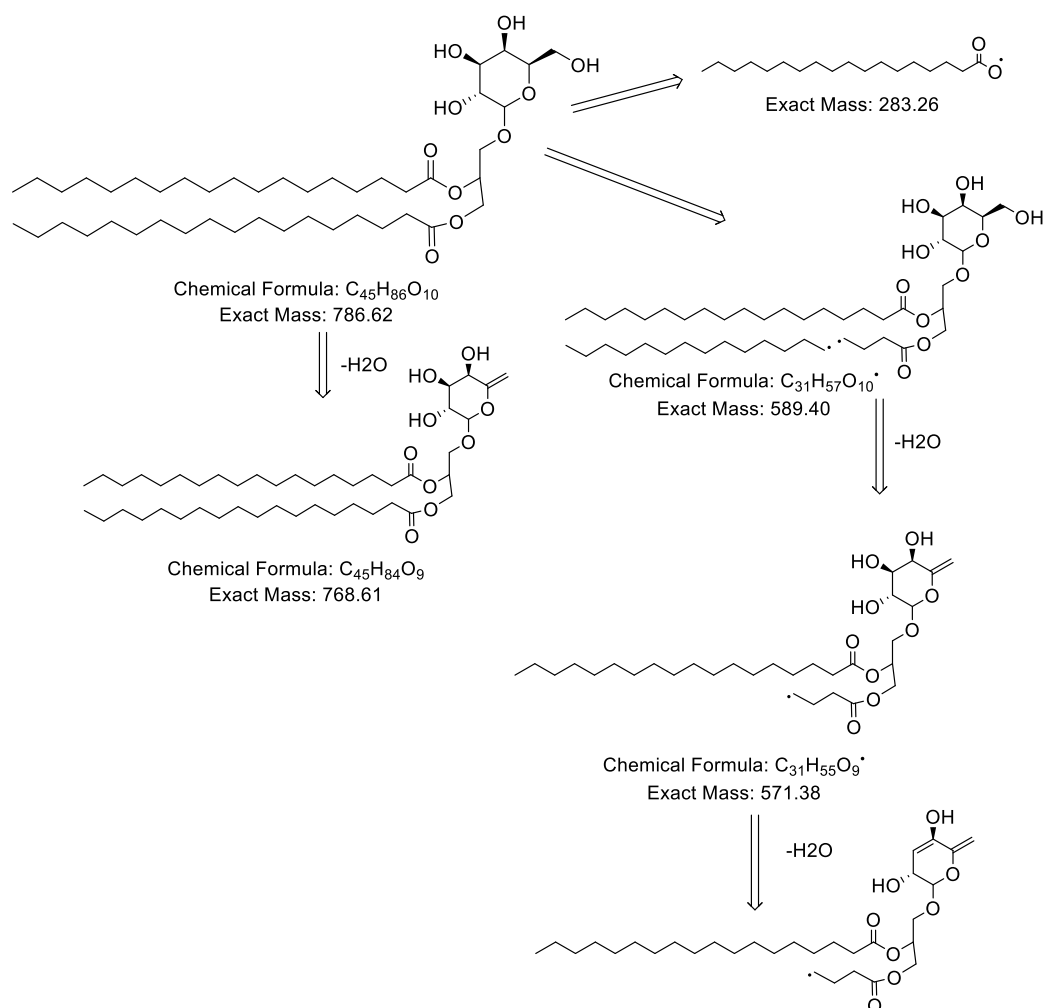
Figure 3-9. Proposed positive mode, electrospray ionization fragmentation pattern of major galactolipid detected in E-h-6B1 and E-g-2A1
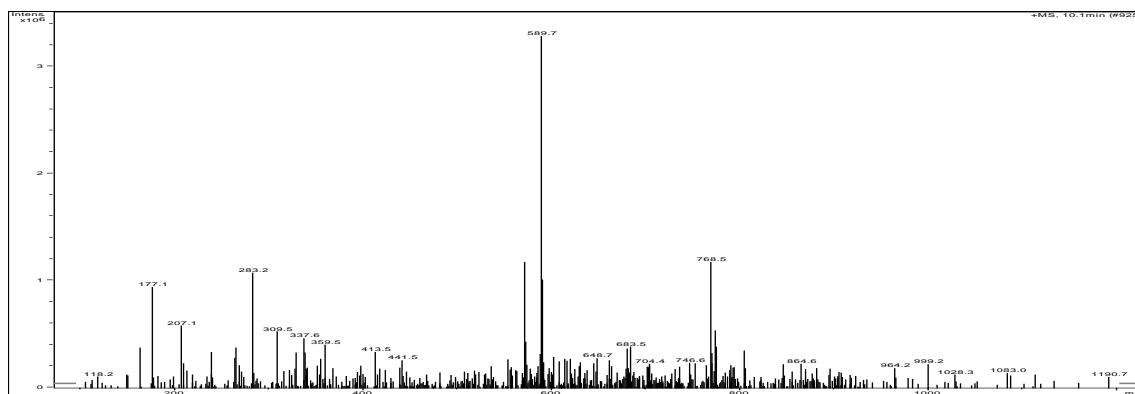
Figure 3-10. Positive mode electrospray ionization mass spectrum of the major compound isolated from E-h-6B1 and E-g-2A1

Next it was sought to identify the compound (E-h-6b1.c) possessing 776.8 m/z [M+H]$^+$ quasimolecular ion. Since the quasimolecular ion was 10 m/z units from the NMR-identity confirmed galactolipid, it was postulated that this compound possessed the same overall skeleton with a total of 5 unsaturated bonds, i.e. linoleoyl-α-linolenoyl-glyceryl-galactoside. Based on the fragmentation pattern, which showed peaks at 279 m/z and 277 m/z, the compound was hypothesized to be linoleoyl-α-linolenoyl-glyceryl-galactoside, although the positions of the fatty acid moieties could not be determined.

The final compound contained within this fraction, E-h-6b1.d, possessed a quasimolecular ion of 779.2 m/z, which corresponded to 3 unsaturated bonds within the skeleton identified by NMR. Based on the fragmentation pattern showing a major fragment at 277.3 m/z and 283 m/z, it was determined that stearoyl and α-linoleoyl moieties were present in this galactolipid. As such, this compound was tentatively identified as stearoyl-α-linoleoyl-glyceryl-galactoside. As with other compounds identified in this manner, the exact linkage between lipid chains and glycerol moiety could not be determined.
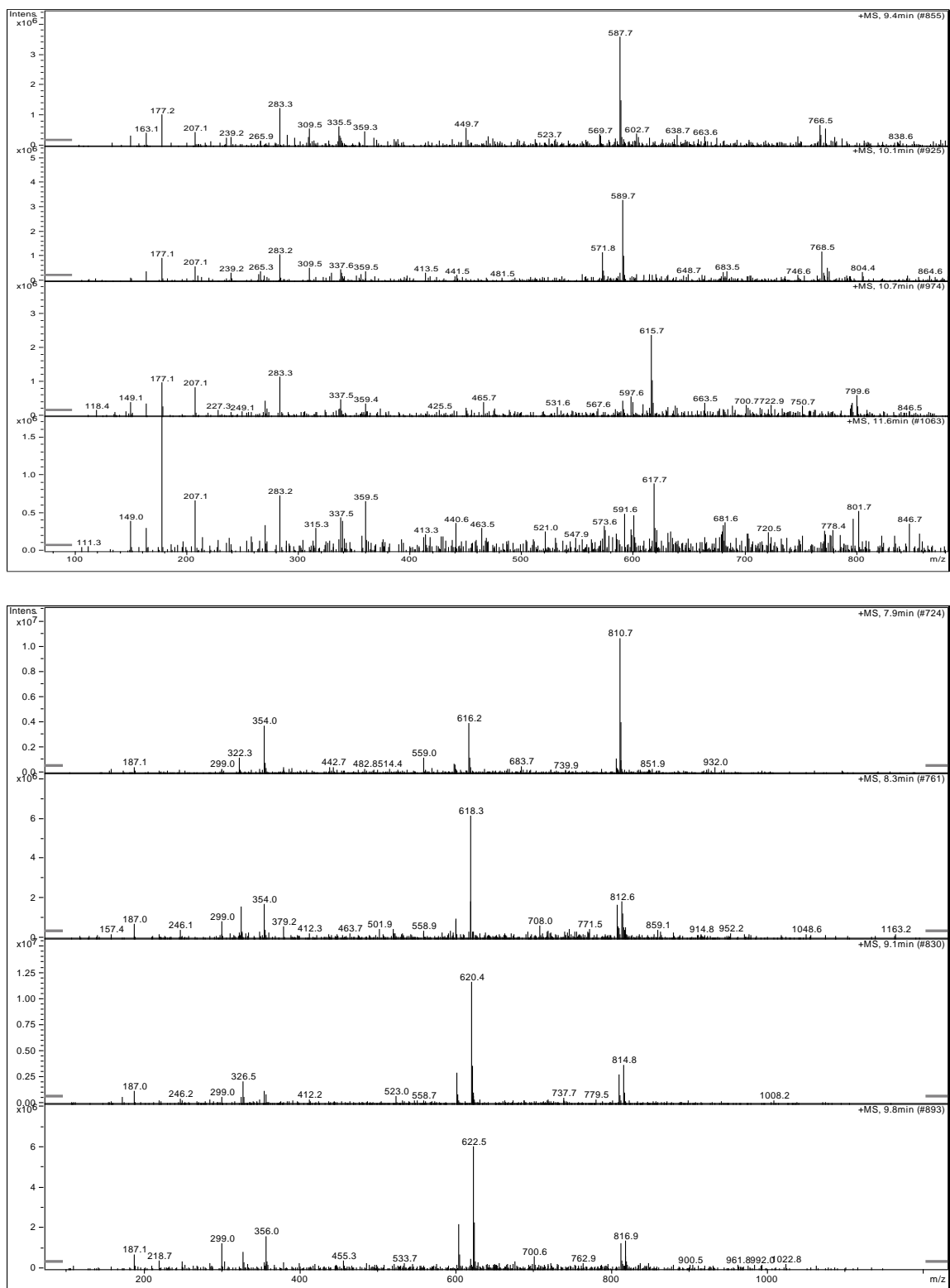
Figure 3-11. Mass spectra of compounds contained within A) E-h-6B1 and B) E-g-2A1

The major compound detected in fraction E-g-2A1 was identical to the major compound detected by LC/MS and NMR in fraction E-h-6B1, di-stearoyl-glyceryl-galactoside by retention time and mass spectrum. There were three other compounds detected possessing quasimolecular ions in negative mode of 789.7 *m/z* (M-H)⁻, 791.9 *m/z* (M-H)⁻, and 793.7 *m/z* (M-H)⁻. In positive mode, the sodium adduct quasimolecular ion was detected at 810.7 *m/z* (M+Na)⁺, identified as the major compound detected above, E-h-6B1.a = E-g-2A1.a. Also detected were E-g-2A1.b: 812.6 *m/z* (M+Na)⁺; E-g-2A1.c: 814.6 (M+Na)⁺; and E-g-2A1.d: 816.9 *m/z* (M+Na)⁺, respectively for the other peaks detected in this fraction.

Compound E-g-2A1.b, detected at peak 789.7 *m/z* (M-H)⁻ and 810.7 *m/z* (M+Na)⁺ corresponded to a reduced analogue of the major galactolipid detected, ca. the galactitol analogue of the di-stearoyl galactolipid characterized previously. While this compound could not be isolated for affirmative structural characterization, the MS fragmentation pattern was consistent with loss of deoxy-galactitol fragment, giving rise to signal at 166 *m/z* (M+) in positive mode. As such, the proposed structure of this compound was distearoyl-glyceryl-galactitol, as shown in Figure 3-12.
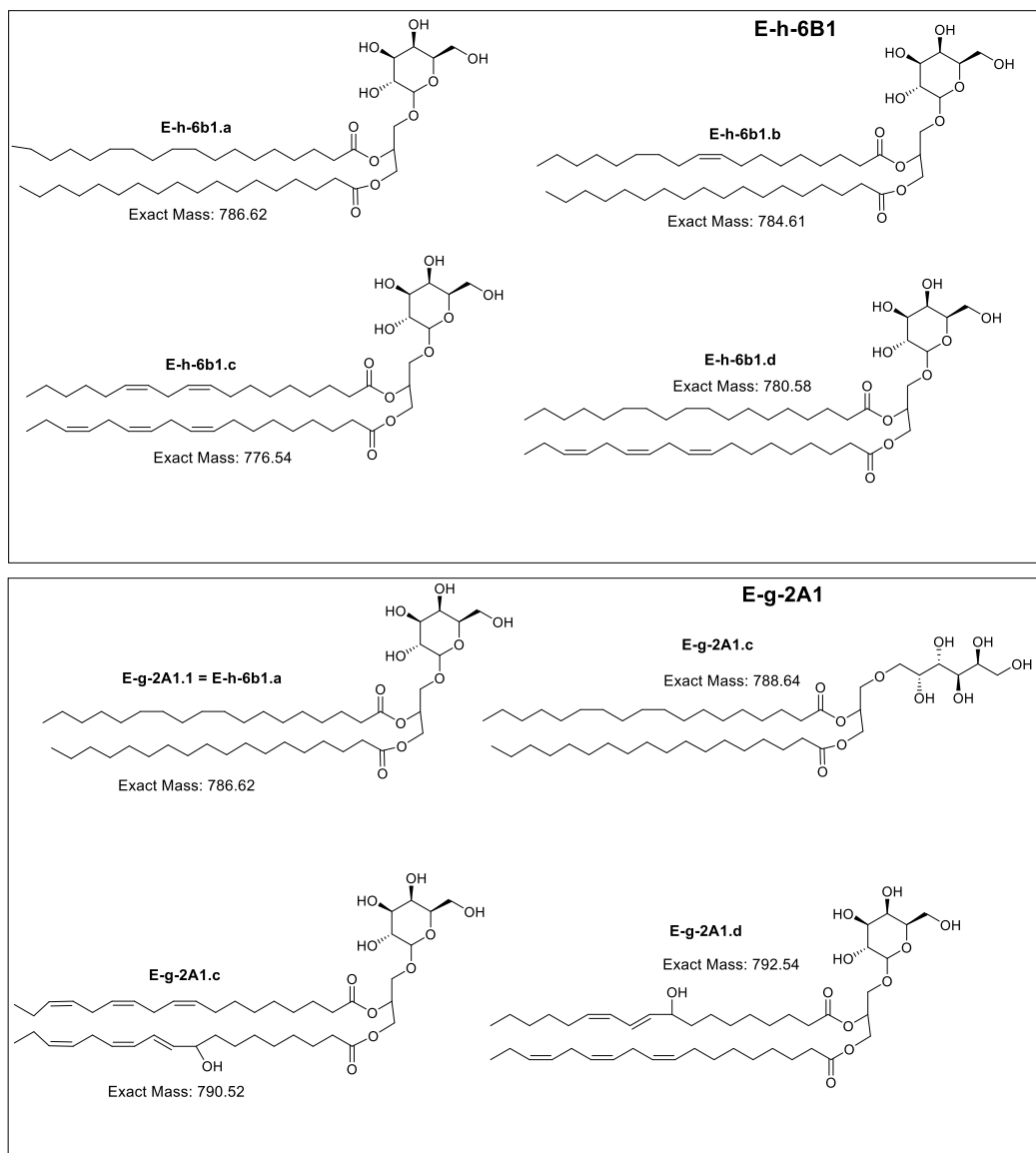
Figure 3-12. Major compound identified by LC/MS, 1H-NMR and COSY analysis (E-h-6b1.a = E.g-2A1.a); Compounds tentatively identified by MS fragmentation patterns in E-h-6B1 and E-g-2A1; exact position assignments for unsaturated side-chains on glycerol backbone was not possible by LC/MS analysis.

The final two constituents (E-g-2A1.c and E-g-2A1.d) presented some difficulty in assigning structural configuration, as the molecular weights extended past what was possible with fatty acids detected in *P. kessleri* biomass. The first indication of possible structure came from comparing the signal from one of these compounds (E-g-2A1.d) to

the signal obtained for E-h-6b1.c (linoleoyl-linolenyl-glyceryl-galactoside), exhibiting quasimolecular ion at 777 *m/z*. Comparing to the signal detected for E-g-2A1.d, which exhibited quasimolecular ion at 793 *m/z*, the difference in these ions was found to be 16 *m/z*, suggesting an oxygen-containing analogue of the E-h-6b1.c. It was therefore proposed that compound E-g-2A1.d was likely an oxidized form of linoleoyl-linolenyl-glyceryl-galactoside. It is well known that preliminary oxidation of unsaturated fatty acid side-chains occurs at the beta position to the first double bond contained starting from the acyl moiety[2], and as such, it was postulated that the oxygen would likely occur beta to the corresponding bond in compound E-g-2A1.d (shown in Figure 3-8). As with other compounds identified strictly by LC/MS characterization, affirmative assignment of the location of the oxidized side chain on the glycerol moiety was not possible.

The final compound (E-g-2A1.c) was separated from E-g-2A1.d by 2 *m/z* in MS analysis. As such, it was proposed that since E-g-2A1.d showed a quasimolecular ion at 793 *m/z* (M+H)[+], and E-g-2A1.c is 2 *m/z* lighter at 791 *m/z*, it is likely that compound E-g-2A1.c contains one more double bond than E-g-2A1.d. Unfortunately, the fragmentation pattern yielded few significant peaks that allowed comparison to absolutely defined structures, and as such the tentative structure is shown in Figure 3-8.

3.4.2.2 E-h-5D1

Compound E-h-5D1 was a brightly yellow-colored compound which exhibited a high degree of lipophilicity in HPLC analysis, and possessed a characteristic UV-Vis spectrum which is typical of xanthophyll structures. These properties greatly reduced the number

of possible molecular structures to consider, and due to the fact that xanthophylls can be

extensively characterized by UV-Vis spectrum. As such, the first analysis conducted was

to   evaluate   the   UV-Vis   spectrum   (shown   in
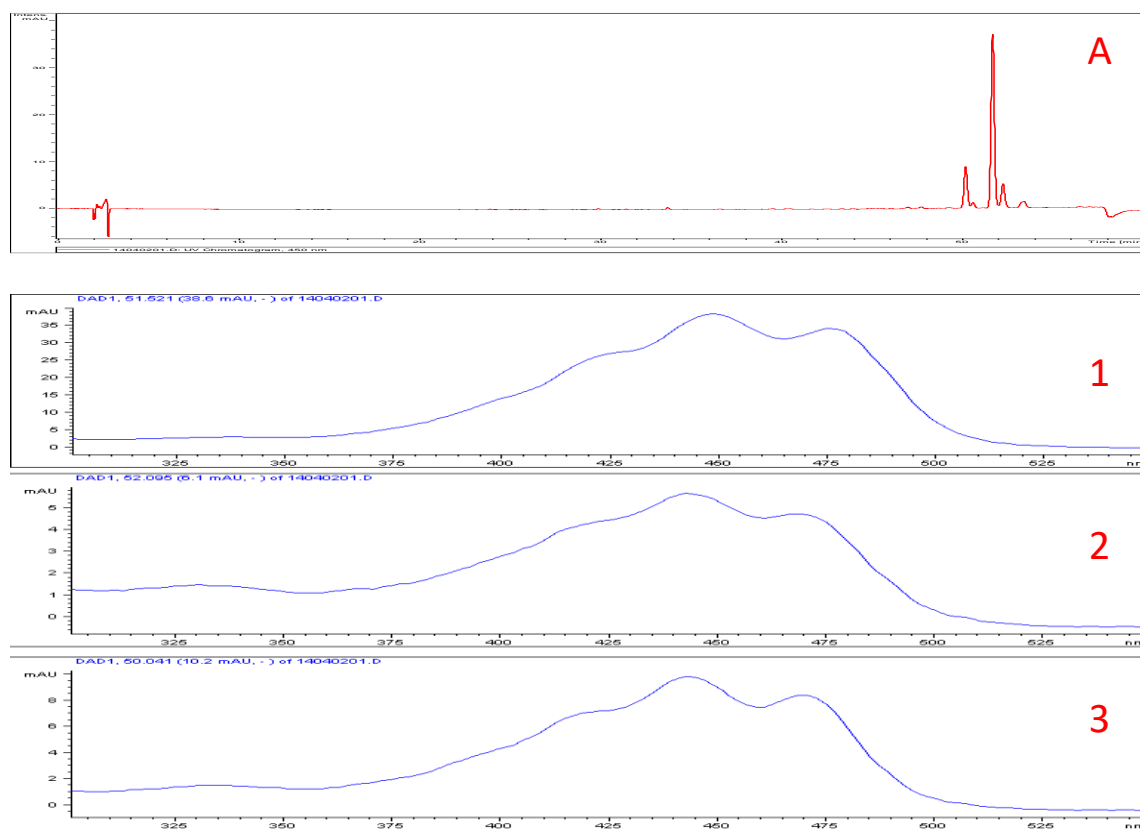
Figure 3-13) to attempt to identify the major structure contributing to the chromophore

of this structure.
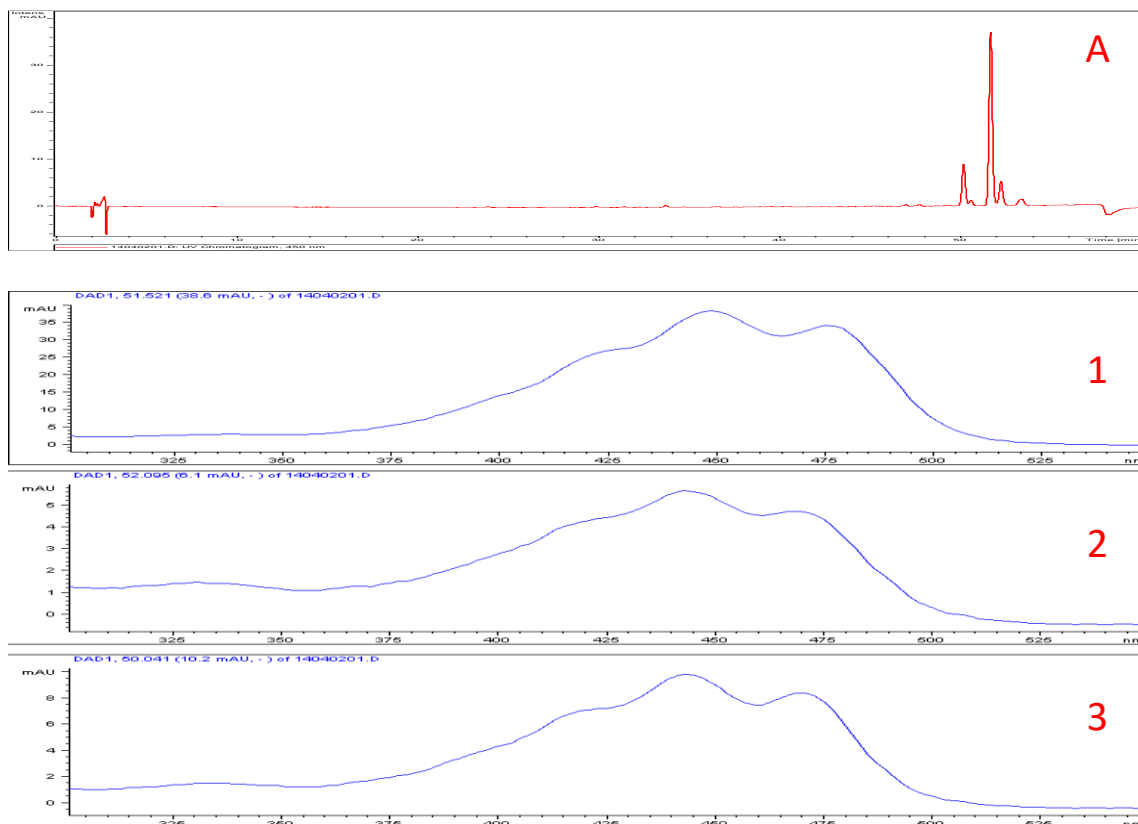
Figure 3-13. HPLC chromatogram of E-h-5D1, showing one major isomer and two minor isomers; 1) UV-Vis spectrum of major isomer, all-trans; 2) UV-Vis spectrum of minor cis isomer, as indicated by peak at 335 nm; 3) UV-Vis spectrum of minor di-cis isomer indicated by peak at 335 nm;

As can be readily seen, the UV-Vis spectrum exhibits a characteristic xanthophyll spectrum[3], with 3 closely adjacent peaks, assymetrically arranged about the center. The absorbance wavelengths and ratio between intensities of two major peaks are characteristic of specific xanthophyll moieties, and can be applied with great utility to the identification of xanthophylls, as is described in detail in section 3.7.2.2 on page 201. As can be seen, the II and III peak in the UV-Vis spectrum are located at 448 nm and 472 nm, respectively, and the I peak was barely detectable, cutting into the shoulder of the response curve. The ratio of intensities of peaks II and III was 42%. The only compound known with current data available that matches these absorption characteristics was

found to be the 19'-butanoyloxy analogue of fucoxanthin[3]. While the known derivative matched characteristic absorbance in UV-Vis spectrum, the data obtained from LC/MS analysis suggested an analogue with a higher molecular weight than the 19'-butanoyloxy analogue of fucoxanthin (Figure 3-14).
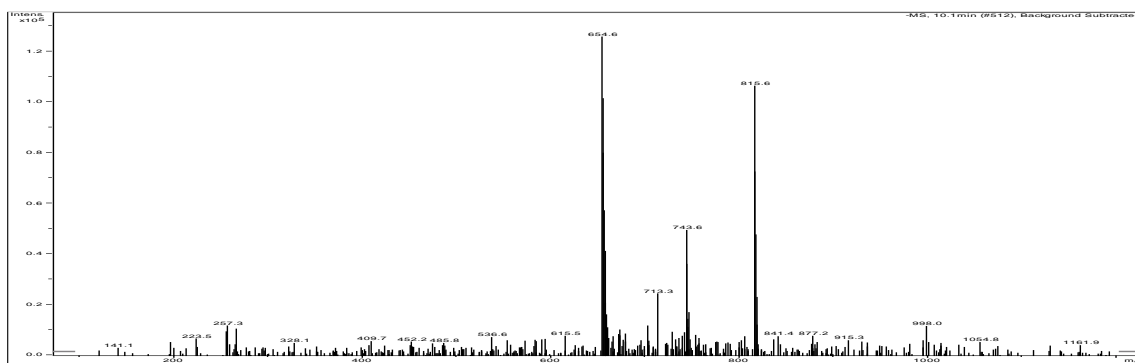
Figure 3-14. Mass spectrum of E-h-5D1 in positive ESI-MS

The quasimolecular ion detected by HPLC/MS was 830.6 m/z (M+H)[+], suggesting an additional 84 Da compared to the known 9'butanoyloxyfucoxanthin[3]. Looking further at the MS data, an ion was detected at 660.1 m/z, suggestive of the fucoxanthin M+H − R group, wherein the R group has a mass of 171 Da. This can be placed into context when examining the reported MS fragmentation of the butanoyloxy fragmentation pattern, showing a loss of the butanoyloxy fragment of 88 m/z in ion-trap MS[3] (and as such the lost ion is neutral, whereas in ESI-MS, one would expect loss of 87 m/z). Taking the 84 Da difference in molecular weight between the unknown compound and the 9'-butanoyloxyfucoxanthin analogue, it was hypothesized that 6 additional methylene groups (6*14 = 84) were present in the unknown compound compared to the 9'-butanoyloxy analogue. As such, the hypothesized structure was 9'-

decanoyloxyfucoxanthin (shown below in Figure 3-15). This structure is consistent with the proposed fragmentation pattern, also shown in Figure 3-15.

As can be readily seen, the major structure fragments into two main fragments; one at 744.4 *m/z*, and the other at 658.4 *m/z*. The 744.4 *m/z* fragment is separated by the quasimolecular ion by 85, which corresponds to a loss of hexyl fragment from the dodecyl ester side-chain. The other fragment at 658.4 *m/z* corresponds to a complete loss of the dodecyloxy group, leaving fucoxanthin radical cation. Unfortunately, since a limited amount of this compound was obtained, no follow up characterization studies could be conducted.
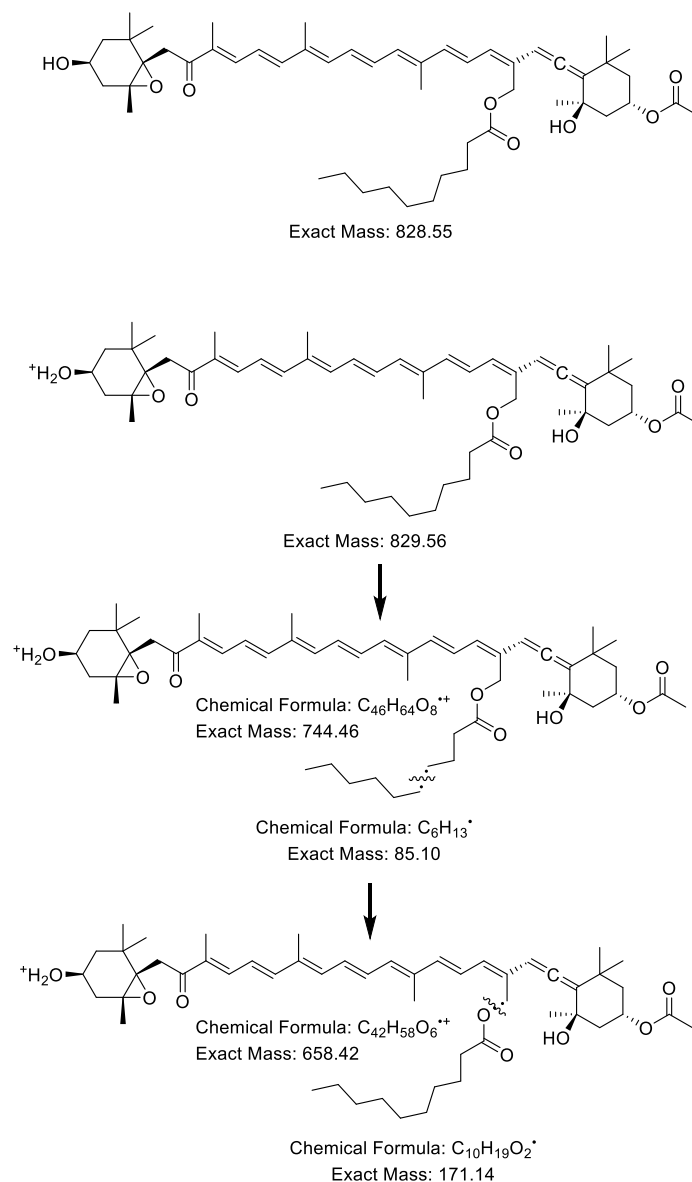
Figure 3-15. Structure of compound isolated in E-h-5D1: 9'-decanoyloxyfucoxanthin (Top); Proposed fragmentation pattern corresponding to positive ESI-MS (Bottom)

3.4.2.3 E-e-0 (stigmasterol)

E-e-0 was obtained as a waxy solid precipitate and analyzed by HPLC/MS. HPLC chromatogram showed a highly pure compound, with very minor impurities (Figure 3-17), absorbing heavily at 210 nm and 254 nm, and to a lesser degree at 280 nm. Based on the

retention time of this compound (R_t = 30.9 min) for a method (14110717.D) which elutes hydrophobic constituents in this range. The MS data were assessed for indications of potential structural assignments. Based on prior experience with sterols in our lab, the quasimolecular ion corresponding to 413.5 *m/z* (M+H)$^+$, and with the long retention time and UV-Vis absorption characteristics, this compound was hypothesized to be stigmasterol, with a molecular weight of 412.7. This was further evidenced by the fragmentation pattern—there was one major fragment at 274.5 *m/z*. Prior experience with sterols suggested that the 274.5 *m/z* fragment corresponded to [M+H − $C_{10}H_9$]$^+$, or loss of the side chain from the sterol skeleton (shown below in Figure 3-18).

To obtain more data to aid in the characterization of this compound, it was decided to inject the pure compound for GC/MS analysis. Mass spectra derived from GC/MS analysis contain data more useful for characterization, especially for sterols and fatty acids. Injection of the purified compound gave one major peak whose mass spectrum was screened for similarity in the NIST GC/MS database. The spectrum with the highest similarity (98) to the compound in E-e-0 was found to be stigmasterol (see Figure 3-16). This hypothesis led to comparison of the compound in E-e-0 to commercially obtained stigmasterol (Figure 3-17), showing co-elution of peaks, confirming the identity of E-e-0 as stigmasterol.
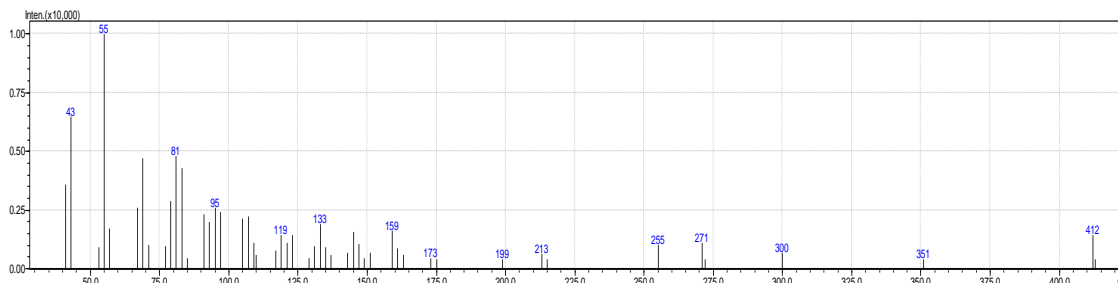
Figure 3-16. GC/MS spectrum obtained from the major compound detected in E-e-0, identified as stigmasterol by comparison to NIST GC/MS database
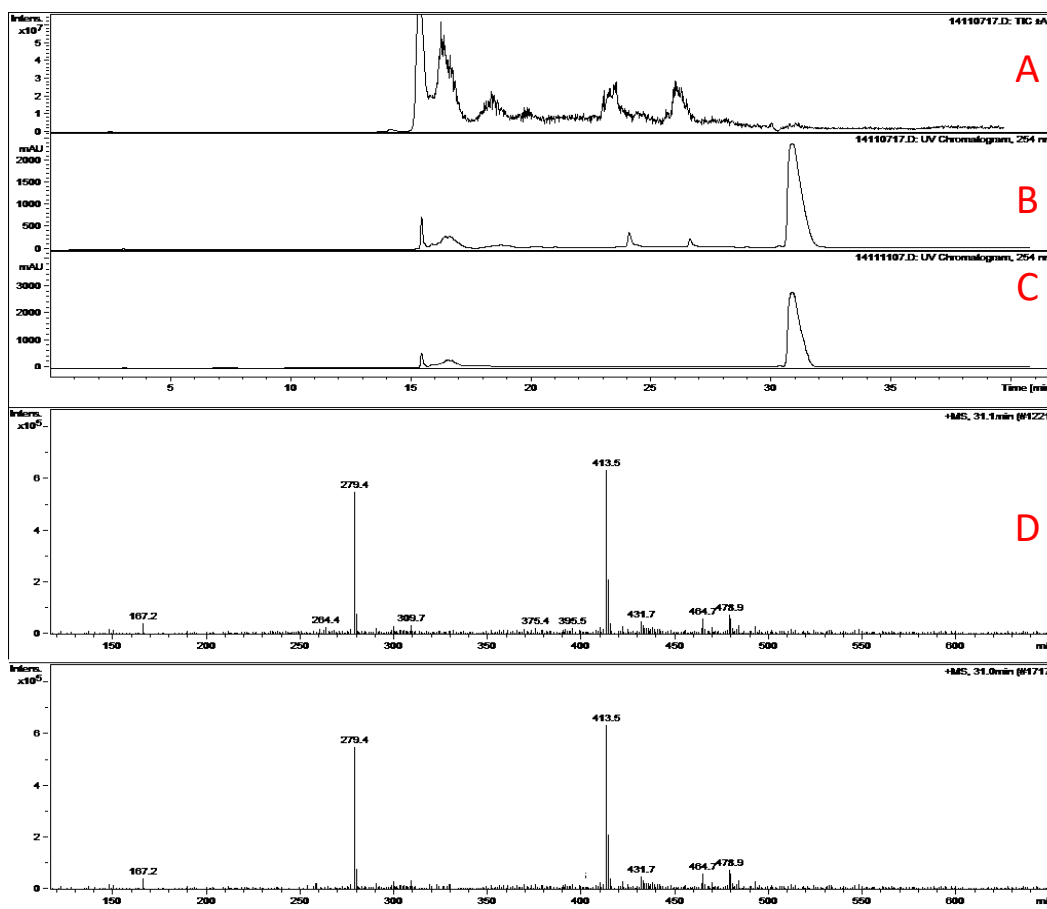
Figure 3-17. HPLC/UV/MS chromatogram of A) Total ion chromatogram of E-e-0 (stigmasterol); B) UV-Vis chromatogram at 254 nm of E-e-0; C) commercially available stimgasterol; and D) positive mode ESI-MS spectrum of E-e-0, showing (M+H)+ quasimolecular ion at 413.5 *m/z*, identical to E) commercially available stigmasterol.

Chemical Formula: $C_{10}H_{19}\cdot$
Exact Mass: 139.15

HO

Exact Mass: 412.37

^+H_2O

Chemical Formula: $C_{19}H_{30}O\cdot^+$
Exact Mass: 274.23
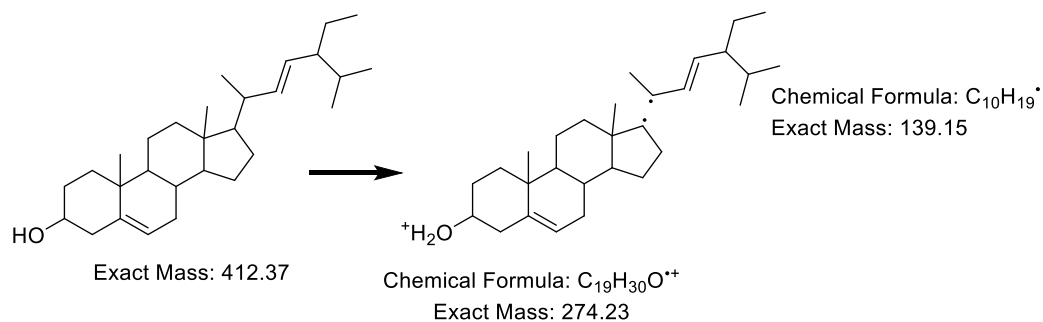
Figure 3-18. Structure of stigmasterol, major compound detected in E-e-0 and MS fragmentation pattern.

3.4.2.4 E-e-A1 (carbendazim)

Fraction E-e-A1 exhibited a highly pure, white solid compound which was soluble in polar solvents such as methanol. This compound presented intense anti-fungal activity during the biological screening assay, and thus its characterization was of great interest. Characterization of E-e-A1 was conducted by HPLC/MS analysis, followed by ^{1}H-NMR characterization, and finally comparison to known reference material. HPLC analysis showed E-e-A1 was highly pure (>99%) by 280 nm UV-Vis spectrum (shown in Figure 3-20). The mass spectrum consisted of only two peaks, at 192.0 *m/z* and 160.1 *m/z*. A search of the literature in SciFinder for articles containing the phrase "192 *m/z*" AND/OR "160 *m/z*" was conducted. Several hundred articles were detected, but the most relevant contained a reference to both phrases. The article referenced analysis of pesticide levels in produce, and cited the detection of carbendazim, a common anti-fungal pesticide, at 192 *m/z* and 160 *m/z* in positive ESI-MS[4]. Further 1H-NMR analysis was conducted, and the following data were obtained: 7.35 ppm (2 H, m) representing the two aromatic protons closer to the nitrogens on the ring, 6.98 ppm (2H, m) for the two distal aromatic

nitrogens at the 6 and 7 positions, and 3.73 ppm (3H, s) for the methyl protons on the ester, consistent with the structure for carbendazim.
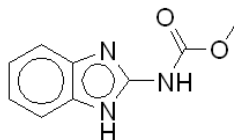
Figure 3-19. Structure of carbendazim, synthetic anti-fungal compound detected in E-e-A1

 These data suggested carbendazim as a probable identity for the compound, although since carbendazim is a synthetic compound not found in nature, its presence in the algal biomass was not immediately understood.   Investigation to possible sources of contamination were conducted, and concluded after we inquired to AL-G Technologies, the producer of the biomass used in this study, about the possible use of fungicides not disclosed previously in this project. They confirmed the presence of carbendazim in their proprietary growth media, used at low levels continuously to ward off fungal infections of the algal biomass. As such, it was concluded that the identity of E-e-A1 was the synthetic compound carbendazim (shown in Figure 3-19), a previously undisclosed contaminant of the algae processing methodology.
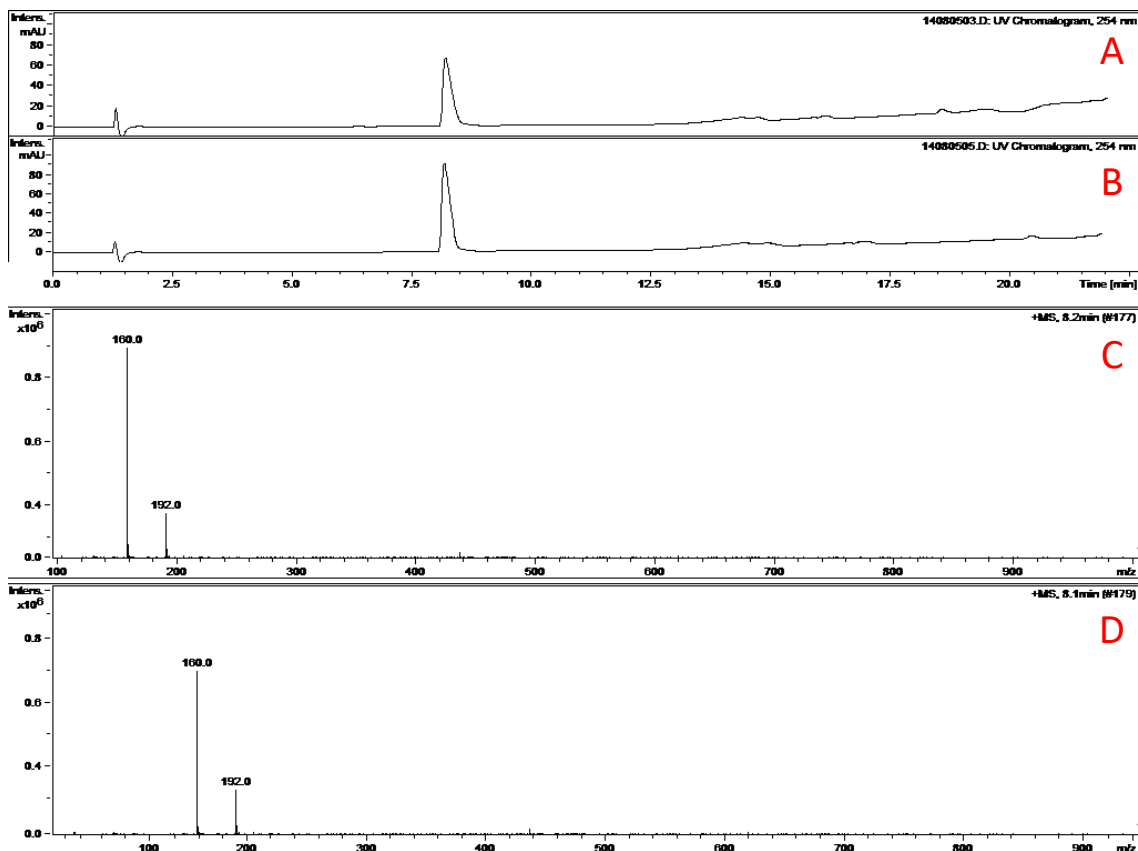
Figure 3-20. HPLC chromatogram at 254 nm of A) E-e-A1 (carbendazim); B) commercially available carbendazim. The mass spectra of C) E-e-A1 and D) carbendazim showed excellent correspondence

3.4.2.5 E-a-1 (ergosterol)

Compound E-a-1 was obtained pure as a white flaky solid after precipitation following chromatographic purification. This compound was analyzed by HPLC/MS to conduct preliminary investigation into its structure. HPLC/MS analysis showed a high concentration of one major compound with intense UV-Vis absorption at 210 nm and slight absorption at 254 nm (see Figure 3-21). The positive mode ESI-MS quasimolecular ion was detected at 397.6 m/z, which due to previous experience identifying sterols in plant material, suggested ergosterol may be a potential identity of this compound, since

it too demonstrates a molecular ion peak at 397 *m/z*. A commercially-obtained sample of ergosterol was injected under the same conditions as E-a-1 for HPLC/MS and was found to co-elute with the unknown compound (see Figure 3-21), confirming its identity as ergosterol. Furthermore, this compound was analyzed via GC/MS, which gives better characteristic fragments compared to LC/MS, and can be utilized with software processing to compare against known compounds in the NIST GC/MS database. The mass spectrum obtained had a high similarity index = 99 (see Figure 3-22) compared to known ergosterol in the NIST GC/MS database, and thus the identity was confirmed as ergosterol.
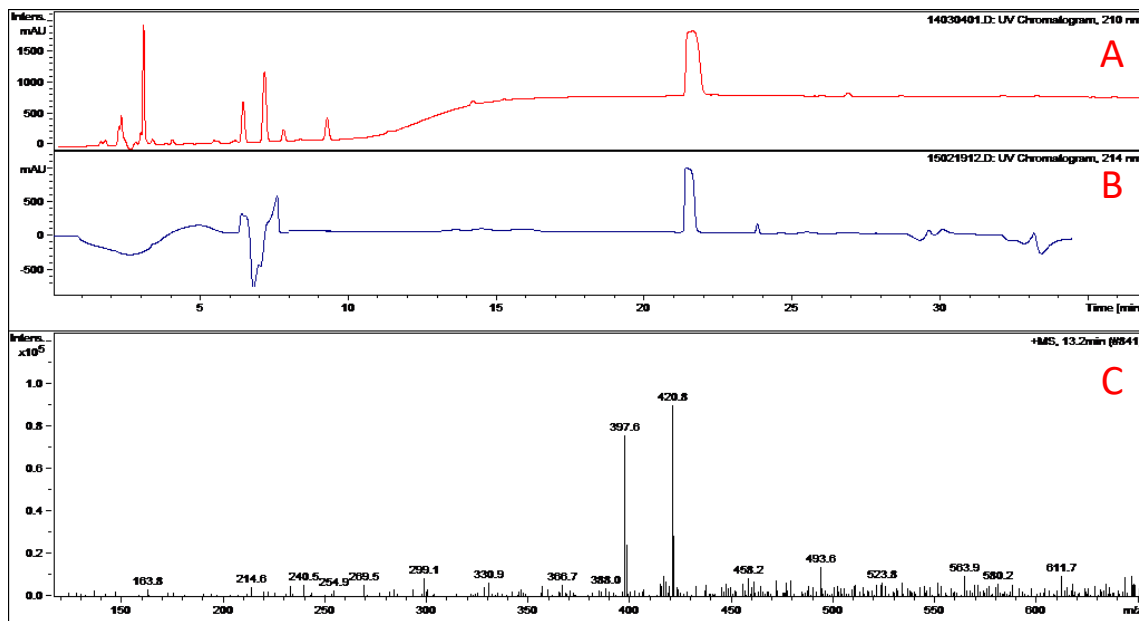
Figure 3-21. HPLC chromatogram at 210 nm of A) fraction E-a-1 (ergosterol) compared to B) commercially available ergosterol. C) ESI-MS spectrum of E-a-1, consistent with ergosterol standard.
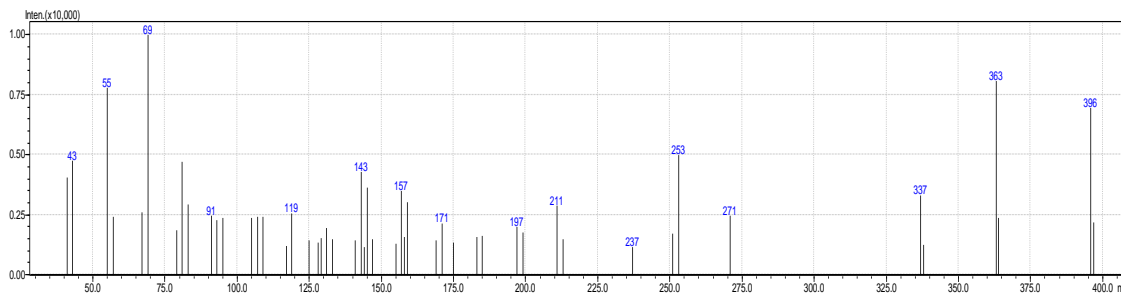
Figure 3-22. GC/MS spectrum of major compound in E-a-1, identified as ergosterol by comparison to NIST GC/MS database

3.5 Investigation of Butanol fraction (B)

3.5.1 Isolation of components contained in B

The butanol fraction of *Parachlorella kessleri* contained a significant quantity of the total mass extracted—8.9 g out of 43 g total extract. Based on the separation achieved via silica TLC with 10% methanol/chloroform, it was decided to utilize column chromatography with fine-grade Silica H. 7.1 g of the butanol fraction was dissolved into 20% methanol/chloroform and loaded onto 10 g Silica H by thorough mixing and drying in the fume hood. After drying, the silica H/butanol fraction slurry was thoroughly mixed by repeated dividing and mixing to ensure complete adsorption to the silica. A 30 cm column of dry Silica H was packed in a 4.5 cm (2") diameter glass column. The butanol / silica H powdered mixture was loaded onto the column and elution was began with 100% chloroform. 200 mL fractions were collected throughout elution. 600 mL chloroform was eluted for the first 3 fractions. A stepwise gradient from 5% to 25% methanol in chloroform was used to collect 30 fractions. TLC comparison of the fractions allowed for many fractions to be combined, yielding 12 fractions (see Figure 3-23).
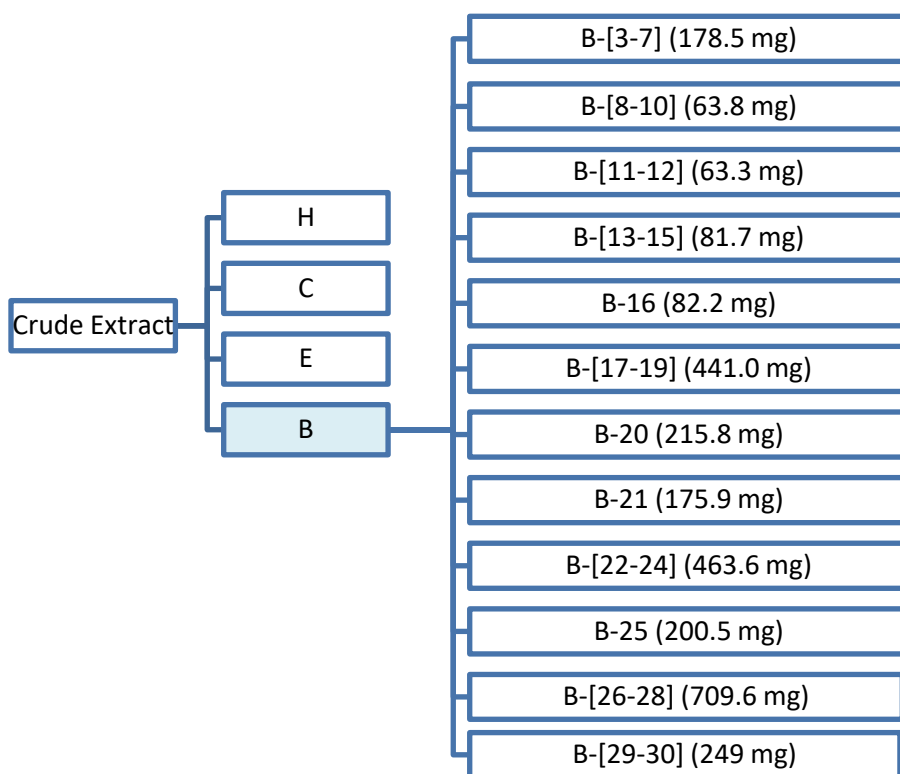
Figure 3-23. Flowchart of preliminary fractionation of butanol fraction (B)

For the sake of clarity, the fractions which consisted of combined portions (e.g. B-[3-7]) were labeled by the first fraction contained in the combination, so B-[3-7] would be B-3, B-[8-10] would be B-8, and so on. These fractioned were then screened in a number of bio-assays, including the mono-acyl glycerol lipase inhibition assay (section 5.1.2.2), fatty acid amide hydrolase (section 5.1.2.1) and pancreatic lipase (section 4.4), however only one sub-fraction exhibited notable activity: B-8, which showed substantial inhibition of pancreatic lipase (Figure 4-6, pg. 222) at a concentration of 100 μg/mL.

As such, B-8 was selected first for sub-fractionation via Sephadex LH-20 column chromatography (15x5 cm) using methanol as an eluent. B-8 (43.2 mg) was dissolved in 1 mL methanol and loaded onto the column. Elution with 200 mL methanol provided three fractions: B-8A (16.4 mg), which was a complex mixture by TLC; B-8C (4.8 mg), which

contained an intensely blue compound which was quite pure by TLC; and B-8B, which contained the same compound as B-8C but with some overlapping green pigments, presumed to be chlorophyll derivatives. A flowchart of the separation scheme is shown in

Figure 3-24.

In order to obtain more of the blue compound contained in B-8C for characterization, B-8B was loaded onto the Sephadex LH-20 column for a second pass. The blue fraction was isolated and returned for a third pass on the Sephadex LH-20 column to obtain B-8B-2 (3.5 mg) which was nearly pure by HPLC/MS (Figure 3-25). This compound was selected for characterization by MS and NMR (section 3.5.2).
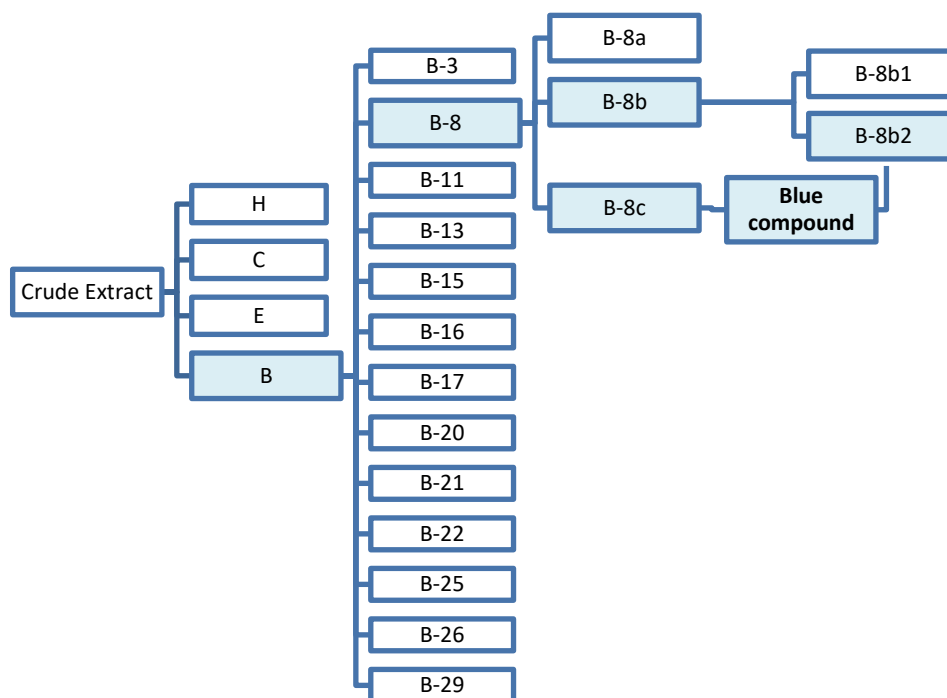
Figure 3-24. Separation flowchart for sub-fraction B-8, containing the unknown blue pigment.
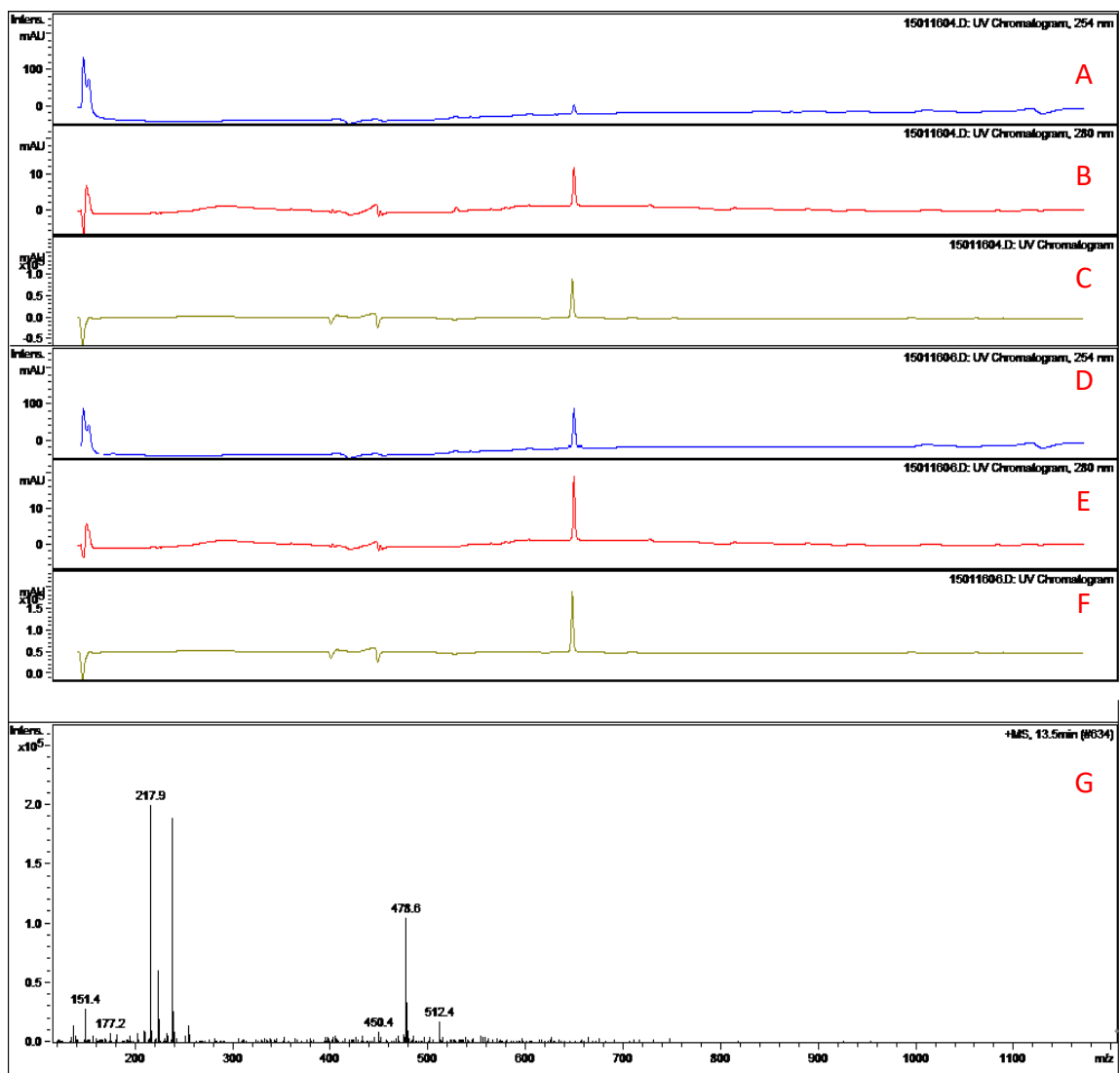
Figure 3-25. HPLC/UV/MS chromatograms of B-8B2 A) 254 nm UV chromatogram; B) 280 nm UV chromatogram; C) 660 nm UV-Vis Chromatogram; and B-8C D) 254 nm UV chromatogram; E) 280 nm UV chromatogram; F) 660 nm UV-Vis Chromatogram; and G) Mass spectrum of B-8C

While the remaining fractions were not active in the assays utilized to screen the biomass,

they contained several major compounds and so effort was taken to isolate and identify

them. Due to the purity of B-20 and B-21, they were selected first for sub-fractionation;

see HPLC chromatograms in
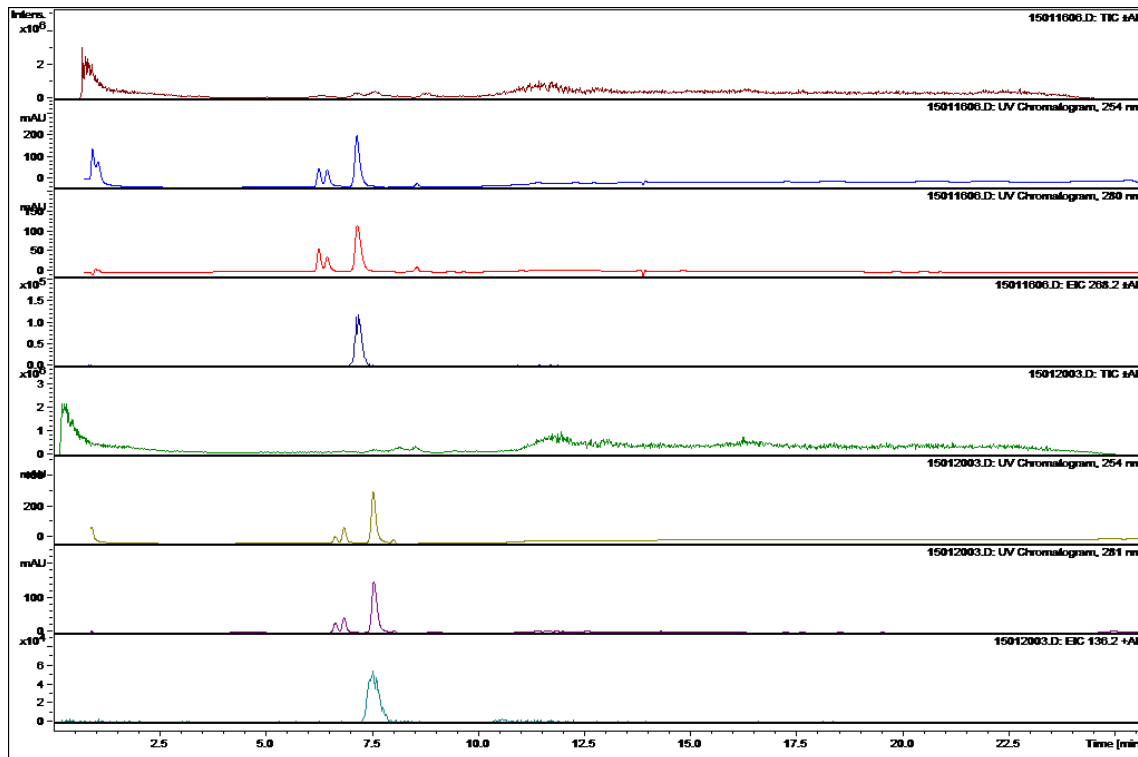
Figure 3-26. B-20 (107.2 mg) was dissolved in minimum methanol and fractionated across a 15x5 cm column of Sephadex LH-20. Elution with methanol provided 3 fractions, wherein B-20c contained the major compound. B-20c was placed in the -20˚C refrigerator overnight while dissolved in methanol, and serendipitously, a precipitate was formed containing the major impurity. The mixture was filtered, giving the filtrate, B-20c-fltr and the precipitate, B-20c-ppt (10.4 mg). B-20c-fltr was quite pure by LC/MS (data not shown) and was selected for characterization. B-21 was purified in a similar fashion—dissolution in methanol followed by precipitation in the -20˚C freezer. The filtrate (B-21-fltr) and the precipitate (B-21-ppt) were separated by gravity filtration while still cold. B-21-fltr (6.8 mg) was relatively pure and was selected for characterization.
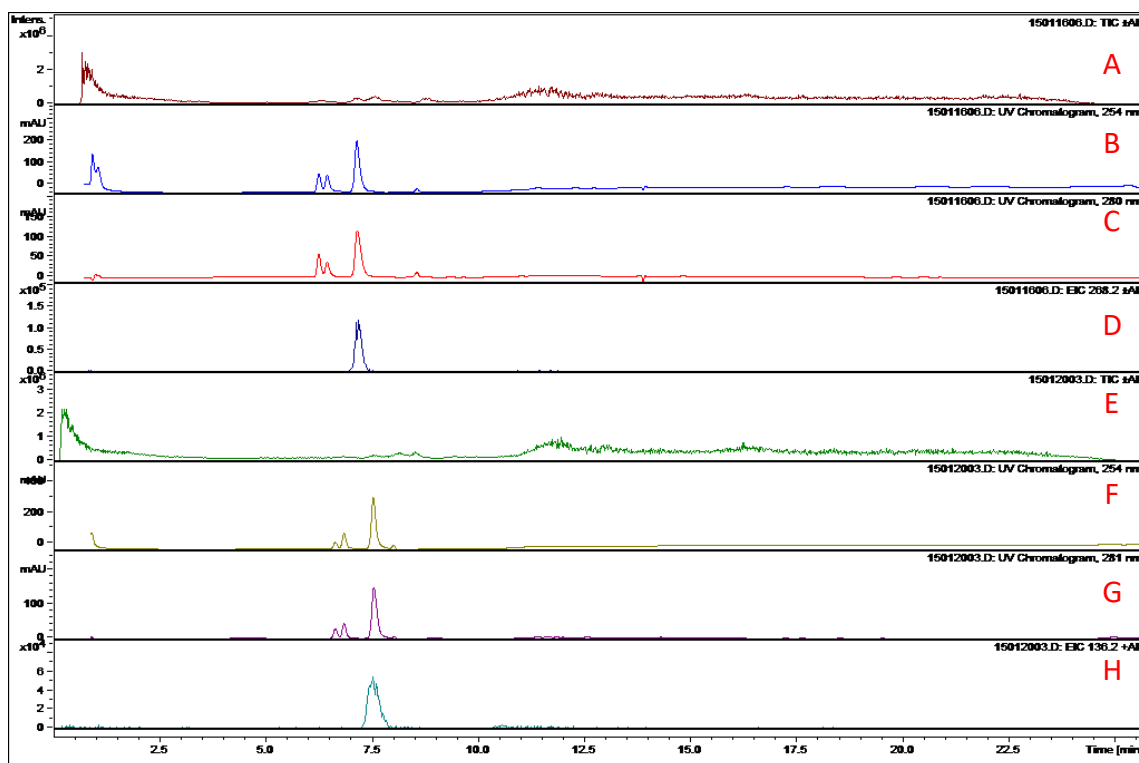
Figure 3-26. HPLC/UV/MS Chromatogram of sub-fractions B-20: A) Total ion chromatogram; B) 254 nm UV-Vis chromatogram; C) 280 nm UV-Vis chromatogram; D) Extracted ion chromatogram of 268.2 *m/z*; and B-21: E) Total ion chromatogram; F) 254 nm UV-Vis chromatogram; G) 280 nm UV-Vis chromatogram; H) Extracted ion chromatogram of 136.2 *m/z*;
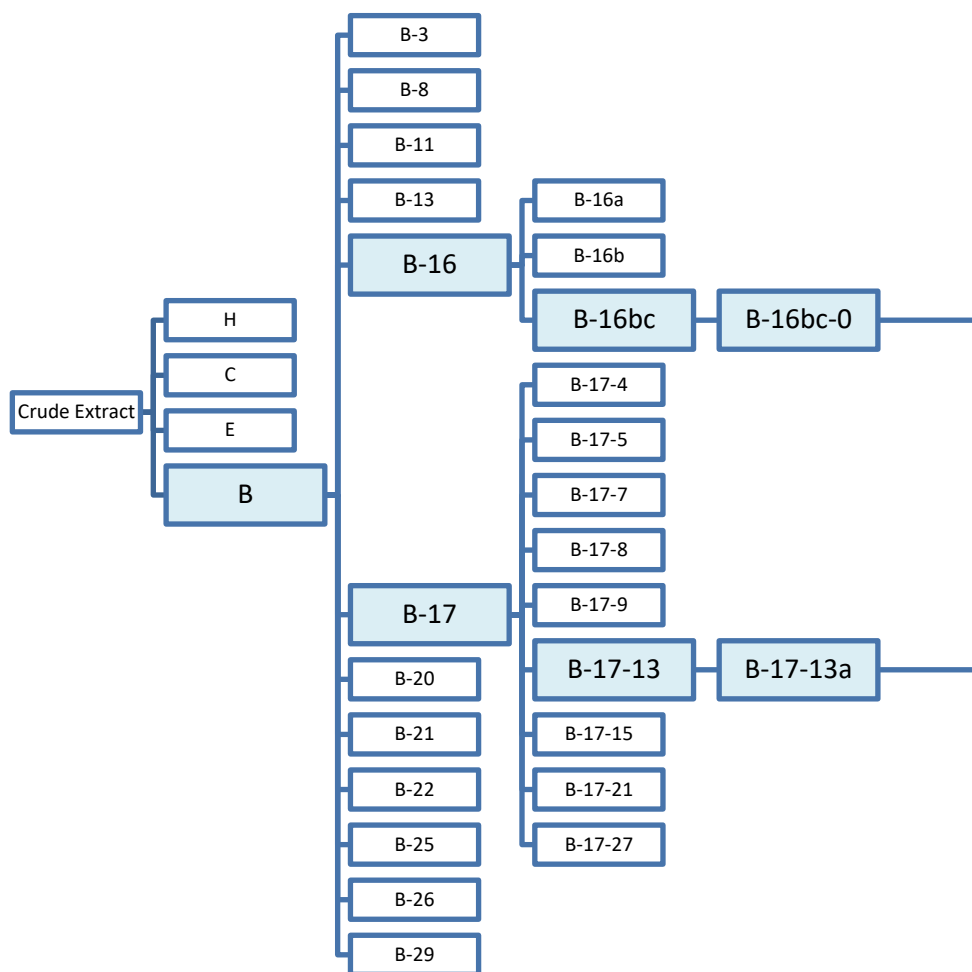
Figure 3-27. Flowchart of sub-fractionation of fractions B-16 and B-17

The next fraction selected for sub-fractionation was B-17. Silica H fractionation was selected due to the separation achievable across silica TLC using methanol/chloroform mixtures. B-17 (440 mg) was dissolved in approximately 5 mL 1:9 methanol/chloroform and loaded onto a column packed to a height of 20 cm at a width of 5 cm with Silica H in 1:19 methanol/chloroform. A total of 30 fractions were collected of a volume of approximately 200-250 mL each. TLC analysis allowed for combination to give 9 final fractions, although only 44% by mass of material eluted from this column, even at high

concentrations of methanol (30% in chloroform). The fractionation flowchart for B-17 is shown in Figure 3-27.

Fraction B-17-13 (17.6 mg) was highly pure by TLC, with a smudge of non-eluting junk, as is the accepted term. By HPLC/UV/MS, this fraction was indeed highly pure, containing one major compound with a shoulder that exhibited identical mass spectrum to the major peak (Figure 3-28). The compound eluted quickly in high polar solvent on reversed-phase HPLC, indicating a high polarity for this compound. To purify for characterization, this compound was selected for separation across a C18 solid-phase extraction cartridge (SPE), which acts as a "mini-column" and is highly useful for cleanups prior to characterization by MS or NMR[5]. A C18 cartridge (1 g solid phase, 2 cc loading volume, Sigma-Aldrich, St Louis, MO) was washed first with 10 mL HPLC grade water, 10 mL HPLC grade methanol, and finally 10 mL HPLC grade water with 1% formic acid. The column was eluted dry. B-17-13 was dissolved in 1:1 water/methanol and loaded onto the column. The first fraction was eluted with 5 mL 1:9 methanol/HPLC grade water; this fraction contained the compound of interest, B-17-13a. Fraction B-17-13a was highly pure by HPLC/UV/MS and was selected for characterization. At this point, it was recognized that B-16 contained a significant quantity of the major compound contained in B-17-13a, and so the fractions were combined. Furthermore, comparison of B-13 to B-17-13a showed that the major compound contained within B-13 was identical to B-17-13a, and was further separated in the same fashion as described below for B-13.

The next fraction selected for separation was B-13, planned for separation on a 5x15 cm Sephadex LH-20 column. Fraction B-13 (63 mg) was dissolved in a minimum quantity of methanol (~ 750 μL) and loaded onto the Sephadex LH-20 column. 18 fractions were eluted with methanol. These fractions were combined by TLC analysis to give 3 fractions: B-13A (2.3 mg), B-13B (2.1 mg) and B-13C (3.1 mg). B-13B contained the major compound of interest, which was quite pure by HPLC/UV/MS (Figure 3-28). This fraction was selected for characterization by MS.
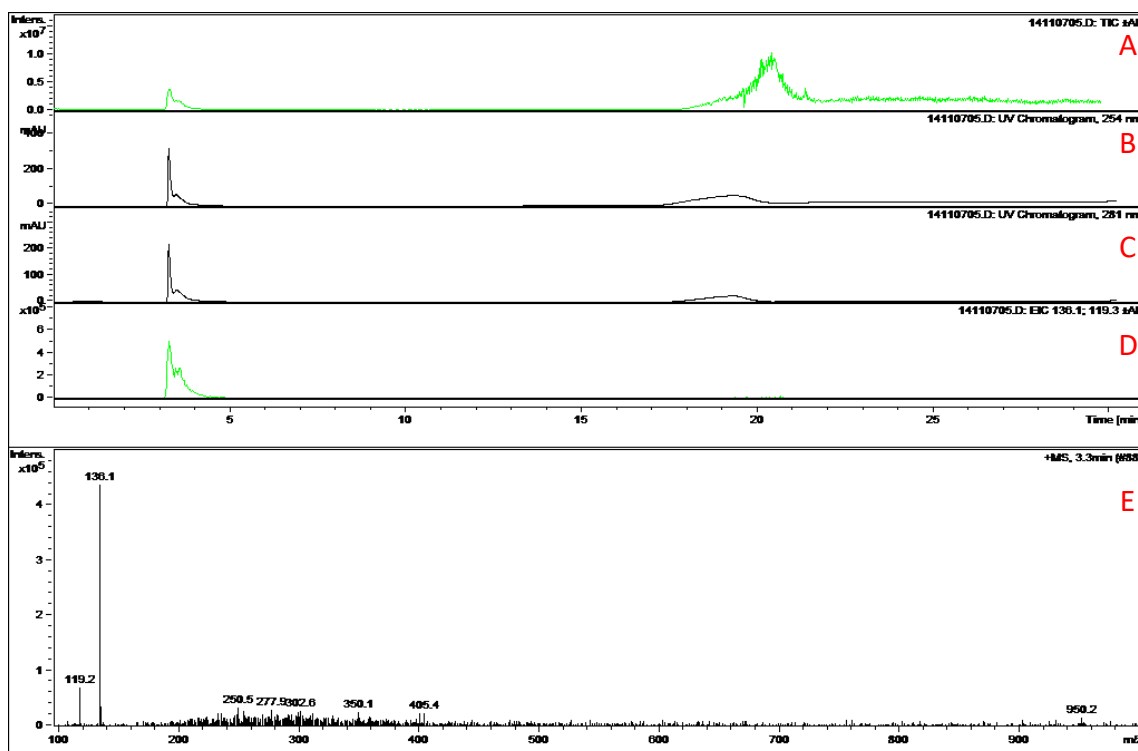
Figure 3-28. HPLC/UV/MS chromatogram of B-13B, also the major constituent in B-16 and B-17-13a; A) Total ion chromatogram; B) 254 nm UV-Vis chromatogram; C) 281 nm UV-Vis chromatogram; D) Extracted ion chromatogram at 136.1 *m/z*; E) Mass spectrum of major compound in B-13B

The next fraction selected for isolation was B-25. B-25 (55 mg) was dissolved in methanol and loaded onto a 5x15 cm Sephadex LH-20 column. A total of 18 fractions were collected

(~10 mL each). By TLC, the fractions were combined to give 4 fractions: B-25-10 (6.9 mg)

and B-25-13 (7.3 mg) were the fractions of interest. HPLC/UV/MS analysis indicated that

B-25-10 and -13 were relatively pure, containing a few minor impurities (
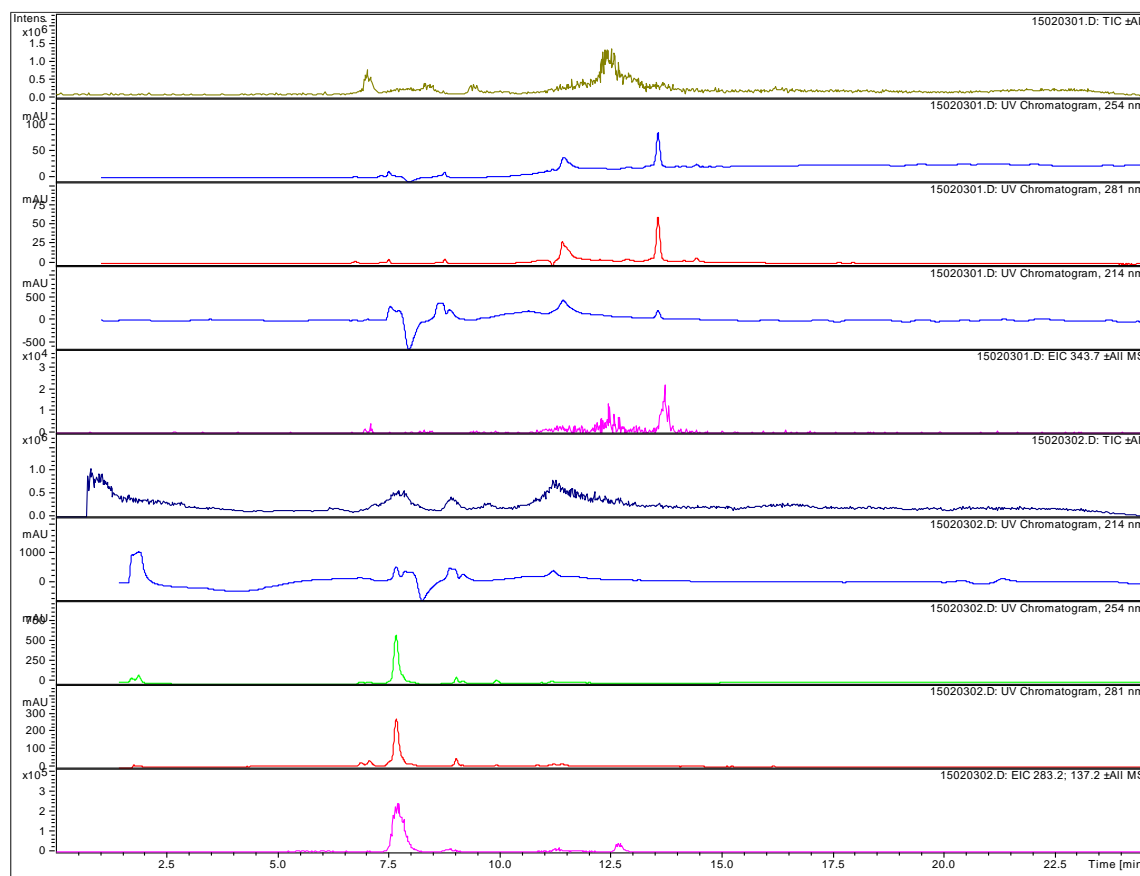
Figure 3-29). The characterization of these compounds is described in the following

section.
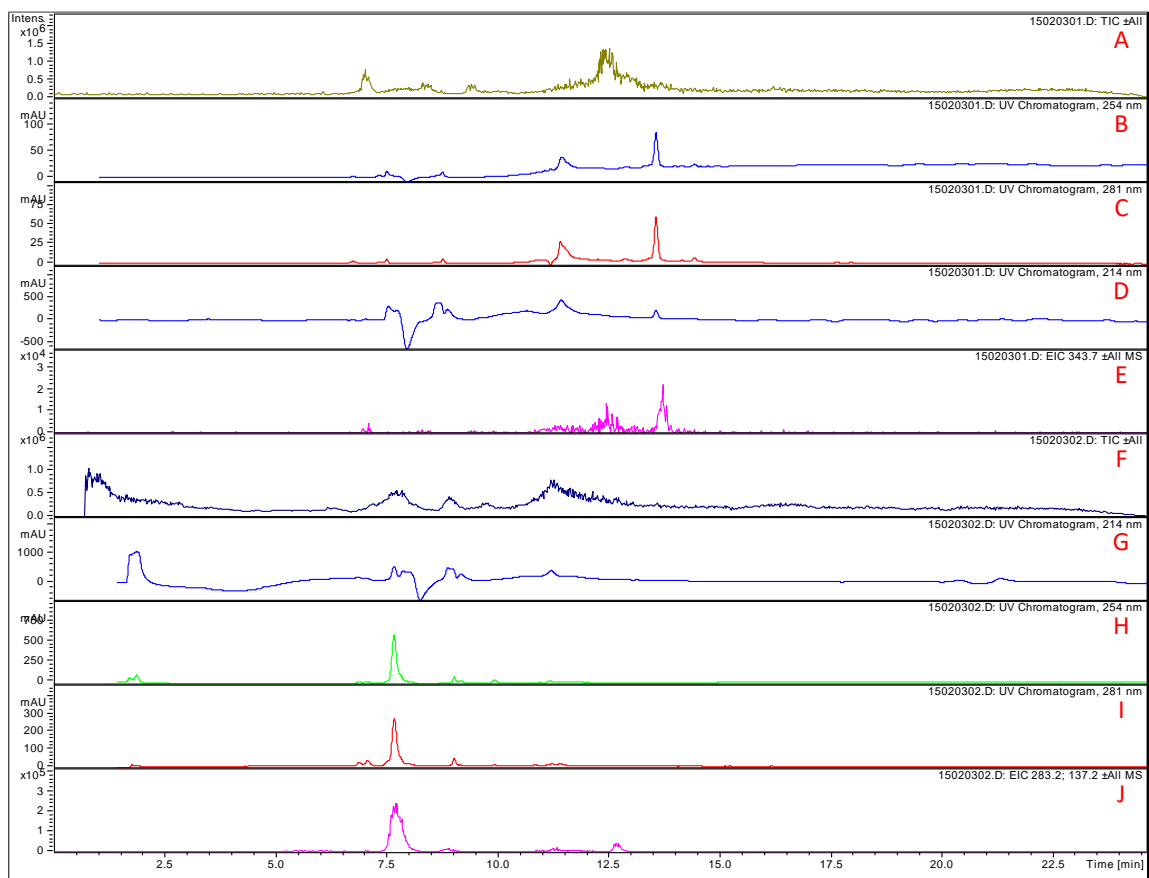
Figure 3-29. HPLC/UV/MS chromatogram of Fractions E-25-10: A) Total ion chromatogram in positive mode; B) 254 nm UV-Vis chromatogram; C) 281 nm UV-Vis chromatogram; D) 214 nm UV-Vis chromatogram; E) Extracted ion chromatogram at 343.7 *m/z*; and E-25-13: F) Total ion chromatogram in positive mode; G) 254 nm UV-Vis chromatogram; H) 281 nm UV-Vis chromatogram; I) 214 nm UV-Vis chromatogram; J) Extracted ion chromatogram at 283.2/137.2 *m/z*;
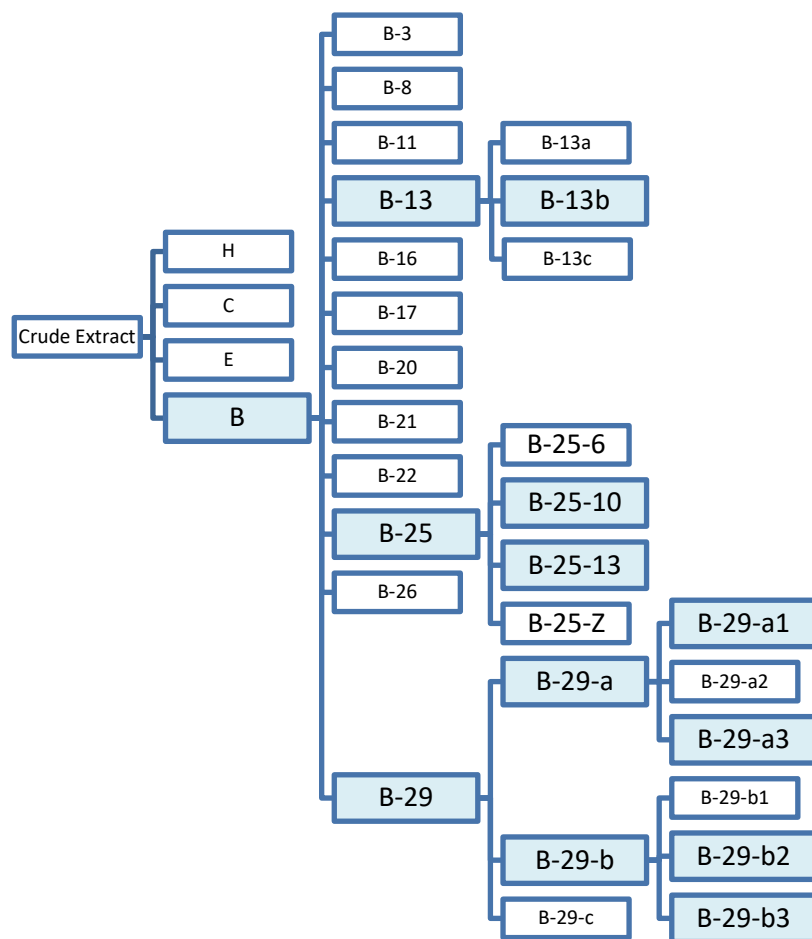
Figure 3-30. Flowchart for fractionation of B-13, B-25 and B-29

The final fraction selected for isolation was B-29, which contained several constituents at relatively high quantities. The fractionation flowchart is shown in Figure 3-30. As adopted in previous fractions, Sephadex LH-20 column chromatography was selected first to sub-fractionate B-29. A solution of B-29 (210 mg) in minimum methanol was loaded onto a 5x15 cm Sephadex LH-20 column. A total of 10 fractions were collected, combined to 3 final fractions by TLC analysis (Silica, 1:9 acetic acid/ethanol). B-29-a (45.2 mg) and B-29-b (57.8 mg) contained the major components of this fraction, which were highly polar, and stained with ninhydrin.

Due to the separation achieved by TLC during analysis of fractions, it was decided to employ prep-TLC for separation of the components in B-29-a and B-29-b. B-29-a (12 mg) and B-29-b (14 mg) were dissolved in 300 µL methanol each and loaded onto individual prep TLC plates (Silica H, 10x20 cm, 250 µm thickness). The plate was thoroughly dried. In a prep-scale TLC reservoir, 50 mL eluent (1:9 acetic acid/ethanol) was added and allowed to condition for 10 minutes. The TLC plates were placed in the reservoir and eluted. The bands were scraped from the TLC plate after visualization with UV light and the compounds extracted into methanol. Six fractions were obtained, three of which were highly pure by TLC: B-29-a3 (2.7 mg), B-29-b2 (4.4 mg) and B-29-b3 (5.5 mg) were selected for characterization (see section 3.5.2).

3.5.2 Characterization of components in B

3.5.2.1 B-8c (blue compound)

Compound B-8c was obtained as a brilliant blue-green residue after fractionation of B-8 by Sephadex LH20 column chromatography. Compound B-8c was intensely colored, which even at high dilutions remained visibly blue. This compound was highly polar, and was soluble in water. Analysis of the UV-Vis spectrum of this compound (shown in Figure 3-31) indicated absorption maximum at λ_{max} = 615 nm, showing a broad peak spanning from 500 nm to the far-red portion of the spectrum (>670 nm, the cutoff for the spectrometer utilized to acquire the data). The UV-Vis absorption characteristics of B-8c were not consistent with known photosynthetic pigments or carotenoids[6]. The color exhibited by B-8c was highly stable: it was observed that several days after TLC analysis,

blue bands were still visible on TLC plates, after all other pigmented bands had faded. The pigment was highly stable in solution as well—attempts to recrystallize the compound from mixtures of ethanol/water, while unsuccessful in obtaining crystals, showed remarkable color stability (> one week) of the major compound in B-8c in solution at room temperature, exposed to oxygen and ambient light, in the mother liquor. The remarkable stability of the color of B-8c suggested the possibility of contamination of the algal biomass with synthetic pigment, which was considered as the characterization of B-8c proceeded.

#FIGURE DISPLAY ERROR#

Figure 3-31. UV-Vis spectrum of B-8c

Characterization of B-8c by HPLC/UV/ESI-MS (shown in Figure 3-32) indicated one major compound by UV-Vis chromatograms and ESI-MS chromatogram, and small quantities of inseparable, unidentifiable, highly-polar impurities. The mass spectrum of the compound in B-8c (Figure 3-32) showed quasimolecular ion at 478.6 *m/z*, presumably $(M+H)^+$, which in positive mode indicates an ion corresponding to a neutrally charged compound with an odd-numbered molecular weight, and thus containing an odd-number of nitrogens in the structure. The other piece of information about the structure obtained from the ESI mass spectrum was the major ion at 239.9 *m/z*, exactly half the base peak ion plus one (479.6 *m/z*, $[M+2H]^{+2}$), suggesting the charge of 239.9 *m/z* is +2. This implies that the structure likely contains at least two nitrogens (and hence 3 nitrogens, since there must be an odd number) to support the doubly-charged cation.
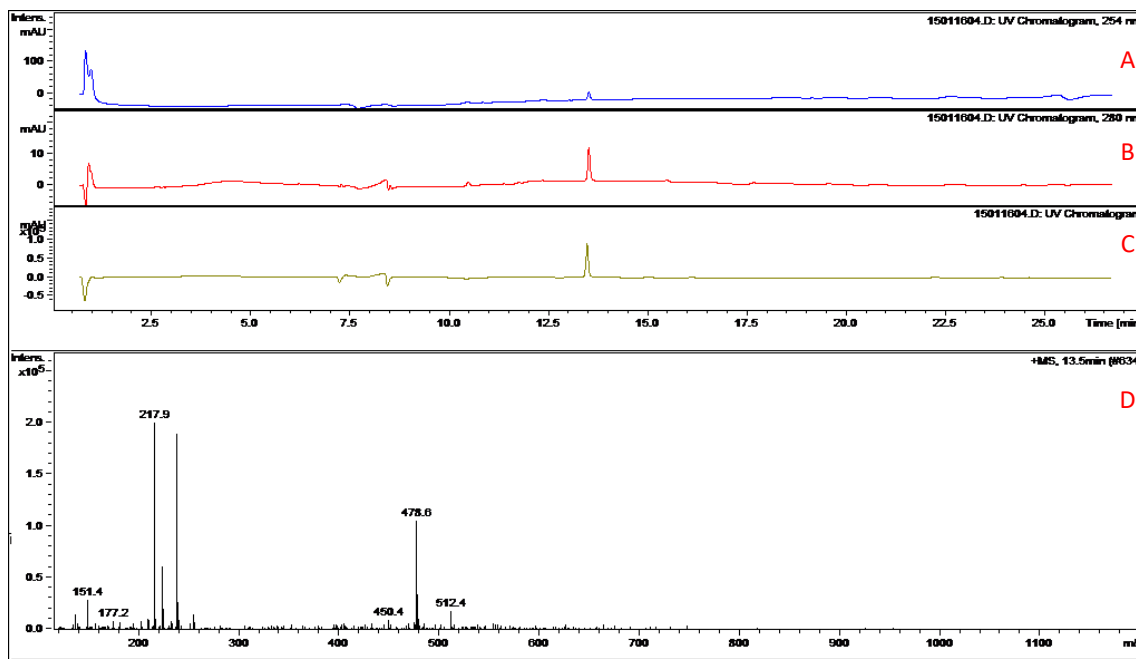
Figure 3-32. HPLC chromatograms of B-8c: A) 254 nm UV-Vis chromatogram; B) 280 nm UV-Vis chromatogram; C) 610 nm UV-Vis chromatogram; D) Positive mode ESI mass spectrum of major compound in B-8c

NMR techniques were employed in an attempt to further elucidate the structure of B-8c. After repeated preparative TLC and Sephadex LH20 column chromatography, ^{1}H-NMR and COSY-NMR analysis were conducted, shown in Appendices (**Error! Reference source not found.**, pg. **Error! Bookmark not defined.**). While HPLC/UV/MS analysis indicated a high relative purity of B-8c, ^{1}H-NMR analysis showed a number of contaminants overlapping signals in the NMR spectrum, rendering complete structural determination by ^{1}H-NMR impossible. COSY-NMR was slightly more useful, allowing for decoupling of the downfield signals from overlapping signals in the aliphatic region—analysis showed several aromatic protons interacting with nearby protons at δ = 4-5 ppm, as well as with other protons at δ = 3 ppm. Aliphatic protons interacted with other aliphatic protons, as well as with the group at δ = 3 ppm. Thus, the structure contained several unique aromatic protons which coupled with other nearby aromatic protons, some of which coupled to

deshielded aliphatic groups. Also indicated were aliphatic groups coupled to the deshielded aliphatic group which is coupled to the aromatic moieties.

With no deterministic structural information obtained from 1H-NMR analysis, and due to the milligram-quantities obtained of this purified fraction, and given the unique properties of the UV-Vis and mass spectra, more extensive investigation into UV-Vis and mass spectral databases was conducted to attempt to identify whether the blue compound in B-8c was a known structure. SciFinder was utilized to conduct a search of references reporting compounds within molecular weight range of 450-520 Da, filtered by keyword phrase combinations of "blue" and "pigment, ink, dye, colorant." These results yielded 1025 references, which were further filtered to those containing "ESI-MS OR electrospray" to eliminate references without reported ESI-MS data. Results were further filtered for references containing the text "478" to narrow down references to those containing the base peak ion detected in our hands by ESI-MS. This search resulted in twenty-two results. Manual screening of these references resulted in two potential relevant hits. The first reference was a master's thesis conducted on the analysis of black writing ink by electrospray MS[7], which reported the detection of the ink "Basic Blue 7" by ESI-MS in positive mode at 478 *m/z*, corresponding to (M-Cl)[+], since Basic Blue 7 is a quaternary-nitrogen with a chloride counterion[8].

The second reference was a forensic study investigating the pigments of blue ballpoint pen[9]. The authors analyzed a wide array of pen inks, and report the ESI-MS data; within this report, the pigment Victoria Blue BO (also known as Basic Blue 7) was detected in

positive mode at 478.6 *m/z* (M-Cl)[+]. Based on the convergence of these two reports, it was hypothesized that the compound in B-8c was the synthetic pigment Basic Blue 7, also known as Victoria Blue BO; the structure is shown in Figure 3-33. There are a number of pieces of evidence supporting this hypothesis: Basic Blue 7 has the same reported molecular ion reported for ESI-MS; Basic blue 7 is a highly-stable blue pigment, with a UV-Vis absorption maximum at λmax = 615 nm, consistent with observations about B-8c; Basic blue 7 contains 3 nitrogens, consistent with earlier observations; there are several aromatic moieties in Basic blue 7, separating aliphatic moieties by deshielded groups, consistent with NMR observations. Therefore, it was determined that the compound in B-8c was the synthetic pigment Basic blue 7, and is likely a product of contamination by pigments used in materials used for the algal growth system.
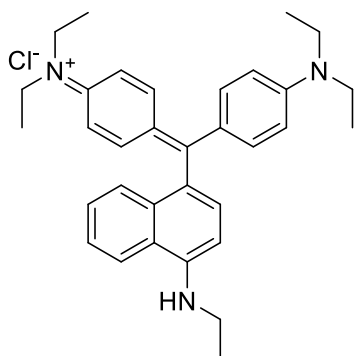
Figure 3-33. Structure of Basic Blue 7, synthetic blue pigment detected in B-8c

3.5.2.2 B-21-fltr – adenosine

Fraction B-21, upon standing, separated into a white precipitate and mother liquor. The mixture was filtered, and the filtrate was designated B-21-fltr. This compound was analyzed by HPLC/MS, which demonstrated a relatively pure compound with several

minor contaminants. The mass spectrum of the major compound was evaluated to establish an identity for the unknown; the positive mode ESI-MS displayed a signal at 268.2 *m/z* and 136.2 *m/z*. A preliminary search was conducted to evaluate detected compounds against ubiquitous biological constituents on several mass spectral databases on the web; massbank.jp quickly revealed a match for these signals, corresponding to adenosine[11]. According to massbank.jp, adenosine possesses two major positive mode ESI-MS signals corresponding to the quasimolecular ion 268.2 *m/z* $(M+H)^+$ and 136.1 *m/z* $(M+H-C_5H_9O_4)^+$, the adenylate ion. This match suggested that the compound detected in B-21-fltr was adenosine, and as such, HPLC comparison between B-21-fltr and commercially obtained adenosine was conducted. Comparison of HPLC chromatograms of B-21-fltr and commercially obtained adenosine confirmed that the main constituent of

B-21-fltr   was   adenosine   (
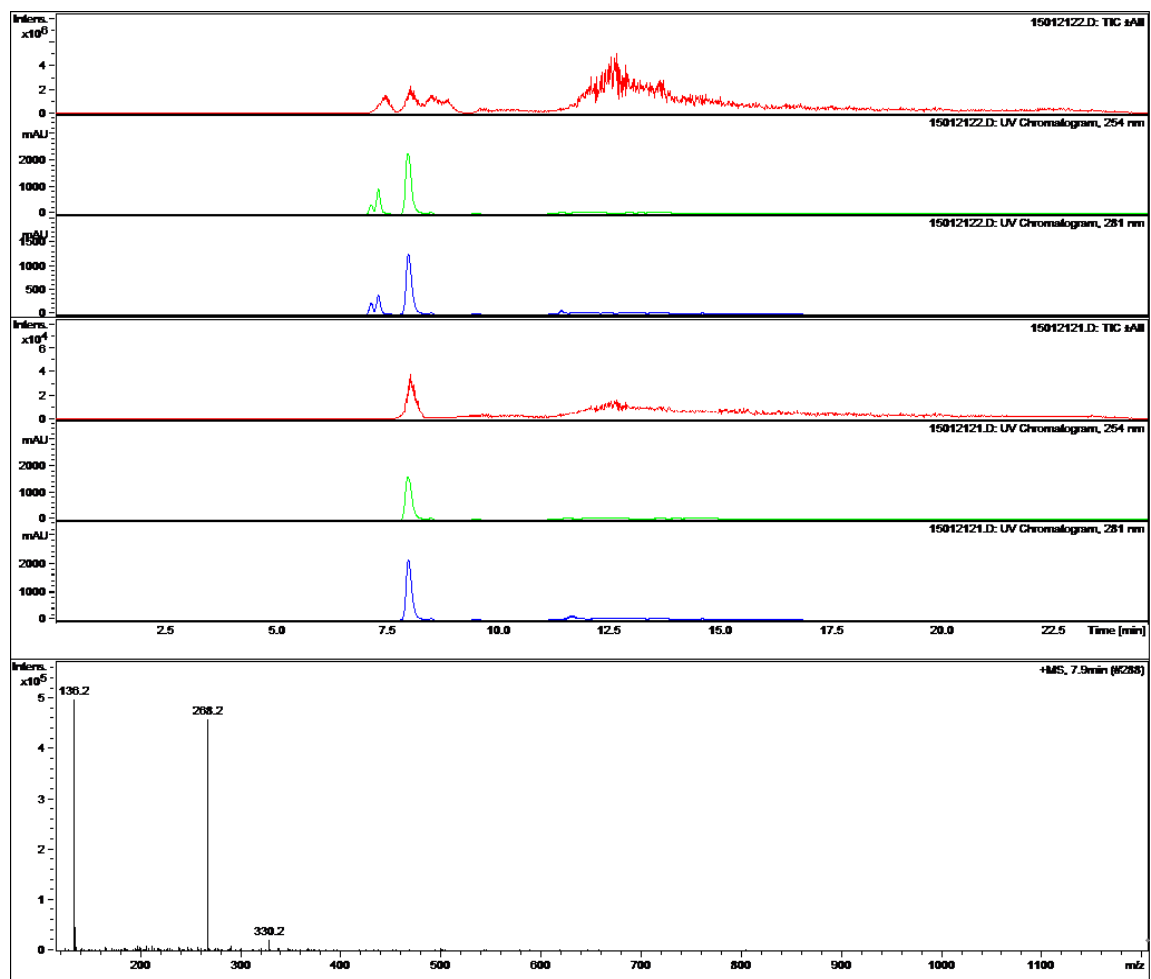
Figure 3-34).
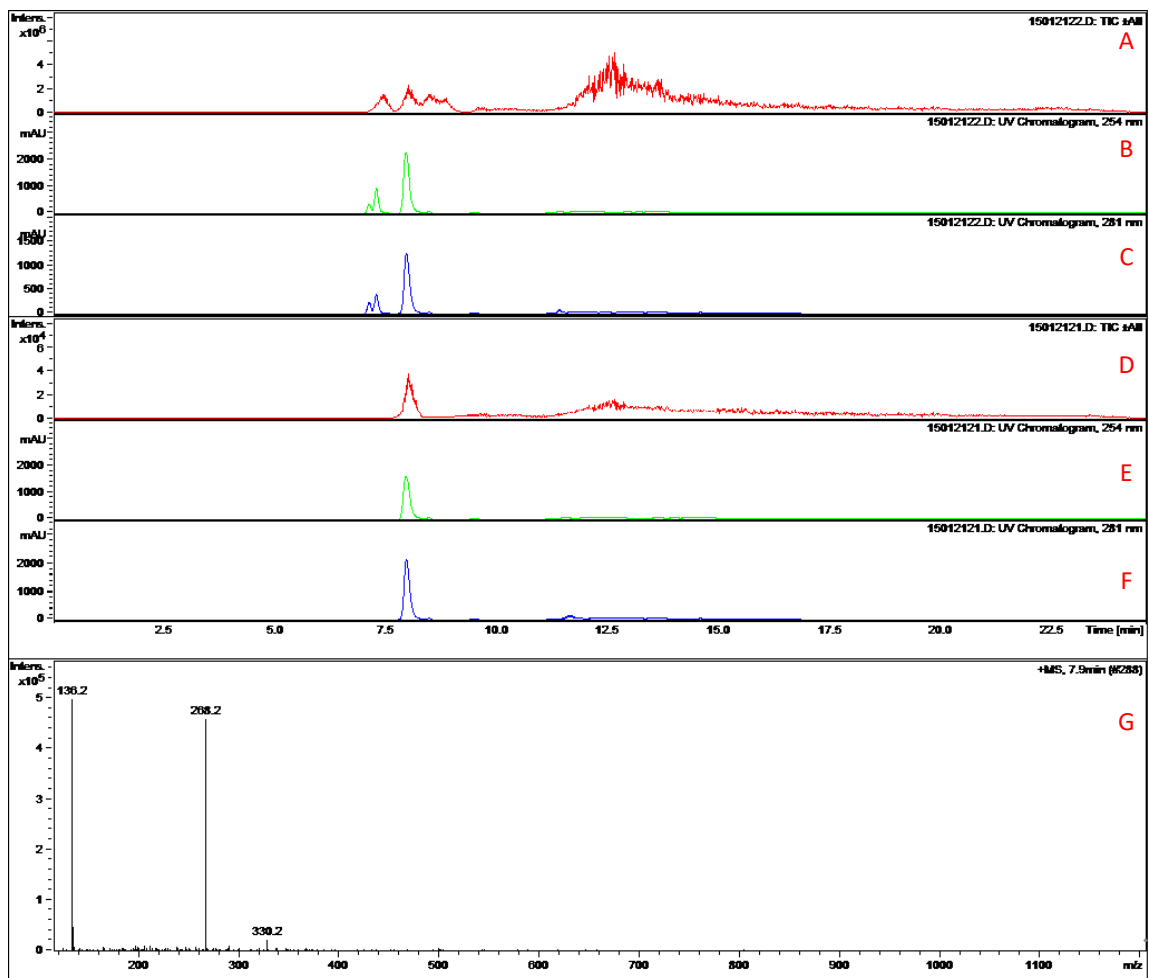
Figure 3-34. HPLC/UV/MS chromatogram comparing Fraction B-21-fltr: A) Total ion chromatogram; B) 254 nm UV-Vis chromatogram; C) 281 nm UV-Vis chromatogram; and commercially available adenosine: D) Total ion chromatogram; E) 254 nm UV-Vis chromatogram; F) 281 nm UV-Vis chromatogram; G) Mass spectrum of fraction B-21-fltr, consistent with adenosine.

3.5.2.3 B-20c - hypoxanthine

The compound detected in fraction B-20c was a highly polar amorphous solid which was readily soluble in water. HPLC/UV/MS analysis showed one major peak and a few minor impurities. The major compound showed UV-Vis absorption maxima at 254 nm and 280 nm, with a single ion detectable by positive mode ESI-MS, presumably (M+H)+

quasimolecular ion. Due to the similarities between the retention characteristics and molecular weight of this compound and adenine, it was postulated that the structure was a purine derivative, and due to its even molecular weight (136 Da), the compound must possess an even number of nitrogens. The purine skeleton has a molecular weight of 120 Da, and so it was proposed that the unknown compound, with a difference of 16 from purine, contained an extra oxygen in the molecular formula; this compound was tentatively identified as hypoxanthin. Comparison of the UV-Vis and mass spectrum obtained from B-20c to published results[11, 10] for hypoxanthin showed good correspondence.

3.5.2.4   B-17-13a (aka B-13B and B-16bc0) - adenine

The highly polar compound obtained from fraction B-17-13 was a white amorphous solid which was reasonably pure by HPLC analysis, however contained some inseparable compounds which made absolute characterization difficult. The compound eluted rapidly, at 5-7% ACN with 0.1% formic acid mixed with H2O with 0.1% formic acid on a C18 column, indicating a high number of polar groups contained within this compound.

The UV-Vis spectrum, shown in
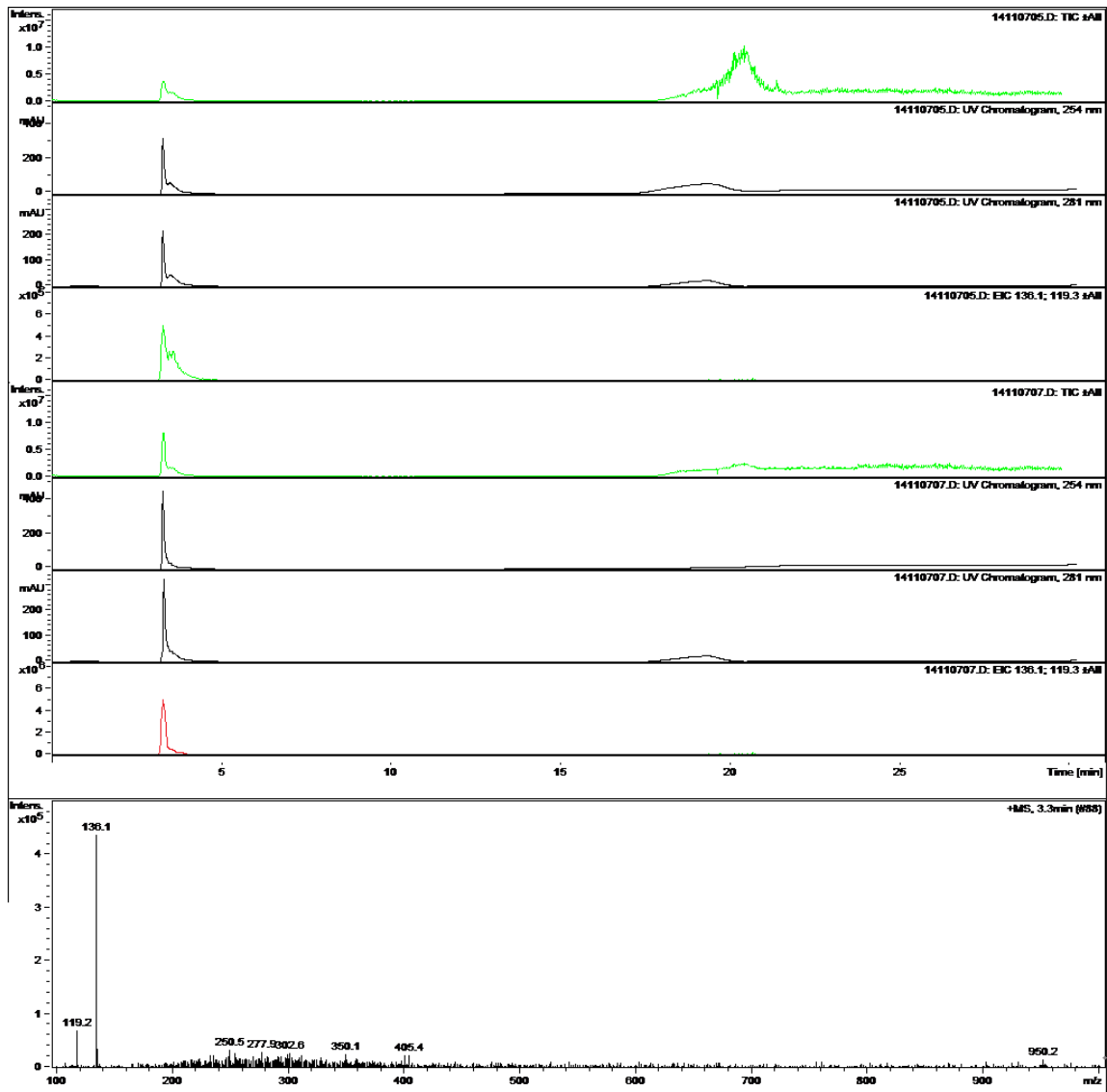
Figure 3-35 showed a major absorbance at 280 nm and 254 nm, suggesting one or more

aromatic hetero groups and unsaturated bonds, respectively. The mass spectrum

obtained from LC/ESI-MS analysis of B-17-13a indicated one peak at 136.2 m/z,

presumably the quasimolecular ion $(M+H)^+$, and another peak at 119.3 m/z, presumably

$(M-NH_3)^+$. This is suggestive of a compound containing an odd number of nitrogens, since

the molecular weight is presumably 135. ^{1}H-NMR analysis in $CDCl_3$ was conducted (see

appendix), however was not of much use in structural characterization due to impurities and lack of material (only 2 mg was obtained). As such, searching through ESI-MS databases available on the internet led to the identification of a possible candidate from massbank.jp11: adenine the nucleoside base, which possessed a mass spectrum containing 136.10 *m/z* (M+H)$^+$ and also at 119.03 (ion not identified). This was further evidence of the identity of B-17-13a, and it was concluded the compound was adenine (structure shown below). Comparison of the HPLC/UV/MS chromatograms of B-17-13a to

commercially   available   adenine   (
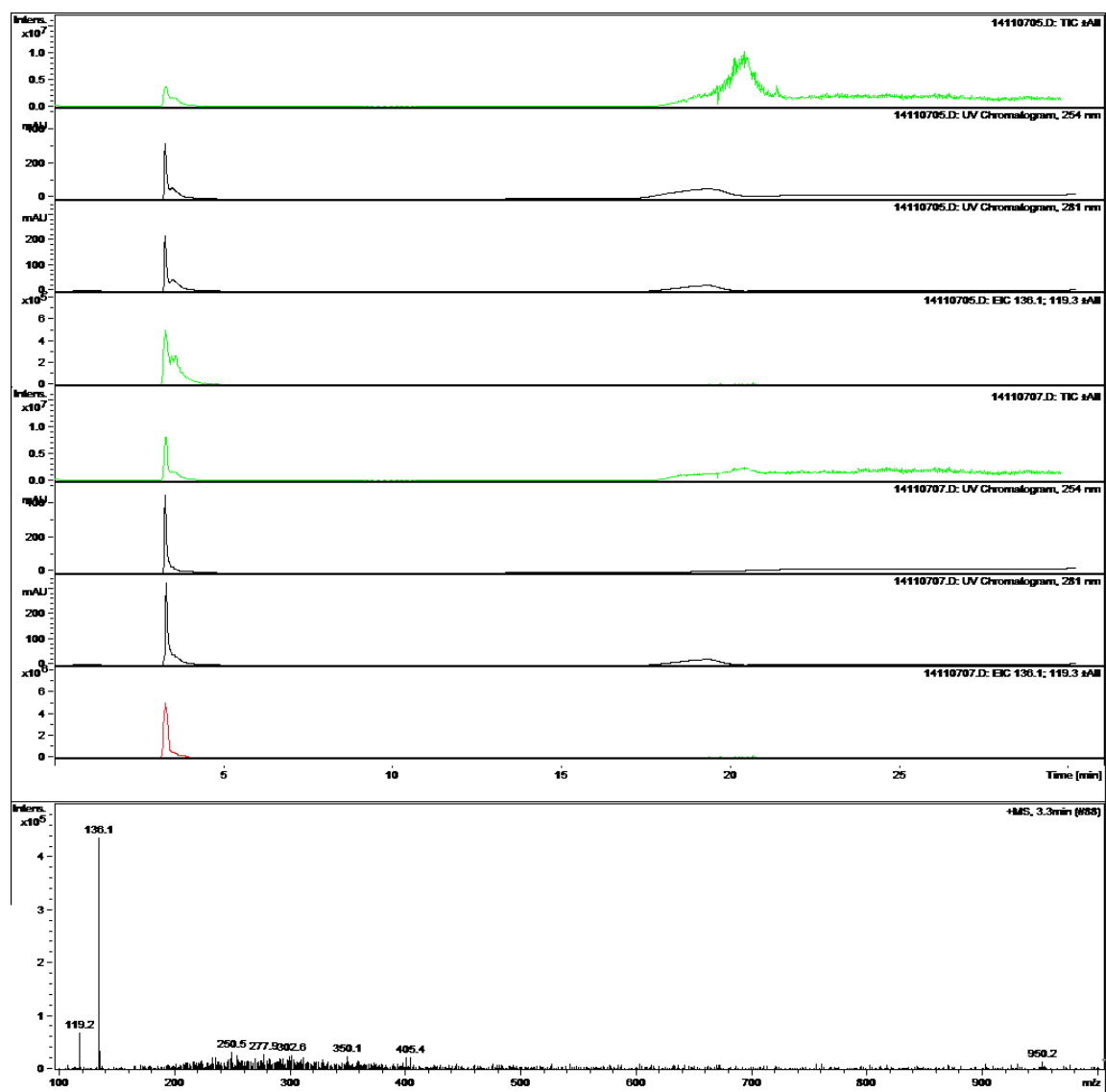
Figure 3-35) showed conclusively the identity of this compound.
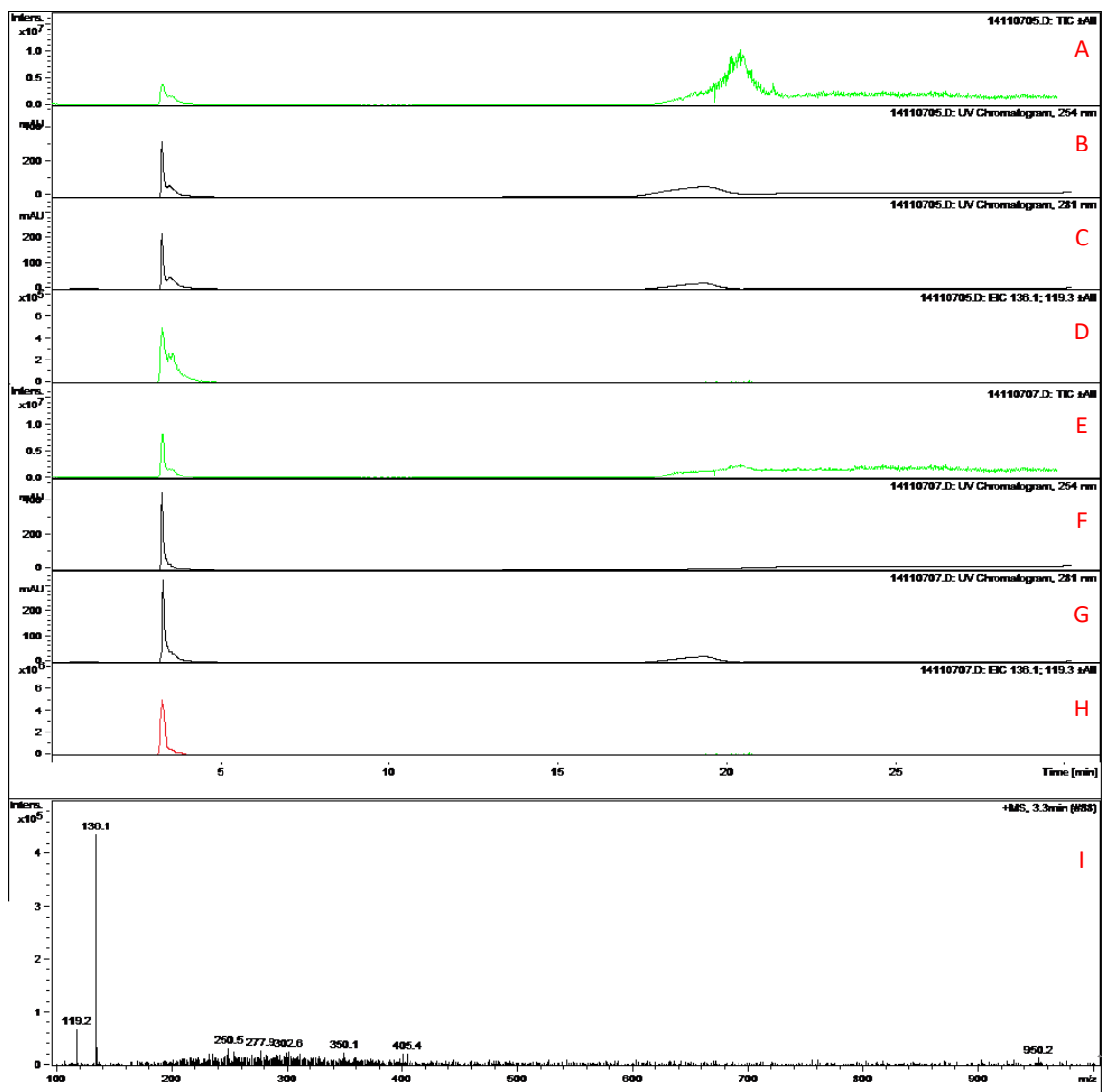
Figure 3-35. UV-Vis and MS chromatograms of B-17-13a: A) Total ion chromatogram; B) 254 nm UV-Vis chromatogram; C) 281 nm UV-Vis chromatogram; D) Extracted ion chromatogram at 136.1 *m/z*; and adenine standard: E) Total ion chromatogram; F) 254 nm UV-Vis chromatogram; G) 281 nm UV-Vis chromatogram; H) Extracted ion chromatogram at 136.1 *m/z*; and I) Mass spectrum of B-17-13a, consistent with adenine;
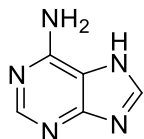
Figure 3-36. Structure of adenine, the major constituent in B-17-13a

3.5.2.5 B-25-8 –adenosine triphosphate

The compound isolated from fraction B-25-8 was a white crystalline solid which was very highly polar by TLC analysis. ESI-MS analysis of this compound showed one major peak, and an inseparable amalgam of components, however the mass spectrum was relatively clean, and first attempts at identification were made directly based on this data. As can

be   seen   below   in
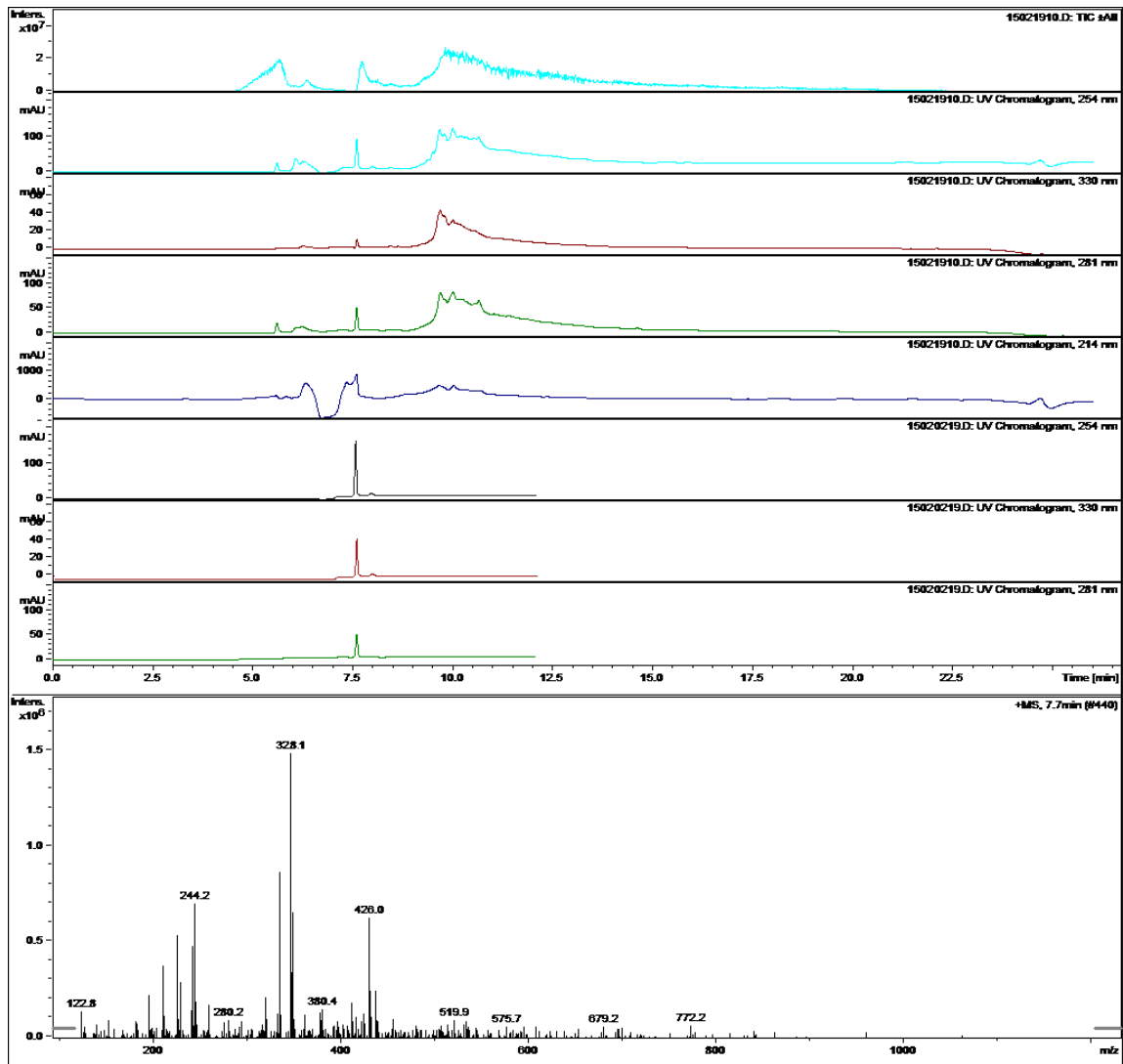
Figure 3-37, there were two major peaks. The MS was run in negative mode, and so

negative adducts were expected. The highest m/z detected for this peak was at 426.0 m/z,

the other peak at 328.1 m/z. As is preliminary protocol for identifying ubiquitous

compounds, the peaks were searched using a number of ESI-MS databanks on the

internet. Quickly a potential match was identified; the records obtained from

massbank.jp [11], indicating a likely identity of adenosine triphosphate, possessing a

quasimolecular ion at 426.0 m/z (M-H-HPO$_4^-$)$^-$, and another major fragment ion at 328.1

m/z (M-H-HPO$_4$-H$_2$PO$_4$)$^-$. The proposed fragmentation pattern is shown below in Figure

3-38.
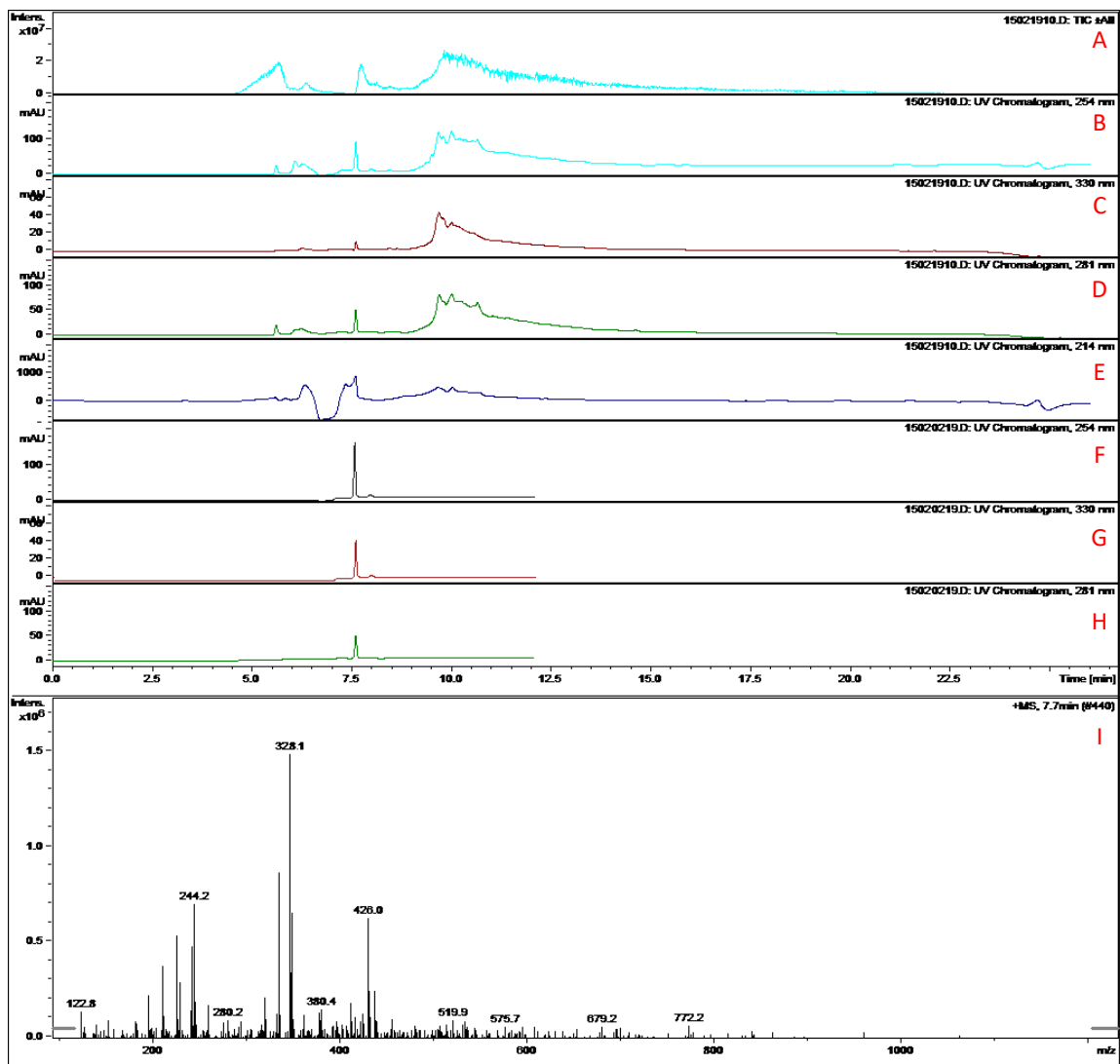
Figure 3-37. HPLC/UV/MS chromatogram of Fractions E-25-8: A) Total ion chromatogram; B) 254 nm UV-Vis chromatogram; C) 330 nm UV-Vis chromatogram; D) 281 nm UV-Vis chromatogram; E) 214 nm UV-Vis chromatogram; and comparison to known standard; and authentic adenosine triphosphate: F) 254 nm UV-Vis chromatogram; G) 330 nm UV-Vis chromatogram; H) 281 nm UV-Vis chromatogram; and I) Mass spectrum of E-25-8, showing excellent correspondence to commercially obtained adenosine triphosphate
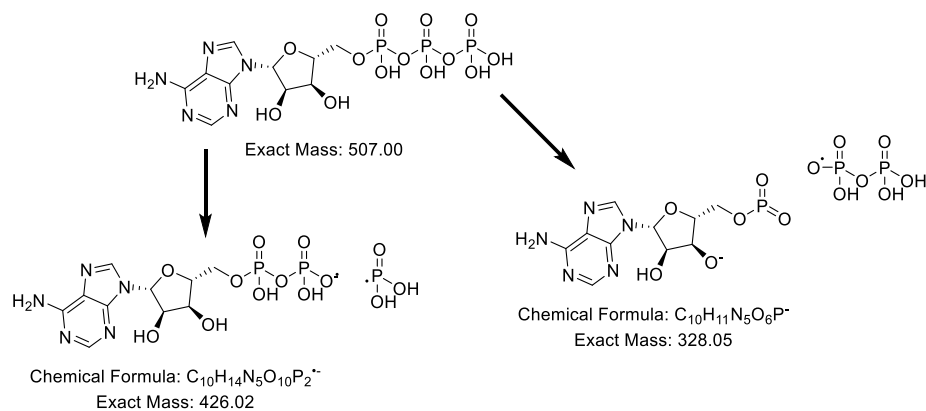
Figure 3-38. Proposed fragmentation pattern of compound detected in B-25-8, adenosine triphosphate

Unfortunately, the compound was not sufficiently pure to obtain NMR data for structural

confirmation, so instead the compound was compared chromatographically to pure

adenosine triphosphate, obtained commercially. Injection of known adenosine

triphosphate resulted in the same response by HPLC/ESI-MS (as shown above in
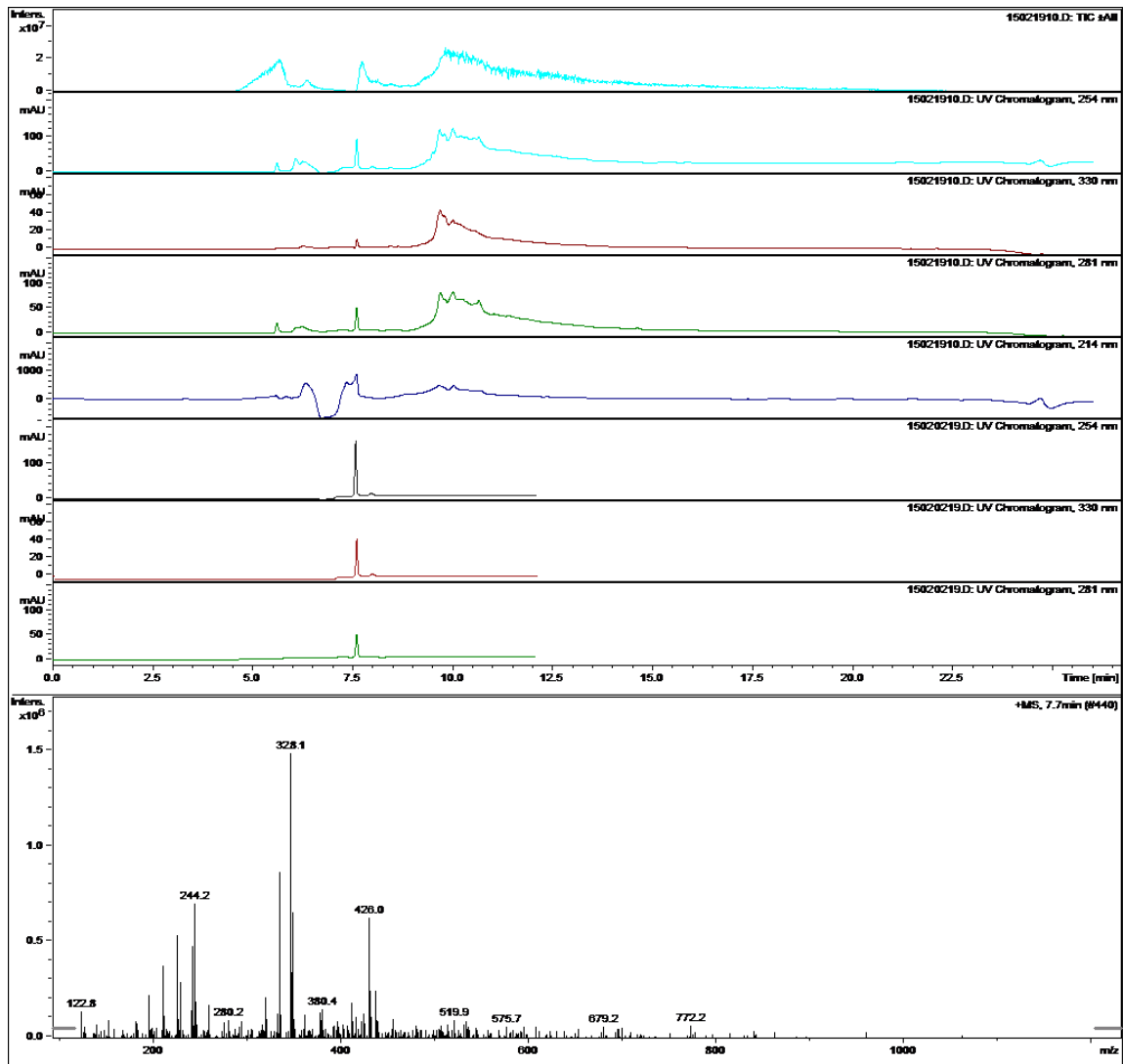
Figure 3-37). As such, the major compound in B-25-8 was confirmed as adenosine

triphosphate (ATP).

3.5.2.6 B-25-10 – cyclic GMP

Compound B-25-10 was identified with facility due to its characteristic LC/ESI-MS

spectrum. Compound B-25-10 was obtained as a white precipitate after removal of

solvent from fraction obtained from preparative scale chromatography. LC/ESI-MS in

positive mode demonstrated that this compound was somewhat pure by LC/MS, but contained substantial impurities. The ESI-mass spectrum of this compound possessed one major peak at 346.0 *m/z* and 152.1 *m/z* detected in positive mode. These peaks were cross-referenced to ESI-MS databases available on the web, and a suitable candidate was detected[11]. The primary candidate suggested based on positive ions 346.0 *m/z* and 152.1 *m/z* was cyclic-guanosine monophosphate (cGMP). The two major peaks reported for cGMP on massbank.jp were 346.05 *m/z* (M+H)$^+$ and 152.1 *m/z* (M+H-C$_5$H$_8$O$_6$P)$^+$. This data suggested a possible identity to the unknown compound detected in B-25-10 as cGMP. To positively ascertain the identity of B-25-10, the compound was injected alongside commercially available cGMP; these compounds showed identical characteristics in HPLC/MS analysis, further indication of the identity of B-25-10 as cGMP (Figure 3-39).
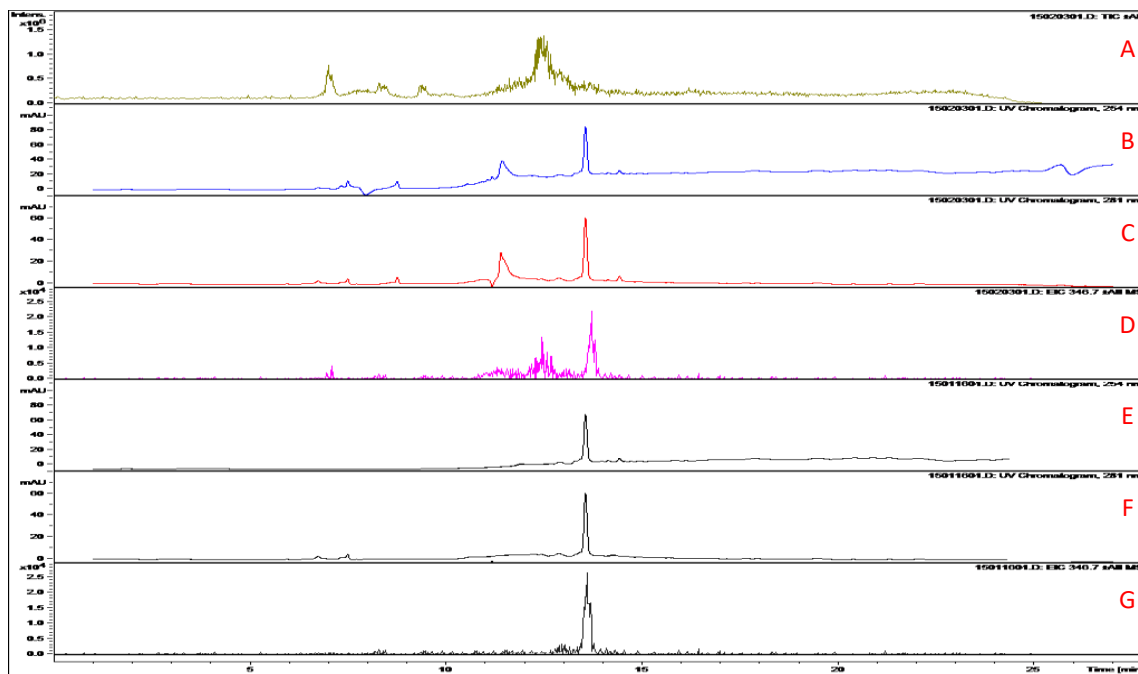
Figure 3-39. HPLC/UV/MS chromatogram of Fraction E-25-10: A) Total ion chromatogram; B) 254 nm UV-Vis chromatogram; C) 281 nm UV-Vis chromatogram; D) Extracted ion chromatogram at 346.7 *m/z*; and comparison to commercially available cyclic GMP: E) 254 nm

UV-Vis chromatogram; F) 281 nm UV-Vis chromatogram; G) Extracted ion chromatogram at 346.7 *m/z*

3.6 Investigation of Hexane (H) and Chloroform fraction (C)

3.6.1 Isolation of components

The hexane (H) and chloroform (C) fractions together represented a substantial portion (44%) of the total extract. The hexane fraction consisted of a waxy oily solid that melted at body temperature, colored orange by the obvious presence of large quantities of β-carotene, as detected by TLC (silica, 20% EtOAc/hexanes). Fraction C was a black-green emulsion/goo which contained large quantities of chlorophyll. Screening of these fractions in the COX-2 inhibition assay (see Figure 5-11, pg. 261) showed that fraction H exhibited the highest inhibitory activity 35.6 ± 1.36% at a concentration of 50 μg/mL, the highest of any fractions screened in this assay. Fraction C was found to inhibit COX-2 activity slightly, although statistically significantly, at 15.1 ± 0.95%. Based on these results, and recognizing that these fractions were crude mixtures of many constituents, it was decided to sub-fractionate H and C followed by evaluation of the sub-fractions using the COX-2 inhibition assay.

Fraction H was selected for separation via Silica gel H column chromatography. Fraction H (2.1 g) was dissolved in minimum volume (~10 mL) 1:9 EtOAc/hexanes. The solution was loaded onto a 5 cm diameter glass column packed with Silica H (Alfa Aesar, Haverhill, MA, ACS grade) to a height of 25 cm in hexanes. The column was eluted with a gradient of hexanes and ethyl acetate from 100% hexanes, to 90% hexanes with ethyl acetate.

Twelve 200 mL fractions were collected and were combined by TLC analysis to give 4 fractions, H-a (650 mg), H-b (205 mg), H-c (580 mg) and H-d (354 mg). These fractions were evaluated using the COX-2 assay which showed activity exclusively in fraction H-c, showing 53% inhibition at 50 µg/mL concentration (Figure 5-11, pg. 261).
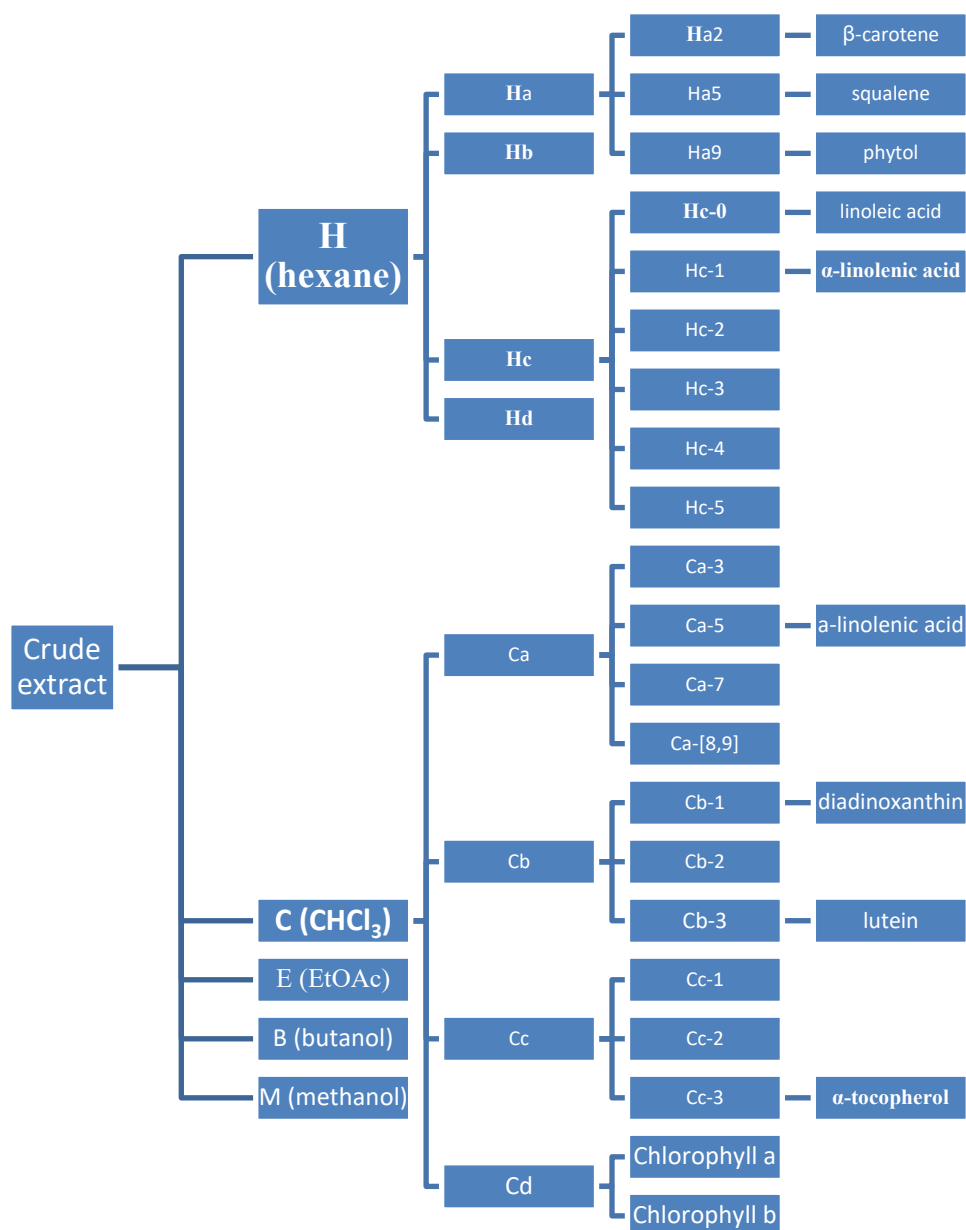
Figure 3-40. Fractionation scheme for Hexane subfraction (H) and Chloroform (C) subfraction

Analysis of Hc was accomplished by derivatization and subsequent GC analysis. Sub-milligram quantities of purified fractions were added to a 1.5 mL autosampler vial and dissolved in 200 µL chloroform. Samples were analyzed by 1.0 µL injection of analyte solutions into Shimadzu TQ8040 GCMS at 280°C injector temperature, with 1:50 split ratio. Samples were separated on a Rxi-5ms fused-silica capillary GC/MS column (30 m

length; 0.25 mm I.D.; 0.25 µm pore size; Restek, p/n 13423) with the following temperature gradient program: 80°C initial temperature, held for 1 minute, ramped linearly to 220°C at a rate of 10°C/min, held at 220°C for 3.5 minutes, and then linearly ramped to 310°C at a rate of 20°C/min, then held 15 minutes at 310°C.

Analysis of H-c indicated two major compounds which were retained similarly on GC, and several minor impurities. Due to the high non-polarity of the components in this fraction, further purification was needed and was achieved by precipitation of impurities from polar solvent mixtures followed by fractional crystallization, following the method described by Hoerr and Harwood (1952)[12] with minor modifications. Approximately 60 mg H-c was dissolved in hot 20% aqueous ethanol (2 mL). The solution was allowed to cool to room temperature and was then placed in an ice bath, then placed in the -20˚C freezer until a precipitate had formed. The supernatant was decanted from the precipitated impurities and the process was repeated several times. The solvent was removed and the residue was dissolved in acetone (600 µL) and cooled stepwise to -10˚C, -20˚C, -35˚C, -50˚C, and -70˚C using a recirculating chiller, with liquid fractions decanted

from solids at each step. The filtrates were separated and analyzed by GC (
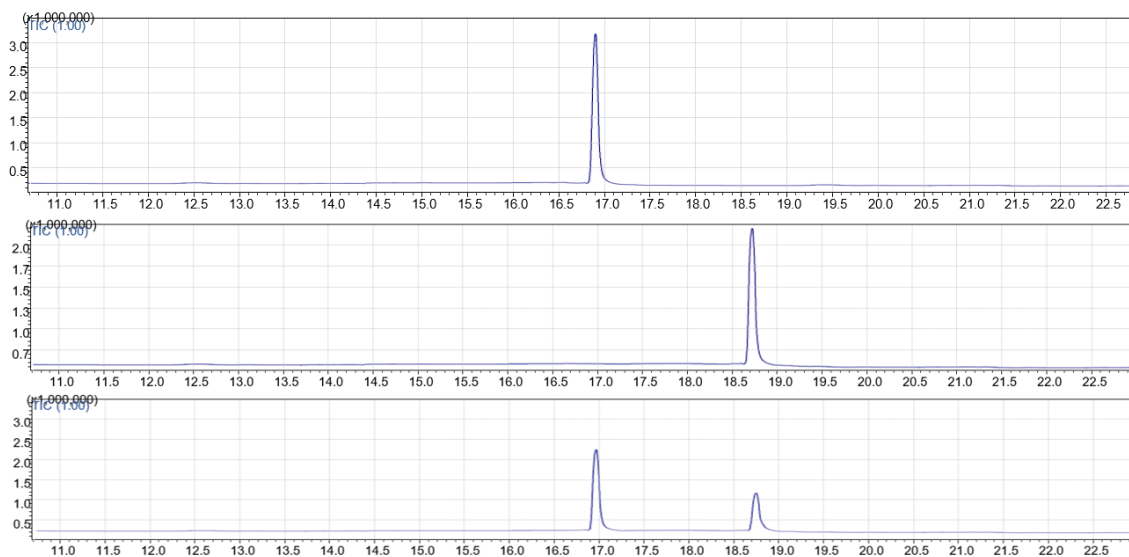
Figure 3-41). Fraction Hc-0 was relatively pure by GC analysis, whereas fraction Hc-1 was

enriched with the second major compound, but still contained significant quantities of

the compound in Hc-0. Multiple recrystallization steps gave analytically pure Hc-0 (10.4

mg), however Hc-1 (22.3 mg) was not completely separable. These compounds were re-

screened using the COX-2 inhibition assay wherein they demonstrated potent inhibition

of COX-2 in the mid-nanomolar range (Figure 5-15 and Figure 5-16, pg. 265). These

compounds were characterized by GC/MS and NMR (see section 3.6.2).
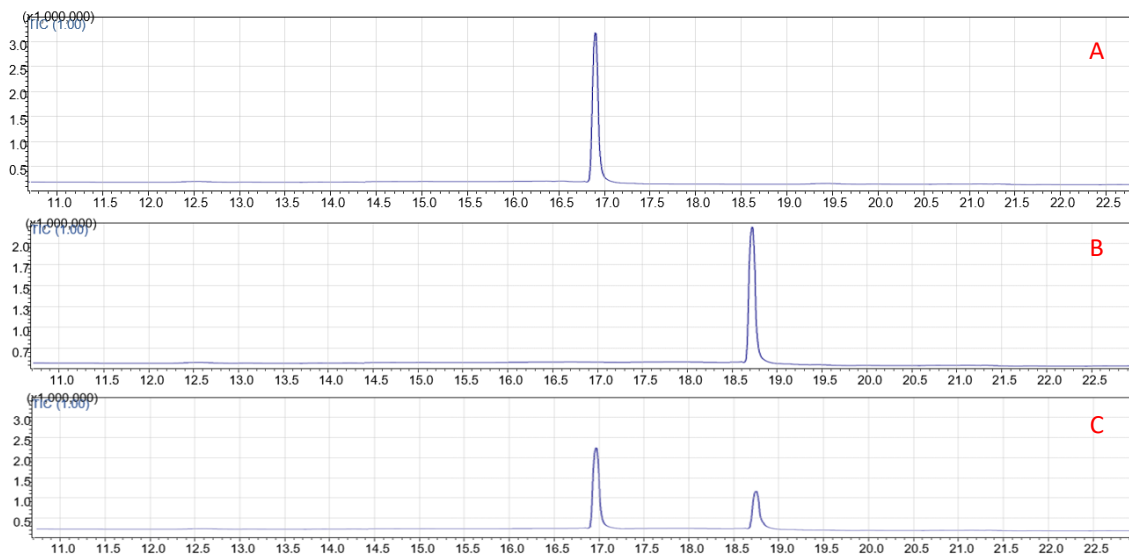
Figure 3-41. GC/MS chromatograms of Fractions A) Hc-0; B) Hc-1; and C) Ca-1, showing Ca-1 consists of a mixture of compounds in Hc-0 and Hc-1

Fraction C also exhibited slight activity in this COX-2 inhibition assay and was sub-fractionated in order to isolate the active constituents. It was decided to employ C_{18} solid phase extraction (SPE) to fractionate highly retained chlorophylls from other constituents in Fraction C. To accomplish this, approximately 500 mg fraction C was dissolved in minimum volume of isopropanol. A 1 g C18 SPE cartridge (Sep-Pak) was washed with 10 mL HPLC grade water, 10 mL methanol, and an additional 10 mL water. The isopropanolic solution of fraction C was loaded onto the column and eluted with a stepwise gradient of 20 mL portions of 50% methanol/water, 75% methanol/water, 100% methanol, and 100% isopropanol to achieve 4 fractions. Of these fractions, only Fraction C-a exhibited activity against COX-2. This fraction was analyzed by GC/MS, and contained a complex mixture

including the presence of compounds in Fractions Hc-0 and Hc-1 was detected (see
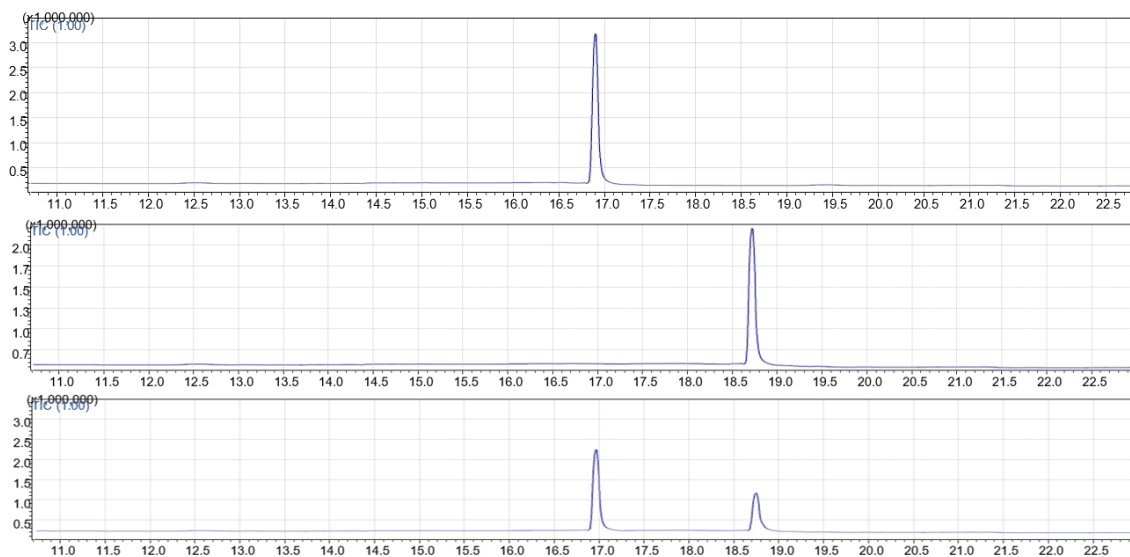
Figure 3-41), explaining the activity detected for this fraction in the COX-2 inhibition assay.

While there were no other sub-fractions of H or C which showed activity in the bio-assays used in screening, effort was made to isolate other major compounds contained within these fractions. Fraction H-a was selected first for fractionation by silica H chromatography. H-a (104 mg) was dissolved in 1:9 ethyl acetate/hexanes and loaded onto a 2.5 diameter column packed to a height of approximately 20 cm in hexane. The column was eluted with 100% hexanes followed by 3% ethyl acetate in hexanes. A total of 40 fractions were collected and combined by TLC to give 10 total fractions, H-a-1 to H-a-10. These fractions were analyzed by GC/MS. Fraction H-a-2 was analyzed by HPLC/UV on a YMC-30 Carotenoid HPLC column using the method described in section 3.7.1.1, *HPLC/MS method for the Analysis of Xanthophylls* (pg. 197). Fraction H-a-5 and H-a-9 were relatively pure by GC/MS and characterized by analysis of their mass spectra. Fraction H-

a-2 was relatively pure, and was recrystallized from dry 95% ethanol to obtain analytically pure product as a bright, orange-red crystals.

There were a number of compounds in the subfractions of C which were isolated. Fraction C-b was subjected to preparative HPLC chromatography using a Phenomenex C18 100x4.6 mm column using an isocratic solvent system consisting of 2:8 water/acetonitrile. Seventy-five 20 mL fractions were collected using the automatic fraction collector. A number of fractions were discarded and others were combined after TLC analysis to give 15 fractions. C-c was subjected to separation by preparative HPLC to give 30 fractions which were combined and discarded by TLC to give 4 final fractions. The sub-fractions of C-b and C-c were analyzed by HPLC/MS (Figure 3-42) and identified by characteristic UV-Vis absorption spectrum, mass spectrum, and comparison to known standards.
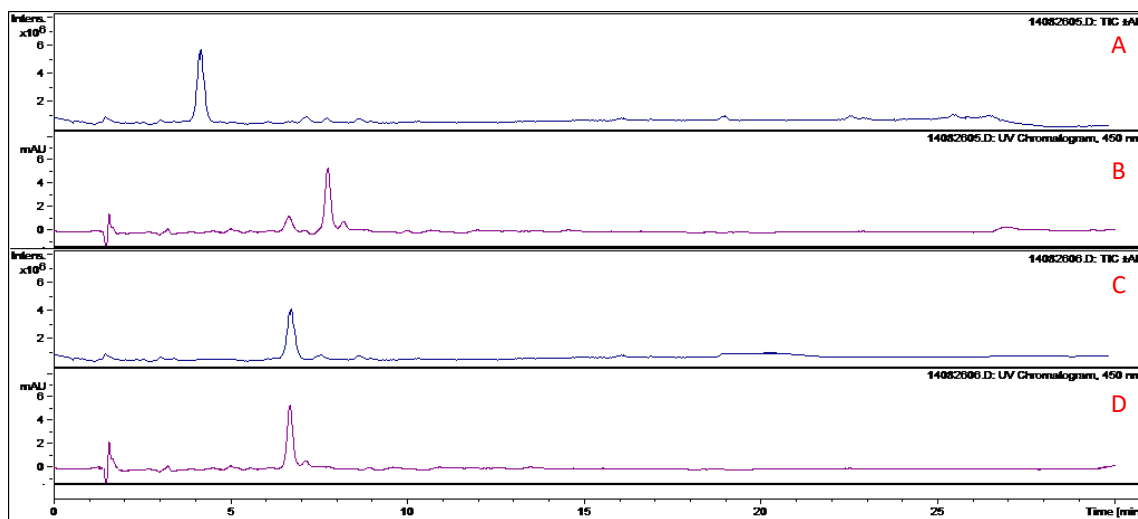
Figure 3-42. HPLC/UV chromatograms of prep-HPLC sub-fractions of C-b: A) Total ion chromatogram; B) 450 nm UV-Vis chromatogram; and C-c : C) Total ion chromatogram; D) 450 nm UV-Vis chromatogram

3.6.2 Characterization of components

3.6.2.1 *Hc-0 – linoleic acid*

Fraction Hc-0 was obtained as a waxy solid, exhibiting high lipophilicity based on its separation characteristics described in detail in (described in detail in section 3.6.1). This compound was selected for identification by GC/MS due to its highly lipophilic characteristics, and since GC/MS analysis yields mass spectra of sufficiently reproducible complexity to compare to known mass spectra in widely-available databases, such as the NIST GC/MS databases. The compound was injected into GC/MS and evaluated according to built-in NIST mass spectral databases for similarity based on deviations from known spectra. Hc-0 was compared to known spectra in the NIST database, and demonstrated highest similarity (S=98) to linoleic acid (Figure 3-43). As can be readily seen, linoleic acid was detected as the major component by GC/MS analysis. Shown below, the unknown compound demonstrates remarkable similarity (S=98) to known linoleic acid in the NIST GC/MS database. For confirmation, commercially available linoleic acid was injected on this system, the mass spectral data is shown below.
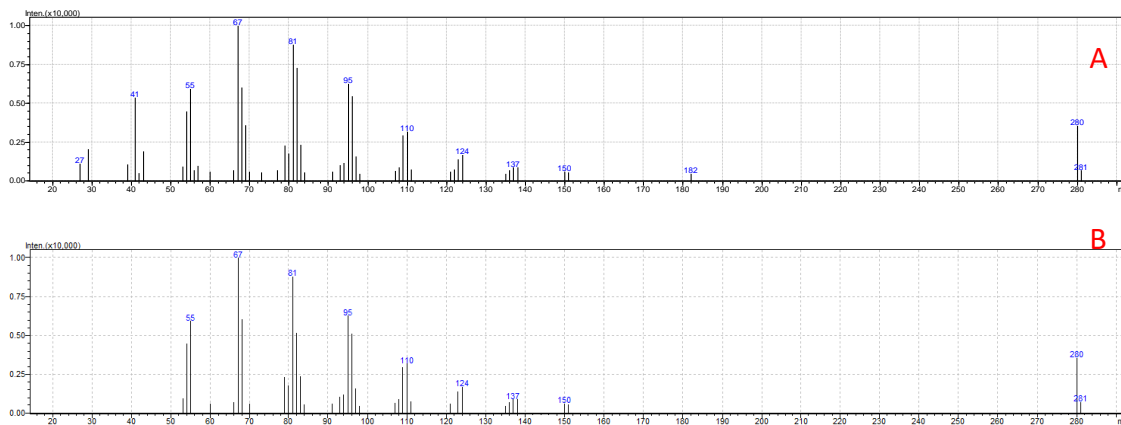
Figure 3-43. Mass spectrum obtained from GC analysis of A) Hc-0 and B) commercially obtained linoleic acid

3.6.2.2 Hc-1 – alpha linolenic acid

Fraction Hc-1 was obtained as a waxy solid, exhibiting high lipophilicity based on its separation characteristics (described in detail in section 3.6.1). This compound was selected for identification by GC/MS due to its highly lipophilic characteristics evident by TLC analysis. Furthermore, since GC/MS analysis yields mass spectra of reproducible and sufficient complexity to compare to known mass spectra in widely-available databases to deduce potential identity of the compound, such as the NIST GC/MS databases. The compound was injected into GC/MS and evaluated according to built-in NIST mass spectral databases for similarity based on deviations from known spectra. Hc-1 was injected on a Shimadzu TQ8040 GCMS and using software algorithms, the mass spectral data was compared to known spectra in the NIST database. Results showed highest similarity (S=97) to alpha-linolenic acid (Figure 3-43). To confirm this assignment,

commercially available alpha-linolenic acid was injected on this system, the mass spectral

data is shown below.
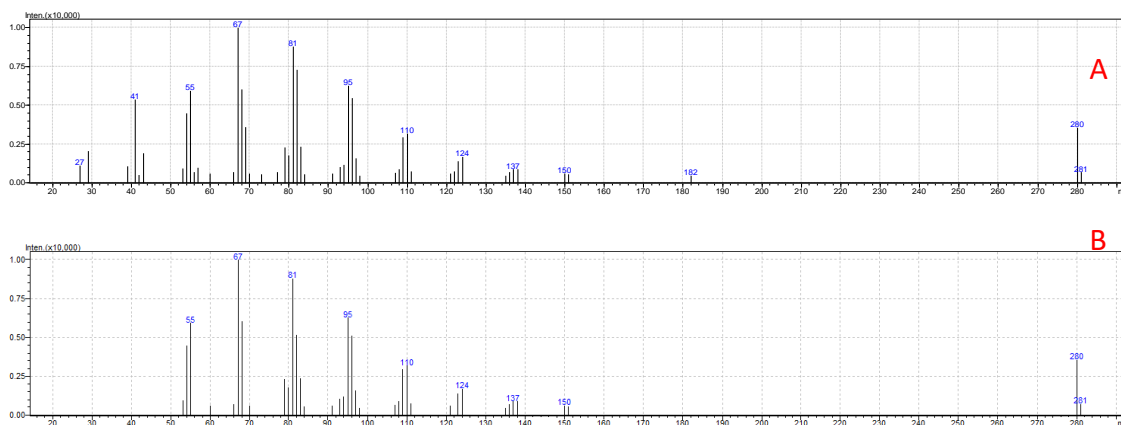
Figure 3-44. Mass spectrum obtained from GC analysis of A) Hc-1 and B) commercially obtained alpha-linolenic acid

3.6.2.3 H-a-2 – beta carotene

H-a-2 was obtained as a bright orange soapy solid which was bright yellow in solution.

Due to its high lipophilicity and characteristic orange color, and the known presence of

significant quantities of β-carotene in this biomass (see section 2.3), this compound was

hypothesized to be β-carotene. Injection of this compound on HPLC showed a highly pure,

extremely lipophilic compound which possessed a UV-Vis spectrum characteristic of β-

carotene, with λ_{max} at 450 nm, exhibiting a broad shoulder peak at 474 nm. Furthermore,

this compound had identical retention time and UV-Vis spectrum as commercially

obtained β-carotene standard. The structure of β-carotene is shown below (Figure 3-46).
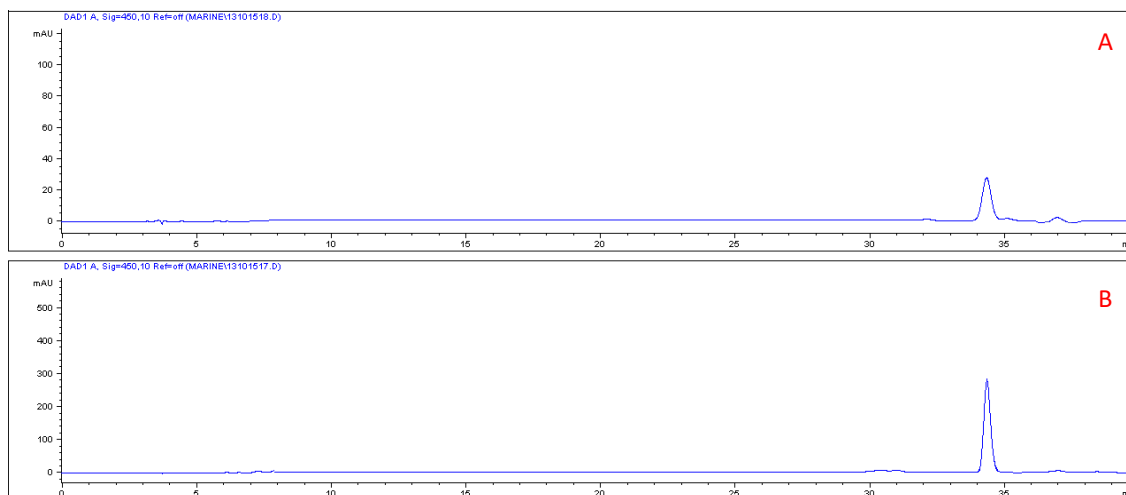
Figure 3-45. HPLC/UV chromatogram at 450 nm of A) H-a-2 and B) β-carotene standard
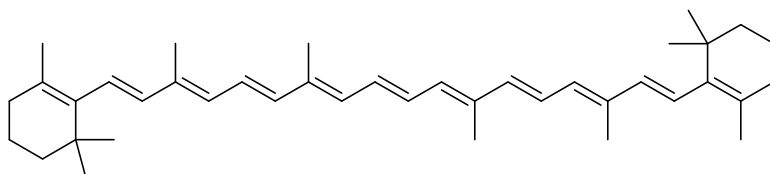
Figure 3-46. Structure of beta-carotene, compound isolated in H-a-2

3.6.2.4   H-a-5 – phytol

Fraction H-a-5 contained one major compound and several contaminants as visible by GC/MS. Due to its highly lipophilic nature, analysis of the mass spectral data obtained from GC/MS was used to characterize the major constituent. Since GC/MS provides reproducible and highly characteristic mass spectral data, mass spectra from unknown compounds can be used to algorithmically compare to databases of known compounds to rapidly identify unknowns with a high degree of certainty. Comparison of the mass spectrum obtained for this compound, shown below in Figure 3-48, indicated a very high similarity to the mass spectrum of phytol in the NIST GC/MS database. Phytol is the side-

chain of chlorophyll, shown in Figure 3-47, and was confirmed as the identity of this compound.
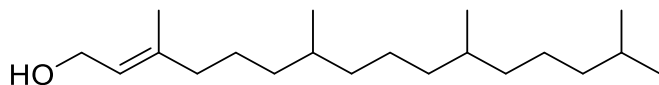
Figure 3-47. Structure of phytol, identified in H-a-5
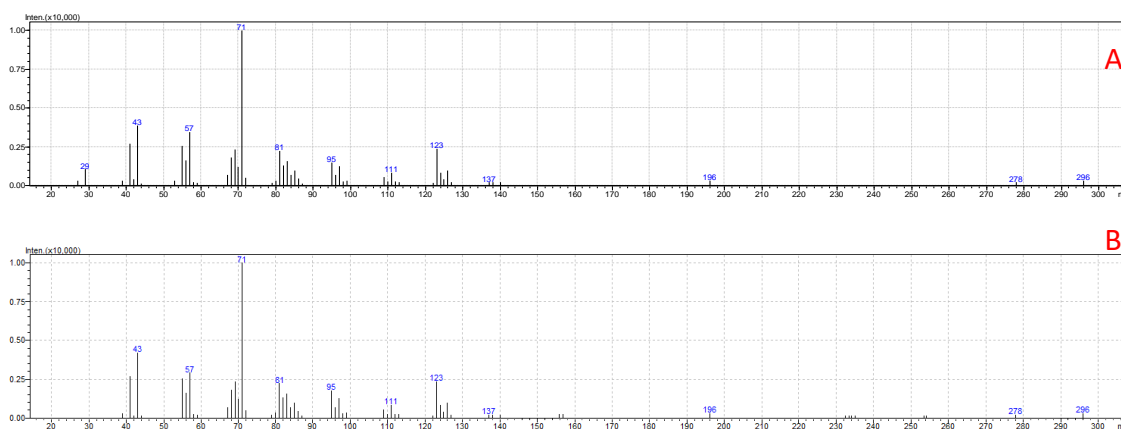
Figure 3-48. GC mass spectra of A) major peak in H-a-5; B) Phytol from NIST GC/MS database

3.6.2.5 H-a-9 – squalene

Fraction H-a-9 was obtained as a white residue which was relatively pure by GC/MS. This compound was highly lipophilic and difficult to detect by TLC analysis, except by developing plates with 10% H_2SO_4 in ethanol and charring with heat gun. Since GC/MS provides highly repeatable fragmentation for most compounds, characterization of this compound was accomplished using mass spectral data by algorithmic comparison to MS data within the NIST GC/MS database, resulting in matches with highly similar mass spectral data. Analysis conducted found a highly similar match in the NIST GC/MS

database, with 98% similarity to the hydrocarbon squalene ($C_{30}H_{50}$), composed of six isoprene units in a chain. The mass spectrum of H-a-9 and squalene are shown below in Figure 3-49, and the structure of squalene in shown in Figure 3-50.
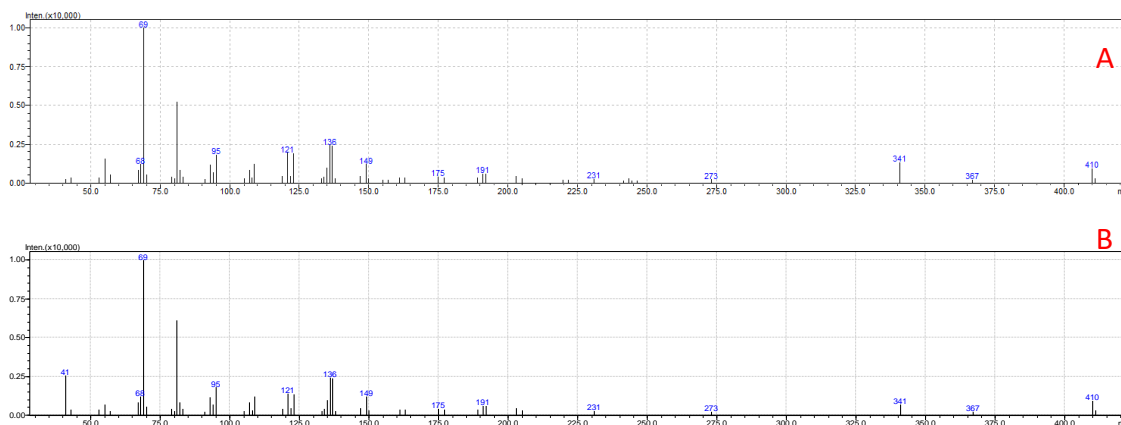
Figure 3-49. Mass spectra of A) H-a-9; B) Squalene from NIST GC/MS database
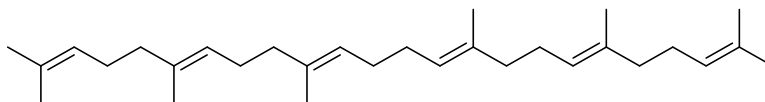
Figure 3-50. Structure of squalene, compound isolated in H-a-9

3.6.2.6 C-b-8 (lutein)

Fraction C-b-8 contained a highly lipophilic compound with a UV-Vis spectrum consistent with the xanthophyll chromophore, and as such it was hypothesized that this compound was one of the many xanthophylls detected in *P. kessleri* see section 3.7 (page 197) for complete details. HPLC analysis of the compound in C-b-8 showed a relatively pure

xanthophyll   (shown   in
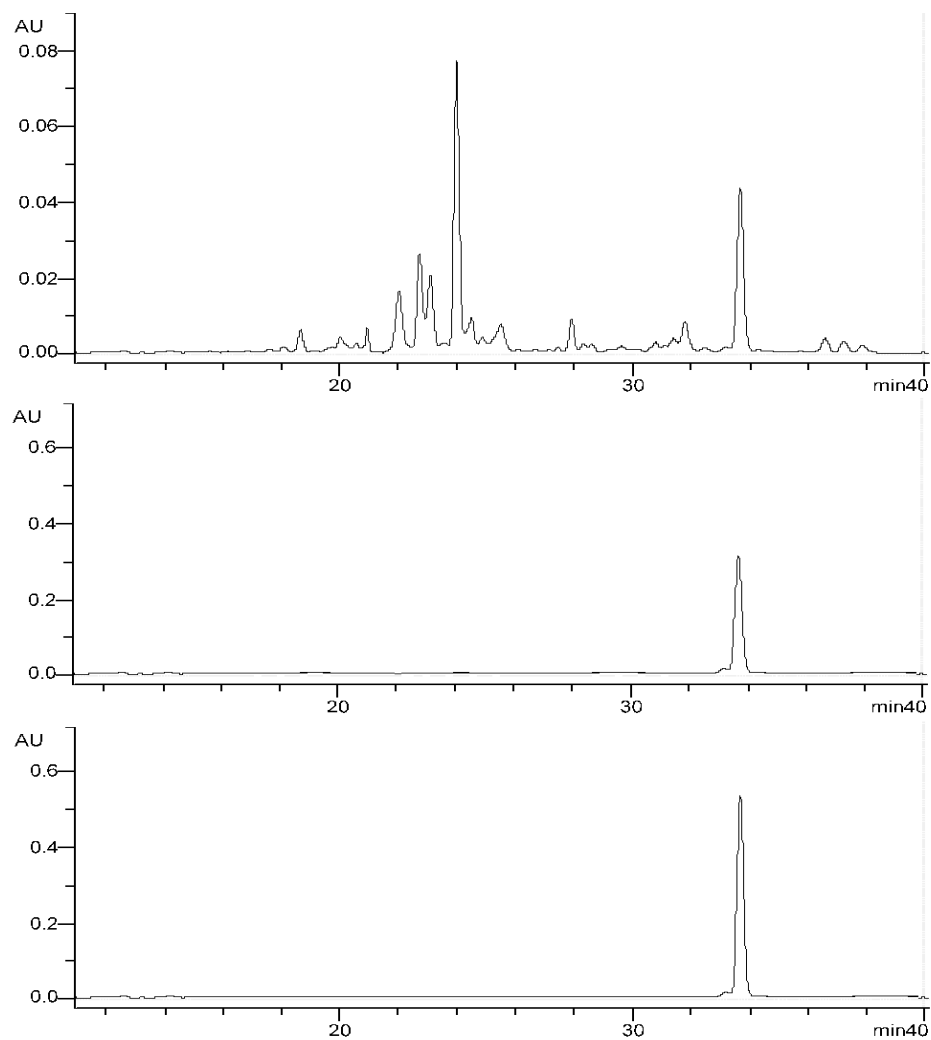
Figure **3-51**), with UV-Vis absorption maxima at 447 nm (peak II), with broad shoulder

peak at 474 nm (peak III), and another slight shoulder at 423 nm (peak I); UV-Vis spectrum

shown in
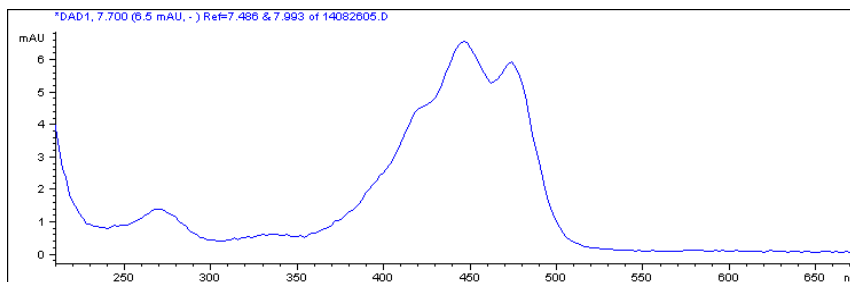
Figure 3-52. The ratio of the bands for peaks II and III is very useful in characterizing xanthophylls[3], and was determined to be 62% (III/II). The UV-Vis spectrum data suggested lutein as a possible identity for this compound. The positive mode ESI mass spectrum was also in agreement with lutein, showing two major peaks: quasimolecular ion at 569.8 *m/z* [M+H]+, and base peak ion at 551.6 *m/z* [M+H-H_2O]+. Comparison to the retention time of this compound to known lutein standard confirmed the identity of C-b-8 (structure shown in Figure 3-53).
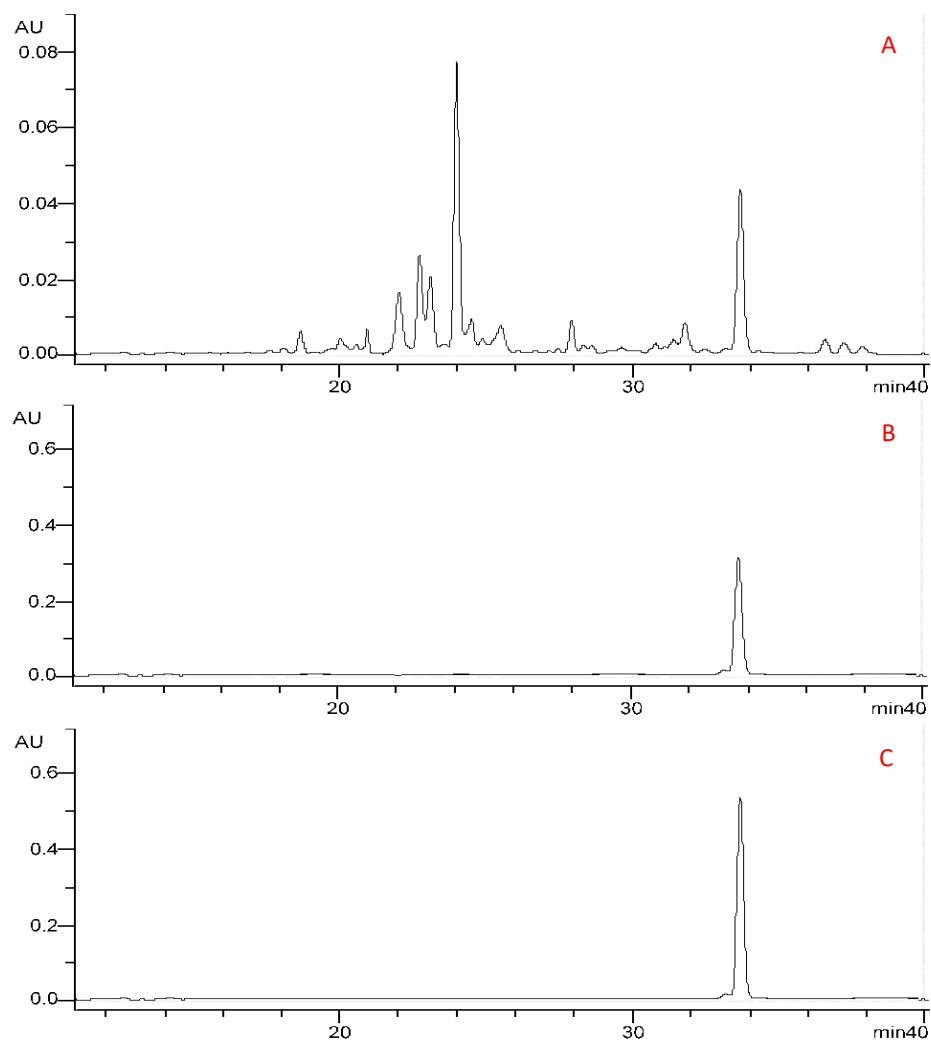
Figure 3-51. 450 nm HPLC/UV chromatogram of A) raw xanthophyll extract from section 3.7; B) fraction C-b-8; C) Lutein standard
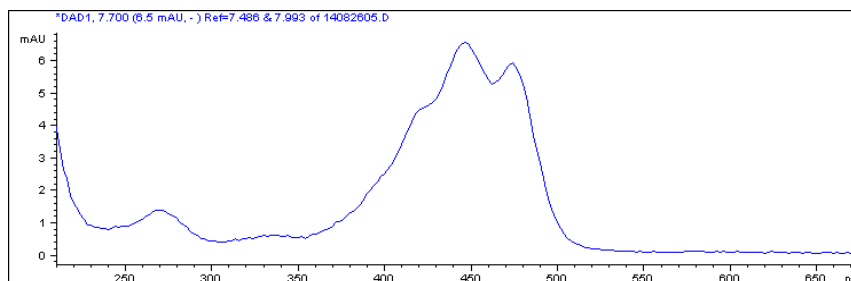
Figure 3-52. UV-Vis spectrum of compound in C-b-8, characteristic of lutein.
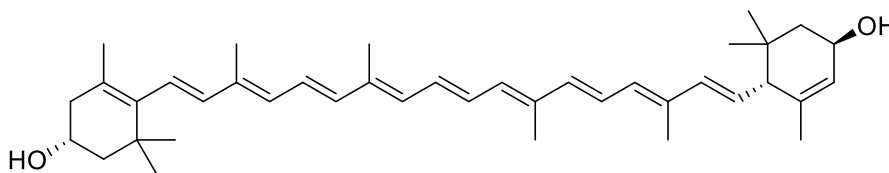
Figure 3-53. Structure of lutein, xanthophyll identified in C-b-8

3.6.2.7 C-b-5 (diadinoxanthin)

C-b-5 was obtained as a bright yellow residue which was highly lipophilic by TLC analysis.

The major compound contained within C-b-5 exhibited strong absorption at 450 nm, and possessed a characteristic xanthophyll absorption spectrum. Detailed analysis of the UV-Vis spectrum (Figure 3-54) showed 3 major bands, the strongest band at 443 (peak II), with broad shoulder at 470 nm (peak III), and minor shoulder peak at 417 nm. The band ratios between III and II was 64%, which is useful in characterizing xanthophylls. Comparison of the UV-Vis spectral data to published data suggests diadinoxanthin as a potential identity for this compound[3]. To further confirm, mass spectral data obtained from LC/ESI-MS showed quasimolecular ion at 583.3 m/z [M+H]$^+$, and fragment at 567.7 m/z [M+H-H$_2$O]$^+$, which were consistent with characteristic ions reported for diadinoxanthin[3]. Comparison of fraction C-b-5 to the xanthophyll extract and to commercially obtained diadinoxanthin by HPLC/UV further confirmed the identity of C-b-5 as diadinoxanthin (see Figure 3-55). The structure of diadinoxanthin is shown below in Figure 3-56.
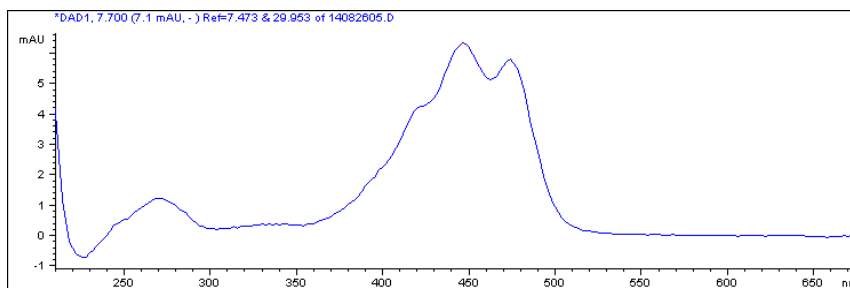
Figure 3-54. UV-Vis spectrum of major compound in C-b-5, diadinoxanthin
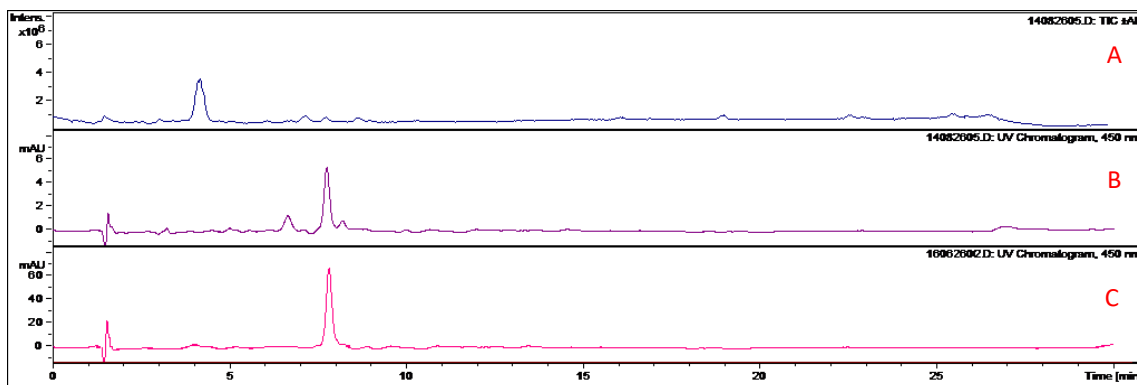
Figure 3-55. HPLC/UV/MS chromatograms of C-b-5 : A) Total ion chromatogram; B) 450 nm UV-Vis chromatogram; compared to diadinoxanthin standard C) 450 nm UV-Vis chromatogram
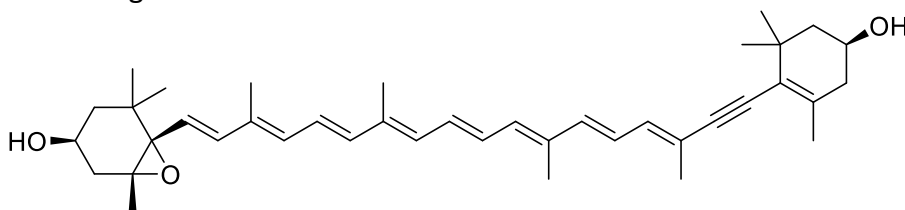
Figure 3-56. Structure of diadinoxanthin, major compound detected in fraction C-b-5

3.6.2.8 C-c-3 (tocopherol)

C-c-3 was obtained as a viscous, non-polar, clear oil with a slight yellow color. HPLC/MS

analysis indicated a substantially hydrophobic compound with a strong absorption at 285

nm. ESI-MS data collected in positive mode (see
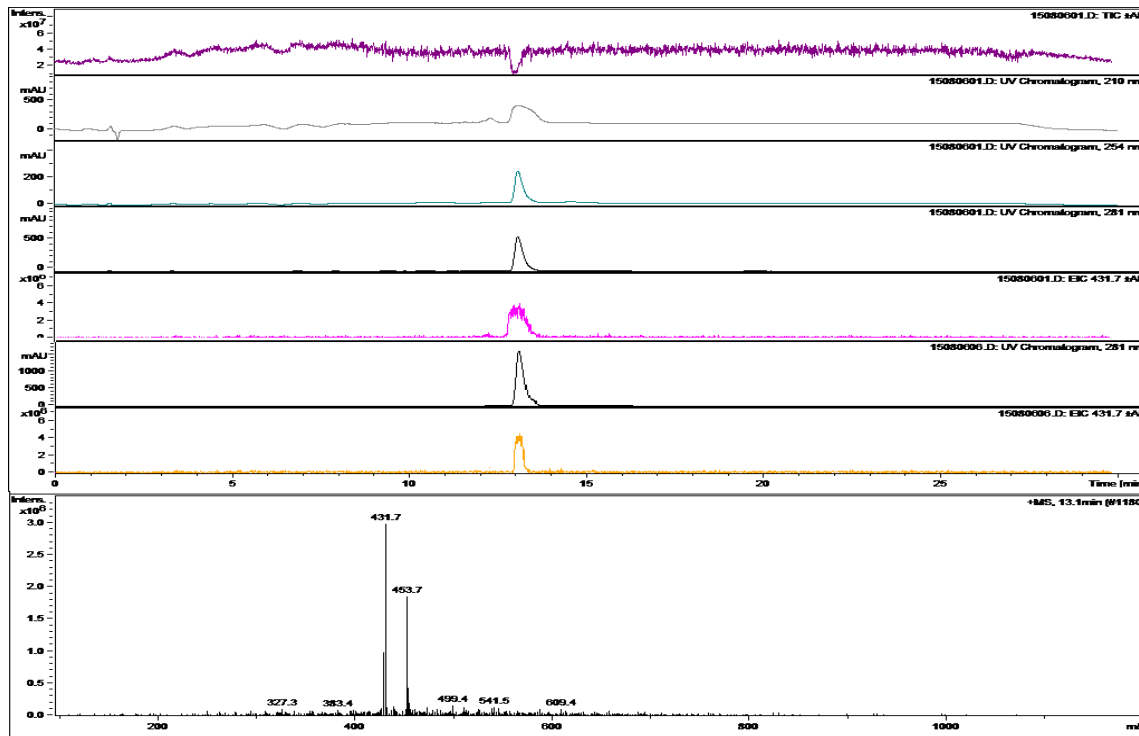
Figure 3-57) exhibited a quasimolecular ion peak 431.2 *m/z* (M+H)$^+$, and sodium adduct ion

at 453.2 *m/z* (M+Na)$^+$. Due to previous experience with tocopherol analysis (see section

2.4), this compound was recognized as sharing a number of features with α-tocopherol,

namely, nearly identical UV-Vis spectrum, and molecular weight of 430 Da, which in

positive mode would yield 431 *m/z* (M+H)$^+$ as the quasimolecular ion. Comparing the

retention time on HPLC to commercially available α-tocopherol confirmed suspicions, as

the compound in C-c-3 co-eluted with known α-tocopherol. For further confirmation,

GC/MS analysis was conducted, wherein characteristic fragmentation patterns can be

obtained and algorithmically compared to a database of known compounds. Results

showed a high similarity between the compound in E-c-3 and database entries for α-

tocopherol (Figure 3-58), thus confirming the identity of E-c-3 as α-tocopherol.
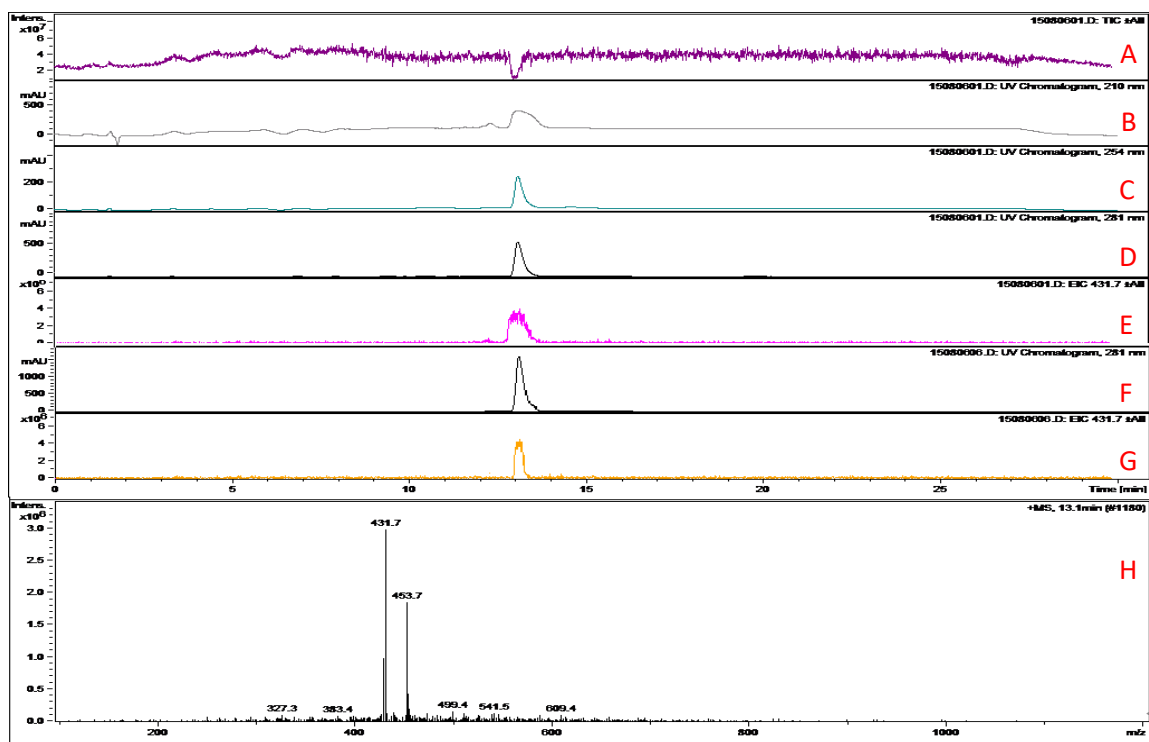
Figure 3-57. HPLC/UV/MS chromatogram and positive mode ESI-mass spectrum of E-c-3 : A) Total ion chromatogram; B) 210 nm UV-Vis chromatogram; C) 254 nm UV-Vis chromatogram; D) 281 nm UV-Vis chromatogram; E) Extracted ion chromatogram at 431.7 *m/z*; F) 281 nm UV-Vis chromatogram of α-tocopherol standard; G) Extracted ion chromatogram at 431.7 *m/z* of tocopherol standard; H) Positive mode mass spectrum of E-c-3, consistent with α-tocopherol
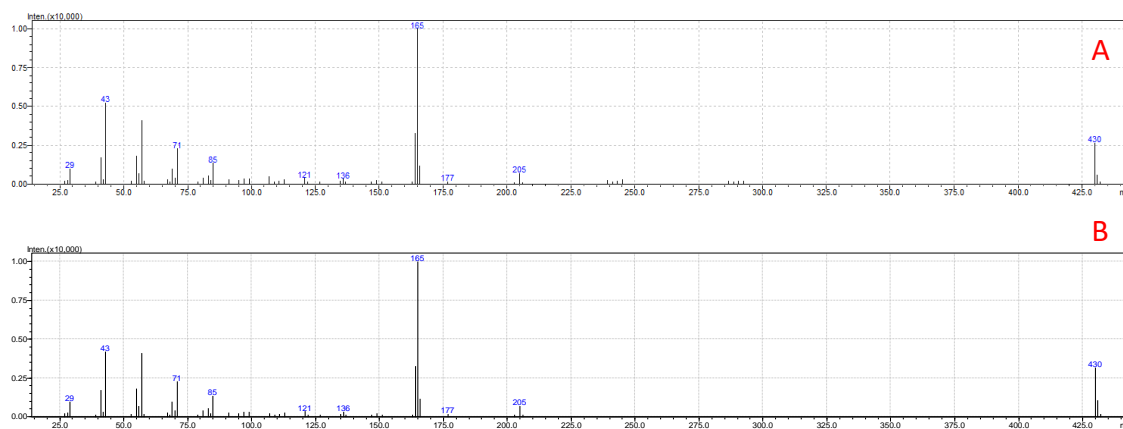
Figure 3-58. GC mass spectra of: A) C-c-3; B) α-tocopherol spectrum from NIST GC/MS database

3.7 Investigation of Xanthophylls

The xanthophyll containing fraction possessed the highest anti-inflammatory activity via inhibition of NO generation (see section 5.4). As such, it was decided to evaluate this fraction for its chemical constituents.

3.7.1 Methodology

3.7.1.1 HPLC/MS method for the Analysis of Xanthophylls

HPLC samples were prepared by filtering each extract through a 0.4 μm nylon syringe filter into an amber HPLC autosampler vial. HPLC separation was performed on an YMC-C30 Carotenoid column, 250 x 4.6 mm, 5 μm (Phenomonex Inc., Torrence, CA). For LC-MS analysis, a Hewlett Packard Agilent 1100 Series LC/MS (Agilent Technologies, Waldbronn, Germany) equipped with autosampler, quaternary pump system, DAD detector, degasser, MSD trap with an electrospray ion source (ESI) was applied, and software HP ChemStation 4.2 was used for data processing. The HPLC mobile phase contains solvent A (0.2% acetic acid with 0.1% NH4OH in water) and B (Methanol with 0.1% formic acid and C (MtBE with 0.1% formic acid) according to the following gradient: Initial solvent composition, 5% A, 90% B and 5% C; linear gradient to 5% A, 75% B and 20% C at 5 minutes; linear gradient to 4% A, 70% B, and 26% C at 10 minutes; linear gradient to 3% A, 57% B and 40% C at 16 minutes; linear gradient to 3% A, 57% B, and 40% C at 34 minutes, and back to 5% A, 75% B, 20% C at 35 minutes. Run time was 40 minutes with 5-minute re-equilibration time. The flow rate was set at 0.8 mL/min with a 1:10 splitter after the output of the UV detector leading ~80 uL/min to the ESI-MS. The UV detector

was set at 210, 254, 280, 370, 450 nm. The eluent was monitored by electrospray ion mass spectrometer (ESI-MS) scanned from *m/z* 100 to 1200. ESI was conducted by using a needle voltage of 3.5 kV. High purity nitrogen (99.999%) was used as dry gas at a flow rate of 8 L/min and capillary temperature was at 350°C. Nitrogen was used as nebulizer at 45 psi, and Helium as collision gas.

3.7.1.2 Xanthophyll Extraction

Approximately 25 mg freeze-dried microalgae samples were added to a 10 mL amber glass centrifuge tube. Extra care was taken with extracts to prevent exposure to light during analysis thus amber glass was used for every step, and exposure to light was limited as much as possible. Samples were extracted 3 times with 5 mL solvent (ethanol, acetone, or 1:1 Acetone/MtBE) by sonication for 5 minutes. Supernatant was decanted and combined. Combined extracts were freed of solvent under reduced pressure. Dried extracts were re-dissolved into 1.00 mL extraction solvent, centrifuged to remove particulates, and stored immediately in amber autosampler vials. Samples were analyzed the same day of preparation. Validation of extraction recovery was accomplished by spiked known amount of lutein to algal biomass prior to extraction. Recovery was quantitated via HPLC/UV by construction of a standard calibration curve (R^2 = 0.9991) using lutein (Sigma-Aldrich, St Louis, MO).

3.7.2   Results and Discussion

3.7.2.1   Optimization of Pigment Extraction

Xanthophylls are quite non-polar and as such are best extracted with non-polar solvent

system. However, due to the location of xanthophylls within the photosystem protein

complex, simple solvent extraction is inefficient; ultrasonic assisted extraction (UAE) has

shown to be a valuable tool to increase extraction efficiency[13]. Additionally, algal biomass

represents a unique problem since the cells of many algae are durable and lysis of cells is

a critical aspect of efficient extraction[14]. Typically, basic hydrolysis would be utilized

during extraction of xanthophylls, however due to the instability of many xanthophylls to

heat and base, it was opted to evaluate milder methods of extraction.

In order to address this problem, a series of solvent systems including mixtures of

different solvents were evaluated in conjunction with ultrasonic extraction to optimize

the extraction process for quantitative analysis of the pigments contained in *P. kessleri*

biomass. The extraction efficiency of ethanol, acetone, and 1:1 acetone/tert-butyl methyl

ether (MtBE) were compared using ultrasonic assisted extraction by comparing the

recovery of lutein and with results presented in Table 3-2. Choice of solvent led to

statistically significant differences in recovery of lutein. The best recovery was obtained

using 1:1 acetone/MtBE, which gave 98.9 ± 1.8% recovery of lutein measured by HPLC.

Another important aspect in regards to the extraction was the relative xanthophyll

content of the extracts. Since the extracts were to be evaluated *in vitro*, it was desirable

to choose the extraction method which resulted in the highest relative content of

xanthophylls, to eliminate non-xanthophyll "impurities" which may also give rise to bio-

activity. The xanthophyll content was estimated via HPLC/UV using a calibration curve

(R^2=0.9991) generated from serial dilutions of stock solutions of lutein. The response was

adjusted by the ratio of the molecular weight determined by LC/MS to that of lutein.

Extracts of 1:1 acetone/MtBE gave the highest "xanthophyll purity" with an average of

81.2 ± 2.6% xanthophylls by mass. Acetone resulted in a "less pure" extract, containing

only 74.2 ± 3.5% xanthophylls by mass, and ethanol resulted in the least relative

xanthophyll content (45.2 ± 6.1%). Presumably this is due to the wide range of compounds

that are soluble in acetone and ethanol in comparison to 1:1 acetone/MtBE.

Table 3-2. Recovery of lutein from spiked *Parachlorella kessleri* biomass using various solvents, and impact on extraction time on recovery of lutein using acetone/MtBE extraction.

Solvent	Recovery of Lutein (n=3)	Content of Xanthophylls[1] (n=3)
Ethanol	78.1 ± 4.8%[A]	45.2 ± 6.1%[D]
Acetone	89.6 ± 3.9%[B]	74.2 ± 3.5%[E]
Acetone/MtBE	98.9 ± 1.8%[C]	81.5 ± 2.6%[F]
Extraction Time (min)[2]	**Recovery of Lutein (n=3)**	**Content of Xanthophylls[1] (n=3)**
1	85.1 ± 4.3%[G]	84.9 ± 4.9%[I]
5	98.9 ± 1.8%[H]	81.5 ± 2.6%[I]
30	75.4 ± 8.9%[G]	72.2 ± 7.1%[I]

[1] Xanthophyll content of extracts was estimated using Lutein calibration curve, by adjusting for the molecular weight as determined by MS
[2] Extraction using 1:1 Acetone/MtBE
[A-I] Entries with different superscripts differ statistically significantly (p < 0.05)

Additionally, the sonication extraction time (from 1 min to 30 min) was evaluated for

impact on recovery of lutein, and 5 minutes was optimal for recovery of lutein, yielding

statistically significantly increased recovery for lutein (98.9 ± 1.8%, p = 0.006); data shown

in Table 3-2 and Figure 3-59. Extraction for 1 minute resulted in incomplete recovery (85.1

± 4.3%), while sonication for 30 minutes resulted in an apparent loss of lutein (75.4 ± 8.9%

recovery, although not significant with respect to 1 minute extraction, p = 0.164), presumably due to oxidation facilitated by prolonged exposure to ultrasound.
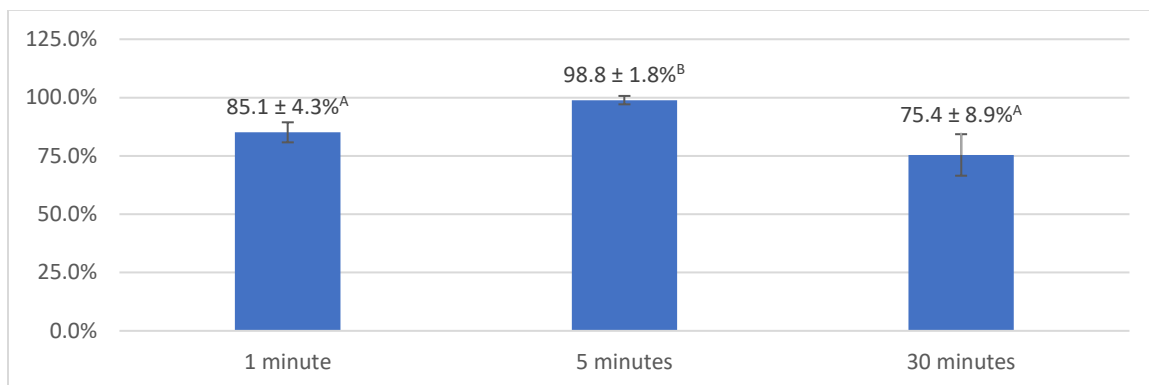
Figure 3-59. Effect of incubation time on lutein recovery for ultrasonic-assisted extraction of xanthophylls with 1:1 acetone/MtBE
A,B: Entries with different superscripts differ statistically significantly (p < 0.05)

Furthermore, effect of extraction time on xanthophyll content was examined. Here, 30-minute extraction time resulted in a lower relative content of xanthophylls (72.2 ± 7.1%) although not statistically significant with respect to 5-minute extraction (p = 0.100). A one minute extraction demonstrated highest xanthophyll content (84.9 ± 4.9%), although the results were not significant with respect to 5-minute extraction (p = 0.348). Therefore, for the extraction of xanthophylls from *P. kessleri*, the optimal procedure utilizes 1:1 acetone/MtBE with ultrasound assisted extraction for 5 minutes, resulting in an extract which is 81.5 ± 2.6% xanthophylls by mass of the extract, a total xanthophyll content of 26.6 ± 8.1 mg/g freeze dried biomass of original algae.

3.7.2.2 Identification of Compounds by HPLC/UV/MS

The elution profile of the pigment extract, prepared as described above, of *P. kessleri* is shown in Figure 3-60. Major compounds were identified by analyzing their mass and UV-

Vis spectra and in comparing to commercially available standards (when available), minor compounds were tentatively identified by comparing data to literature references. Xanthophylls exhibit characteristic ratios between bands in the UV-Vis spectrum; the ratio of bands II and III can be used as an identifying feature[15]. The identities of the compounds are shown in Table 3-3. The xanthophyll present in highest content was diatoxanthin (compound **4**), identified by characteristic quasimolecular ion [M+H]$^+$ at 567.5 *m/z*. Additionally, its UV-Vis spectrum was consistent with data reported by Strain et al. (1970). Lutein (compound **9**) is also a major constituent of the pigment extract, identifiable by its quasimolecular ion [M+H]$^+$ at 569.8 *m/z* and major fragment at 551.6 *m/z* corresponding to a loss of a molecule of water. The UV-Vis spectrum is consistent with the reported spectrum of lutein[16].

Table 3-3. Identification of compounds in pigment extract by UV-Vis and MS data.

#	RT	Identity	UV-Vis	(%III:II)	*m/z* (positive mode ESI-MS)
1	21.9	Diadinochrome	412, *424*, 451	62	583.5 [M+H]$^+$
2	22.7	Diadinoxanthin	(417), *443*, 470	64	583.3 [M+H]$^+$, 567.7 [M+H-H$_2$O]$^+$
3	23.1	9'-cis-neochrome	402, *425*, 451	90	601.5 [M+H]$^+$, 583.6 [M+H-H$_2$O]$^+$
4	23.9	Diatoxanthin	(415), *450*, 478	33	567.5 [M+H]$^+$
5	24.5	Unidentified Xanthophyll 1	(421), *442*, (464)	5	567.5 [M+H]$^+$, 549.5 [M+H-H$_2$O]$^+$
6	25.5	cis-Diadinochrome	(400), *419*, 445	80	583.5 [M+H]$^+$
7	27.8	Unidentified Xanthophyll 2	*418*, 447, 474	25	593.4 [M+H]$^+$
8	31.7	Dihydro loroxanthin	400, *423*, 450	68	587.6 [M+H]$^+$, 569.6 [M+H-H$_2$O]$^+$
9	33.6	Lutein	(423), *447*, 474	62	569.8 [M+H]$^+$, 551.6 [M+H-H$_2$O]$^+$
10	36.5	Loroxanthin dodecanoate	418, *443*, 470	25	767.5 [M+H]$^+$, 583.6 [M+H-C$_{12}$H$_{23}$O$_2$]$^+$
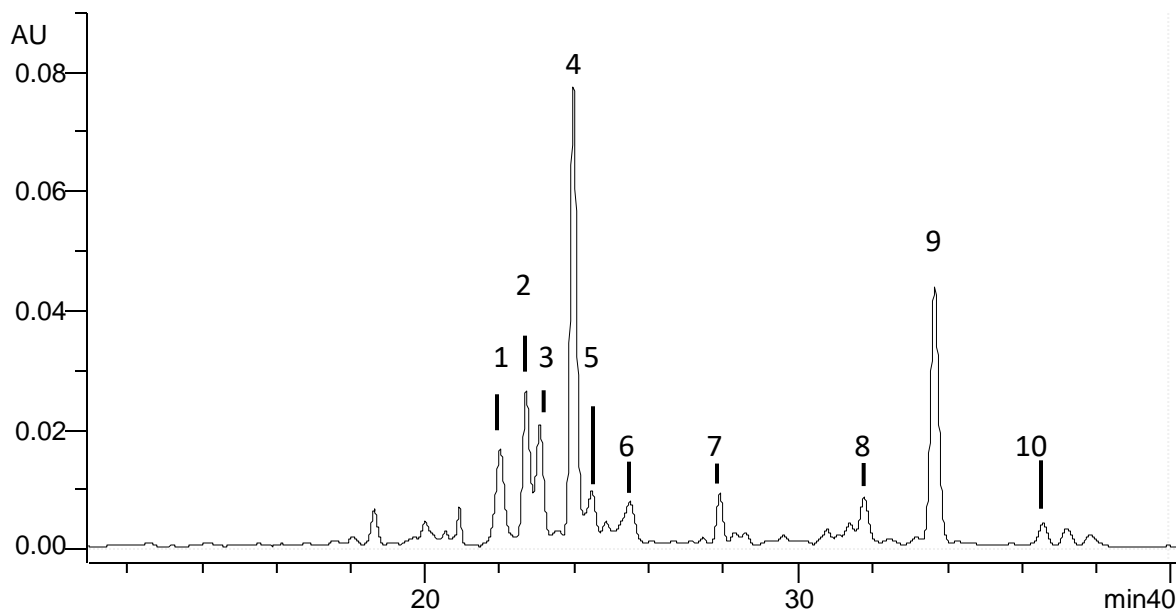
Figure 3-60. A representative UV-Vis chromatogram at 450 nm of *Parachlorella kessleri* pigment extracts. Compound IDs and data listed in Table 3-3.

Diadinochrome (compound **1**) was identified by its unique blue-shifted absorption spectrum, with λ_{max} at 424 nm, exhibiting the characteristic band ratio of 62% III/II (Egeland, 2011). The mass spectrum is consistent with diadinochrome, with quasimolecular ion [M+H]$^+$ at 583.5 *m/z*. Diadinoxanthin (compound **2**) was distinguished by the UV-Vis band ratio of 48, and a λ_{max} measured at 443, consistent with reported data. Additionally, the quasimolecular ion for diadinoxanthin was observed at 583.3 *m/z*, and fragment at 567.7 *m/z* corresponding to loss of a molecule of water. 9'-cis-neochrome (compound **3**) was readily identified by its unique quasimolecular ion [M+H]$^+$ at 601.5 *m/z*, with fragment corresponding to loss of a molecular of water at 583.6 *m/z*. The UV-Vis spectrum of compound 3 was blue-shifted, with λ_{max} at 425 nm, and III/II band ratio of 90%, consistent with reported data.

In addition to the major xanthophylls that were present, three minor compounds were also detected and assigned tentatively based on MS and UV-Vis data. Compound 6 exhibited a unique blue-shifted UV-Vis spectrum, with a λ_{max} at 419 nm, 30 nm down-field from λ_{max} of lutein, suggesting one fewer double bond in conjugation according to Woodward-Fieser rules for conjugated dienes[17]. This suggests either a dihydro moiety, or a cyclized moiety as in diadinochrome and neochrome. Based on the UV-Vis spectrum and quasimolecular ion [M+H]$^+$ at 583.5 m/z, compound 6 was tentatively identified as cis-diadinochrome. Compound 8 exhibited a similar blue-shift, with a λ_{max} at 423 nm, and a quasimolecular ion [M+H]$^+$ at 587.6 m/z, and was tentatively identified as dihydro-loroxanthin. Compound 10 exhibited an absorption spectrum nearly identical to loroxanthin with a quasimolecular ion [M+H]$^+$ at 767.5 m/z, as such was identified as loroxanthin dodecanoate.

There were two xanthophylls which eluded identification due to inconsistencies with UV-Vis spectral data in comparison to reported literature. Compound 5 had a molecular weight very close to diatoxanthin, however possessed a unique UV-Vis spectrum, wherein band I and III were present only as shoulders. Compound 7 possessed a unique quasimolecular ion [M+H]$^+$ at 593.4 m/z. It is possible that compound 7 has a molecular formula of $C_{40}H_{48}O_4$. The UV-Vis spectrum of this compound is very unique, where band I was at the λ_{max} at 418 nm.

3.8   References

[1] Jung, J. H., Lee, H., & Kang, S. S. (1996). Diacylglycerylgalactosides from Arisaema amurense. *Phytochemistry*, *42*(2), 447-452.

[2] Rahman, S. M., Wang, Y. M., Yotsumoto, H., Cha, J. Y., Han, S. Y., Inoue, S., & Yanagita, T. (2001). Effects of conjugated linoleic acid on serum leptin concentration, body-fat accumulation, and β-oxidation of fatty acid in OLETF rats. *Nutrition*, *17*(5), 385-390.

[3] "Xanthophylls", Phytoplankton Pigments. 1st ed. Cambridge: Cambridge University Press, 2011. pp. 728-822. Cambridge Books Online. Web. 16 March 2015.

[4] Anastassiades, M; Lehotay, S. J.; Stajhbaher, D.; Schenck, F. J. Fast and easy multiresidue method employing acetonitrile extraction/partitioning and "Dispersive Solid-Phase Extraction" for the determination of pesticide residues in produce. J. AOAC Int. 2003, 86, 412-431.

[5] Berrueta, L. A., Gallo, B., & Vicente, F. (1995). A review of solid phase extraction: basic principles and new developments. *Chromatographia*, 40(7-8), 474-483.

[6] Lichtenthaler, H. K., & Buschmann, C. (2001). Chlorophylls and carotenoids: Measurement and characterization by UV-VIS spectroscopy. *Current protocols in food analytical chemistry*.

[7] Moody, C. M. (2010). Black Writing Ink Analysis By Direct Infusion Electrospray Mass Spectroscopy.

[8] Kim S, Thiessen PA, Bolton EE, Chen J, Fu G, Gindulyte A, Han L, He J, He S, Shoemaker BA, Wang J, Yu B, Zhang J, Bryant SH. PubChem Substance and Compound databases. *Nucleic Acids Res.* 2016 Jan 4; 44(D1):D1202-13. Epub 2015 Sep 22 [PubMed PMID: 26400175] doi: 10.1093/nar/gkv951

[9] Brewer, J. D., Hagan, K. A., & Egan, J. M. (2005). Forensic analysis of blue ballpoint pen inks using capillary electrophoresis. *Forensic Sci. Commun*, *7*(3).

[10] P.J. Linstrom and W.G. Mallard, Eds., **NIST Chemistry WebBook, NIST Standard Reference Database Number 69**, National Institute of Standards and Technology, Gaithersburg MD, 20899, http://webbook.nist.gov, (retrieved January 7, 2017).

[11] "MassBank: A public repository for sharing mass spectral data for life sciences", H. Horai, M. Arita, S. Kanaya, Y. Nihei, T. Ikeda, K. Suwa. Y. Ojima, K. Tanaka, S. Tanaka, K. Aoshima, Y. Oda, Y. Kakazu, M. Kusano, T. Tohge, F. Matsuda, Y. Sawada, M. Yokota Hirai, H. Nakanishi, K. Ikeda, N. Akimoto, T. Maoka, H. Takahashi, T. Ara, N. Sakurai, H. Suzuki, D. Shibata, S. Neumann, T. Iida, K. Tanaka, K. Funatsu, F. Matsuura, T. Soga, R. Taguchi, K. Saito and T. Nishioka, *J. Mass Spectrom*., **45**, 703-714 (2010).

[12] Hoerr, C. W., & Harwood, H. J. (1952). The solubilities of oleic and linoeic acids in common organic solvents. *The Journal of Physical Chemistry*, *56*(9), 1068-1073.

[13] Vilkhu, K., Mawson, R., Simons, L., & Bates, D. (2008). Applications and opportunities for ultrasound assisted extraction in the food industry—A review. *Innovative Food Science & Emerging Technologies*, 9(2), 161-169.

[14] Zheng, H., Yin, J., Gao, Z., Huang, H., Ji, X., & Dou, C. (2011). Disruption of Chlorella vulgaris cells for the release of biodiesel-producing lipids: a comparison of grinding, ultrasonication, bead milling, enzymatic lysis, and microwaves. *Applied biochemistry and biotechnology*, *164*(7), 1215-1224.

[15] Rodriguez-Amaya, D. B., & Kimura, M. (2004). *HarvestPlus handbook for carotenoid analysis.* Washington, DC, USA: International Food Policy Research Institute (IFPRI). Chicago

[16] Jeffrey, S. W., Mantoura, R. F. C. and Bjørnland, T. (1997). Data for the identification of 47 key phytoplankton pigments. In Phytoplankton Pigments in Oceanography: Guidelines to Modern Methods, ed. S. W. Jeffrey, R. F. C. Mantoura and S. W. Wright. Paris: UNESCO Publishing, pp. 449–559.

[17] Woodward, R. B. (1941). "Structure and the Absorption Spectra of α,β-Unsaturated Ketones". *J. Am. Chem. Soc.* **63** (4): 1123

Chapter 4   Screen for Bioactivity

A major goal of this dissertation is to evaluate the compounds contained within algae biomass for biological activity relevant to disease. As such, a series of assays were utilized to rigorously interrogate the chemistries within the available algae species. This chapter will focus upon the following specific screens: anti-oxidant activity, anti-bacterial activity, anti-fungal activity, pancreatic lipase inhibition activity and α-glucosidase inhibition activity. Chapter 5 follows with focusing on anti-inflammation activity and bioassays conducted to explore the role of compounds in algae on inflammation.

In general, the approach was to evaluate a number of crude solvent extracts of the algal biomass in each of the assays described in this section. Care was taken to prepare extracts with a broad range of compounds varying in polarity. For crude extracts of *P. kessleri* which demonstrated significant activity, the assays were repeated with sub-fractions and pure compounds obtained from the natural products isolation described in Chapter 3.

4.1   Anti-oxidant activity

4.1.1   Methodology

Algal extracts were prepared from freeze-dried algal biomass. Approximately 100 mg biomass was extracted 3x with 100% ethanol, followed by triplicate extraction with 70% methanol/water. Solvent was removed by rotary evaporation. To remove residual water from extracts, they were dried by azeotrope with benzene, followed by drying under a stream of N_2 at 40˚C.

The methodology utilized to measure free radical absorption capacity is based upon the well-known and widely published Trolox Equivalent Antioxidant Capacity assay, which has been reviewed extensively by many authors[1-4]. The Trolox Equivalent Antioxidant Capacity assay measures the degree of radical absorption compared to Trolox (a water-soluble form of Vitamin E). A solution of ABTS (2,2'-azino-bis(3-ethylbenzothiazoline-6-sulphonic acid)) was reacted with Potassium Persulfate (radical generator) to produce the stable colored ABTS radical cation (stable for ~1 hour at room temperature). The disappearance of this colored radical is measured at 734 nm, allowing for the quantification of radical absorption capacity. A calibration series of Trolox was prepared ranging from 632 µg/mL to 19.75 µg/mL.

ABTS (38.4 mg) and Potassium Persulfate (6.6 mg) were mixed in 10 mL water and stored in the dark for 12 hrs. 990 uL of the ABTS reagent was combined with 10 µL of the algae extracts or calibration solution. The mixture was placed in a cuvette and measured using an Agilent G1111AA UV-Vis Spectrophotometer, set at 734 nm. All samples were run in triplicate. Results are reported as µmol trolox / g, reported as average of three runs ± standard deviation.

4.1.2   Results and Discussion

Each of the algal extracts analyzed using this assay demonstrated significant free radical absorption capacity using the Trolox Equivalent Antioxidant Capacity assay with ABTS radical as the free-radical source. Solvent extracts were prepared of each algal strain evaluated in this assay, and results are reported as µmol Trolox equivalents per gram of

freeze-dried biomass. Results are shown in Figure 4-1. *Tetraselmis chuii* exhibited the highest activity, at 68.2 µmol Trolox/g freeze dried biomass. *Parachlorella kessleri* and *Isochrysis galbana* (Caribbean strain) possessed similar antioxidant capacity at 43.5 ± 4.80 µmol Trolox/g and 45.9 ± 5.60 µmol Trolox/g respectively. *T. chuii, P. kessleri*, and *I. galbana* exhibited superior antioxidant activity compared to red grapes and commercially available green alga *Chlorella vulgaris*. Red grapes have been reported to possess a trolox equivalent absorption capacity (TEAC) of 36.0 ± 1.10 µmol / g[5]; *T. chuii* has nearly double that activity, and *P. kessleri* and *I. galbana* have comparable activity. Additionally, *I. galbana* and *P. kessleri* are superior to *Chlorella vulgaris,* with a reported TEAC of 15.5 ± 0.51 µmol / g[6].

The activity of *Pavlova lutheri*, *Chaetoceros calcitrans*, and *Chaetoceros neogracile* exhibited less activity than the other evaluated alga. *C. calcitrans* exhibited the least activity with 4.8 ± 2.80 µmol / g TEAC. *C. neogracile* exhibited similar activity as reported for *C. vulgaris*[6]. *P. lutheri* showed TEAC of 13.6 ± 3.2 µmol / g.

Based on these results, algal biomass is clearly a rich source of compounds capable of free radical absorption, and hence acting as anti-oxidants. Due to the substantial content of β-carotene, α-tocopherol, and xanthophylls (see sections 2.3, 2.4, and 5.4.2.1 respectively), which are known free-radical scavengers, we hypothesize that these algal species would be rich source of antioxidants and find, we did such high radical scavenging activity in the algal biomass.
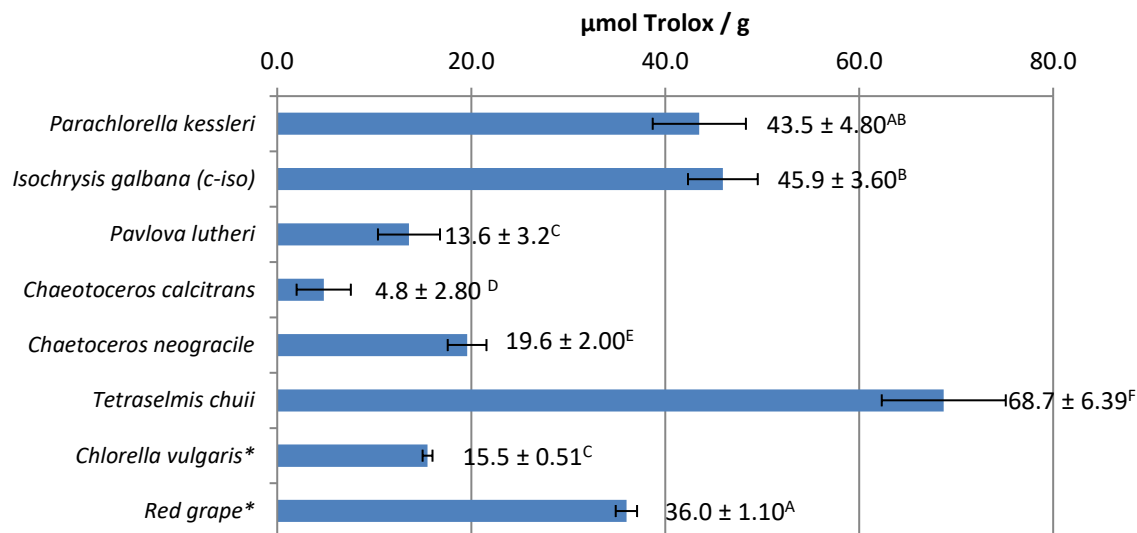
Figure 4-1. Trolox equivalent antioxidant capacity (TEAC) of crude extracts of algal biomass
Results with different superscripts were not statistically significant by Students T-Test ($p < 0.05$)
* Results for *Chlorella vulgaris*[6] and Red grape[5] obtained from published data

4.2 Anti-bacterial activity

4.2.1 Methodology

4.2.1.1 Agar Disc Diffusion Method

The agar disc diffusion method has been used for nearly a century to screen compounds for antimicrobial activity[7], and the methods used in this work were adapted from learnings discussed in a detailed review of the numerous technical adaptations of this method[8]. A culture of *E. coli* was kept in LB broth in a shaking incubator at 37˚C. The culture was diluted to an $OD_{600} = 0.1$ by UV-Vis spectrometer. Stock solutions of the chloroform, ethyl acetate, and butanol fractions of PK extract were prepared in 95% ethanol. A 1cm diameter paper disc (sterilized previously in 95% ethanol) was saturated with each solution and set to dry in sterile conditions. As control, a disc was immersed in kanamycin (5 mg/mL) in 95% ethanol, and a disc that was immersed in only 95% ethanol.

Agar plates containing MH broth were prepared earlier and autoclaved. The plates were inoculated with the E. coli culture, and dried discs were placed immediately onto the plates. The plates were sealed with Parafilm and placed in a gently shaking incubator at 37°C for 24 hours in the dark. The radius of the zone of inhibition was measured to determine relative inhibition.

4.2.1.2 Broth micro-dilution assay

The broth micro-dilution assay was used to assess inhibitory activity in 96-well plate format; the methodology was adapted from published techniques[9]. A culture of *E. coli* was kept in LB broth in a shaking incubator at 37°C. The culture was diluted to an OD600 = 0.1 by UV-Vis spectrometer. Stock solutions of PK extracts were prepared in DMSO and diluted serially using sterile LB media. In a 96-well plate, 50μL extract solution and 50μL LB broth were added and thoroughly mixed. 5 μL of diluted bacterial culture was added to each well. Control-wells were kept for blank, media/bacteria/kanamycin, media/vehicle, and media/vehicle/control to ascertain whether the DMSO vehicle had any effect on the bacterial growth. The plate was wrapped in Parafilm and placed in a 37°C shaking incubator overnight in light or dark/. Bacterial growth was determined by measuring the OD_{600} using a 96-well plate reader. MIC_{50} was determined as the minimum concentration wherein no bacterial growth could be detected.

4.2.2   Results and Discussion

The algal extracts were evaluated for anti-bacterial method using two techniques: the agar disc diffusion technique[8] and the broth microdilution technique[9]. These techniques

are widely cited in the literature, consisting of numerous adaptations and refinements (discussed in detail in the excellent review[8] by Wiegand, I., Hilpert, K., & Hancock, R. E. , 2008) , and serve as the principal technique utilized to screen natural products, extracts, and pharmaceuticals for antimicrobial activity.

The agar disc diffusion method is the earliest described method for the evaluation of antibacterial activity[7], and as such, its simplicity is inimitable. Briefly, compounds/extracts are dissolved in a volatile solvent such as ethanol or chloroform at known concentrations. Small circles of filter paper are sterilized in ethanol, dried in sterile conditions. Then a small amount of each compound/extract and dried, such that a known mass of compound/extract is added to each circle. Meanwhile, suitable microbes (in this case, *Escheria coli*) are cultured in suitable media and divided so they are kept in log phase, i.e. rapidly dividing. Sterile agar plates containing suitable medium are inoculated with bacteria, and the filter paper circle is added to the center of each plate. A positive control plate was prepared using known anti-microbial kanamycin, and a negative control containing solvent vehicle was also prepared. The plates are incubated overnight at 37˚C in atmospheric conditions. After 24 hours, the plates were examined. The radius of the inhibition of growth detected around the circles is measured using a caliper and presented as the data point for each sample.

The results of the agar disc diffusion assay are shown below in Table 4-1. The ethanolic extracts of algae biomass did not show any appreciable antibacterial activity versus

vehicle control. As none of these strains of algae have been reported to contain antibacterial compounds or show antibacterial activity, the results were expected.

Table 4-1. Results of agar disc-diffusion assay for anti-bacterial activity

	Isochrysis galbana (Caribbean)	*Isochrysis galbana* (Tahitian)	*Pavlova lutheri*	*Chaetoceros calcitrans*
Radius of inhibition (mm)	0.005	0.005	0.005	0.005
	Chaetoceros negracile	***Parachlorella kessleri***	**Vehicle Control**	**Kanamycin**
Radius of inhibition (mm)	0.005	0.005	0.005	6.0

Assays done in triplicate

The broth microdilution assay is the modern and academically accepted assay to utilize when determining the anti-bacterial activity of plant extracts/compounds of interest. The preference in the broth microdilution resides in the shortcomings of other techniques— within the agar disc diffusion method, for example, some compounds adhere strongly to the paper disc, and do not diffuse readily into the medium. The broth microdilution technique consists of a solution or stable suspension of extract/compound of interest, growth media, and bacteria. Thus, determination of the effective concentration of anti-bacterial activity is much more reliable using this technique. One of the major drawbacks in utilizing this technique for crude plant extracts is that it may be difficult to solubilize many components of plant extract in growth medium without adding solubilizing agents which may in turn effect the assay results. Solubilizing surfactants and solvents may themselves inhibit bacterial growth, and as such should be avoided in this assay. Especially lipophilic components need to be removed prior to analysis, and this can be accomplished by simple precipitation of insoluble material from the media by microcentrifuge. It is crucial to recover the precipitated mass in order to adjust for the

concentration of the extract dissolved in the media. One obvious and unavoidable caveat is that false negatives may arise due to compounds that may be active but are sparingly soluble in the assay medium.

Table 4-2. Results of broth microdilution assay for anti-bacterial activity

	Isochrysis galbana (Caribbean)	*Isochrysis galbana* (Tahitian)	*Pavlova lutheri*	*Chaetoceros calcitrans*
MIC_{50} (µg/mL)	>5000	>5000	>5000	>5000
	Chaetoceros negracile	***Parachlorella kessleri***	**Vehicle Control**	**Kanamycin**
MIC_{50} (µg/mL)	>5000	>5000	>5000	4

The results of the broth microdilution assay conducted for the algal extracts is summarized in Table 4-2. Each algal extract again demonstrated negligible activity, showing no inhibition of bacterial growth even at extremely high concentrations (5000 µg/mL). Due to the extremely high concentration at the highest end of the assay, it was concluded that the algal extracts demonstrated no anti-bacterial activity. These results are congruent with the results from the agar disc diffusion assay, and as such, it was decided to discontinue the investigation of anti-bacterial activity in algal extracts.

4.3 Anti-fungal activity

4.3.1 Methodology

The anti-fungal assay used in this work was adapted from the commonly employed MTT assay to determine metabolic activity in yeasts[10]. Baker's yeast (Fleishmans, ShopRite, North Brunswick, NJ) was activated in a warm solution of 1% sucrose, heated to 45˚C. After 10 minutes, it was clearly evident that the yeast had become activated. A volume of 190 µL of the suspension of activated baker's yeast was then pipetted into 96-well plates.

A solution of 10 µL of the fraction to be evaluated dissolved in DMSO was pipetted into corresponding wells. 10 µL DMSO was pipetted into the vehicle control wells. The 96-well plate was incubated overnight at 37˚C. The following morning, a solution of 3-[4,5-dimethylthiazol-2-yl]-2,5-diphenyltetrazolium bromide (MTT) was added and the well plate was incubated for 10 minutes. Results were measured on a scale from 1-4, where 1 showed complete color change to blue, and 4 represented no detectable color change.

4.3.2   Results and Discussion

The anti-fungal assay performed allowed for the assessment of the lethality of the fractions derived from *Parachlorella kessleri* to fungi, namely, yeast. This is accomplished by incubation of activated yeast with fractions dissolved in DMSO. After 24 hours, the metabolic activity of the yeast is measured using 3-[4,5-dimethylthiazol-2-yl]-2,5-diphenyltetrazolium bromide (MTT). MTT has been widely used due to its unique ability to turn into a dark blue colored compound upon action from mitochondrial reductase—as such MTT has found major utility as a marker for the flux of $NADP(H_2)^+$, therefore metabolic activity, and hence, living cells[11]. A schematic of this reaction is shown in Figure 4-2.
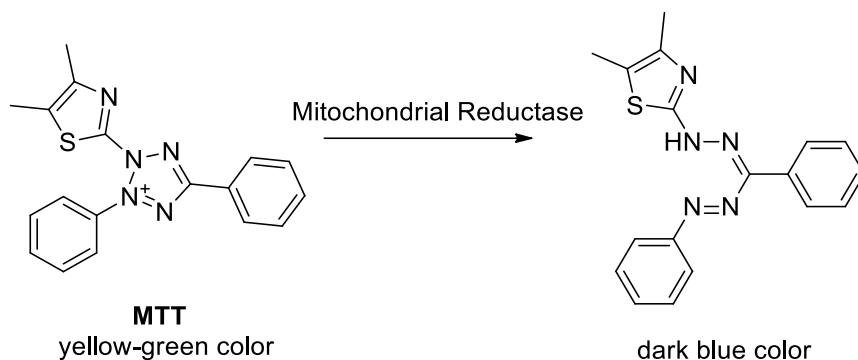
Figure 4-2. Diagram of reduction of MTT to form colored product for the detection of metabolic activity

Of the 48 fractions evaluated for anti-fungal activity (see **Chapter 3** for preparation and fractionation scheme), only two fractions showed any signs of anti-fungal activity (Table 4-3). Anti-fungal activity was assessed by measuring the metabolic activity of the yeast using MTT, as described above, where a lack of anti-fungal activity would yield a dark blue product, and complete inhibition of fungal growth would result in a yellow-green color, unchanged from vehicle control samples. A qualitative score from 1 (no detectable change in ATP metabolism, yielding dark-blue wells), 2 (slight reduction in ATP metabolism, slightly lighter blue wells) 3 (moderate reduction in ATP metabolism, yielding very light blue-green coloring) to 4 (complete inhibition of ATP metabolism, resulting in yellow-green wells indistinguishable from control). Fraction E-e-a demonstrated slight activity, with a rating of 2. From fraction E-e-a, a white crystalline material was recovered and designated as E-e-a-0. Accordingly, fraction E-e-a-0 demonstrated very high activity, with complete inhibition of metabolic activity. This fraction possessed the highest anti-

fungal activity, and as such a thorough characterization of this compound was conducted

(see section 3.4.2.4, pg. 141 for more details).

Table 4-3. Anti-fungal activity of fractions derived from *Parachlorella kessleri* measured by change in metabolic activity by MTT (ATP-analogue) colorimetric assay*

E-H-[2,3,4]-1	E-H-6B1-[19]	E-H-5-[17-19]	E-H-5-[1-4]	E-H-5B1	E-H-6A	E-H-5-[14-16]	E-H-B2
1	1	1	1	1	1	1	1
E-H-5C-[10-12]	E-H-6C	E-G-[1,2]	E-a	E-G-2B	E-G-2A3	E-G-2A1	B-[16]-B
1	1	1	1	1	1	1	1
B-[25]-[6,7]	B-[25]-[14]	B-[25]-[15]	E-e-a	E-e-a-0	E-e-0	E-e-c	E-e-b
1	1	1	2	4	1	1	1
E-G-2A	E-g-3	E-B	B-[3]	B-[4]	B-[5]	B-[6]	B-[7]
1	1	1	1	1	1	1	1
B-[8]	B-[9]	B-[10]	B-[11]	B-[12]	B-[13]	B-[14]	B-[15]
1	1	1	1	1	1	1	1
B-[17-19]	B-[20]	B-[21]	B-[22]	B-[23]	B-[24]	B-[25]	B-[26]
1	1	1	1	1	1	1	1

* Qualitative scale from 1-4: 1 indicates normal ATP metabolism (no color change compared to control, no anti-fungal activity); 2 indicates slight reduction in ATP metabolism (slight color change, slight anti-fungal activity); 3 indicates moderate inhibition of ATP metabolism (moderate color change, moderate anti-fungal activity); 4 indicates complete inhibition of ATP metabolism (complete loss of color, total inhibition of fungal growth)

The structure of the compound isolated in fraction E-e-a-0 was identified by LC/MS and

^{1}H-NMR spectrum (described in detail in section 3.4.2.4). The compound was identified

to be Methyl 1H-benzimidazol-2-ylcarbamate, commonly known as carbendazim.

Carbendazim is a synthetic compound which is a broad-spectrum fungicide, widely used

commercially for the control of mold and yeast growth in industry. The presence of

carbendazim readily explains the potent anti-fungal activity measured for fraction E-e-a-

0, as well as the slight activity of E-e-a, since the former was purified from the latter. Yet,

how did this compound arise in the sample? Carbendazim has been widely demonstrated

to act on yeast as a fungicide by inhibition of respiration and fermentation[12,13,14].
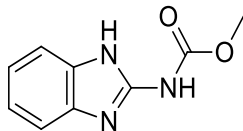
Figure 4-3. Chemical structure of carbendazim (fraction E-e-a-0)

The presence of carbendazim in the algal extracts was initially perplexing—carbendazim is not a natural product, and has not been detected in plant or algal species from natural origin. Carbendazim is a widely used synthetic product, and it was hypothesized that perhaps the presence of carbendazim was left over from proprietary treatments conducted by AL-G Technologies to optimize the growth of their algal system. As such, the researchers at AL-G Technologies were contacted and confirmed that carbendazim was employed at low concentrations to control the growth of fungi on the algal membranes, and thus a contaminant due to the system used to grow the algae biomass.

In conclusion, although anti-fungal activity was detected in fraction E-e-a-0, the compound responsible, carbendazim, was not of natural origin. Carbendazim is widely employed in industrial use for the control of fungi and molds and was employed exactly for this purpose by the technicians at AL-G Technology. Thus, the anti-fungal activity detected in *Parachlorella kessleri* can be readily explained by the addition of carbendazim to the growth media by the technicians who produced the algal biomass. While these results are less than satisfying, it represents the power of analytical chemistry and bioactivity assays to readily detect compounds of interest in extracts from algal biomass.

4.4   Lipase inhibition activity

Pancreatic triacylglycerol lipase is a key enzyme family responsible for metabolism of triacylglycerides for absorption into the blood-stream by hydrolysis of the α and α' ester bond to release free fatty acid and diacylglycerides. Pancreatic triacylglycerol lipase is secreted by the pancreas and are responsible for 50-70% of total lipid metabolism[15], and as such they are critical to the balance of lipid metabolism, and therefore of interest in the treatment of diseases such as obesity and hyperlipidemia. Inhibition of pancreatic tracylglycerol lipase is an attractive target for the development of pharmaceutical therapies for the treatment of obesity and hyperlipidemia, and in 1999, Orlistat, developed by Roche, was approved by the FDA for the treatment of obesity by inhibition of pancreatic lipase[16]. Due to the wide range of interesting fatty acid derivatives detected in *Parachlorella kessleri*, a thorough investigation of the inhibitory activity of sub-fractions on pancreatic lipase was conducted.

4.4.1   Methodology

Ethanol extracts of marine and freshwater algae were prepared and stripped of solvent. The residue was taken up in DMSO to prepare stock solutions of approximately 30 mg/mL. Serial dilutions were prepared spanning a range from 30 mg/mL to 29 µg/mL. The determination of lipase inhibition activity was conducted by treatment of Porcine pancreatic lipase (Type II, Sigma Aldrich) with 4-methylumbelliferyl butyrate, a substrate for lipase which is fluorescent after hydrolysis of the butyrate, which in competition with purified fractions, allows for determining competitive inhibition of lipase activity[17]. Porcine Lipase (Type II, Sigma Aldrich) was prepared in pH 7.0 Phosphate Buffer (Sigma

Aldrich) to a concentration of 39.2 µg/mL. 150 µL buffer, 10 µL inhibitor solution, 10 µL enzyme solution were added to each well in a polystyrene 96-well plate. One column was left empty as a blank, and another column contained 10 µL DMSO as a control to measure activity without inhibitor present. Finally, 40 µL substrate solution, containing 4.371mM 4-methyl umbelliferyl butyrate (Sigma Aldrich) was added to initiate the reaction. The total volume was 210 µL, with a final substrate concentration of 833 µM, a final enzyme concentration of 1.86 µg/mL. After 20 minutes of incubation at 37˚C, the plates were read using a fluorimetric plate-reader with excitation wavelength of 360 nm and an emission wavelength at 460 nm. Results were calculated as percentage inhibition by calculating the percentage fluorescence detected compared to wells containing no inhibitor.

4.4.2 Results and discussion

The inhibition of porcine pancreatic triacylglycerol lipase by extracts and fractions of *Parachlorella kessleri* biomass was investigated thoroughly as part of the bio-guided fractionation effort to identify relevant bio-activities in the algal biomass. There has been great interest in recent years into pancreatic lipase inhibitors as effective treatment for hyperdipidemia, as discussed in detail in the previous section. Utilizing an assay to measure the competitive inhibition of porcine pancreatic lipase, which is closely phylogenetically related to human pancreatic lipase[18], and is often used to evaluate inhibitors *in vitro*, a variety of fractions of *Parachlorella kessleri* were screened for anti-triacylglycerol lipase inhibitory activity. Compounds were screened against vehicle control and positive control *orlistat*, a well-known, commercially available pancreatic lipase inhibitor currently available over-the-counter[19].

A preliminary screen for triacylglycerol lipase inhibition was conducted on the primary fractions obtained from fractionation of *Parachlorella kessleri* biomass and compared to the activity of the raw biomass. The primary fractions screened were the hexane fractions (H), the chloroform fraction (C), the ethyl-acetate fraction (E), and the butanol fraction (B). For detailed descriptions of the preparation of these fractions, see Chapter 3. These fractions were solubilized in DMSO at a screening concentration of 100 µg/mL. Orlistat, a known inhibitor of pancreatic lipase, was used as a positive control at a screening concentration of 10 µM. The results are shown in Figure 4-4. Crude *P. kessleri* extract showed slight, although statistically significant, inhibitory activity (37%, p = 0.029), as did the ethyl acetate sub-fraction E (38%, p = 0.019); and the butanol exhibited the weakest activity that was still statistically significant from vehicle control sub-fraction B (26% inhibition, p = 0.031). As such, fractions E and B were selected for sub-fractionation to isolate and identify possible triacylglycerol lipase (TGL) inhibitors.
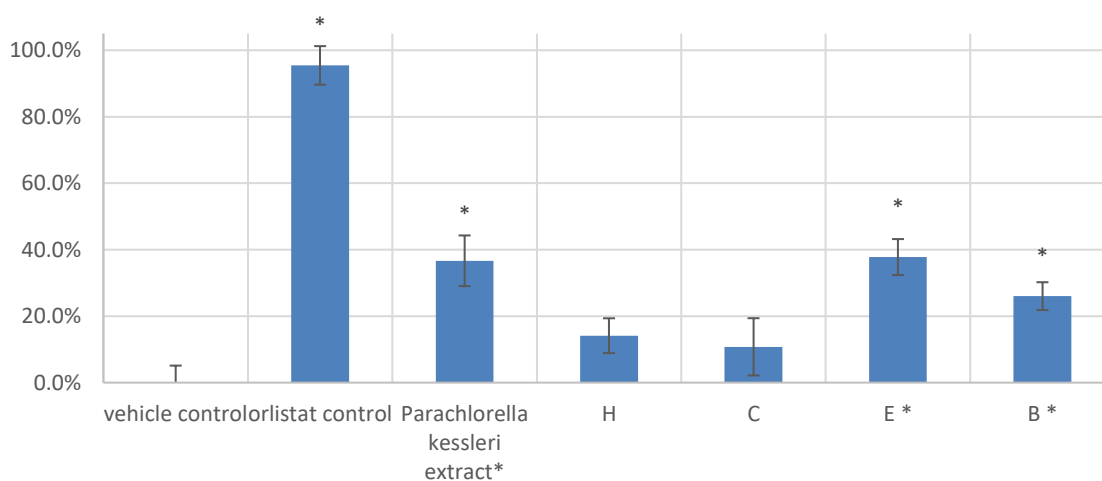
Figure 4-4. Results of porcine pancreatic lipase inhibition assay for primary hexane (H), chloroform (C), ethyl acetate (E), and n-butanol (B) sub-fractions of *Parachlorella kessleri*
* Exhibited statistically significant difference from vehicle control (student's t-test, two-tailed, p < 0.05)

The butanol fraction was sub-fractionated as described in section 3.5.1 (page 145), obtaining 21 sub-fractions (B-3 to B-25, wherein B-17 through B-19 were combined as B-17). These fractions were assayed against TGL for inhibitory activity at a concentration of 100 µg/mL; the results are shown below in Figure 4-5. Unfortunately, none of the sub-fractions exhibited statistically significant inhibitory activity, and it was hypothesized that the appearance of slight activity in the butanol sub-fraction was due to interference of UV-Vis absorbing and/or fluorescent contaminants with the assay, due to the highly complex nature of butanol fraction (B). As such, the butanol fraction was not pursued further for evaluation of lipase inhibition.
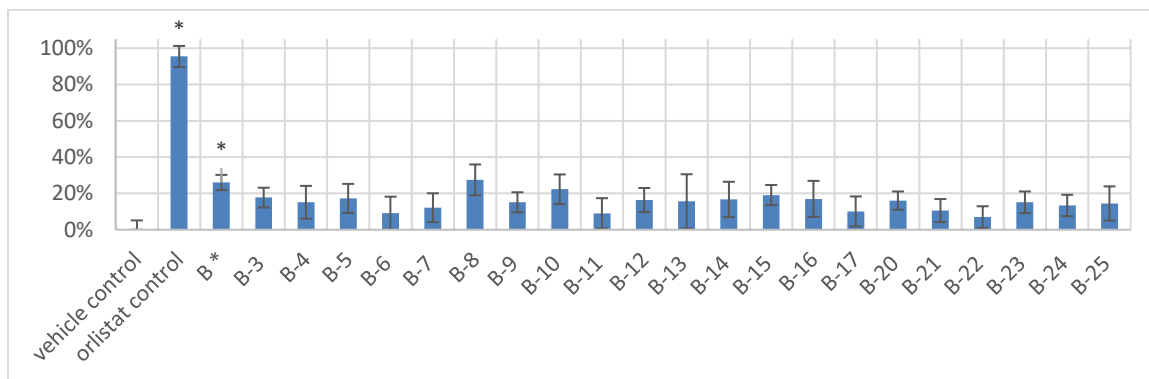
Figure 4-5. Screening of sub-fractions of butanol fraction (B) for porcine triacylglycerol pancreatic lipase inhibition at 100 µg/mL
* Exhibited statistically significant difference from vehicle control (student's t-test, two-tailed, $p < 0.05$)

Next, attention was focused on the ethyl-acetate fraction (E), which was fractionated into 7 sub-fractions (E-a through E-h), as described in section 3.4.1 (page 109). These fractions were assayed for porcine TGL inhibitory activity at a concentration of 100 µg/mL) against vehicle control and orlistat, as a positive control; results are shown in Figure 4-6.
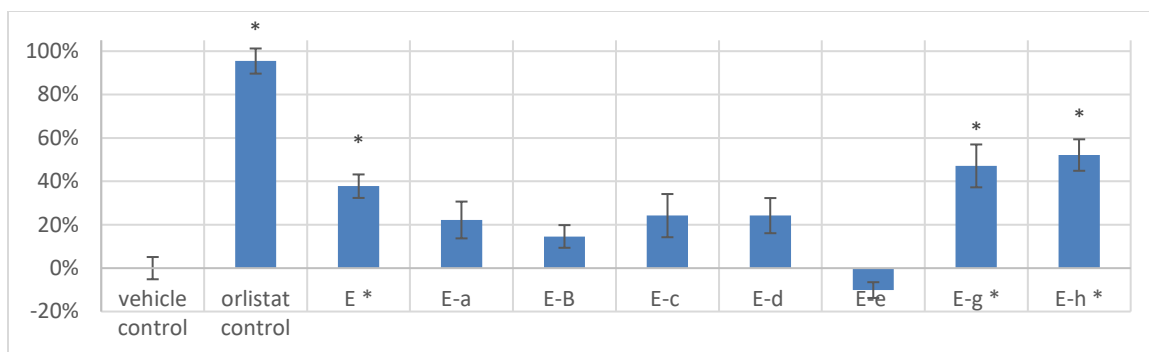
Figure 4-6. Porcine pancreatic lipase inhibition of major fractions from *Parachlorella kessleri* biomass
* Exhibited statistically significant difference from vehicle control (student's t-test, two-tailed, p < 0.05)

Two fractions exhibited significant TGL inhibition at a greater level than the parent fraction. Fraction E-g inhibited TGL at 47% (p = 0.026) and fraction E-h inhibited TGL at 52% (p = 0.014), both at a level of 100 μg/mL compared to an inhibition of 38% for the parent fraction E at a level of 100 μg/mL. Fractions E-g and E-h were selected for further separation and TGL inhibitor assay screening.
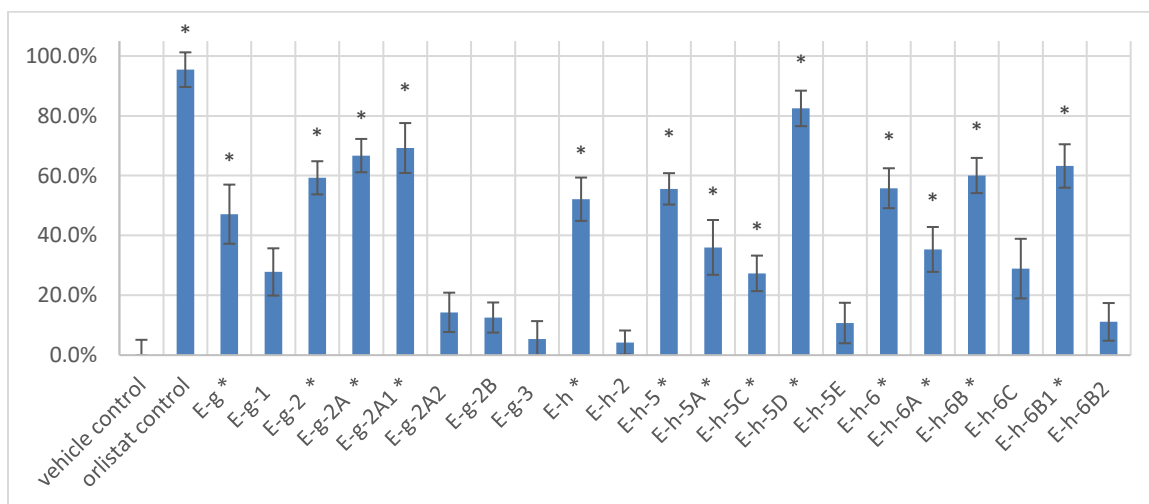
Figure 4-7. Porcine pancreatic lipase inhibition of major sub-fractions of fraction E-g and E-h
* Exhibited statistically significant difference from vehicle control (student's t-test, two-tailed, p < 0.05)

Fraction E-g was separated into E-g-1, E-g-2, and E-g-3. Screening of these sub-fractions showed reduced activity in E-g-1 (27.8 ± 7.90%, not significant compared to vehicle control, p = 0.052). Fraction E-g-2 inhibited TGL (59.3 ± 5.94%, p = 0.008) to a higher degree than its sister-fractions or its parent fraction. Fraction E-g-3 did not appreciably inhibit TGL, and so fraction E-g-2 was thus selected for further fractionation and analysis. E-g-2 was separated into two sub-fractions, E-g-2A and E-g-2B, both of which were screened for TGL inhibitory activity. Fraction E-g-2A, with 69.2 ± 5.56% (p = 0.006), retained activity, whereas E-g-2B showed a loss of inhibition (12.6 ± 5.03%, p = 0.133, not significant from vehicle control). Fraction E-g-2A was selected for further purification and screening.

Fraction E-g-2A was sub-fractionated into E-g-2A1 and E-g-2A2, both of which were screened for TGL inhibition activity at 100 ug/mL concentration against vehicle control and orlistat. Fraction E-g-2A1 exhibited strong inhibition of TGL (69.2 ± 8.34%, p = 0.009) whereas E-g-2A2 lost inhibitory activity. Results suggested E-g-2A1 contained the TGL inhibiting compound(s). Characterization of E-g-2A1 is discussed in detail in section 3.4.2.1 (page 121), and due to similarities of compounds detected in E-h and sub-fractions, E-g-2A1 will be discussed together with sub-fractions of E-h below in the text.

Fraction E-h exhibited significant activity in this assay, and as such it was further fractionated and the resultant sub-fractions were further analyzed to isolate the active compound. Fractionation of E-h yielded three major sub-fractions, E-h-2, E-h-5, and E-h-6, which were all screened against the parent fraction (Figure 4-7). Fractions E-h-5 and E-

h-6 gave the highest inhibition at 55.6 ± 5.24% (p = 0.009) and 55.8 ± 6.67% (p = 0.011) respectively. Based on similarities between E-h-6 and E-g-2 found in LC/MS analysis, fraction E-h-6 was selected first for further analysis.

Fraction E-h-6 was sub-fractionated into fractions E-h-6A, E-h-6B, and E-h-6C. The fractions were screened for TGL inhibition activity. Fraction E-h-6B exhibited the highest activity (60.1 ± 5.88%, p = 0.008), whereas fraction E-h-6A (35.3 ± 7.50%, p = 0.031) and E-h-6C (28.9 ± 9.97%, not statistically significant from vehicle control, p = 0.067) both showed reduced inhibition compared to the parent fraction E-h-6 (55.6 ± 5.24%, p = 0.009). E-h-6B was selected for further fractionation.

Fractionation of E-h-6B by preparative TLC analysis, described in detail in section 3.4.1 (page 109), yielded a major fraction E-h-6b1 which was identified as a mixture of galactolipids (section 3.4.2.1, page 121) which were also found in E-g-2A1, and a minor fraction E-h-6b2 which contained a mixture and due to its low activity, was not characterized further. These fractions were both screened for TGL inhibition activity; Fraction E-h-6B1 showed increased activity (63.2 ± 7.26%, p = 0.009), whereas fraction E-h-6B2 showed very low activity (11.1 ± 6.30%, difference not statistically significant compared to control, p = 0.192). One compound was isolable from the mixture of galactolipids in E-h-6B1 and E-h-2A1, compound E-h-6B1.a, identified as the galactolipid distearoyl-glycerol-galactoside. This compound was isolated in milligram quantities, and a dose-response curve for porcine pancreatic lipase inhibition was prepared using the isolated material, shown below in Figure 4-8. From this data, using linear approximation

as a power function (of the form y = Ae^{Bx}), an excellent fit (R^2 =0.9549) was found for the data spanning 50% inhibition, from 155.6 µM to 19.5 µM, which gave the following equation: [C]= 183.07*[% inhibition]$^{1.7205}$. Solving for concentration [C] at 50% inhibition, gives an IC$_{50}$ value of 58.93 µM.
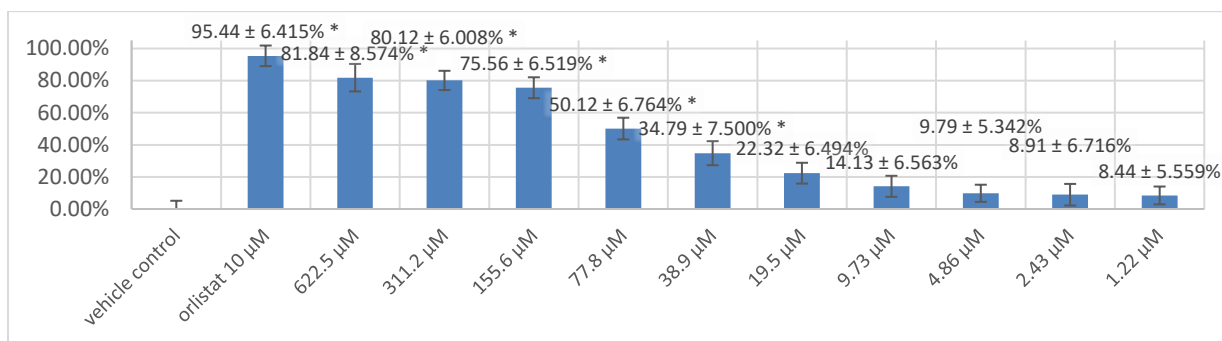
Figure 4-8. Dose response curve for porcine pancreatic lipase inhibition for galactolipid E-h-6B1.a
* Exhibited statistically significant difference from vehicle control (student's t-test, two-tailed, p < 0.05)

The inhibition detected from compound 5-hB1.a is not unexpected, as galactolipids have been shown to interact with pancreatic lipase[20], and can by hydrolyzed by pancreatic lipases to release fatty acids[21,22,23]. As such, it was hypothesized that the galactolipid 5-hB1.a was likely a competitive substrate for porcine pancreatic lipase, and as such, it was hypothesized that the inhibitory activity would decrease in a time-dependent manner. As such, the assay was repeated, and E-h-5B1 was incubated with porcine pancreatic lipase for various times (5 minutes – 24 hours) prior to initiating the assay by adding fluorescent substrate. The results are shown below in Figure 4-9. As can be seen, there was a distinctive loss of inhibitory activity with increasing incubation time, suggesting that compound 5-hB1.a was hydrolyzed as a substrate of porcine pancreatic lipase, and no

longer participated as an inhibitor. These results agree with previously reported data showing hydrolysis of diacylglyceryl-galactolipids to monoacylglyceryl-galactolipids by pancreatic lipase[13,14,15], which show a time frame of approximately 1-2 hours velocity for hydrolysis of galactolipids.

Figure 4-9. Time-based inhibition assay; 100 µM E-h-5B1.a was incubated with porcine pancreatic lipase for various times prior to running inhibition assay
* Exhibited statistically significant difference from 0-minute incubation control (student's t-test, two-tailed, $p < 0.05$)

As can be seen in Figure 4-9, there is a statistically significant reduction in the inhibition of porcine pancreatic lipase after just 15 minutes' incubation with respect to 0-minute incubation control. After 30 minutes, the inhibition has been reduced to 26.95 ± 7.765%, which is not significant compared to vehicle control. However, the inhibitory activity is significant even after 15 minutes' incubation, and as such has relevant implications for use as pancreatic lipase inhibitors, since triglyceride metabolism via pancreatic secretion of lipase enzymes occurs within the first minutes of eating[24]. Galactolipids have been postulated to interfere at the lipid-water interface of lipase, preventing binding of colipase and the closure of a hinge segment, significantly slowing hydrolysis[20], competing

with the hydrolysis of triacylglycerides. According to Chu et al., incubation of human pancreatic lipase with a mixture of galactolipids and lecithins/triacylglycerides induces a significant lag time, up to 16.52 ± 0.17 minutes into the overall time required to hydrolyze lecithins/triacylglycerides, consistent with the 15-minute mark where inhibition of lipase by 5-h-6b1.a started to significantly decrease. Decrease of the lipolysis of lipids in the first stages of digestion prior to transfer of digested food to the ileum promotes secretion of hormones which promote a feeling of satiety—this "feeling full" reduces appetite and has positive indications for the treatment of hyperlipidemia[25]. Chu et al. postulate that the interference of lipid metabolism on pancreatic lipase is a surface-based phenomenon, arising from the interference of galactolipids with the absorption of lipids into the protein matrix, and further interfere with surface phenomena induced from bile acids in digestion which aid in lipid metabolism[20]. Pancreatic lipase inhibition by constituents of *Parachlorella kessleri* has not been previously reported.

The final fraction analyzed for sub-fractionation and bioactivity screening was E-h-5D, which showed the highest activity ($82.5 \pm 5.39\%$, p = 0.004) of all fractions screened. E-h-5D was relatively pure, and was repeatedly purified by prep-TLC, as described in section 3.4.1 (page 109), to obtain E-h-5D1, which was highly pure by TLC, but contained a few minor contaminants by HPLC. The dose response curve for E-h-5D1 was obtained. As can be easily seen in Figure 4-10, this compound exhibited strong inhibition of porcine pancreatic lipase even into sub-micromolar concentrations. This data was used to estimate the IC_{50} for this compound by linear approximation of the points flanking 50% inhibition in Figure 4-10, i.e. the points spanning 1.3 µM (60.12%) to 162 nM (10.98%).

Construction of exponential function to fit this data based on y=Ae^Bx was accomplished using Microsoft Excel, giving the following equation: $[C]= 〖 0.1319e 〗 \char`\^(3.8572*[\% \text{ inhibition}])$. Solving for concentration $[C]$ at 50% inhibition gives an IC_{50} value of 751 nM.
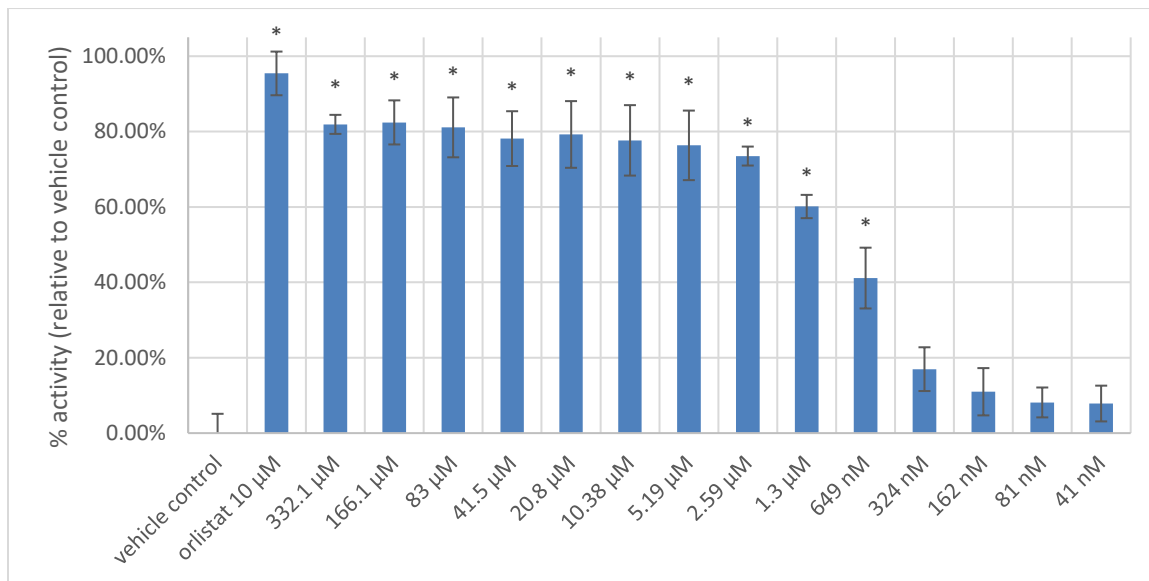
Figure 4-10. Dose response curve of the compound E-h-5D1, identified as 19'-decanoyloxy-fucoxanthin in section 3.4.2.2
* Exhibited statistically significant difference from vehicle control (student's t-test, two-tailed, $p < 0.05$)

This compound was further studied to determine whether the ester moiety in E-h-5D1 is hydrolyzed by the enzyme during incubation, and so an experiment with extended incubation with pancreatic lipase prior to assaying inhibitory activity was conducted, as for E-h-6B1.a described in the above text. E-h-5D1 was incubated at 10 µM concentration for various times (0 minutes to 24 hours) before initiation of the assay; the results are shown in Figure 4-11. Results showed that there was no significant change in inhibition due to incubation with pancreatic lipase prior to inhibition assay, indicating that E-h-5D1 is not a substrate for porcine pancreatic lipase.

Xanthophylls have been previously described as inhibitors for pancreatic lipase derived from rats. Mastumoto et al. have shown that fucoxanthin and its metabolite fucoxanthinol (both structural relatives of E-h-5D1) inhibit lipolysis activity of rat pancreatic lipase[26] *in vitro* and *in vivo*. The authors showed that oral treatment of rats by gavage with fucoxanthin or fucoxanthinol significantly reduced triacylglyceride absorption into rat blood serum. The IC_{50} values of fucoxanthin and fucoxanthinol were reported to be 660 nM and 764 nM, respectively—the IC_{50} value determined for fucoxanthin derivative 19'-decanoyloxy-fucoxanthin (structure shown in Figure 3-15 on page 138) was 751 nM, consistent with results described by Matsumoto et al.[27]
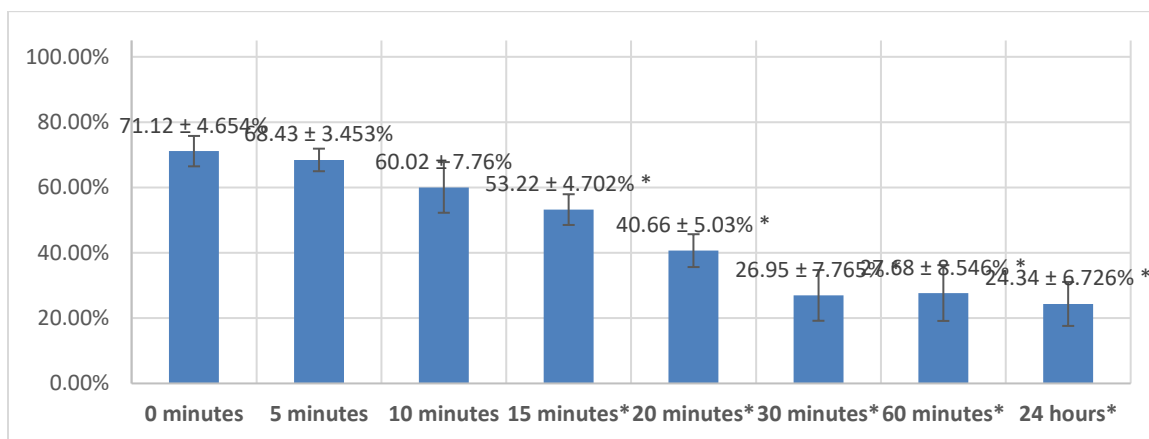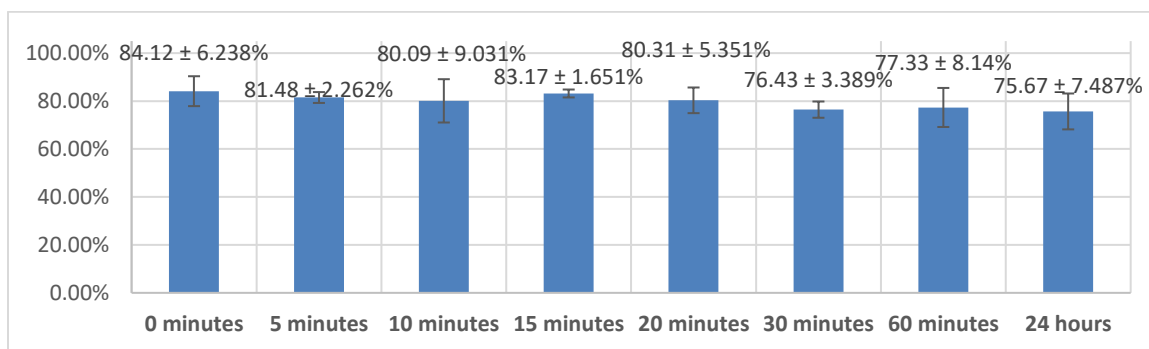

Figure 4-11. Time-based inhibition assay; 10 µM E-h-5D1 was incubated with porcine pancreatic lipase for various times prior to running inhibition assay
* No results exhibited statistically significant difference from 0-minute control (student's t-test, two-tailed, $p < 0.05$)

While the IC_{50} value of this compound suggested it is a rather potent inhibitor of porcine pancreatic lipase, due to the low levels of E-h-5D1 detected in *P. kessleri*, it would not be feasible to obtain the levels necessary for inhibition by ingestion of algal biomass alone, rather this compound would need to be supplemented after extraction. The IC50 value (751 nM) was about >100-fold greater than reported for orlistat (6.8 nM). However,

orlistat has significant side effects, such as stomach pain and diarrhea, and investigation of milder alternatives remains an attractive clinical option[28].

4.5 α-Glucosidase inhibition activity

The metabolism of polysaccharides is a critical step in extracting energy from foodsources, and there are many highly specialized enzymes suited to this purpose. α-Glucosidase is the first enzyme to act in the sequence of polysaccharide metabolism, as it is present in saliva, and immediately begins acting on starches during mastication (chewing)[29]; α-Glucosidase acts on starches and disaccharides by breaking α(1->4) bonds, releasing glucose[29]. Because of its role in releasing glucose for absorption into the blood stream, α-glucosidase has become a target of interest in pharmaceutical development for the treatment of diabetes mellitus, as inhibition of α-glucosidase can be utilized to control blood sugar by reducing and delaying absorption of starches[30]. Acarbose, a competitive, reversible inhibitor of α-glucosidase, is currently marketed for the treatment of diabetes in the US and EU[31]. Fractions of *Parachlorella kessleri* were screened for inhibitory activity against α-glucosidase.

4.5.1 Methodology

The α-glucosidase inhibitory activity was assessed by the standard method, with slight modifications[32]. Briefly, a volume of 60 µL of fraction to be screened for inhibition dissolved in DMSO at a concentration of 0.1 mg/mL and 1 mg/mL depending on the activity level of extract in the initial screen. 50 µL of 0.1 M phosphate buffer (pH 6.9) containing α-glucosidase (Sigma-Aldrich, St. Louis, MO) solution at a concentration of 0.2

Units/ml was incubated in 96-well plates at 37˚C for 20 minutes. After pre-incubation, 50 µL of 5 mM p-nitrophenyl-α-D-glucopyranoside (PNPG) solution in 0.1 M phosphate buffer (pH 6.9) was added to each well and incubated at 37˚C for another 20 min. Then the reaction was stopped by adding 160 µL of 0.2 M NaCO$_3$ into each well, and absorbance readings (A) were recorded at 405 nm by micro-plate reader and compared to a vehicle control, in which the only difference is the addition of 60 µL of DMSO in place of the extract in the well. To establish the background absorbance for samples which absorbed in the 405 nm range, buffer was added instead of the enzyme solution and absorbance recorded. The α-glucosidase inhibitory activity was expressed as inhibition % and was calculated as follows:

$$\%_{inhibition} = 100\% - \frac{Abs_{inhibitor} - Abs_{blank}}{Abs_{vehicle}}$$

4.5.2 Results and Discussion

Using an enzymatic *in vitro* assay, primary fractions obtained from *Parachlorella kessleri* fractionation were evaluated for α-glucosidase inhibitory activity. Primary fractions were tested at a screening concentration of 750 µg/mL, which was 15% of the competitive

substrate   concentration.   The   results   are   shown   in
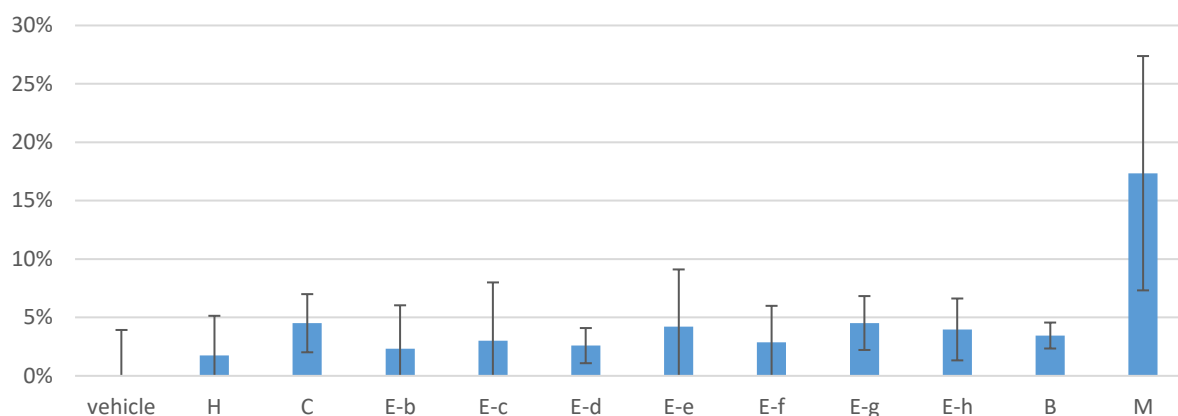
Figure 4-12. The only primary fraction that exhibited α-glucosidase inhibitory activity was the methanol fraction M, demonstrating slight activity with an inhibition of 17.35 ± 10.030% at a concentration of 750 μg/mL. While this result differed statistically significantly from the vehicle control (p = 0.049), the standard deviation of the result was much higher than in other fractions. It was hypothesized that since β4 was the most polar fraction, from which was obtained a starchy, crumbly biomass that was macroscopically similar to polysaccharide-rich biomass, it is likely that β4 contained a high concentration of α-glucosidase active polysaccharides, which would account for its apparent activity.
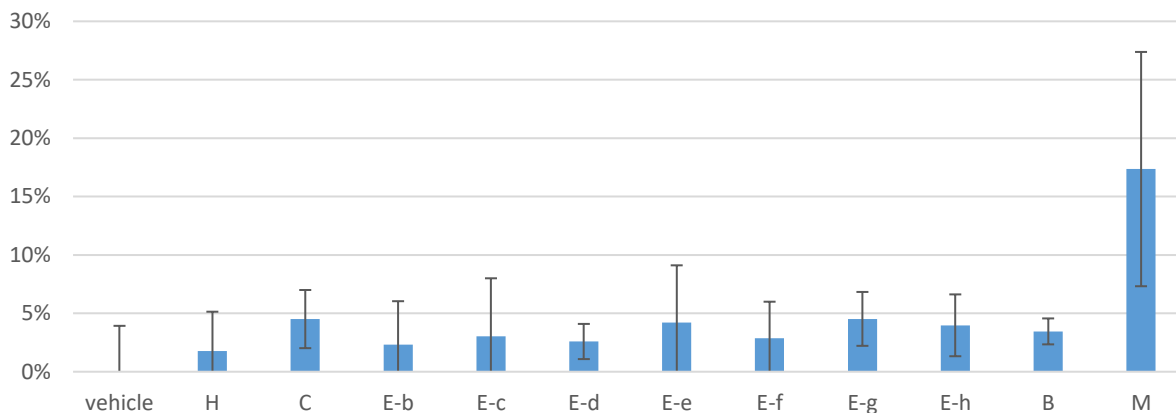
Figure 4-12. Results of screen of primary fractions of *Parachlorella kessleri* for α-glucosidase inhibitory activity
*Exhibited statistically significant difference from vehicle control

In order to test this hypothesis, Fraction M was incubated with α-glucosidase for increasing times prior to treatment with competitive substrate for the inhibition assay. If Fraction M is a substrate for α-glucosidase and hydrolyzes to inactive monosaccharides, a time-dependent response should be detected as Fraction M is consumed by α-glucosidase as time continues. If Fraction M contains *bona fide* inhibitors of α-glucosidase, the inhibition should not decrease due to pre-incubation. The results of this experiment are shown in Figure 4-13.
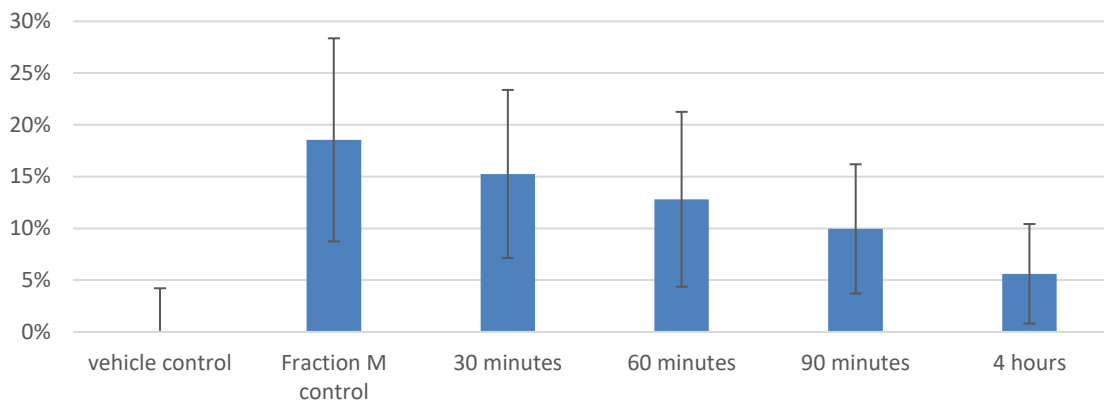
Figure 4-13. Results of screen of Fraction M fraction for α-glucosidase inhibition after pre-incubation for increasing times; Results show that Fraction M is a substrate for α-glucosidase, not an inhibitor.
*Exhibited statistically significant difference from vehicle control

As expected, Fraction M exhibited a time-dependent inhibitory response for α-glucosidase inhibitory activity, suggesting that Fraction M contains substrates for α-glucosidase, not inhibitors. True competitive inhibitors of Fraction M should not demonstrate time-dependent inhibition based on pre-incubation with enzyme, on the contrary, inhibition should achieve consistent dose-dependent equilibrium regardless of amount of time interacting with enzyme without the presence of metabolism or excretion. These results suggest that Fraction M is hydrolyzed by α-glucosidase and thus contains glucose-bearing polysaccharides which act as a substrate for this enzyme. Pre-incubation of Fraction M with α-glucosidase for as little as 60 minutes reduced inhibitory activity which differed only slightly significantly with respect to vehicle control ($p = 0.07$). It was thus concluded that while the methanol fraction Fraction M contained polysaccharides which served as substrates for α-glucosidase, there was no evidence to support inhibitory activity by primary fractions of *Parachlorella kessleri*.

4.6   References

[1] MacDonald-Wicks, L. K., Wood, L. G., & Garg, M. L. (2006). Methodology for the determination of biological antioxidant capacity in vitro: a review. *Journal of the Science of Food and Agriculture*, *86*(13), 2046-2056.

[2] Huang, D., Ou, B., & Prior, R. L. (2005). The chemistry behind antioxidant capacity assays. *Journal of agricultural and food chemistry*, *53*(6), 1841-1856.

[3] Karadag, A., Ozcelik, B., & Saner, S. (2009). Review of methods to determine antioxidant capacities. *Food analytical methods*, *2*(1), 41-60.

[4] Magalhães, L. M., Segundo, M. A., Reis, S., & Lima, J. L. (2008). Methodological aspects about in vitro evaluation of antioxidant properties. *Analytica chimica acta*, *613*(1), 1-19.

[5] Fu, L., Xu, B. T., Xu, X. R., Gan, R. Y., Zhang, Y., Xia, E. Q., & Li, H. B. (2011). Antioxidant capacities and total phenolic contents of 62 fruits. *Food Chemistry*, 129(2), 345-350.

[6] Li, H. B., Cheng, K. W., Wong, C. C., Fan, K. W., Chen, F., & Jiang, Y. (2007). Evaluation of antioxidant capacity and total phenolic content of different fractions of selected microalgae. *Food Chemistry*, 102(3), 771-776.

[7] McLeod, J. W., & Govenlock, P. (1921). THE PRODUCTION OF BACTERICIDINS BY MICRO-ORGANISMS. *The Lancet*, *197*(5096), 900-903.

[8] Wiegand, I., Hilpert, K., & Hancock, R. E. (2008). Agar and broth dilution methods to determine the minimal inhibitory concentration (MIC) of antimicrobial substances. *Nature protocols*, *3*(2), 163-175.

[9] Zgoda, J. R., & Porter, J. R. (2001). A convenient microdilution method for screening natural products against bacteria and fungi. *Pharmaceutical Biology*, *39*(3), 221-225.

[10] Levitz, S. M., & Diamond, R. D. (1985). A rapid colorimetric assay of fungal viability with the tetrazolium salt MTT. *Journal of Infectious Diseases*, *152*(5), 938-945.

[11] Berridge MV, Herst PM , and Tan AS. Tetrazolium dyes as tools in cell biology: new insights into their cellular reduction. Biotechnology Annual Review, 11: 127-152 (2005).

[12] Fokkema, N. J., Dik, A. J., & Daamen, R. A. (1987). Use of carbendazim and carbendazim-resistant yeasts to create different yeast densities on wheat leaves for field studies on biological control. *Netherlands Journal of Plant Pathology*, *93*(6), 273-283.

[13] Chiba, M., Bown, A. W., & Danic, D. (1987). Inhibition of yeast respiration and fermentation by benomyl, carbendazim, isocyanates, and other fungicidal chemicals. *Canadian journal of microbiology*, *33*(2), 157-161.

[14] Dik, A. J. (1991). Interactions among fungicides, pathogens, yeasts, and nutrients in the phyllosphere. In *Microbial Ecology of Leaves* (pp. 412-429). Springer New York.

[15] Birari, R. B., & Bhutani, K. K. (2007). Pancreatic lipase inhibitors from natural sources: unexplored potential. *Drug discovery today*, *12*(19), 879-889.

[16] Cooke, D., & Bloom, S. (2007). The obesity pipeline: current strategies in the development of anti-obesity drugs.

[17] Roberts, I. M. (1985). Hydrolysis of 4-methylumbelliferyl butyrate: a convenient and sensitive fluorescent assay for lipase activity. *Lipids*, *20*(4), 243-247.

[18] Hide, W. A., Chan, L., & Li, W. H. (1992). Structure and evolution of the lipase superfamily. *Journal of lipid research*, *33*(2), 167-178.

[19] Lunagariya, N. A., Patel, N. K., Jagtap, S. C., & Bhutani, K. K. (2014). Inhibitors of pancreatic lipase: state of the art and clinical perspectives. *EXCLI journal*, *13*, 897.

[20] Chu, B. S., Rich, G. T., Ridout, M. J., Faulks, R. M., Wickham, M. S., & Wilde, P. J. (2009). Modulating pancreatic lipase activity with galactolipids: effects of emulsion interfacial composition. *Langmuir*, *25*(16), 9352-9360.

[21] Lowe, M. E. (2002). The triglyceride lipases of the pancreas. *Journal of lipid research*, *43*(12), 2007-2016.

[22] Sias, B., Ferrato, F., Grandval, P., Lafont, D., Boullanger, P., De Caro, A., ... & Carrière, F. (2004). Human pancreatic lipase-related protein 2 is a galactolipase. *Biochemistry*, *43*(31), 10138-10148.

[23] Whitcomb, D. C., & Lowe, M. E. (2007). Human pancreatic digestive enzymes. *Digestive diseases and sciences*, *52*(1), 1-17.

[24] Chu, B. S., Rich, G. T., Ridout, M. J., Faulks, R. M., Wickham, M. S., & Wilde, P. J. (2009). Modulating pancreatic lipase activity with galactolipids: effects of emulsion interfacial composition. *Langmuir*, *25*(16), 9352-9360.

[25] Karhunen, L. J., Juvonen, K. R., Huotari, A., Purhonen, A. K., & Herzig, K. H. (2008). Effect of protein, fat, carbohydrate and fibre on gastrointestinal peptide release in humans. *Regulatory peptides*, *149*(1), 70-78.

[26] Matsumoto, M., Hosokawa, M., Matsukawa, N., Hagio, M., Shinoki, A., Nishimukai, M., ... & Hara, H. (2010). Suppressive effects of the marine carotenoids, fucoxanthin and fucoxanthinol on triglyceride absorption in lymph duct-cannulated rats. *European journal of nutrition*, *49*(4), 243-249. Found in: reference (19) cited above

[27] Matsumoto, M., Hosokawa, M., Matsukawa, N., Hagio, M., Shinoki, A., Nishimukai, M., ... & Hara, H. (2010). Suppressive effects of the marine carotenoids, fucoxanthin and fucoxanthinol on triglyceride absorption in lymph duct-cannulated rats. *European journal of nutrition*, *49*(4), 243-249. Found in: reference (19) cited above

[28] Barbier, P., Hadvary, P., & Lengsfeld, H. (2004). *U.S. Patent No. 6,756,364*. Washington, DC: U.S. Patent and Trademark Office.

[29] Van de Laar, F. A., Lucassen, P. L., Akkermans, R. P., Van de Lisdonk, E. H., Rutten, G. E., & Van Weel, C. (2005). Alpha-glucosidase inhibitors for type 2 diabetes mellitus. *The Cochrane Library*.

[30] He, Lebovitz (1998). Alpha-glucosidase inhibitors as agents in the treatment of diabetes. *Diabetes review*, *6*, 132-145.

Martin, A. E., & Montgomery, P. A. (1996). Acarbose: an alpha-glucosidase inhibitor. *American journal of health-system pharmacy*, *53*(19), 2277-2290.

[31] Martin, A. E., & Montgomery, P. A. (1996). Acarbose: an alpha-glucosidase inhibitor. *American journal of health-system pharmacy*, *53*(19), 2277-2290.

[32] Kaskoos, R. A. (2013). In-vitro α-glucosidase inhibition and antioxidant activity of methanolic extract of Centaurea calcitrapa. *Iraq. American Journal of Essential Oils and Natural Products*, 1(1), 122-125.

Chapter 5   Anti-inflammatory activity

5.1   Endocannabinoid reuptake inhibition

Named after the first known ligand for the receptor, cannabinoid receptors have become an expanding area of interest since they were first reported[1]. The cannabinoid receptors CB1 and CB2 are activated by the psychoactive constituent of cannabis, tetrahydrocannabinol (THC), to illicit a number of effects including the suppression of pain and inflammatory[2]. The endogenous ligands for these receptors, anandamide and 2-arachidonyl-glycerol, known as endocannabinoids, play a key role in cellular signaling and in the regulation of inflammatory processes. Anandamide is hydrolyzed and deactivated by fatty acid amide hydrolase (FAAH)[2], whereas 2-arachidonoyl-glycerol is hydrolyzed by mono-acyl glycerol lipase (MAGL)[3]. Thus inhibition of FAAH and MAGL is a potential strategy for the modulation of inflammatory effects.

5.1.1   Methodology

5.1.1.1   Fatty Acid Amide Hydrolase (FAAH) inhibition

In order to quantify the inhibitory effect that algae extracts and fractions had on endocannabinoid reuptake enzyme Fatty Acid Amide Hydrolase (FAAH), a commercially available kit was obtained from Cayman Chemical (Ann Arbor, MI).

To prepare the assay buffer, 3 mL concentrated assay buffer (Cayman Chem, cat #700301) was diluted to 30.0 mL with HPLC-grade water. The final concentration was 125 mM Tris-HCl, pH 9.0, containing 1 mM EDTA. The enzyme solution was prepared by dilution of 120

μL human recombinant FAAH (Cayman Chem, cat #700302) with freshly prepared assay buffer. A positive control solution was prepared using JZL-195, a known inhibitor of FAAH. JZL-195 (Cayman Chem, cat. #700307) was dissolved in 1.00 mL of DMSO to produce a 20 μM solution. The FAAH substrate (Cayman Chem, cat. #700303) was 400 μM 7-amino-4-methyl-coumaryl-arachidonamide (AMC-AA) was used as provided. AMC-AA produces fluorescence upon hydrolysis by FAAH.

The assay was performed in a 96-well plate. All wells were prepared in triplicate. Vehicle control wells were prepared by addition of 170 μL assay buffer, 10 μL FAAH enzyme solution, 10 μL AMC-AA substrate, and 10 μL DMSO (vehicle). Background wells were prepared by adding 180 μL assay buffer to 10 μL DMSO, 10 μL AMC-AA substrate, with 10 μL extract/fraction. Inhibitor wells were prepared by adding 170 μL assay buffer, 10 μL FAAH solution, 10 μL AMC-AA substrate, and 10 μL of extract/fraction to each well. Finally, positive control wells were prepared by adding 170 μL assay buffer, 10 μL FAAH solution, 10 μL AMC-AA substrate, and 10 μL JZL-195 solution. The plates were covered and incubated for 30 minutes at 37˚C. The well plate was read at 350 nm excitation wavelength, 460 nm emission wavelength. Results were reported as percent inhibition relative to vehicle control by the following equation: $100\% - \frac{Em - Em_{veh}}{Em_{veh}}$ where Em is the emission of the sample, Em_{veh} is the emission of the vehicle control. Blanks were subtracted from samples which absorbed at 350-460 nm.

5.1.1.2 MAGL inhibition

To evaluate the inhibition of mono-acyl glycerol lipase (MAGL) by extracts/fractions of *Parachlorella kessleri*, an enzymatic *in vitro* assay was performed. Commercially available, human-recombinant MAGL was obtained (Cayman Chem. Cat #705194) and stored at -80°C until use. Working enzyme solution was prepared by diluting 30 µL enzyme solution with 570 µL assay buffer (10 mM Tris-HCl, pH 7.2, containing 1 mM EDTA in HPLC grade water). 4-nitrophenyl acetate was selected as the substrate, prepared to a 4.25 mM ethanolic solution. JZL-195, a known inhibitor of MAGL was selected for use as a positive control (this same inhibitor was used in section 5.1.1.1), and was prepared by dilution to 80 µM in DMSO. The assay was performed in a 96-well plate, each well was performed in triplicate. For the vehicle control wells, designated as 0% inhibition, 150 µL assay buffer (10 mM Tris-HCl, pH 7.2, containing 1 mM EDTA in HPLC grade water), 10 µL MAGL solution, and 10 µL DMSO. For the positive control well, 150 µL assay buffer (10 mM Tris-HCl, pH 7.2, containing 1 mM EDTA in HPLC grade water), 10 µL MAGL solution, and 10 µL JZL-195 solution (4.25 mM in DMSO) was added. For the background control well, 150 µL buffer (10 mM Tris-HCl, pH 7.2, containing 1 mM EDTA in HPLC grade water), 10 µL MAGL solution, and 10 µL DMSO was added. To initiate the reaction, 10 µL nitrophenyl acetate solution (4.25 mM) was added to each well, except for the background control wells. The final concentration of nitrophenyl acetate in each well was 236 µM, which has a K_m of 500 µM. The plate was carefully shaken to mix, and the plate was incubated at room temperature for 10 minutes. The plate was read at 410 nm. Results were reported as percent inhibition relative to vehicle control by the following equation: $100\% -$

$\frac{Abs - Abs_{veh}}{Abs_{veh}}$ where *Abs* is the absorbance at 410 nm of the unknown, and Abs_{veh} is the

absorbance at 410 nm of the vehicle control.

5.1.2   Results and Discussion

5.1.2.1   Fatty Acid Amide Hydrolase (FAAH) inhibition

To thoroughly interrogate the mechanism of anti-inflammatory activity in the algal

biomass, it was necessary to investigate whether the endocannabinoid pathway was

involved.   Fatty acid amide hydrolase (FAAH) is the key enzyme responsible for the

breakdown of anandamide, one of the two chief endocannabinoids in the human body[4].

Excess concentrations of endocannabinoids activate the cannabinoid receptors in the

central nervous system, promoting anti-inflammatory effects.   The assay performed

allowed for the evaluation of inhibition of FAAH by evaluating the total enzyme activity

upon treatment with extracts/fractions derived from algal biomass compared to enzyme

activity under normal conditions. Reduction in enzyme activity while in competition

demonstrates competitive inhibitor activity.

The percentage inhibition for the algal fractions evaluated using this assay is shown in

Figure 5-1. The extracts demonstrated little to no inhibition of FAAH in this assay. With

the exception of the known inhibitor JZL-195, there were no results that were statistically

significantly different ($p<0.05$) with respect to vehicle control. From these results, there

is clearly no evidence that algal extracts act on FAAH in order to induce anti-inflammatory

effect. Concentrated fractions of *Parachlorella kessleri* demonstrated insignificant or

negligible activity, and as such it is unlikely that compounds derived from *Parachlorella*

kessleri would provide use as modulators of FAAH for the control of inflammation.
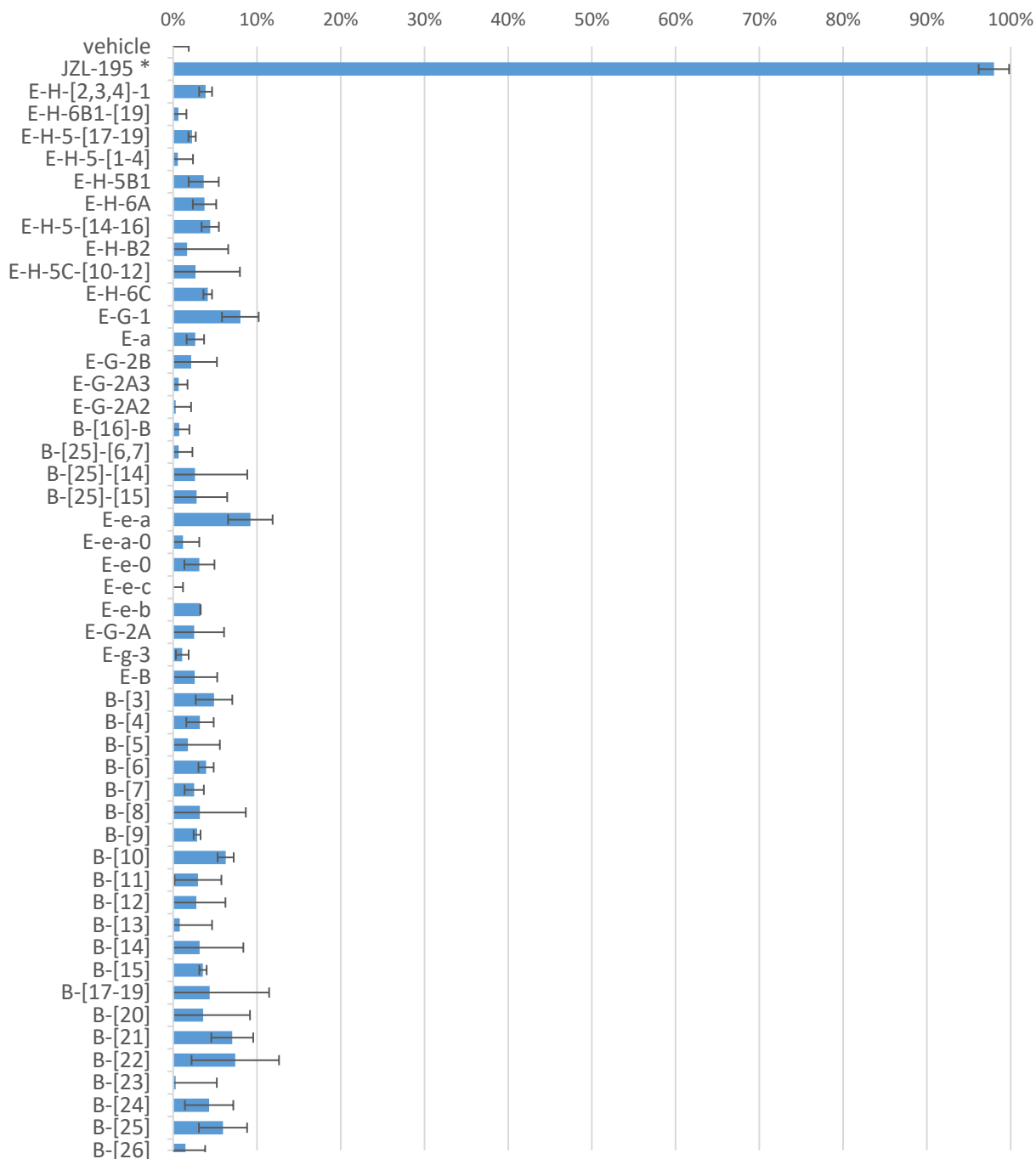
Figure 5-1. Percent inhibition of Fatty Acid Amide Hydrolase by sub-fractions of *Parachlorella kessleri*

* results differed significantly from vehicle control (p < 0.05).

5.1.2.2   Mono-acyl glycerol lipase (MAGL) inhibition

Possible anti-inflammatory activity in *Parachlorella kessleri* biomass, was continued to be investigated relative to whether the endocannabinoid pathway was involved, but this time, relative the involvement of MAGL. Mono-acyl glycerol lipase (MAGL) is responsible for the hydrolysis of 2-arachidonoyl-glycerol, and the second of the two chief endocannabinoids in the human body. Excess concentrations of endocannabinoids activate the cannabinoid receptors in the central nervous system, promoting anti-inflammatory effects, and thus inhibition of MAGL attenuates inflammatory symptoms[5].

The assay performed allowed for the evaluation of inhibition of MAGL by evaluating the total enzyme activity upon treatment with extracts/fractions derived from algal biomass compared to enzyme activity under normal conditions. Reduction in enzyme activity while in competition with extracts demonstrates inhibitor activity. The assay was performed using the Cayman Chemical MAGL inhibitor screening kit (Cayman Biochem, Ann Arbor, MI; p/n 705192) according to the protocol provided in the kit.

The percentage inhibition for the algal fractions evaluated using this assay is shown in Figure 5-2. Here again, the extracts demonstrated little to no inhibition of MAGL in this assay. Except for five fractions and the known inhibitor JZL-195, there were no fractions demonstrating inhibition that differed statistically significantly ($p < 0.05$) in comparison to vehicle control. Of the fractions that indicated statistical significance with respect to vehicle control, they all demonstrated inhibition of less than 10% at concentrations exceeding 1 mg/mL, and as such, these fractions were deemed inactive.

From these results, there is clearly no evidence that algal extracts act on MAGL in order to induce anti-inflammatory effect. Concentrated fractions of *Parachlorella kessleri* demonstrated insignificant or negligible activity, and as such it is unlikely that compounds derived from *Parachlorella kessleri* would provide use as modulators of MAGL for the control of inflammation.
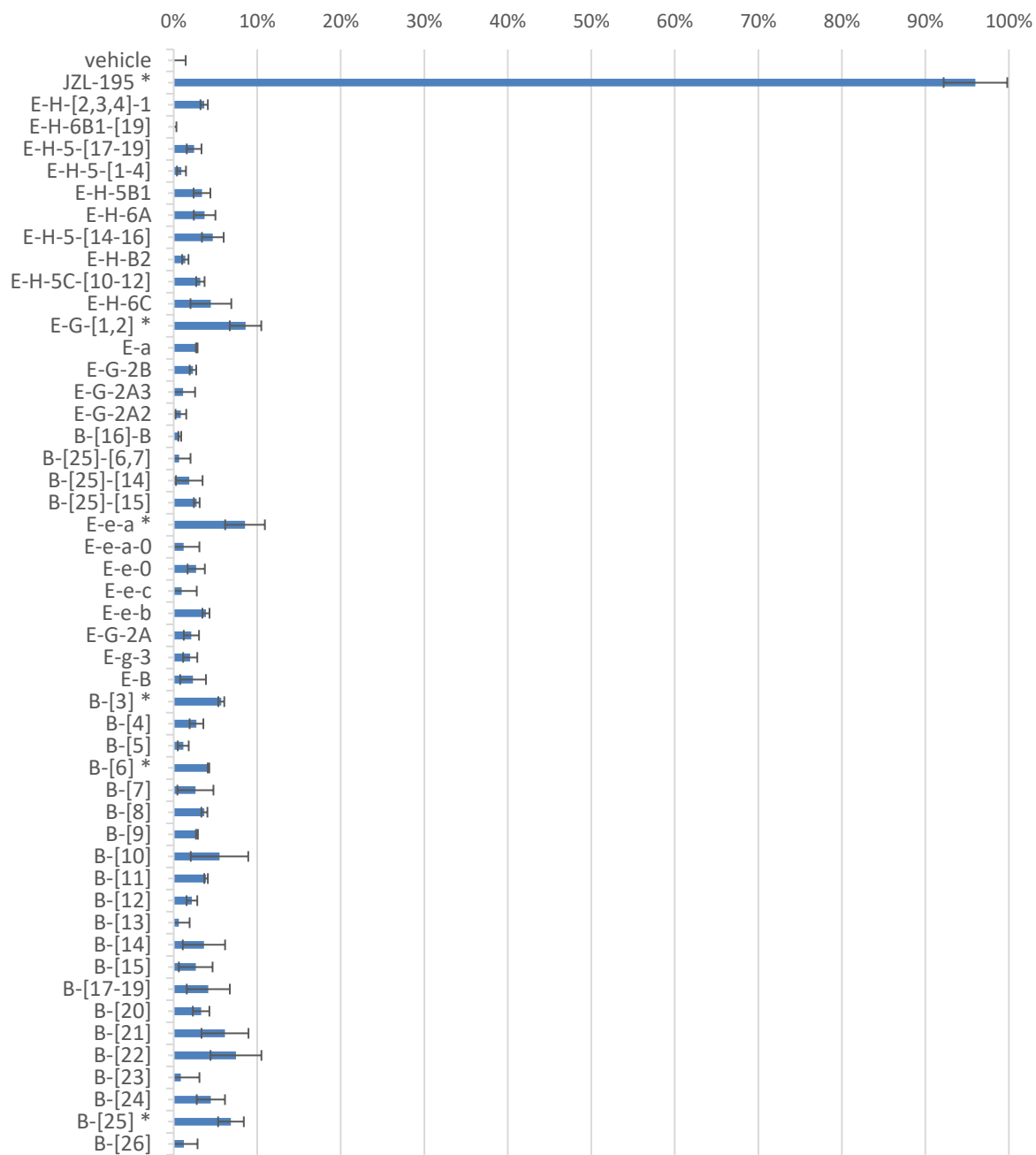
Figure 5-2. Results of screen of *Parachlorella kessleri* fractions for MAGL inhibition

* results differed significantly from vehicle control ($p < 0.05$).

5.2   Phospholipase A2 inhibition

Phospholipase A2 is a family of proteins responsible for catalyzing the hydrolysis of phospholipids at the sn2 position of glycerol to give a free fatty acid and lysophospholipid. In general, human phospholipase A2 (PLA2) takes two forms, the extracellular secreted PLA2 (sPLA2) or cytosolic PLA2 (cPLA2). sPLA2 is secreted by the pancreas to aid with digestion of dietary phospholipids in animals, and is the major component of many venoms including bees and snakes[6]. The role of sPLA2 in the promotion of inflammation through the arachidonic acid pathway involves catalyzing the release of arachidonic acid from the phospholipid. Arachidonic acid is subsequently cyclized via cyclooxygenase-2 to yield prostaglandins (see section 1.3.3 for a thorough review of the biochemistry). sPLA2 is thought to contribute to many inflammatory diseases such as coronary artery disease, atherosclerosis [7] . Additionally, increased sPLA2 activity has been observed in the cerebrospinal fluid of patients with Alzheimer's disease and multiple sclerosis. As such, sPLA2 is an attractive target for the mitigation of symptoms of inflammation.

5.2.1   Methodology

The measurement of sPLA2 activity was accomplished by developing an assay which was based on a modification of a commercially available assay to assess intrinsic sPLA2 activity. Cayman Chemical supplies an assay to detect sPLA2 activity which makes use of a thio-ester phospholipid derivative, diheptanoly-thio-phosphocholine (Cayman Chemical cat #765014). This compound can be readily lysed by sPLA2, yielding thioglycerate ion which goes on to react with dithionitrobenzoate (DTNB) yielding the yellow colored thionitrobenzoate ion which can be detected by UV-Vis spectroscopy (see Figure 5-3)[8].

This detection system provides a convenient and effective tool for the evaluation of sPLA2 inhibition by way of competition for the binding site. Competition for the binding site by inhibitors will reduce the concentration of thionitrobenzoate formed over the course of incubation in the presence of an enzyme, and this reduction is easily detected by UV-Vis spectroscopy.
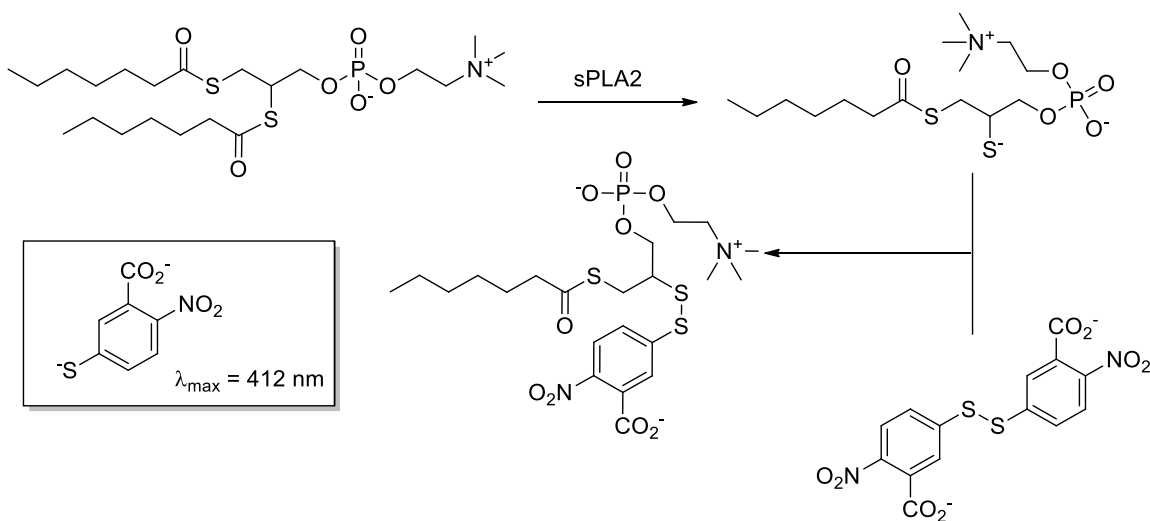
Figure 5-3. System of detection of sPLA2 activity utilized for inhibition assay

Human recombinant sPLA2 (Type V) was obtained from Cayman Chemical (Ann Arbor, MI). This isoform is responsible for arachidonic acid release and prostaglandin production in macrophages[9]. Assay buffer was prepared containing 25 mM Tris-HCl, pH 7.5, with 10 mM $CaCl_2$, 100 mM KCl, and 0.3 mM Triton X-100. 10 μL sPLA2 was diluted with 990 μL assay buffer. DTNB (Cayman Chem, Cat # 765012) was diluted with 1.0 mL HPLC grade water with 0.4M Tris-HCl, pH 8.0 to yield 10 mM DTNB solution. 12 mL assay buffer was

used to reconstitute Diheptanoyl Thio-PC (Cayman Chem, #765014) to achieve a final concentration of 1.66 mM.

Assay reagents were added to a clear polypropylene 96-well-plate. To blank wells was added 10 µL DTNB, 10 µL assay buffer and 5 µL DMSO. To vehicle control wells was added 10 µL DTNB, 10 µL sPLA2 enzyme solution, and 5 µL DMSO. Screening for inhibitors was accomplished by dissolving algal extracts to a concentration of 4.5 mg/mL. Purified fractions were prepared at a concentration of 1126 µg/mL in DMSO. Inhibitor screening wells were prepared by adding 10 µL DTNB, 10 µL sPLA2 enzyme solution, and 5 µL inhibitor solutions in DMSO. The reaction was initiated by adding 200 µL Diheptanoyl Thio-PC to each well, giving a final concentration of 1.475 mM. The screening concentration of 100 µg/mL for crude fractions and 25 µg/mL for purified fractions. The plates were incubated for 10 minutes at room temperature and the absorbance was measured at 412 nm using a 96-well-plate reader.

5.2.2 Results and Discussion

There has been great interest lately in sPLA2 inhibitors as effective treatment for cardiovascular inflammation and disease [10], and for the treatment of hypercholesterolemia[11]. Utilizing an assay to measure the competitive inhibition of sPLA2 by a variety of fractions of *Parachlorella kessleri* provided an opportunity to evaluate the potential for compounds derived from algae to act as anti-inflammatory therapeutics. A preliminary screen for sPLA2 inhibition was conducted on the primary fractions obtained from fractionation of *Parachlorella kessleri* biomass. The primary fractions screened were

the combined hexane fractions (H), the butanol fraction (β3), the methanol fraction (Fraction M), and the polyamide fractions derived from the ethyl acetate fraction (E-B through E-H). For detailed descriptions of the preparation of these fractions, see Chapter 3. These fractions were solubilized in DMSO at a screening concentration of 100 µg/mL. KH604, a known inhibitor of sPLA2 was used as a positive control at a screening concentration of 500 nM. The results are shown in Figure 5-4. There was one fraction that exhibited statistically significant inhibition of human type V sPLA2 and that was E-h (p = 0.037). E-h exhibited 33.9 ± 3.07% at a concentration of 100 µg/mL.
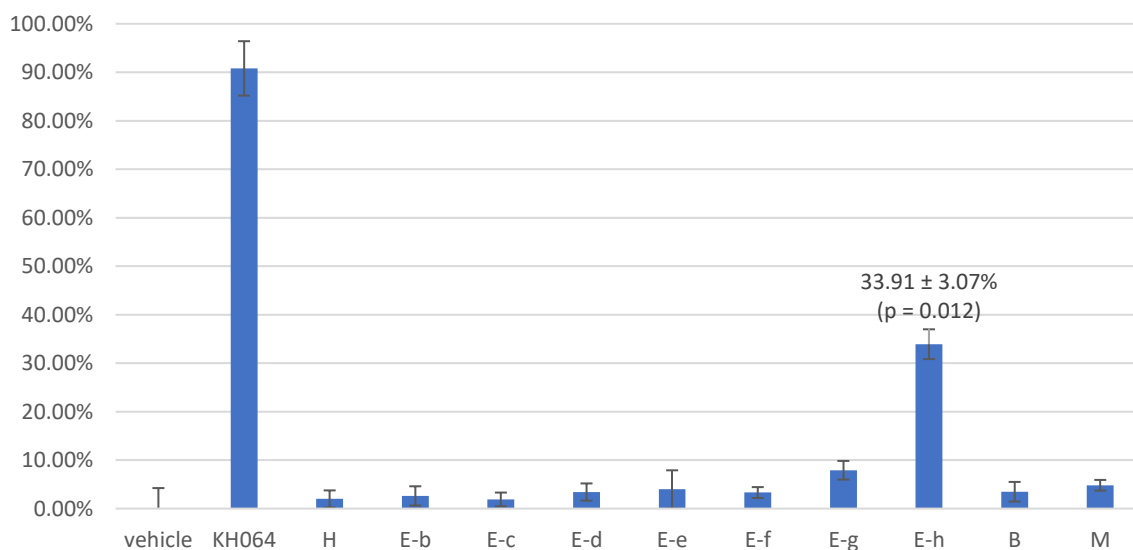
Figure 5-4. sPLA2 inhibition of primary fractions derived from *Parachlorella kessleri*
* Exhibited statistically significant difference from vehicle control (student's t-test, two-tailed, $p < 0.05$)

E-h was sub-fractionated in order to determine the active constituent. E-h was separated by Sephadex into three major fractions, E-h-2, 5, and 6. The fractions were assayed at a concentration of 100 µg/mL. Results are shown in Figure 5-5. Of these, the only fraction with activity was the largest fraction, E-h-5 which demonstrated a significant inhibition of

sPLA2 (21.8 ± 3.05%, p = 0.018). This fraction contained one major compound and several minor compounds, and was sub-fractionated using preparative TLC (Silica H) to obtain E-h-6a, b, and c (Figure 5-5). These fractions were screened at a concentration of 25 µg/mL, at which concentration only E-h-6b demonstrated significant activity (p = 0.016), exhibiting 31.0 ± 4.77% inhibition.
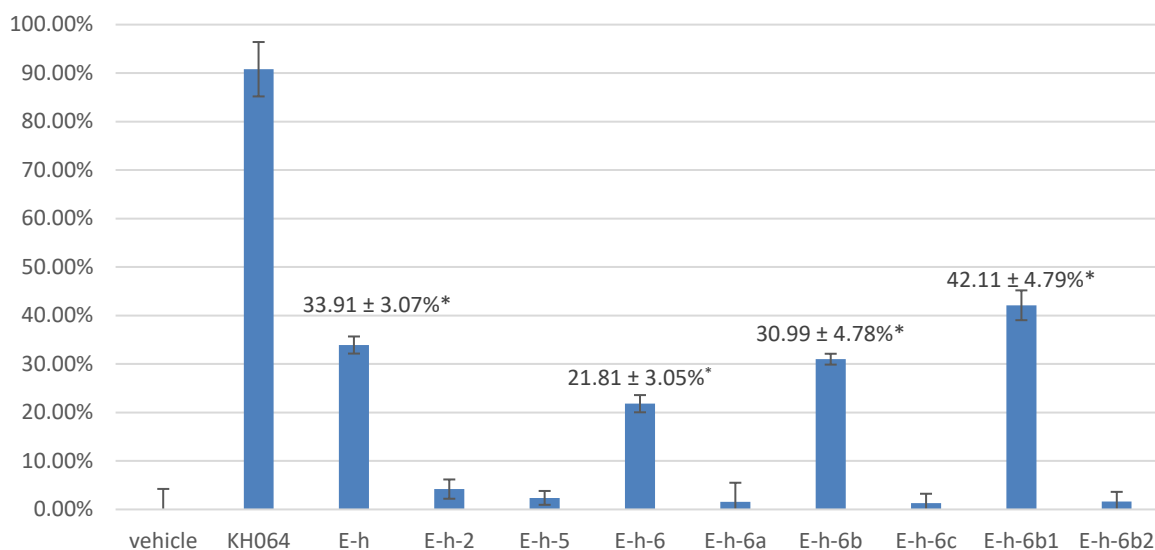
Figure 5-5. sPLA2 inhibition of purified fractions of E-h
* Statistically significant difference from vehicle control (student's t-test, two-tailed, p < 0.05)

In order to purify this fraction further for chemical characterization, E-h-6b was subjected to Sephadex separation to give the major product E-h-6b1 and minor components in fraction E-h-6b2. E-h-6b1 demonstrated significant inhibition (p = 0.009) of sPLA2 at 42.1 ± 4.78%. LC/MS analysis showed E-h-6b1 was a mixture of 4 analogues with molecular weight 783.3, 785.6, 775.8, and 778.2. By NMR, the skeleton of the compound was determined to be galactolipids of variously unsaturated fatty acids (Figure 5-6).

Molecular Weight: 785.14

Molecular Weight: 783.13

Molecular Weight: 779.09

Molecular Weight: 775.06
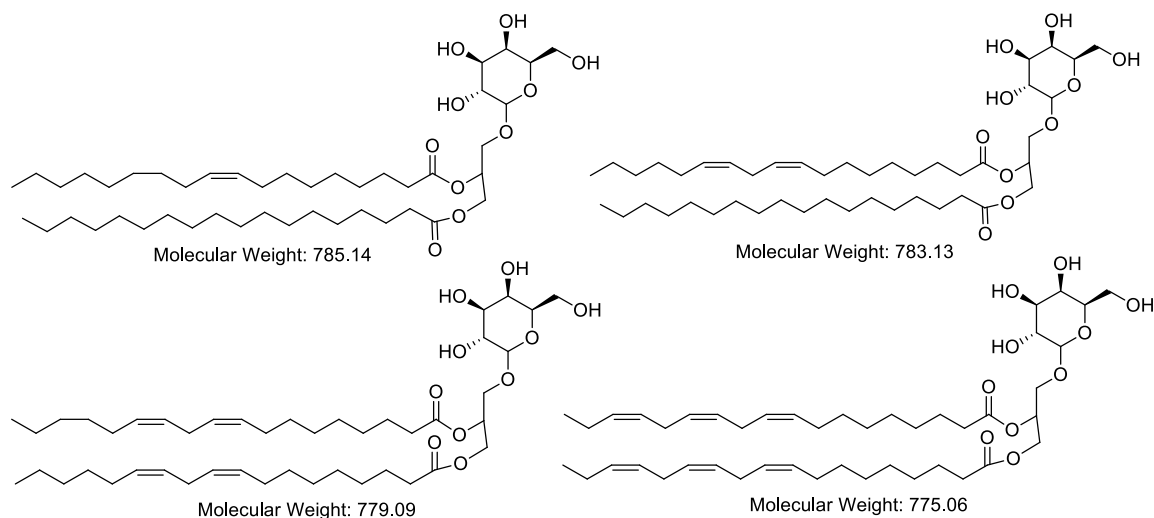
Figure 5-6. Structure of compounds identified in active fraction E-h-6b1

These compounds were inseparable by preparative chromatography, and as such were assayed as a mixture. Since LCMS showed relatively equal amounts of each analogue and NMR showed no detectable contaminants, the average molecular weight (780.73 Da) was used to calculate molarity for the dose response curve. E-h-6b1 was assayed at a range of 77.8 μM to 152 nM to establish a dose response curve (in Figure 5-7). As is clearly illustrated, there was a significant dose dependent response observed. E-h-6b1 exhibited statistically significant inhibition at concentrations of 2.43 μM and higher. E-h-6b1 achieved a maximal inhibition at a concentration of 38.9 μM; treatment at higher concentration (77.8 μM) did not increase inhibition significantly ($p = 0.41$). At a concentration of 38.9 μM or higher, inhibition of sPLA2 did not differ significantly from results obtained for known inhibitor KH064 ($p = 0.366$). Using a third order polynomial regression curve, the IC50 value was calculated to be 10.41 μM.
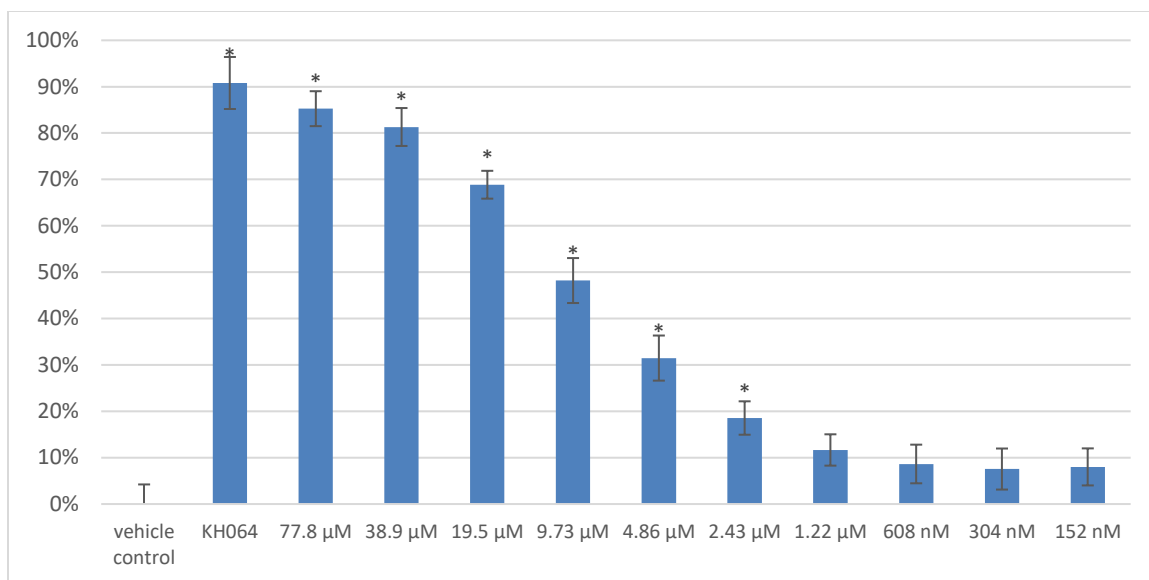
Figure 5-7. Dose response curve for sPLA2 inhibition for E-h-6b1
*Statistically significant difference from vehicle control (student's t-test, two-tailed, p < 0.05)

The mechanism of inhibition was postulated to be competition for the binding site since the galactolipid derivatives share such resemblance to phospholipid molecules. It has been reported that human pancreatic phospholipase can hydrolyze galactolipids during digestion[12], further supporting evidence that the algae-derived galactolipids compete for the active site of sPLA2. It was postulated that since sPLA2 can hydrolyze galactolipids, the inhibitory response would be lost quickly. To test this, three inhibition experiments were conducted in parallel using E-h-6b1 at a concentration of 7 µM. Each trial was pre-incubated with sPLA2 for differing times to allow for hydrolysis of galactolipids prior to addition of competitive substrate for detection. The results of this experiment are shown in Figure 5-8. Pre-incubation with enzyme showed a slight impact on inhibitory activity which increased in a time dependent manner. Pre-incubation for 30 minutes reduced inhibitory activity from 40.8 ± 3.91% to 31.2 ± 4.52% (p = 0.049). Incubation for 60 minutes further reduced inhibitory activity to 28.9 ± 3.82% (p = 0.02). The difference between 30

minute incubation and 60 minute incubation was slight and not statistically significant (p
= 0.54) and as such it was hypothesized that the lysogalactolipid formed due to hydrolysis
from sPLA2 is an active inhibitor, although is less potent than the original galactolipid.
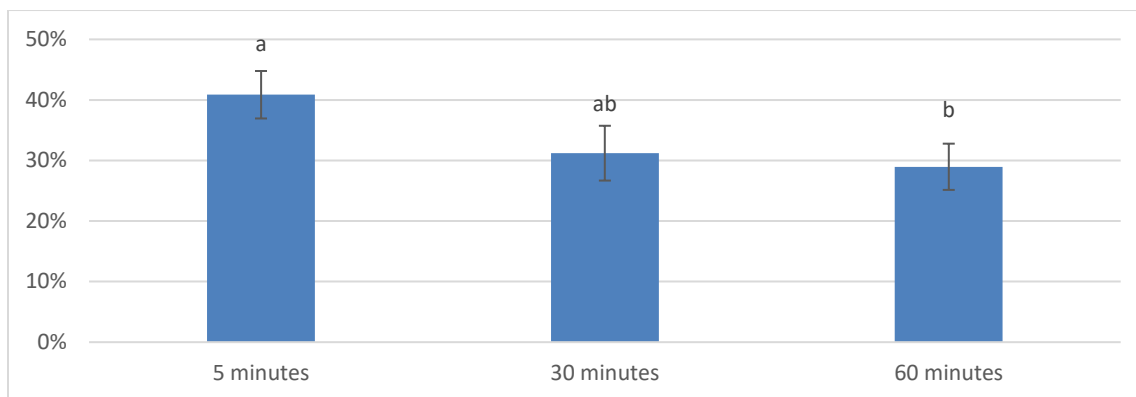
Figure 5-8. Results of inhibition assay for E-h-6b1 with various enzyme incubation times
Bars with shared superscripts did not differ significantly (p < 0.05) by student's t-test.

In conclusion, four galactolipid derivatives isolated from *Parachlorella kessleri* biomass
exhibited dose dependent inhibition of human type V secretory phospholipase A2. Due
to the myriad roles of sPLA2 in the regulation of inflammatory response, inhibition of
sPLA2 is an attractive target for therapeutic modulation of chronic inflammatory diseases.
Based on these results, the galactolipid and lysogalactolipid structure represent
interesting lead molecules for sPLA2 inhibition. Stabilized derivatives which mimic the
galactolipid or lysogalactolipid structures and retain key binding interactions at the active
site would be expected to significantly inhibit sPLA2. Modulation of structure to improve
drug-like characteristics (logP, molecular weight, stability to metabolism) through rational
drug design is the next logical step in the drug-design process to optimize this lead
compound.

5.3   COX-2 inhibition

The therapeutic role of cyclooxygenase proteins has been exploited for over a century since the development of Aspirin by Bayer in the late 19th century (citations). Since then, an explosion in pharmaceuticals marketed for the attenuation of pain and common symptoms of cold have led to countless small molecules capable of interfering with cyclooxygenase, known as non-steroidal anti-inflammatory drugs (NSAIDs) (citations). Although inflammatory response is the immune system's response to infection and injury, the inflammatory response itself can lead to excessive fever, discomfort as well as pain and injury in chronic diseases such as arthritis (See section 1.3.1 for the earlier detailed discussion of inflammation and disease). As such, reduction of inflammation is a key therapeutic strategy to mitigate pain, fever, and swelling.

Despite widespread use of NSAIDs, the mechanism of therapeutic action was not elucidated until the 1970s. Vane (1971) proposed that NSAIDs suppress inflammation via inhibition of cyclooxygenase and hence prostaglandin synthesis [13] . Prostaglandins promote inflammatory reactions via activation of CREB transcription factor (discussed in detail in section 1.3.3) and lead to an activation of the innate immune response. Inhibition of prostaglandin synthesis at the point of injury reduces swelling and pain; this effect can also lead to a reduction in fever[14].

There are two major isoforms of cyclooxygenase, imaginatively named COX-1 and COX-2. COX-1 is constitutively expressed in nearly all tissue types under basal conditions and it is thought that the major function of COX-1 is to regulate "housekeeping" functions in which

prostaglandins play a crucial role[15]. COX-1, however, does not play a large role in active control of inflammatory processes. By contrast, COX-2 is tightly regulated, and is dramatically upregulated during inflammation. As such, COX-2 inhibition activity is the hallmark of non-steroidal anti-inflammatory therapeutics. The ability of compounds derived from *Parachlorella kessleri* biomass to inhibit prostaglandin synthesis by way of COX-2 was evaluated utilizing an enzymatic *in vitro* assay.

5.3.1 Methodology

5.3.1.1 Theory of Assay

In order to measure the inhibition of cyclooxygenase, specifically COX-2, by extracts and compounds derived from *Parachlorella kessleri*, an *in vitro* enzymatic assay was employed. This assay is available commercially for the quantification of COX-2 inhibition by various ligands (Cayman Chemical, Cat #701080). The theoretical premise of this assay is elegant although fairly complex, and as such warrants a detailed explanation prior to practical description of the assay.

As discussed in detail in section 1.3.3 *Lipid signaling*, COX-2 is the enzyme responsible for the synthesis of prostaglandins (PGs) in response to cellular stress or damage. This assay relies on measuring the concentration of PGs produced by COX-2 with and without the presence of inhibitor. The relative difference between these results is a measure of percent inhibition of COX-2. The method utilized to detect the concentration of PGs produced by COX-2 for this assay relies on immunochemistry. The 96-well plates used for this assay are coated with a mouse anti-rabbit IgG which binds very selectively to rabbit antiserum. Rabbit antiserum is obtained which tightly binds PG. The assay is based upon

the competition of binding between PGs produced by COX-2 and synthetic PG-acetylcholineserase (PG-AChE) conjugate tracer. A diagram of this process is shown below in Figure 5-9. Competition between PGs produced by COX-2 and PG-AChE for a limited quantity of PG-specific rabbit antiserum allows for a means of measuring the activity of COX-2. When limited PG is present due to COX-2, relatively large quantities of PG-AChE are bound to the PG-specific rabbit antiserum, which binds the mouse anti-rabbit IgG antibodies bound to the well plate. Treatment of the bound PG-AChE with acetylthiocholine yields thiocholine which upon treatment with 5-5'-dithio-bis-(2-nitrobenzoic acid) yields 5-thio-2-nitrobenzoate (see Figure 5-10). 5-thio-2-nitrobenzoate is intensely colored and gives quantifiable response that is proportional to the concentration of bound PG-AChE, and of course inversely proportional to the quantity of PG present due to COX-2 activity. This complicated although elegant procedure allows for indirect measurement of PG production by COX-2 and serves as the basis for this assay[16].

Figure 5-9. Diagram of theoretical premise of detection of PGs in COX-2 inhibitor assay
Modified from Cayman Chemical product manual[8].

Figure 5-10. Schematic diagram of mechanism of colorimetric response for COX-2 inhibitor assay

5.3.1.2 Assay Protocol

Fractions and compounds derived from *Parachlorella kessleri* were dissolved in DMSO for use in this assay. For screening solutions were prepared at a concentration of 460 µg/mL to give a screening concentration of 50 µg/mL. Purified fractions were tested at a concentration of 10 µg/mL. Fractions that showed significant activity were re-evaluated across a range of concentrations to establish IC_{50} values. Indomethacin (Sigma-Aldrich, St. Louis, MO) was used as a positive control at a screening concentration of 500 nM. All other reagents were obtained from Cayman Chemical (COX-2 inhibitor screening assay kit, #701080).

Reaction buffer was prepared by dilution of 5 mL stock solution obtained from Cayman with 45 mL ultrapure water to make 50 mL 0.1 M Tris-HCl, pH 8.0, with 5 mM EDTA and 2 mM phenol. Buffer was equilibrated to 37°C prior to use. 960 µL buffer was added to 40 µL Heme in DMSO. A solution of arachidonic acid was prepared in 1/1 ethanol:0.1M KOH and diluted with ultrapure water to obtain a concentration of 5 mM in order to achieve a screening concentration of 217 µM.

To achieve a reading for background absorbance of COX-2 due to non-specific adsorption by antibodies (NSB), a small amount of COX-2 was transferred to a microcentrifuge and boiled for 3 minutes. To a microcentrifuge tube was added 160 µL reaction buffer, 10 µL of Heme solution, and 10 µL inactive COX-2. The vehicle (DMSO) was used to control for inhibition due to solvent; to the vehicle control microcentrifuge tube was added 160 µL reaction buffer, 10 µL Heme, and 10 µL COX-2, and 10 µL DMSO. To measure the inhibition

by algal fractions, to individual microcentrifuge tubes was added 160 μL reaction buffer, 10 μL Heme, 10 μL COX-2, and 10 μL algal fraction. A positive control was prepared by adding 160 μL reaction buffer, 10 μL Heme, 10 μL COX-2, and 10 μL indomethacin (500 nM final concentration). All tubes were incubated for 10 minutes at 37˚C. 10 μL arachidonic acid solution was added to each reaction tube followed by exactly 2 minutes' incubation at 37˚C. 30 μL saturated stannous chloride in 1.0 M HCl was added to each tube to halt the reaction.

To quantify the formation of PGs, a specialized 96-well plate coated with mouse anti-rabbit IgG was utilized. EIA buffer was prepared by dilution of 10 μL stock solution (Cayman chemical, cat # 400060) with 90 μL ultrapure water. A calibration dilution series of prostaglandins was prepared from the supplied stock solution (Cayman Chem, Cat # 414026) by serial dilution in EIA buffer over a range of 2000 pg/mL – 15.6 pg/mL. This was prepared to ensure that results stayed within the precision range specified by the product manual. 50 μL each prostaglandin standard was added to two sets of eight wells. 50 μL was aliquoted from the non-specific binding background absorption sample (NSB) microcentrifuge tube (prepared as described above from denatured COX-2) was added to two wells. 50 μL of the vehicle control solution was added from the reaction tube to two wells. 50 μL of the inhibitor test solutions prepared from algal fractions was added in duplicate to wells. 50 μL of PG-AChE conjugate tracer was added to each well except for the blank wells. Finally, 50 μL PG-screening rabbit antiserum was added to each well except the blank wells and the background absorption wells. The plate was covered with plastic wrap and incubated for 18 hours at room temperature with gentle shaking.

Ellman's reagent was prepared by reconstituting 1 vial of Ellman's reagent (Cayman Chemical, Cat # 400050) with 20 mL ultrapure water. The wells were emptied and washed 5x with wash buffer. The wash buffer was prepared by diluting Wash Buffer 400x concentrate (Cayman Chem, Cat # 400062) to a volume of 2.0 L with ultrapure water and adding 1 mL Polysorbate 20 (Cayman Chem, Cat #400035). After sufficient washing of the plate, 200 µL Ellman's Reagent was added to each well. 5 µL of PG-AChE conjugate tracer was added to the total-activity wells. The plate was covered with plastic film and developed by shaking gently for 70 minutes on an orbital shaker. The absorbance for each well on the plate was read on a well-plate reader at a wavelength of 410 nm when the background wells read an absorbance of at least 0.3 OD.

5.3.1.3 Data processing

Due to non-specific binding of the antiserum to the well-plate-bound antibodies, the absorbance measured for the NSB wells (see 5.3.1.2) was measured to establish a non-specific binding correction factor abs_{NSB}, equal to the average of the absorbance at 410 nm of the NSB wells. This factor was subtracted from the average of the absorbance of the vehicle control wells to obtain abs_0, the adjusted absorption representing 0% inhibition. The absorbance of the inhibitor samples abs_n was adjusted by the specific binding correction factor to give the adjusted inhibitor absorbance $abs_i = abs_n - abs_{NSB}$. The percent inhibition is therefore easily calculable from the following ratio:

$$\%inhibition = \frac{abs_i}{abs_0}.$$

To determine statistical significance with respect to vehicle control, the student's t-test was performed (two-tails, unpaired). Results were deemed significant if $p < 0.05$.

5.3.2 Results and Discussion

During the process of isolation of natural products derived from *Parachlorella kessleri*, bio-guided fractionation was employed in order to identify the constituents responsible for activity. The separation process is described in detail in Chapter 3 involving sequential chromatography with a variety of solvents and stationary phases. Eleven fractions were selected for initial screening which spanned a wide range of lipophilicity. Among the fractions were the crude combined hexane fraction (H), the crude combined chloroform fraction (C), the crude butanol fraction (B), and the crude methanol fraction (M). The ethyl acetate fraction (E) was fractionated prior to screening due to its high content of xanthophylls and polar lipid derivatives, and 6 sub-fractions from polyamide gel separation were included in the preliminary screen.

The concentration of fractions used in the preliminary screen for COX-2 activity was 50 µg/mL. Indomethacin, a synthetic, commercially available COX inhibitor and well-characterized prescription non-steroidal anti-inflammatory drug (NSAID) was selected as a positive control and assayed at a concentration of 179 ng/mL (500 nM). Results are reported as % inhibition relative to untreated and vehicle control groups (Figure 5-11).
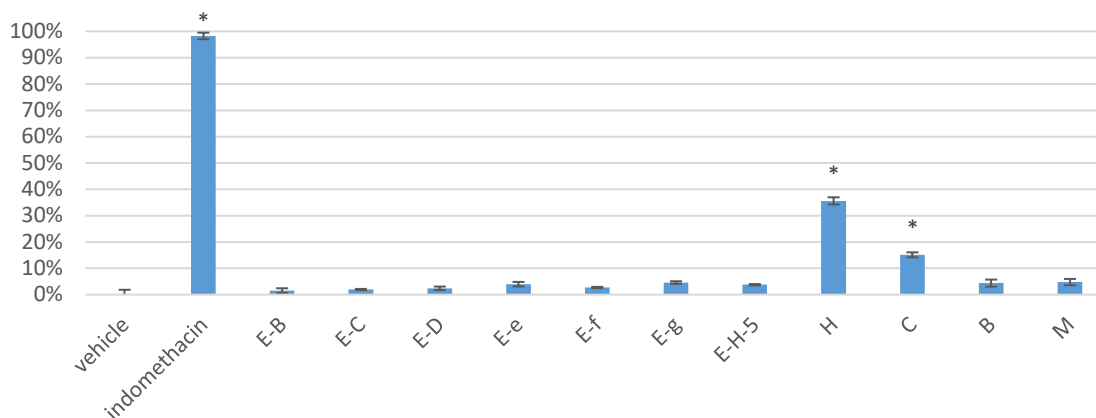
Figure 5-11. Percent inhibition of COX-2 by *Parachlorella kessleri* fractions (see Chapter 3)
* Differed statistically significantly from vehicle control (student's t-test, two tailed, unpaired, p < 0.05)

Indomethacin, as expected, exhibited nearly complete inhibition of COX-2 (98.3%) As can be readily seen, only two fractions, H and C, demonstrated statistically significant (p = 0.002 and 0.009 respectively) inhibition relative to vehicle control (denoted with an asterisk in Figure 5-11). Fraction H was found to inhibit COX-2 activity by 35.6 ± 1.36% at a concentration of 50 µg/mL, the highest of any fractions screened in this assay. Fraction C was found to inhibit COX-2 activity at 15.1 ± 0.95% (p = . Based on these results, and that these fractions were crude mixtures of many constituents, it was decided to sub-fractionate H and C followed by evaluation of the sub-fractions using the COX-2 inhibition assay.

Fractions H and C were sub-fractionated as described in section 3.6. Obtained from H were 3 sub-fractions, H-a, Hb, and Hc. Fraction Hc contained two major compounds, and one minor compound, and was re-fractionated in order to isolate these compounds, obtaining Hc-0, Hc-1, and Hc-2. Hc-0 and Hc-1 was obtained as highly pure white flaky solids after evaporation of the solvent, while Hc-2 was a yellow residue. Two major

fractions of C, Ca and Cb were also screened for activity. These fractions were assayed to assess COX-2 inhibitory activity; the results are shown in Figure 5-13.
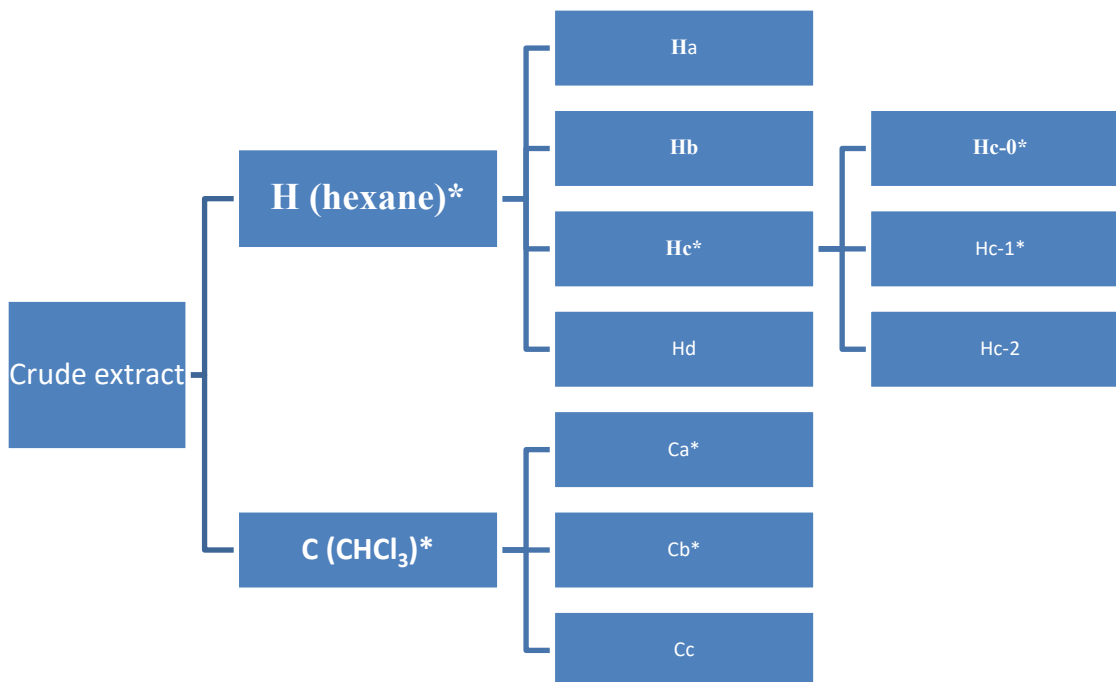
Figure 5-12. Bioguided fractionation diagram for fractions showing COX-2 inhibition activity
*COX-2 inhibition activity differed significantly from vehicle control in assay (student's t-test, two tailed, unpaired, p < 0.05), see Figure 5-13

Of the sub-fractions of H evaluated for COX-2 inhibition, only two exhibited statistically significant activities. It is key to note that Hc-0, Hc-1, and Hc-2 were assayed at a concentration of 50 μg/mL, while fractions H, Hb, and Hc were evaluated at 10 μg/mL. The most active sub-fraction was Hc-0, exhibiting 42.3 ± 3.61% inhibition of COX-2, a marked increase over the parent-fraction H with half the treatment concentration. The sister fraction, Hc-1, also relatively pure, exhibited the second most activity, yielding 29.3 ± 1.25% inhibition of COX-2 at 10 μg/mL. A sub-fraction of C, Ca, also demonstrated

statistically significant inhibition of COX-2 (16.8 ± 1.21%), although at a 50 µg/mL

(compared to 10 µg/mL for H sub-fractions).
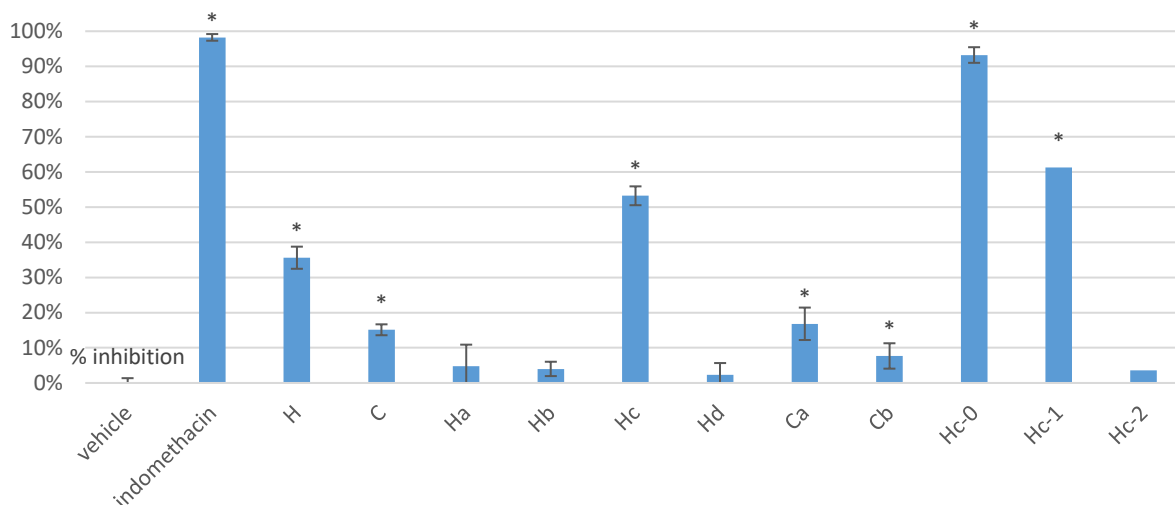
Figure 5-13. Percent inhibition of COX-2 by *Parachlorella kessleri* sub-fractions of H and C
*Results differed significantly from vehicle control (student's t-test, two tailed, unpaired, $p < 0.05$)
Subfractions of H were tested at a concentration of 10 µg/mL. Results demonstrated increased
activity in fraction Hc-0 and Hc-1.

Based on these results and their relative purity, Hc-0 and Hc-1 were selected for further

study and structural characterization. In order to prepare analytically pure samples of the

two active components, preparative TLC was carried out as described in section 3.6.1.

After purification, the compounds were identified by LC/MS, GC/MS, and ^{1}H-NMR (see

sections 3.6.2.1 and 3.6.2.2 for details about structural characterization). Fraction Hc-0

was identified as (Z, Z)-9,12-octadecadienoic acid, commonly known as linoleic acid.

Fraction Hc-1 was identified as (Z,Z,Z)-9,12,15-octadecatrienoic acid, commonly known as

α-linolenic acid. The structures of these compounds are shown in Figure 5-14.
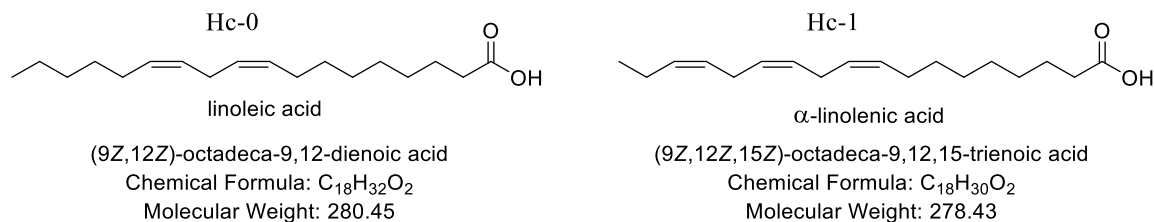
Figure 5-14. Structures of compounds found in COX-2 inhibiting fractions

Once the structure of the active compounds was solved, the COX-2 inhibition assay was repeated across a range of concentrations in order to construct a dose response curve and evaluate the molar potency of these compounds. The purified compounds were assayed at a concentration range from 7 µM to 56 nM. Indomethacin was used as a positive control. Linoleic acid (LA) demonstrated a dose-dependent response. LA showed excellent potency, exhibiting statistically significant inhibition of COX-2 at a concentration of 223 nM and higher. The dose response for linoleic acid is shown in Figure 5-15. The maximal inhibition (85.6 ± 3.61%) was reached at a concentration of 2 µM—COX-2 inhibition at higher concentrations did not vary significantly from inhibition at 1.79 µM. At concentrations of 7.14 µM and 3.57 µM, COX-2 inhibition did not differ significantly from 500 nM indomethacin (p = 0.216 and 0.092 respectively). In order to calculate the IC_{50} value for LA, a third order polynomial was fit to the data. The IC_{50} value for linoleic acid was found to be 557 nM.
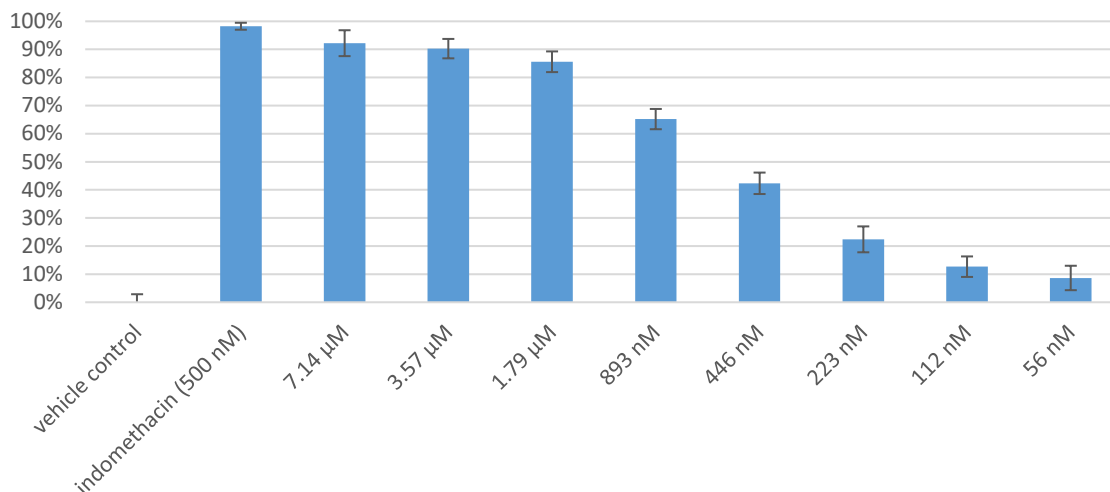
Figure 5-15. Dose response curve for COX-2 inhibition by Hc-0, identified as linoleic acid (IC$_{50}$ = 557 nM)
* Differed significantly from vehicle control (student's t-test, two tailed, unpaired, $p < 0.05$)
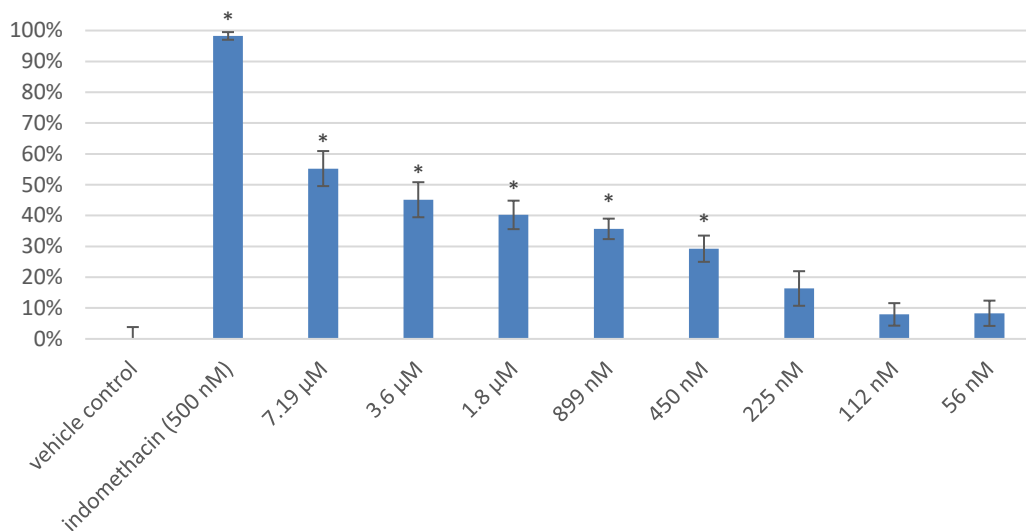
Figure 5-16. Dose response curve for COX-2 inhibition by Hc-1, identified as α-linolenic acid
* Differed significantly from vehicle control (student's t-test, two tailed, unpaired, $p < 0.05$)

α-linolenic acid was evaluated across the same range of concentrations as linoleic acid. α-linolenic acid (ALA) demonstrated a dose-dependent response; the dose response for linoleic acid is shown in Figure 5-16. ALA showed activity as a partial inhibitor, attaining maximum inhibition at 45.13 ± 5.680% inhibition at 7.19 µM. During the screen when this

fraction was tested at 35 µM, COX-2 inhibition of 45.28 ± 3.610% was detected. In order to calculate the IC_{50} value for ALA, a third order polynomial was fit to the data. The IC_{50} value for linoleic acid was found to be 11.9 µM.

The activity of linoleic acid as a COX-2 inhibitor is not unprecedented. Jäger et al. (2008) reported the isolation of linoleic and α-linolenic acid as the active COX inhibitors in rose hip[17]. The authors report IC_{50} values consistent with the results found in this work: linoleic IC_{50} 0.6 µM for COX-2, consistent with 557 nM found in this work, and IC_{50} = 12 µM, consistent with the IC_{50} value of 13.8 µM detected in this work. This is the first time COX-2 inhibitor activity has been reported for *Parachlorella kessleri*.

Inhibition of cyclooxygenase-2 is a target of myriad over-the-counter non-steroidal anti-inflammatory drugs (NSAIDs). NSAIDs, such as acetaminophen (Tylenol®), ibuprofen (Advil®), and acetylsalicylic acid (aspirin). NSAIDs are the most prescribed and utilized drugs, with 70 million prescriptions and 30 billion over-the-counter (OTC) medications sold[18]. As COX-2 inhibitors, NSAIDs inhibit the production of prostaglandin E2 from arachidonate (see section 1.3.3 for a detailed discussion about the role of COX-2 in inflammation). The data show that *Parachlorella kessleri*-derived linoleic and α-linolenic acid have the potential to mitigate symptoms of inflammation due to their COX-2 inhibition activity. Inhibition of COX-2 leads to a decrease in prostaglandin formation which in turn would lead to a reduction in inflammatory symptoms such as edema and pain.

5.4   iNOS inhibition

Inducible nitric oxide synthase is an important enzyme involved in the regulation of inflammatory responses. Nitric oxide (NO) is a critical cellular signaling molecule which is generated *in situ* by oxidation of L-arginine by iNOS involved in immune response to cellular damage[19]. NO is a potent vasodilator, and a reactive molecule which subsequently generates reactive oxygen species (ROS) used by leukocytes to lyse bacteria, pathogens, and infected cells[20]. NO propagates the inflammatory signal to other cells, stimulating the immune response in other cells. Quenching of NO or inhibition of iNOS can therefore mitigate inflammation. There has been a substantial effort in the pharmaceutical industry to identify therapeutic iNOS inhibitors for the treatment of inflammation[21].

5.4.1   Methodology

5.4.1.1   Trolox Equivalent Antioxidant Capacity (TEAC) determination

The Trolox Equivalent Antioxidant Capacity assay measures the degree of radical absorption compared to Trolox (a water-soluble form of Vitamin E). A solution of ABTS (2,2'-azino-bis(3-ethylbenzothiazoline-6-sulphonic acid)) was reacted with Potassium Persulfate (radical generator) to produce the stable colored ABTS radical cation (stable for 1 hour at room temperature). The disappearance of this colored radical is measured at 734 nm, allowing for the quantification of radical absorption capacity. A calibration series of Trolox was prepared ranging from 632 µg/mL to 19.75 µg/mL.

ABTS (38.4 mg) and Potassium Persulfate (6.6 mg) were mixed in 10 mL water and stored in the dark for 12 hrs. 990 uL of the ABTS reagent was combined with 10 µL of the algae

extracts or calibration solution. The mixture was placed in a cuvette and measured using an Agilent G1111AA UV-Vis Spectrophotometer, set at 734 nm. All samples were run in triplicate. Results are reported as µmol trolox / g, reported as average of three runs ± standard deviation.

5.4.1.2 Cell Culture

RAW 264.7 cells, derived from murine macrophages, were procured from the American Type Culture Collection (Rockville, MD). The cells were cultured in RPMI-1640 (without phenol red) supplemented with 10% endotoxin-free, heat-inactivated fetal calf serum (GIBCO, Grand Island, NY), 100 units/mL penicillin, and 100 mg/mL streptomycin. When the RAW 264.7 cells reached a density of (2-3) 106 cells/mL, they were activated by incubation in the medium containing *Escherichia coli* lipopolysaccharide (LPS, 100 ng/mL).

Various concentrations of test compounds dissolved in dimethyl sulfoxide (DMSO) were combined together with LPS. The cells were cultured in 100 mm tissue culture dishes and incubated with 100 ng/mL of LPS for 12 h (Kim et al, 1995). The cells were treated with 0.05% DMSO with LPS as vehicle control. The cells were then harvested and plated in a 24-well plate and treated with LPS only or with LPS and different concentrations of test compounds for a further 12 h. Indomethacin treated cells were used as a positive control, and since exhibiting a near complete inhibition in NO production (98% at 20 µM treatment), this control was defined as 100% inhibition to relative to the algal extracts for the purposes of IC_{50} calculation.

5.4.1.3 Nitrite Assay

The RAW 264.7 cells were treated with various compounds and LPS or LPS only. At the end of incubation time, 100 μL of the culture medium was collected for nitrite assay (Kim et al. 1995). The amount of nitrite, an indicator of NO synthesis, was measured using the Griess reaction. Briefly, supernatants (100 μL) were mixed with the same volume of Griess reagent (1% sulfanilamide in 5% phosphoric acid and 0.1% naphthylethylenediamine dihydrochloride in water) in duplicate on 96-well plates. After incubation at room temperature for 10 min, absorbance at 570 nm was measured with the ELISA reader (Thermo Labsystems, Multiskan Ascent, Finland). The values are expressed as means ± standard error of triplicate tests.

5.4.1.4 Statistical Analysis

Values are presented as means ± standard deviation. Data were analyzed by unpaired, two-tailed student's t-test to identify significant differences ($p < 0.05$).

5.4.2 Results and Discussion

5.4.2.1 Trolox Equivalent Antioxidant Capacity (TEAC)

The antioxidant capacity of extracts of *Parachlorella kessleri* were evaluated by generating the stable 2,2'-azino-bis(3-ethylbenzothiazoline-6-sulphonic acid) radical cation (ABTS$^+$) through single electron oxidation. ABTS$^+$ is colored dark blue, and as the radical is quenched, the color turns clear proportionately. This allows for the quantitative

measure of the chemical quenching of ABTS$^+$ of unknown materials by comparison to Trolox, a water-soluble form of Vitamin E used as a reference standard.

Using this technique, the free radical absorption capacity of the xanthophyll extract was measured in comparison to the depigmented extract. The *P. kessleri* xanthophyll extract possessed substantial antioxidant activity (3915 ± 52.3 µM Trolox equivalent / g extract). The depigmented extract also possessed radical scavenging activity (35.6 ± 3.91 µM trolox equivalents / g extract), but was over 100x less potent than the xanthophyll extract.

5.4.2.2 Inhibition of inducible Nitric Oxide Synthase (iNOS)

In order to evaluate the effect of *P. kessleri* xanthophyll extract on the inhibition of iNOS, extracts were prepared as described in the section 5.4.2.1. Solutions of the pigment extract with standard concentrations were prepared in DMSO. The xanthophyll extract of *P. kessleri* exhibited a dose-dependent response in the inhibition of iNOS (Figure 5-17). The IC_{50} value determined for the xanthophyll extract was found to be 78 µg/mL. In order to estimate a molar IC_{50} value, the average molecular weight was calculated by weighted average of molecular weights determined in Table 3-3, weighted by peak area percent. Using this method, the molar IC_{50} value was calculated to be 94 µM.

The activity of compounds contained in the depigmented biomass was evaluated by recovering the insoluble material by centrifugation following extraction of pigment. This depigmented material was collected, dried, and dissolved in DMSO, and referred to as "depigmented extract." In contrast, the depigmented extract, containing no xanthophylls, possessed negligible activity at any concentration (Figure 5-17), and was thus determined

to be inactive. It is clear from this evidence that the xanthophyll extract of *P. kessleri*

possessed inhibitory activity on the production of NO from iNOS in murine macrophages

in vitro.
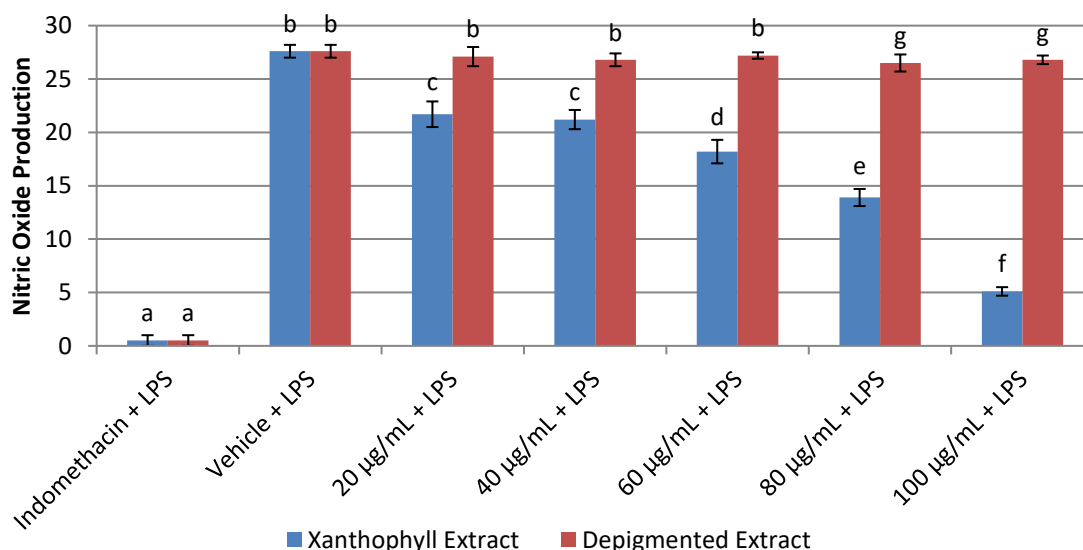
Figure 5-17. Dose response of xanthophyll extract and depigmented extract inhibition of nitric oxide production by inducible nitric oxide synthase (iNOS) in RAW264.7 murine macrophage cells

Bars with matching superscripts did not differ significantly (student's t-test, two-tailed, unpaired, $p < 0.05$).

Treatment of RAW264.7 macrophage cells with lipopolysaccharide (LPS) derived from *E.*

coli causes an inflammatory response in these cells. LPS binds to lipopolysaccharide-

binding protein (LBP); this complex in turn binds to CD14 or TLR4 receptors located on the

cell surface, activating a cellular signaling pathway leading to activation of the

proinflammatory transcription factor NF-κB, which induces the expression of iNOS[22]. iNOS

catalyzes the production of nitric oxide (NO) in the cells. The NO content is then quantified

according to the Greiss reaction[23], which has been used for nearly a century to quantify

nitrogen oxides. This reaction allows for direct colorimetric measurement of inhibition of

NO production in cells which have been treated with xanthophylls derived from

Parachlorella kessleri. *In vivo*, iNOS is typically induced by stimulation from pro-inflammatory cytokines such as IL-1, TNF-α and IFNγ, which induce transcription of iNOS in macrophages via NF-κB pro-inflammatory transcription factor[22].

Inducible nitric oxide synthase is an important enzyme involved in the regulation of inflammatory responses. Nitric oxide (NO) is a critical cellular signaling molecule which is generated *in situ* by oxidation of L-arginine by iNOS involved in immune response to cellular damage[19]. NO is a potent vasodilator, and a reactive molecule which subsequently generates reactive oxygen species (ROS) used by leukocytes to lyse bacteria, pathogens, and infected cells[20]. NO propagates the inflammatory signal to other cells, stimulating the immune response in other cells. Quenching of NO or inhibition of iNOS can therefore mitigate inflammation. There has been a substantial effort in the pharmaceutical industry to identify therapeutic iNOS inhibitors for the treatment of inflammation[21].

The xanthophylls contained in *Parachlorella kessleri* demonstrated a dose-dependent inhibition of the generation of NO by iNOS (IC_{50} = 94 μM, calculated from IC_{50} = 78 μg/mL). There was a statistically significant (p = 0.0016) decrease in NO production at 29.7 μM (calculated from 20 μg/mL) compared to vehicle control. The depigmented extract possessed statistically insignificant activity over vehicle control. The extracts exhibited *in vitro* antioxidant activity: extracts quenched free radicals generated by oxidation of ABTS (3915 μmol trolox equivalents / g extract). This data suggests the possibility that the xanthophyll extract may act to decrease NO generation by quenching the NO radical. The role of xanthophylls in the inhibition of iNOS is not unprecedented. Rafi and Shafaie

(2007) demonstrated that treatment with 10 µM lutein modulates iNOS protein expression in RAW 264.7 cells[24]. Slevaraj and Klasing (2006) have shown that iNOS mRNA levels are modulated by lutein in chickens and HD11 cell lines[25]. Astaxanthin has been shown to significantly reduce the expression of iNOS in keratinocytes[26]. These results are evidence to support the hypothesis that some xanthophylls modulate the expression of iNOS to induce inhibitory effects.

Due to the widespread prevalence of chronic inflammatory diseases (e.g. atherosclerosis), the identification of natural products which can modulate inflammatory response remains an important aspect of research. In this work, an optimized method to extract xanthophylls from algae biomass was developed in order to extract xanthophylls without the need of hydrolysis. The solvent and extraction time via ultrasound assisted solvent extraction were optimized for recovery of lutein. Extracts of *P. kessleri*, containing >90% xanthophylls by mass, were chemically profiled using HPLC/UV/MS using a C_{30} HPLC column. Ten xanthophylls were detected, 8 were tentatively identified by analyzing UV and MS data and by comparison with commercially available standards and literature references. The xanthophyll extract prepared was evaluated for anti-inflammatory activity in RAW 264.7 murine macrophage cells by measuring the inhibition of iNOS. It was confirmed that the pigment extract possessed low micromolar potency, with an estimated IC_{50} of 94 µM, whereas extracts of biomass without xanthophylls possessed no activity. Our results show that pigment extracts of *P. kessleri* demonstrate the potential to modulate inflammatory response by the inhibition of NO production by iNOS, demonstrating the potential for xanthophylls derived from *P. kessleri* to be potentially

useful as an anti-inflammatory, algae-derived phytomedicine. Subsequent work is currently being conducted to identify unknown xanthophylls and elucidate the molecular mechanism of inhibition.

5.4.2.3 *Proposed Mechanism of Action*

Since the characterization of xanthophylls and carotenoids and the discovery of their role in myriad biochemical pathways such as photosynthesis[27], the synthesis of retinal for vision[28], and as anti-oxidants which protect cells from oxidative damage[29], there has been great interest in these structures as possible modulators of physiological function and disease. A detailed discussion of the roles of xanthophylls and carotenoids in human health and disease is presented in section 1.1.2 (pg. 8). An excellent review of the role of carotenoids and xanthophylls as scavengers of oxidative byproducts of photosynthesis was published by Telfer (2002)[30], which concludes that β-carotene participates in photosystem II by absorption of singlet oxygen, preventing the oxidation of chlorophyll during photosynthesis. Astaxanthin, a red-yellow xanthophyll isolated from *Hematococcus pluvialis* has also been comprehensively studied for its properties as an anti-oxidant, and there have been numerous reviews assembled which indicate the capability of astaxanthin and similar xanthophylls to absorb oxidative byproducts[31,32,33,34].
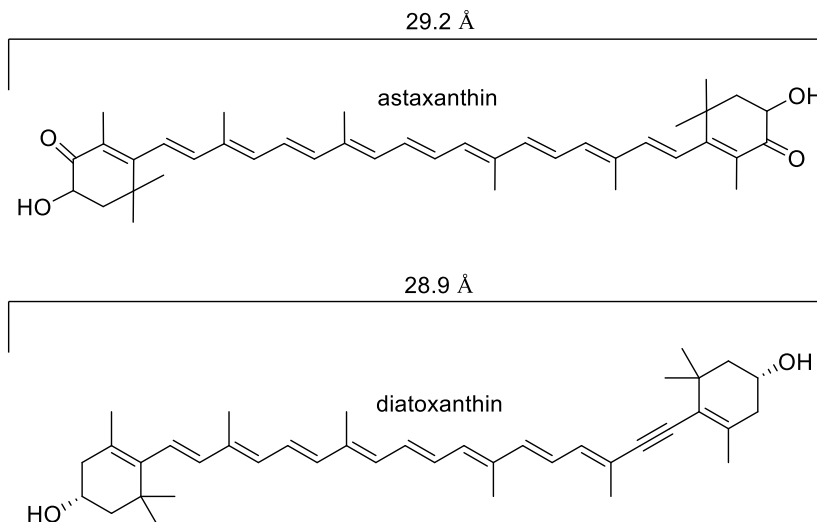
Figure 5-18. Structures of astaxanthin and diatoxanthin

Kidd (2011) proposed that astaxanthin acts as a membrane-nutrient, showing that astaxanthin spans cell membranes, allowing for the reactive oxygen species generated within a cell to be exported by way of conducting electron oxidation through membrane-bound astaxanthin[35]. Examining the chemical structure of astaxanthin is helpful to understand the potential mechanism of this action; the key is the long chain of conjugated double bonds, spanning 11 ethylenes with a conjugated carbonyl at the ring on each flank, spanning 29.2 Å (Figure 5-18). The average length of the lipid bilayer in a cell-membrane is approximately 30 Å, and because of the polar groups at the flank of each side of astaxanthin, the molecule can span the lipid-portion of the membrane[36]. Since the conjugated system extends from end to end, the astaxanthin structure, when bound in the membrane, can conduct electrons from oxidative byproducts from within the cell across the membrane to external antioxidants[35,36]. Due to the similarities in structure between astaxanthin and the diatoxanthin, major xanthophyll detected in *P. kessleri* (Figure 5-18), it was postulated that diatoxanthin acts to quench oxidative byproducts in

RAW264.7 macrophages (as discussed in section 5.4.2.2, pg. 270) by the same mechanism as astaxanthin—by spanning cell membranes and allowing for the conduction of oxidative byproducts to the extracellular media. A schematic depiction of this mechanism is shown in Figure 5-19, which was adapted from Kidd (2011)[35].
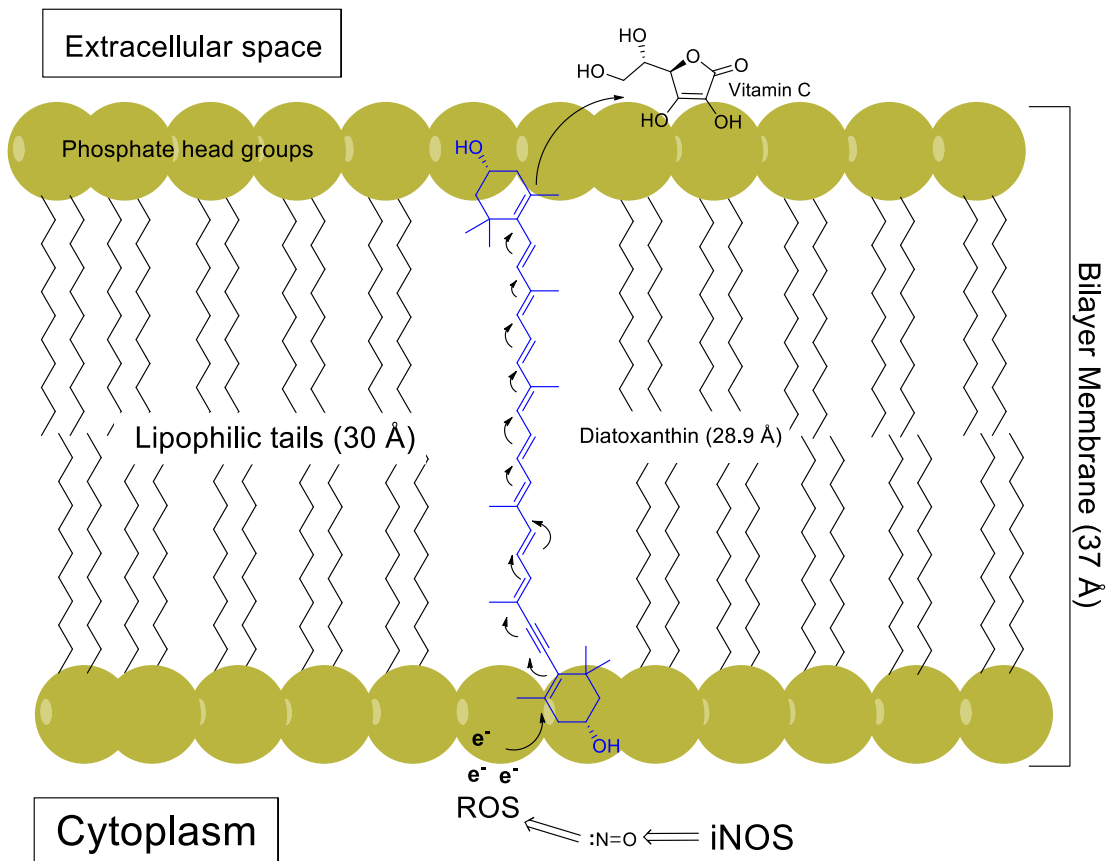

Figure 5-19. Proposed mechanism of reduction of nitric oxide production in murine macrophages by xanthophylls
Adapted from Kidd (2011)[35]

5.5   References

[1] Matsuda, L. A., Lolait, S. J., Brownstein, M. J., Young, A. C., & Bronner, T. I. (1990). Structure of a cannabinoid receptor and functional expression of the cloned cDNA. *Nature*, *346*(6284), 561.

[2] Di Marzo, V., & Petrosino, S. (2007). Endocannabinoids and the regulation of their levels in health and disease. *Current opinion in lipidology*, *18*(2), 129-140.

[3] Stella, N., Schweitzer, P., & Piomelli, D. (1997). A second endogenous cannabinoid that modulates long-term potentiation. *Nature*, *388*(6644), 773-778.

[4] Ahn, K., Johnson, D. S., Mileni, M., Beidler, D., Long, J. Z., McKinney, M. K., ... & Lazerwith, S. (2009). Discovery and characterization of a highly selective FAAH inhibitor that reduces inflammatory pain. *Chemistry & biology*, *16*(4), 411-420.

[5] Anderson, W. B., Gould, M. J., Torres, R. D., Mitchell, V. A., & Vaughan, C. W. (2014). Actions of the dual FAAH/MAGL inhibitor JZL195 in a murine inflammatory pain model. *Neuropharmacology*, *81*, 224-230.

[6] Valentin, E., Ghomashchi, F., Gelb, M. H., Lazdunski, M., & Lambeau, G. (2000). Novel human secreted phospholipase A2 with homology to the group III bee venom enzyme. *Journal of Biological Chemistry*, *275*(11), 7492-7496.

[7] Mallat, Z.; Lambeau, G.; Tedgui, A. (November 2010). "Lipoprotein-Associated and Secreted Phospholipases A2 in Cardiovascular Disease: Roles as Biological Effectors and Biomarkers".*Circulation* **122** (21): 2183–2200.

[8] Cayman Chemical (2015). sPLA2 activity assay kit; Product instruction manual. Ann Arbor, MI.

[9] Balboa, M.A., Balsinde, J., Winstead, M.V., Tischfield, J.A., & Dennis, E.A. (1996). Novel group V phospholipase A2 involved in arachidonic acid mobilization in murine P388D1 macrophages. *Journal of Biological Chemistry*, 271, 32381-4.

[10] Mallat, Z., Lambeau, G., & Tedgui, A. (2010). Lipoprotein-Associated and Secreted Phospholipases A2 in Cardiovascular Disease Roles as Biological Effectors and Biomarkers. *Circulation*, *122*(21), 2183-2200.

[11] Rosenson, R. S., Elliott, M., Stasiv, Y., & Hislop, C. (2010). Randomized trial of an inhibitor of secretory phospholipase A2 on atherogenic lipoprotein subclasses in statin-treated patients with coronary heart disease. *European heart journal*, ehq374.

[12] Andersson, L., Bratt, C., Arnoldsson, K. C., Herslöf, B., Olsson, N. U., Sternby, B., & Nilsson, A. (1995). Hydrolysis of galactolipids by human pancreatic lipolytic enzymes and duodenal contents. *Journal of lipid research*,*36*(6), 1392-1400.

[13] Vane, J. R. (1971). Inhibition of prostaglandin synthesis as a mechanism of action for aspirin-like drugs. *Nature, 231*, 232–235

[14] Ricciotti, E., & FitzGerald, G. A. (2011). Prostaglandins and Inflammation. *Arteriosclerosis, Thrombosis, and Vascular Biology*, *31*(5), 986–1000.

[15] Crofford, L. J. (1997). COX-1 and COX-2 tissue expression: implications and predictions. *The Journal of Rheumatology. Supplement*, *49*, 15-19.

[16] Cayman Chemical (2015). COX-2 (human) inhibitor assay screening kit; Product instruction manual. Ann Arbor, MI.

[17] Jäger, A. K., Petersen, K. N., Thomasen, G., & Christensen, S. B. (2008). Isolation of linoleic and α-linolenic acids as COX-1 and-2 inhibitors in rose hip. *Phytotherapy Research*, *22*(7), 982-984.

[18] Green, G. A. (2001). Understanding NSAIDs: from aspirin to COX-2. *Clinical cornerstone*, *3*(5), 50-59.

[19] Hong, C. H., Hur, S. K., Oh, O. J., Kim, S. S., Nam, K. A., & Lee, S. K. (2002). Evaluation of natural products on inhibition of inducible cyclooxygenase (COX-2) and nitric oxide synthase (iNOS) in cultured mouse macrophage cells. *Journal of Ethnopharmacology*, *83*(1), 153-159.

[20] Lander, H. M. (1997). An essential role for free radicals and derived species in signal transduction. *The FASEB journal*, *11*(2), 118-124.

[21] Bonnefous, C., Payne, J. E., Roppe, J., Zhuang, H., Chen, X., Symons, K. T., Phan M. Nguyen, Sablad, M. , Rozenkrants, N., Zhang, Y., Wang, L., Severance, D., Walsh J.P., Yazdani N., Shiau, A.K., Noble, S.A., Rix, P., Rao T.S., Hassig, C.A., & Smith, N. D. (2009). Discovery of inducible nitric oxide synthase (iNOS) inhibitor development candidate KD7332, part 1: Identification of a novel, potent, and selective series of quinolinone

iNOS dimerization inhibitors that are orally active in rodent pain models. *Journal of medicinal chemistry*, *52*(9), 3047-3062.

[22] Xie, Q. W., Kashiwabara, Y., & Nathan, C. (1994). Role of transcription factor NF-kappa B/Rel in induction of nitric oxide synthase. *Journal of Biological Chemistry*, *269*(7), 4705-4708.

[23] Bartholomew, R. P. (1928). THE QUANTITATIVE DETERMINATION OF NITRITES IN SOIL. *Soil Science*, *25*(5), 393-398.

[24] Rafi, M. M., & Shafaie, Y. (2007). Dietary lutein modulates inducible nitric oxide synthase (iNOS) gene and protein expression in mouse macrophage cells (RAW 264.7). *Molecular nutrition & food research*, *51*(3), 333-340.

[25] Selvaraj, R. K., & Klasing, K. C. (2006). Lutein and eicosapentaenoic acid interact to modify iNOS mRNA levels through the PPARγ/RXR pathway in chickens and HD11 cell lines. *The Journal of nutrition*, *136*(6), 1610-1616.

[26] Yoshihisa, Y., & Shimizu, T. (2014). Astaxanthin, a xanthophyll carotenoid, inhibits ultraviolet-induced apoptosis in keratinocytes. *Experimental dermatology*, *23*(3), 178-183.

[27] Frank, H. A., & Cogdell, R. J. (1996). Carotenoids in photosynthesis. *Photochemistry and photobiology*, *63*(3), 257-264.

[28] Olson, J. A., & Hayaishi, O. (1965). The enzymatic cleavage of beta-carotene into vitamin A by soluble enzymes of rat liver and intestine. *Proceedings of the National Academy of Sciences*, *54*(5), 1364-1370.

[29] Sies, H., & Stahl, W. (1995). Vitamins E and C, beta-carotene, and other carotenoids as antioxidants. *The American journal of clinical nutrition*, *62*(6), 1315S-1321S.

[30] Telfer, A. (2002). What is β–carotene doing in the photosystem II reaction centre?. *Philosophical Transactions of the Royal Society of London B: Biological Sciences*, *357*(1426), 1431-1440.

[31] Higuera-Ciapara, I., Felix-Valenzuela, L., & Goycoolea, F. M. (2006). Astaxanthin: a review of its chemistry and applications. *Critical reviews in food science and nutrition*, *46*(2), 185-196.

[32] Naguib, Y. M. (2000). Antioxidant activities of astaxanthin and related carotenoids. *Journal of agricultural and food chemistry*, *48*(4), 1150-1154.

[33] Guerin, M., Huntley, M. E., & Olaizola, M. (2003). Haematococcus astaxanthin: applications for human health and nutrition. *TRENDS in Biotechnology*, *21*(5), 210-216.

[34] Pashkow, F. J., Watumull, D. G., & Campbell, C. L. (2008). Astaxanthin: a novel potential treatment for oxidative stress and inflammation in cardiovascular disease. *The American journal of cardiology*, *101*(10), S58-S68.

[35] Kidd, P. (2011). Astaxanthin, cell membrane nutrient with diverse clinical benefits and anti-aging potential. *Altern Med Rev*, *16*(4), 355-64.

[36] Park, J. S., Chyun, J. H., Kim, Y. K., Line, L. L., & Chew, B. P. (2010). Astaxanthin decreased oxidative stress and inflammation and enhanced immune response in humans. *Nutrition & metabolism*, *7*(1), 18.

Chapter 6   Conclusions

6.1   Summary of impact

In this work, six marine algae and one freshwater algae were chemically profiled for nutritional compounds. A number of important nutritional components relevant to human health were detected in the freshwater and marine algal species. To address limitations of current techniques, an extraction and derivatization method was developed for the quantitation of fatty acids; fifteen fatty acids were detected, importantly, the two essential fatty acids linoleic acid and linolenic acid, the omega-3 fatty acids eicosapentaenoic acid and docosahexaenoic acid. Pro-vitamin A (β-carotene), and vitamin E (α-tocopherol) was also detected in the algal biomass. Results showed that the algal biomass was a rich source of many vitamins and fatty acids relevant to inflammation and nutrition.

The freshwater alga *Parachlorella kessleri* was selected for scale-up production to produce enough biomass material for a bio-guided fractionation guided by investigation of various bio-activities, including anti-bacterial activity, anti-fungal activity, and several enzymatic inhibition assays, such as α-glucosidase inhibition activity, pancreatic lipase inhibition activity, inhibition of endo-cannibinoid reuptake enzymes FAAH and MAGL, inhibition of pro-inflammatory enzymes COX-2, iNOS, and PLA2. Using these assays, evaluation of primary fractions obtained by prep-scale chromatographic separation allowed for selection of active fractions for further purification. Sequential evaluation of

active fractions led to the isolation of eight compounds bio-active fractions, and the identification of 15 compounds in inactive fractions.

Screens demonstrated that compounds isolated from *Parachlorella kessleri* were active in a number of bioactivity assays. Six galactolipids were characterized and identified as potential pancreatic lipase inhibitors using an *in vitro* porcine pancreatic lipase inhibitor assay. This is the first report of galactolipids or pancreatic lipase inhibition activity reported for *Parachlorella kessleri*. Additionally, a new xanthophyll, 19'-decanoyloxy-fucoxanthin was detected and determined to inhibit pancreatic lipase (IC_{50} = 751 nM); this is the first report of 19'-decanoyloxy-fucoxanthin and its activity. α-glucosidase inhibition activity was detected in the methanol sub-fraction of *P. kessleri*, however it was determined that this activity was due to the fact that the major constituents of the methanol sub-fraction were starches which were substrates of α-glucosidase which competed with the assay substrate.

Several assays were conducted to evaluate potential anti-inflammatory activity. COX-2 inhibition was detected and α-linolenic acid and linoleic acid were identified by bio-guided fractionation, with IC50 values for COX-2 inhibition measured at 13.8 μM and 11.9 μM respectively. The inhibition of NOS by the xanthophyll extract of *P. kessleri* was evaluated in RAW264.7 macrophages; the IC50 was determined to be 94 μM. This is the first study of xanthophylls reported for *P. kessleri*. The major galactolipids isolated from *P. kessleri* showed PLA2 inhibition activity, with an IC50 calculated to be 10.41 μM—PLA2 inhibition activity has not previously been reported for *P. kessleri*. These results portend the

potential for utilizing *Parachlorella kessleri* biomass as potential sources of compounds capable of mitigating pro-inflammatory responses. Inhibition of endo-cannabinoid reuptake lipase enzymes MAGL and FAAH was not detected in any fractions evaluated.

In summary, results of the bioactivity-guided fractionation of *Parachlorella kessleri* biomass resulted in the identification of thirteen bioactive compounds with a range of enzymatic inhibitory properties. The quantity of nutritionally relevant constituents and large number of hits acquired from the small quantity of *P. kessleri* biomass (~100 g) obtained for this work confirms the hypothesis that the exploration of algal biomass in the context of medicinal chemistry represents an exciting new venue for identification of new sources of nutraceuticals and bioactive compounds.

6.2   Recommendations for future work

The next steps to be taken following this work involve the scale-up of methodology used to produce algal biomass. A major limiting factor confronted in this work was the minimal amount of material obtained after purification of constituents due to the difficulty in obtaining large quantities of starting material. Researchers in our lab are currently working with the Institute of Marine and Coastal Sciences at Rutgers to develop and optimize the aquaculture process to maximize biomass output.

After obtaining sufficient quantities of purified materials, a series of cell-based bioassays should be conducted to establish the viability of the bioactivities detected in this work *in vivo*. Concurrently, simple structural analogues of these compounds should be synthesized which eliminate labile moieties, such as ester bonds and glycoside linkages,

and replaced with more stable linkages. Following confirmatory cell-based assays, these compounds should be screened for toxicity in cell culture models to establish whether the concentration range required for activity causes toxicity in other cell lines (e.g. hepatocytes). Finally, after establishing bioactivity and lack of activity in cell lines, activity of these compounds in mouse models should be conducted to confirm cell-based evidence of activity.